

Optimizing the sequence of targeted therapy in EGFR-mutant lung adenocarcinoma

By

Catherine Belle Meador

Dissertation

Submitted to the Faculty of the

Graduate School of Vanderbilt University

in partial fulfillment of the requirements

for the degree of

DOCTOR OF PHILOSOPHY

in

Cancer Biology

August, 2015

Nashville, Tennessee

Approved:

Rebecca Cook, Ph.D.

Jennifer Pietenpol, Ph.D.

Christine M. Lovly, M.D., Ph.D.

William Pao, M.D., Ph.D.

To my mother

## ACKNOWLEDGMENTS

This work would not have been possible without the enduring support of family, friends, co-workers, and mentors. Words cannot fully express my gratitude for each and every person who has contributed mentorship, scientific conversation, challenging feedback, and words of encouragement through the years. First and foremost I would like to thank my graduate mentor, Dr. William Pao, for his investment in my training. Dr. Pao taught by example, combining efficiency with scientific rigor and holding himself and his students to the highest of standards. His love for new data, his endless optimism, and his confidence in his trainees made him the best graduate mentor I could have asked for. I feel lucky to have had the opportunity to train with someone with such a strong vision for the future of oncology and with such a strong work ethic. I would also like to very sincerely thank Dr. Christine Lovly for her willingness to mentor me during my final year of graduate school and support me in finishing up my thesis work. I am grateful for her investment of time and energy, and I appreciate all she has taught me from my early days in the lab up through the final stretch. I continue to be inspired by both Dr. Pao and Dr. Lovly's work in cancer biology and oncology drug development and hope to continue to learn from both of them through the years.

I would also like to thank my lab mates, fellow students in the Department of Cancer Biology, MSTP classmates, medical school classmates, and friends for the company, encouragement, reagents, protocols, coffee runs, feedback, happy hours, and perspective they have offered over the years. I am better for having had each one

of you around me. I would like to especially thank my fellow graduate students in the Pao and Lovly labs – Caroline, Katie, J-N, and Merrida – for the support they have each offered in their own way. Thank you also to former and current postdocs and research technicians for their scientific and life advice through the years – especially Kadoaki, Monica, Eiki, Karinna, and Hailing. Thank you to Abudi for sharing your lunch and for making my life run smoothly in every way. Thank you to all of you for brightening my days.

I would also like to thank my committee chair, Dr. Rebecca Cook, for her mentoring during the past few years. I am especially grateful for her guidance during times of transition. To Dr. Jennifer Pietenpol, I would like to express very sincere gratitude for her confidence in me and for her investment in my scientific progress and professional development from the time of my rotation in her lab to her joining my thesis committee.

In addition, I am grateful for having had wonderful collaborators on these projects, both within Vanderbilt and at other institutions. Specifically, I would like to thank Dr. Zhongming Zhao and his group, especially Dr. Peilin Jia, with whom I have collaborated extensively over the past several years and from whom I have learned much about processing and interpretation of next-generation sequencing data. I am grateful to Dr. Kimberly Dahlman and her team in the Innovative Translational Research Shared Resource for their assistance and scientific discussion on multiple projects. I would also like to thank Dr. Katerina Politi and her lab at the Yale Cancer Center, especially Dr. Valentina Pirazzoli, for several enjoyable collaborations over the years. I

am also thankful to many collaborators at Memorial Sloan Kettering Cancer Center, especially Dr. Marc Ladanyi, Dr. Lu Wang, and Dr. Elisa de Stanchina.

To the current and former members of the Vanderbilt MSTP Leadership Team, I extend my deepest gratitude for all of their support throughout this graduate school phase. It seems no question or problem is too small or too big for them, and because of that I am never left without someone to turn to. In addition, they are all wonderful people to be around. Between help with paperwork and logistics to generously inviting me into their homes for dinner and into their offices for advice, they have provided me with more support than I've deserved. Many thanks to Melissa, Jim, Larry, Michelle, Danny, Sally, and Terry for all they have done.

I would be remiss not to also thank Dr. Robert Coffey and Dr. Yang Wang, who were the first to teach me to love the lab and to love the EGF receptor. Their patience and faith in me is what opened doors and led me to pursue a career in research, and for that, I am deeply indebted to them. Finally, I would like to thank my family, for all of their support throughout the years. Thanks to Hannah for being my biggest cheerleader, to John for always generously offering to edit my papers, to Katie for adopting me as her own, and to my dad for his unconditional support and willingness to talk through anything I find myself facing. It is only with help from all of you that I have gotten this far, and I will continue to count on you as I navigate the years ahead.

## TABLE OF CONTENTS

	Page
ACKNOWLEDGMENTS .....	iv
LIST OF TABLES.....	xiv
LIST OF FIGURES .....	xvi
LIST OF PUBLICATIONS .....	xix
Chapter I: Introduction .....	1
Overview .....	1
Non-small cell lung cancer (NSCLC) .....	1
Historical classification and treatment of NSCLC.....	1
Genetic alterations and driver mutations in lung adenocarcinoma.....	2
Targeted therapies in lung adenocarcinoma.....	6
Diagnostic platforms for molecular classification of tumors in the clinic.....	8
Routine molecular subtyping of solid tumors by known driver mutations.....	13
EGFR-mutant lung adenocarcinoma .....	14
Epidermal Growth Factor Receptor .....	14
Lung adenocarcinoma-associated EGFR mutations.....	17
First-generation anti-EGFR therapies .....	20
Acquired resistance to first-generation EGFR TKIs .....	23
Second-generation EGFR TKIs and antibody+TKI combinations .....	26
Mutant-selective third-generation EGFR TKIs .....	29
Purpose of these studies .....	32
Chapter II: Next-generation sequencing of paired tyrosine kinase inhibitor-sensitive and -resistant EGFR mutant lung cancer cell lines identifies spectrum of DNA changes associated with drug resistance.....	35
Significance .....	35
Introduction.....	36
Results .....	39
Spectrum of genetic alterations associated with isogenic pairs of drug-sensitive and drug-resistant cells.....	39
Sample relatedness .....	52
Mutation patterns .....	55

Mutations shared across resistant cells .....	59
Driver gene specification.....	59
Discussion .....	61
Materials and methods .....	65
 Chapter III: Optimizing the sequence of anti-EGFR targeted therapy in EGFR-mutant lung cancer... 71	
Introduction.....	71
Results .....	73
AZD9291 versus afatinib + cetuximab in T790M+ cell lines.....	73
Derivation of afatinib + cetuximab-resistant cell lines .....	79
AZD9291 overcomes afatinib + cetuximab resistance .....	80
Afatinib + cetuximab does not overcome AZD9291 resistance.....	82
Discussion .....	85
Materials and methods .....	91
 Chapter IV: Acquired resistance to mutant-selective EGFR inhibitor AZD9291 is associated with increased dependence on RAS signaling in preclinical models .....	99
Introduction.....	99
Results .....	101
Generation of EGFR mutant cell populations resistant to AZD9291 and other EGFR TKIs .....	101
Resistance to AZD9291 and other EGFR TKIs is often associated with increased sensitivity to MEK inhibition .....	101
Comparison of genetic alterations across multiple populations of EGFRm or EGFRm/T790M cells resistant to AZD9291 and other EGFR TKIs.....	107
Modifications of RAS genes can drive resistance to EGFR inhibition .....	109
In vitro a combination of AZD9291 with selumetinib delays or prevents resistance emerging in EGFRm and EGFRm/T790M cells .....	111
In vivo a combination of AZD9291 + selumetinib caused regression of AZD9291 resistant tumors in transgenic models.....	117
Basal levels of RAS-MAPK pathway components do not predict MEK inhibitor sensitivity across resistant populations .....	122
Discussion .....	122
Materials and methods .....	126
 Chapter V: Mechanisms of resistance to combined EGFR/MEK inhibition in <i>EGFR</i> -mutant non-small cell lung cancer.....	128
Introduction.....	128
Results .....	130

Establishing models of resistance to AZD9291 + selumetinib .....	130
AZD9291+selumetinib-resistant cells are sensitive to ERK inhibition .....	133
AZD9291+selumetinib-resistant cells are sensitive to alternative MEK inhibitor, trametinib .....	134
Increased RAS-GTP in AZD9291+selumetinib-resistant cells .....	140
Discussion .....	142
Materials and methods .....	143
 Chapter VI: Conclusions and Future Directions .....	 146
Summary of findings .....	146
Future directions .....	149
T790M-negative, EGFR-dependent resistance to first-generation EGFR TKIs.	149
Heterogeneity in mechanisms of resistance to first-generation EGFR TKIs .....	150
Mechanisms of resistance to AZD9291 .....	152
Mechanisms of resistance to AZD9291 + selumetinib .....	153
Immune microenvironment of solid tumors .....	154
Conclusion .....	155
 Appendix .....	 158
Supplementary information for Chapter I .....	158
Supplementary information for Chapter II .....	159
Supplementary information for Chapter III .....	182
Supplementary information for Chapter IV .....	188
Supplementary information for Chapter V .....	212
Supplementary information for Chapter VI .....	217
 REFERENCES .....	 218

## LIST OF TABLES

### MAIN TABLES

<b>Table 1.</b> Alterations in signaling enzymes known to be associated with sensitivity to available targeted therapies in NSCLC. ....	9
<b>Table 2.</b> Types of clinical molecular tests and variants detected. ....	11
<b>Table 3.</b> List of EGFR TKIs currently approved or in clinical development. ....	21
<b>Table 4.</b> Summary of data derived from next-generation sequencing of 9 EGFR mutant cell lines ....	42
<b>Table 5.</b> Summary of single nucleotide variants (SNVs) and small insertions/deletions (indels) unique to each cell line .....	42
<b>Table 6.</b> Summary of validation studies on putative SNVs and indels .....	43
<b>Table 7.</b> List of validated SNVs and indels in parental cell lines .....	44
<b>Table 8.</b> Summary of copy number variation (CNV) regions identified in whole-exome sequencing (WES) samples using two software tools .....	53
<b>Table 9.</b> List of genetic alterations associated with drug-resistance for each cell line .....	60
<b>Table 10.</b> Drug-sensitive and –resistant cell lines used in this study .....	75
<b>Table 11.</b> IC <sub>50</sub> (μM) values from cell growth inhibition assays comparing compound sensitivity between parental and resistant cell populations. ....	103

### APPENDIX TABLES

<b>Table 12.</b> List of validated SNVs and indels in PC-9/ER cells. ....	169
<b>Table 13.</b> CNV regions in PC-9/ER .....	171
<b>Table 14.</b> List of validated SNVs in cell line PC-9/BRc1 .....	172
<b>Table 15.</b> CNV regions in PC-9/BRc1 .....	173
<b>Table 16.</b> List of validated SNVs in cell line HCC827/R1 .....	174
<b>Table 17.</b> CNV regions in HCC827/R1 .....	175

<b>Table 18.</b> List of validated SNVs in cell line HCC827/R2.....	176
<b>Table 19.</b> CNV regions (>100kb) in HCC827/R2 .....	178
<b>Table 20.</b> List of validated SNVs in cell line HCC4006/ER .....	179
<b>Table 21.</b> Distribution of SNVs in 5' versus 3' UTRs and within the gene body across the different cell lines. ....	180
<b>Table 22.</b> Summary of kinase genes harboring non-silent SNVs/indels in each cell line.....	181
<b>Table 23.</b> Generation of resistant cell populations.....	204
<b>Table 24.</b> Small molecule inhibitors.....	207
<b>Table 25.</b> IC <sub>50</sub> (μM) values from cell growth inhibition assays comparing compound sensitivity between parental and resistant cell populations. ....	208
<b>Table 26.</b> Genetic analysis of resistant cell populations. ....	209
<b>Table 27.</b> RPPA analysis of phosphorylated and total protein levels in PC9 and NCI-H1975 AZD9291 resistant populations compared to respective parental cells.....	211

## LIST OF FIGURES

### MAIN FIGURES

<b>Figure 1.</b> Examples of types of “driver” genomic alterations found in cancer. ....	3
<b>Figure 2.</b> Routine molecular subtyping of NSCLCs. ....	15
<b>Figure 3.</b> Frequency of resistance mechanisms identified in clinical samples of acquired resistance to gefitinib or erlotinib. ....	25
<b>Figure 4.</b> Description of cell lines examined. ....	38
<b>Figure 5.</b> Sanger sequencing chromatograms of mutations “lost” in drug-resistant cell lines compared with matched drug-sensitive cell lines. ....	45
<b>Figure 6.</b> Copy number variation (CNV) regions on chromosome 7 for HCC827/R1, HCC827/R2, and HCC4006/ER cells. ....	50
<b>Figure 7.</b> Pairwise comparison of samples. ....	54
<b>Figure 8.</b> Patterns of mutations that uniquely occurred in each resistant cell line. ....	56
<b>Figure 9.</b> Patterns of SNV frequencies (A, B) and signatures (C-F) across different stratifications of genomic material. ....	58
<b>Figure 10.</b> Afatinib plus cetuximab (A+C) versus AZD9291 in T790M+ cell lines. ....	77
<b>Figure 11.</b> Afatinib plus cetuximab (A+C)-resistant cell lines are sensitive to growth inhibition by AZD9291. ....	83
<b>Figure 12.</b> AZD9291-resistant cell lines are resistant to growth inhibition by A+C. ....	86
<b>Figure 13.</b> RAS-MAPK signaling inhibition by selumetinib in EGFR inhibitor resistant cell lines. ....	105
<b>Figure 14.</b> Determining the functional role of NRAS modifications in acquired resistance to EGFR inhibitors. ....	112
<b>Figure 15.</b> Determining the functional role of KRAS gain in acquired resistance to EGFR inhibitors. ....	114
<b>Figure 16.</b> In vitro combination of AZD9291 with selumetinib induces more profound phenotype inhibition. ....	118

<b>Figure 17.</b> In vivo combination of AZD9291 and selumetinib can overcome acquired resistance to AZD9291 in mutant EGFR transgenic models of lung cancer.....	120
<b>Figure 18.</b> <i>In vitro</i> modeling of resistance to AZD9291 + selumetinib. ....	131
<b>Figure 19.</b> AZD9291+selumetinib-resistant cells are sensitive to ERK inhibition. ....	135
<b>Figure 20.</b> AZD9291+selumetinib-resistant cells are sensitive to alternative MEK inhibitor, trametinib. ....	138
<b>Figure 21.</b> AZD9291+selumetinib-resistant cells demonstrate increased RAS activation. ....	141
<b>Figure 22.</b> Potential sequential application of targeted therapies in <i>EGFR</i> -mutant lung cancer.....	147

## APPENDIX FIGURES

<b>Figure 23.</b> Effect of erlotinib and WZ4002 (T790M-specific small molecule) on the growth of PC-9 (A) and PC-9/ER cells (B).....	159
<b>Figure 24.</b> Analysis pipeline. ....	160
<b>Figure 25.</b> Copy number variation (CNV) changes in PC-9/ER compared to PC-9/S1 by Control-FREEC.....	161
<b>Figure 26.</b> Copy number variation (CNV) changes in PC-9/BRc1 compared to PC-9/S2.....	162
<b>Figure 27.</b> Effect of erlotinib and WZ4002 (T790M-specific small molecule) on the growth of HCC827 (A), HCC827/R1 (B), and HCC827/R2 (C) cells.....	163
<b>Figure 28.</b> Copy number variation (CNV) changes in HCC827/R1 compared to HCC827. ....	164
<b>Figure 29.</b> Copy number variation (CNV) changes in HCC827/R2 compared to HCC827. ....	165
<b>Figure 30.</b> Effect of erlotinib and WZ4002 (T790M-specific small molecule) on the growth of HCC4006 (A) and HCC4006/ER (B) cells.....	166
<b>Figure 31.</b> Copy number variation (CNV) changes in HCC4006/ER compared to HCC4006.....	167
<b>Figure 32.</b> Illustration of location of mutations in kinase genes detected in the cell lines. ....	168
<b>Figure 33.</b> Schematic of derivation ‘lineages’ for drug-sensitive and –resistant cell lines used in this study. ....	182
<b>Figure 34.</b> Characterization of T790M+ cell lines. ....	183

**Figure 35.** Characterization of A+C-resistant cell lines..... 185

**Figure 36.** Characterization of AZD9291-resistant cell lines. .... 186

**Figure 37.** Comparison of genetic alterations across multiple populations resistant to AZD9291 and other EGFR TKIs ..... 196

**Figure 38.** Treatment of resistant populations with AZD9291..... 197

**Figure 39.** Detection and Validation of a novel NRAS E63K mutation. .... 199

**Figure 40.** Lysates were prepared from parental PC9 and resistant populations analysed for levels of total and phosphorylated ERK, NRAS and KRAS by western blot..... 200

**Figure 41.** The novel NRAS E63K mutation is an activating mutation that when expressed enhances resistance to cell growth inhibition by gefitinib or AZD9291 in EGFRm cell lines..... 201

**Figure 42.** In vitro combination of AZD9291 with selumetinib induces more profound phenotype inhibition..... 203

**Figure 43.** Characterization of additional cell line models of AZD9291 + selumetinib resistance..... 212

**Figure 44.** Increased phospho-ERK and/or phospho-AKT signaling in setting of AZD9291 + selumetinib resistance. .... 214

**Figure 45.** Characterization of AZD9291 + selumetinib-resistant cell lines not sensitive to ERK inhibition..... 215

**Figure 46.** Characterization of AZD9291 + selumetinib-resistant cell lines not sensitive to trametinib. .... 216

## LIST OF PUBLICATIONS

Jia P, Jin H, **Meador CB**, Xia J, Ohashi K, Liu L, Pirazzoli V, Dahlman KB, Politi K, Michor F, Zhao Z, Pao W. Next-generation sequencing of paired tyrosine kinase inhibitor-sensitive and –resistant EGFR mutant lung cancer cell lines identifies spectrum of DNA changes associated with drug resistance. *Genome Research*. 2013 September; 23(9): 1434-45.

**Meador CB**, Micheel CM, Levy MA, Lovly CM, Horn L, Warner JL, Johnson DB, Zhao Z, Anderson I, Sosman JA, Vnencak-Jones CL, Dahlman KB, Pao W. Beyond Histology: translating tumor genotypes into clinically effective targeted therapies. *Clinical Cancer Research*. 2014 May; 1:20(9): 2264-75.

**Meador CB**, Jin H, de Stanchina E, Nebhan CA, Pirazzoli V, Wang L, Lu P, Vuong H, Hutchinson KE, Jia P, Chen X, Eisenberg R, Ladanyi M, Politi K, Zhao Z, Lovly CM, Cross DA, Pao W. Optimizing the sequence of anti-EGFR-targeted therapy in EGFR-mutant lung cancer. *Mol Cancer Ther*. 2015 February; 14(2): 542-52.

**Meador CB** and Pao W. Old Habits Die Hard: Addiction of BRAF-Mutant Cancer Cells to MAP Kinase Signaling. *Cancer Discov*. 2015 April; 5(4): 348-50.

Eberlein CA, Stetson D, Markovets AA, Al-Kadhimi KJ, Lai Z, Fisher PR, **Meador CB**, Spitzler P, Ichihara E, Ross SJ, Ahdesmaki MJ, Ahmed A, Ratcliffe LE, O'Brien ELC, Barnes CH, Brown H, Smith PD, Dry JR, Beran G, Thress KS, Dougherty B, Pao W, Cross DAE. Acquired resistance to mutant-selective EGFR inhibitor AZD9291 is associated with increased dependence on RAS signaling in preclinical models. *Cancer Res*. 2015 June; 75: 2489.

**Meador CB** and Lovly CM. Revealing dynamic resistance mechanisms in solid tumors with liquid biopsies. *Nat Med*, in press.

Pirazzoli V, Ayeni D, **Meador CB**, Sanganahalli BG, Hyder F, Goldberg S, Pao W, Politi K. Afatinib plus cetuximab delays resistance compared to single agent erlotinib or afatinib in mouse models of TKI-naïve EGFR L858R-induced lung adenocarcinoma. *Submitted*.

## Chapter I: Introduction

### Overview

The goal of this introductory chapter is to supply background information on concepts relevant to the original scientific data presented in this manuscript. As such, the following text will first provide a historical perspective on the clinical categorization and treatment of non-small cell lung cancer, including the discovery of “driver” oncogenes in lung cancer and the shift from histological to molecular stratification. Subsequent sections will describe broadly the available targeted therapies for various molecular subsets of lung cancer and current status of technologies used for detection of therapeutically ‘actionable’ driver oncogenes in the clinic. The final section will provide a more in-depth discussion of *EGFR*-mutant lung cancer, including the biology of the epidermal growth factor receptor (EGFR) in its wild-type and mutant forms, the multiple generations of anti-EGFR targeted therapies that have been developed to treat this disease, and known mechanisms of resistance to these therapies at the time this work was initiated.

### Non-small cell lung cancer (NSCLC)

#### *Historical classification and treatment of NSCLC*

Lung cancer is responsible for approximately one-third of all cancer-related deaths worldwide [8]. Lung cancer has classically been histologically subdivided broadly

into small cell lung cancer (SCLC) and non-small cell lung cancer (NSCLC). NSCLC can be further subdivided into adenocarcinoma, squamous cell carcinoma, and large cell carcinoma. Standard of care for advanced NSCLCs, which were previously lumped together clinically, has historically consisted of combination chemotherapy regimens such as cisplatin and paclitaxel [8]. The median overall survival rate with this combination is approximately 8-10 months, similar to other combinations of chemotherapeutic agents [9]. A phase III trial published in 2006 demonstrated a 20% higher response rate (35% versus 15%) and an increase of 2 months in overall survival (12.3 months versus 10.3 months) with addition of bevacizumab, an anti-VEGF monoclonal antibody [10]. In general, new cytotoxic chemotherapy regimens for unselected NSCLCs have not substantially improved survival of lung cancer patients in recent years.

### ***Genetic alterations and driver mutations in lung adenocarcinoma***

Since the original discovery that oncogenes were mutated forms of normally expressed genes in human cells [11], somatic genomic alterations have been recognized as causative in the initiation and progression of cancer. These genetic changes can take many forms, including point mutations, insertions, deletions, combined insertions/deletions (indels), duplications, inversions, and translocations. In some cases, tumors harbor these mutations in oncogenes (in particular, tyrosine kinases and serine-threonine kinases), which render them exquisitely sensitive to targeted small-molecule inhibitors (**Figure 1**) [12].

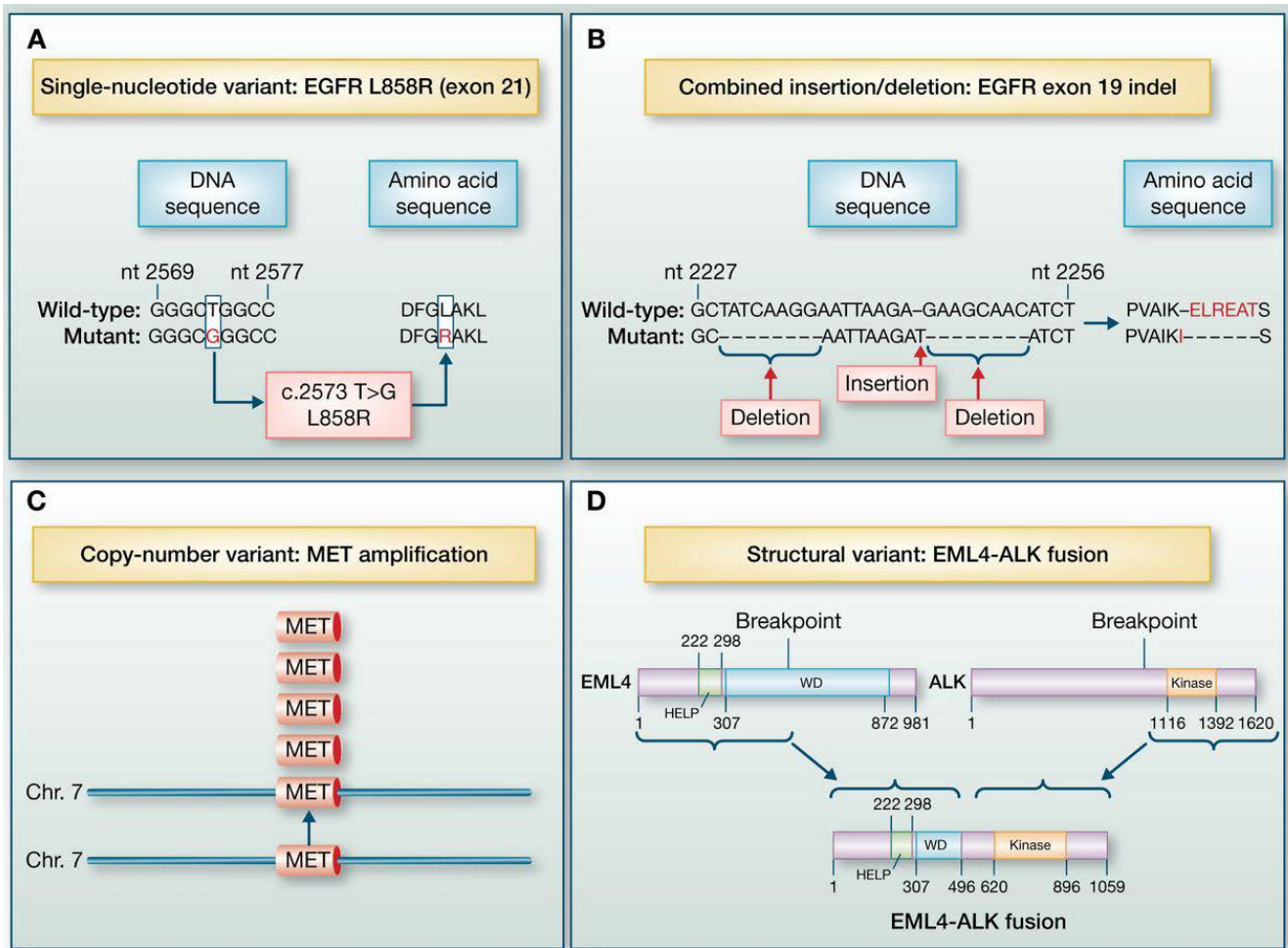


**Figure 1. Examples of types of “driver” genomic alterations found in cancer.**

Schematic representations of mutations known to occur in NSCLC, including point mutations, insertions/deletions, CNVs, and structural variants. **A**, SNV in exon 21 of *EGFR* (c.2573 T>G) encoding a substitution of arginine for leucine at codon 858 (L858R). **B**, combined insertion/deletion (indel) in exon 19 of *EGFR* confer sensitivity to EGFR TKIs. Red, a nucleotide or amino acid that has been altered in the mutant form. Amplification of *MET* (C) and structural variants resulting in *EML4-ALK* fusions confer sensitivity to crizotinib (D). Adapted from Meador, CB et al, Clin Cancer Res, 2014 [7].

Despite the enormous genetic complexity present in the tumor, these specific genomic alterations, or “driver mutations”, cause tumors to become ‘oncogene addicted’, i.e. ultimately reliant on specific signaling pathways such that inhibition of those pathways results in cell death [12]. In the past decade, research efforts have revealed that a large percentage of NSCLCs harbor recurrent alterations in known oncogenes. The discovery of these genomic subsets has prompted a paradigm shift in the treatment of NSCLC, especially in lung adenocarcinoma. Rather than empiric treatment based on histological classification, molecular classifications of lung adenocarcinomas are increasingly informing clinical decision-making.

Known and/or putative driver oncogenes in lung adenocarcinoma identified to date include mutated *KRAS*, *EGFR*, *ERBB2*, *BRAF*, *PIK3CA*, *MAP2K1*, *AKT1*, *MET*, *NRAS*, *HRAS*, *RIT1*, amplified *MET* and *ERBB2*, and translocated *ALK*, *ROS1*, *RET*, and *NTRK1* [13-15]. For the most part, these identified driver alterations occur in receptor tyrosine kinases (RTKs) or downstream pro-proliferative and survival (RAS/RAF/MEK) signaling pathways. Driver mutations are typically considered mutually exclusive; however, several of these genomic alterations have occasionally been found to be co-occurring (especially *PIK3CA* mutations with *EGFR* and/or *KRAS* mutations) [13].

Identification of clinically actionable molecular drivers in NSCLC and other solid tumors has been a tour de force for the oncology community during the past 10-15 years. Traditionally, these discoveries have been made by identifying the underlying molecular mechanisms in individual tumors or cells lines demonstrating particular phenotypes. With the recent explosion of available next-generation sequencing (NGS)

technologies, we are now able to detect the whole spectrum of somatic genomic alterations in cancers using a limited number of assays and minimal amounts of tumor tissue. However, because a solid tumor may have up to 400 mutations per megabase (Mb) [16], the task of distinguishing ‘driver’ (causative) versus ‘passenger’ (non-functional) mutations from the pool of somatic mutations observed in tumor genomes is not trivial. Thus, the most challenging task in the identification of targetable oncogenic ‘drivers’ is the integration of the diverse range of available genomic data into biologically and clinically relevant information.

In order to begin to discern potentially functional genomic alterations from the myriad of mutations and structural variants present in solid tumors, large sequencing efforts have been initiated that provide greater statistical power for discovering genomic alterations of biological importance. One such example is The Cancer Genome Atlas (TCGA), which is an initiative sponsored by the National Institutes of Health (NIH) that aims to catalog systematically genetic changes occurring in more than twenty types of human cancers, including lung adenocarcinoma [14, 17]. This analysis is made possible by the availability of fresh frozen surgically resected specimens and matched blood samples, which in most cases provide more than enough tissue for multi-platform analysis of somatic alterations at the DNA, RNA, or protein level. This is especially important, given that efforts to identify drivers at the genomic level (even in extensive studies with 200+ tumor specimens) reveal known or putative driver mutations in only about 75% of analyzed tumors [14].

## ***Targeted therapies in lung adenocarcinoma***

Such ‘driver’ genomic alterations serve as a mechanism by which tumors can be sub-classified regarding their likelihood of response to pharmacological inhibition of their activated pathways. While effective inhibitors are not yet available for all molecular subtypes of lung adenocarcinomas, significant progress has been made in recent years to develop rational therapeutic approaches to treatment of lung adenocarcinomas. The goal of this work is to, whenever possible, deliver the ‘right drug to the right patient, at the right time.’

The first great success regarding targeted therapy in lung adenocarcinoma was the discovery that tumors harboring activating mutations in *EGFR* are exquisitely sensitive to EGFR tyrosine kinase inhibitors [18-20]. A more in-depth discussion of *EGFR*-mutant lung cancers and available anti-EGFR therapies follows in the subsequent section (“EGFR-Mutant Lung Adenocarcinoma”). Another success story of targeted therapies drastically improving patient outcomes was the discovery and rational treatment of tumors harboring genetic fusions involving *ALK* tyrosine kinase [21]. *ALK* fusions (most commonly with *EML4*) are found in about 3-7% of NSCLCs and confer sensitivity to crizotinib, a small molecule inhibitor of *ALK* as well as *MET* tyrosine kinases [22, 23]. There are multiple novel *ALK* inhibitors currently in clinical trials for TKI-naïve and crizotinib-resistant *ALK*-positive lung cancer, such as ceritinib and alectinib, among others [24, 25].

While *EGFR* mutations and *ALK* rearrangements are the most common known genomic alterations in ‘never-smokers’ (defined as fewer than 100 cigarettes in one’s

lifetime), *KRAS*-mutant lung cancer remains the largest known genomic subtype of NSCLC overall [14]. Unfortunately, there are no direct inhibitors of mutant *KRAS* available, making this a less ‘targetable’ group of tumors. Efforts thus far to develop rational therapeutic strategies for *KRAS*-mutant tumors have been aimed at inhibiting downstream signaling molecules, such as MEK1/2. Based on promising preclinical data in *KRAS*-mutant NSCLC, a phase II study testing the addition of a MEK1/2 inhibitor, selumetinib, to standard chemotherapeutic agent docetaxel was initiated. This study revealed that the addition of selumetinib was associated with a 3.2 month increase in PFS (5.3 versus 2.1 months) and achieved a 37% objective response rate (compared to 0% with docetaxel alone) [26]. However, a phase II study combining another MEK1/2 inhibitor, trametinib, with docetaxel showed no improvement over docetaxel alone [27]. Similarly disappointing are data from a small recent multi-histology phase II basket study demonstrated a mere 11% response rate in *KRAS*-mutant NSCLC treated with selumetinib alone [28].

A recent study, designed based on preclinical data suggesting the need for co-targeting of MEK/AKT signaling in *KRAS*-mutant tumors, tested the combination of selumetinib with AKT inhibitor MK-2206 and demonstrated only a 25% (3/13) response rate in *KRAS*-mutant NSCLC [29]. Thus, although new therapeutic strategies are actively being pursued for this molecular cohort, identification of an effective first-line targeted therapy for treatment of *KRAS*-mutant tumors remains an unmet clinical need. Case reports and retrospective analyses have shed light on potential targeted agents for smaller genomic subsets of NSCLC. A summary of known genomic subtypes of NSCLC, along with their sensitivity/resistance to targeted agents, is listed in **Table 1**.

### ***Diagnostic platforms for molecular classification of tumors in the clinic***

A relevant consideration for clinical application of widespread sequencing efforts to identify molecular drivers in tumors is the limited amount and variability in quality of available tumor tissue (usually formalin-fixed and paraffin-embedded, FFPE). This, along with cost of testing, issues around reimbursement policies, and the bioinformatics expertise necessary for interpretation of results are current barriers to the feasibility of routinely translating certain genomics-based assays into the clinic.

Despite the challenges, development of new and updated platforms for detection of single nucleotide variants (SNVs), copy number variants (CNVs), and structural variants (SVs) with minimal amounts of input genetic material is rapidly evolving. Increasingly precise and comprehensive sequencing technologies are regularly emerging, including technologies necessary for sequencing DNA extracted from single cells or circulating cell-free DNA [30-34]. However, the adoption of appropriate technologies from the research to the clinical realm takes time. **Table 2** describes currently available technologies for molecular profiling of tumors for clinical decision-making.

For SNVs and small insertions, deletions, or indels, PCR followed by dideoxynucleotide sequencing remains a cost-effective, reliable method for detection of known variants. However, direct sequencing is low-throughput as well as limited in its sensitivity, detecting only variant alleles present at a frequency of at least 20-25%. By contrast, multiplexed assays such as SNaPshot and Sequenom mass ARRAY can

**Table 1. Alterations in signaling enzymes known to be associated with sensitivity to available targeted therapies in NSCLC.**

Oncogene		Targeted therapy	Level of evidence	Associated publications
ALK fusions		Crizotinib	Phase III trial	Shaw et al. 2013 [23]
		IPI-504	Phase II trial	Sequist et al. 2010 [35]
		Ganetespib	Phase II trial	Socinski et al. 2013 [36]
		Ceritinib (LDK378)	Phase I trial	Shaw et al. 2014 [24]
		AP26113	Phase I trial	Camidge et al. 2015 [37]
		Alectinib	Phase I/II trial	Seto et al. 2013 [25]
ALK	Fusion + G1269A	Ganetespib	Case report	Sang et al. 2013 [38]
BRAF	Y472C	Dasatinib	Case report	Sen et al. 2012 [39]
	V600E	Vemurafenib	Case report	Gautschi et al. 2012 [40]
		Dabrafenib	Case report	Rudin et al. 2013 [41]
DDR2	S768R	Dasatinib	Case report	Pitini et al. 2013 [42]
		Dasatinib + erlotinib	Case report	Hammerman et al. 2011 [43]
EGFR	Exon19del/ L858R	Gefitinib	Phase III trial	Mok et al. 2009 [44] Mitsudomi et al. 2010 [45] Maemondo et al. 2010 [46]
		Erlotinib	Phase III trial	Zhou et al. 2011 [47] Rosell et al. 2012 [48]
		Afatinib	Phase III trial	Sequist et al. 2013 [49]
		Dacomitinib	Phase II trial	Ramalingam et al. 2012 [50]
	Exon 19ins	Erlotinib Gefitinib Afatinib	Retrospective analysis	He et al. 2012 [51]
	Exon 20ins (A763_Y764insFQEA)	Erlotinib Gefitinib Afatinib	Preclinical data	Yasuda et al. 2013 [52]
	G719A/C/S	Gefitinib Neratinib	Case report Phase II trial	Lynch et al. 2004 [20] Sequist et al. 2010 [53]
	L861Q	Gefitinib	Case report	Lynch et al. 2004 [20]
	T790M	Rociletinib	Phase I trial	Sequist et al. 2015

				[54]
		AZD9291	Phase I trial	Janne et al., 2015 [55]
<i>ERBB2</i>	Exon20ins/ G776L	Afatinib	Phase II trial	De Greve et al. 2012 [56]
		Trastuzumab + paclitaxel	Case report	Cappuzzo et al. 2006 [57]
		Trastuzumab + chemo	Retrospective analysis	Mazieres et al., 2008 [58]
<i>FGFR1</i>	Amplification	BGJ398	Case report	Malchers et al. 2013 [59]
<i>KRAS</i>	<sup>a</sup> G12A/R/D/C/S/V <sup>a</sup> G13D	Selumetinib + docetaxel	Phase II trial	Janne et al. 2013 [26]
<i>MEK1</i>	K57N	Selumetinib	Preclinical data	Marks et al., 2008 [60]
<i>MET</i>	Amplification	Crizotinib	Case report	Ou et al. 2011 [61]
<i>NRAS</i>	<sup>b</sup> Q61L/R/K	Selumetinib Trametinib	Preclinical data	Ohashi et al. 2013 [62]
<i>PIK3CA</i>	H1047R	BKM120	Phase I trial	Bendell et al. 2012 [63]
<i>RET</i> fusions		Cabozantinib	Phase II trial	Drilon et al. 2015 [64]
		Vandetinib	Case report	Gautschi et al. 2013 [65]
		Ganetespib	Preclinical data	Sang et al. 2013 [38]
<i>ROS1</i> fusions		Crizotinib	Case report	Bergethon et al. 2012 [66]
			Phase I trial	Shaw et al. 2014 [67]
		Ganetespib	Preclinical data	Sang et al. 2013 [38]

<sup>a</sup>Specific mutations listed are those found in references cited. Other substitutions in *KRAS* codons 12, 13, and 61 have been found in NSCLC; differences in their sensitivity to selumetinib + docetaxel are unknown at this time.

<sup>b</sup>Specific mutations listed are those found in references cited. Other substitutions in *NRAS* codons 12, 13, and 61 have been found in NSCLC; differences in their sensitivity to selumetinib and trametinib are unknown at this time.

Adapted from Meador, CB et al, Clin Cancer Res, 2014 [7].

**Table 2. Types of clinical molecular tests and variants detected.**

Molecular Methodology	Variant Types			
	SNVs	Small duplications, insertions, deletions, indels	Exon duplications, deletions or gene copy number changes	SVs
Allele-specific PCR	✓			
PCR and Sanger dideoxy sequencing	✓	✓		<sup>a</sup>
PCR and pyrosequencing	✓	•		
PCR and MS	✓	•		
PCR and single base extension	✓			
MLPA	✓		✓	
FISH			<sup>b</sup>	✓
NGS – custom panels (amplicon capture)	✓	✓		
NGS – custom panels (hybridization capture)	✓	✓	✓	•
NGS – whole exome sequencing	✓	✓	✓	•
NGS – whole genome sequencing	✓	✓	✓	✓

✓ Variant detected. • Variant detected with difficulty. <sup>a</sup> Variant detected if fusion RNA is extracted first. <sup>b</sup> Variant in gene copy number only. FISH = fluorescence *in situ* hybridization; indels = mutations including both insertions and deletions; MLPA= multiplex ligation-dependent probe amplification; MS = mass spectrometry; NGS = next-generation sequencing; PCR = polymerase chain reaction; SNVs = single nucleotide variants; SVs = structural variants. Adapted from Meador, CB et al, Clin Cancer Res, 2014 [7].

query already known mutations in several genes at once, detecting variant alleles present at frequencies as low as 1.56% [68-71]. NGS, in the form of targeted/custom panels, whole exome sequencing (WES), or whole genome sequencing (WGS) offers deep coverage (i.e. high sensitivity) and the highest possible throughput in terms of detecting many somatic SNVs, small insertions and/or deletions at once. However, the use of NGS does not necessarily imply comprehensiveness; for example, multiplexed amplicon-based targeted re-sequencing assays that encompasses panels of cancer-associated genes often interrogate only specific exons and may therefore miss detection of certain novel mutations in other locations. Capture-based targeted re-sequencing methods have similar drawbacks; thus, data outputs from these assays must be carefully interpreted and not assumed to be exhaustive in their detection of potentially functional genomic alterations.

While fluorescence *in situ* hybridization (FISH) and multiplex ligation-dependent probe amplification (MLPA) remain the clinical standard for targeted detection of CNVs, NGS technologies afford higher throughput and unbiased detection of CNVs. Finally, NGS, in particular WGS, provides a mechanism for genome-wide detection of structural variants, eliminating the need for previous knowledge of potential fusions or input of RNA (more easily degraded in FFPE samples and thus logistically more difficult to obtain and preserve on a large scale).

Management, analysis, and reporting of NGS data back to the treating physician all remain significant hurdles to widespread adoption of NGS technologies, but algorithms for more automated and accurate variant calling are improving. A relevant consideration regarding the practicality and ethics of NGS is the question of 'how much

is too much?’ These platforms are invaluable for discovery, but adoption into routine patient care will require careful stewardship and meticulous, integrated analysis of these large datasets.

### ***Routine molecular subtyping of solid tumors by known driver mutations***

For tumors harboring known drivers with well-understood implications for existing and emerging targeted therapies, translation to the clinic can be achieved by the design of targeted molecular genotyping assays that are accurate, sensitive, timely, and cost-effective for cancer patients. Indeed, many such academic, commercial, and government-sponsored targeted genotyping efforts are in progress at centers all over the world. Encouragingly, the multitude of clinical tumor genotyping efforts currently underway are too numerous to name, and they are generating an enormous amount of data about the genetic landscape of solid tumors while also facilitating access of patients to personalized cancer therapy.

Among 1,003 NSCLC specimens (predominantly adenocarcinoma) genotyped by SNaPshot sequencing [68] at Vanderbilt University Medical Center (VUMC) between 2010-2013, 424 harbored known driver mutations, including *KRAS* (22.9%), *EGFR* (14.8%), *PIK3CA* (2.1%), *BRAF* (1.9%), *ERBB2* (0.9%), *MEK1* (0.8%), *NRAS* (0.5%), and *AKT1* (0.3%) (**Figure 2A**). These mutations are typically mutually exclusive, except for *PIK3CA* mutations, which often co-occur with *EGFR* or *KRAS* mutations. This breakdown is similar to what has been published in the literature for each of these mutations [13, 14]. In addition to these tumors harboring activating mutations detectable

by SNaPshot sequencing, a subset of lung adenocarcinomas harbor fusions (which are tested for separately) in genes encoding receptor tyrosine kinases anaplastic lymphoma kinase (*ALK*; 3-7%), c-ros oncogene 1 (*ROS1*; 2%), and *RET* (rearranged during transfection; 1%) [21, 65, 72].

## **EGFR-mutant lung adenocarcinoma**

### ***Epidermal Growth Factor Receptor***

As described previously, mutations in the kinase domain of EGFR are found in 10-35% of NSCLCs. EGFR is the first of four epidermal growth factor receptor family members, which also include ErbB2/HER2, ErbB3/HER3, and ErbB4/HER4. Originally discovered in the early 1980s [73-75], decades of research have further elucidated its complex signaling mechanisms, critical role in epithelial cell homeostasis, and widespread dysregulation in human cancers [76-80].

Each of the ErbB receptors consists of an extracellular domain, a single hydrophobic transmembrane domain, and an intracellular domain. The extracellular domain is further subdivided into domains I-IV. Extracellular domains I and III participate in ligand binding, and extracellular domains II and IV commonly form disulfide bonds, including those needed for receptor dimerization. The intracellular domain contains a juxtamembrane segment, tyrosine kinase domain, and carboxyterminal tail [74, 78]. As an aside, there are two numbering systems widely used to describe the peptide sequence of ErbBs. The first includes the 24-amino acid signal peptide, and the second

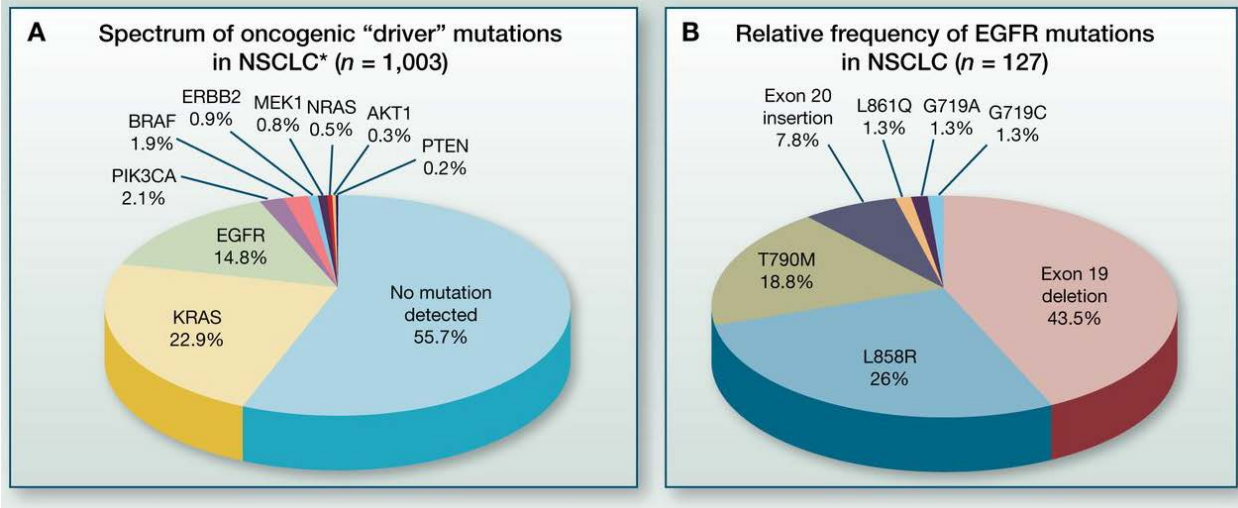


**Figure 2. Routine molecular subtyping of NSCLCs.**

Routine molecular subtyping of NSCLCs. Frequency of mutations identified by SNaPshot genotyping through Vanderbilt's PCMI from July 2010 to August 2013. **A**, frequency of lung cancer–associated mutations. 34 lung tumor specimens contained multiple mutations in the genes listed. \*, ALK FISH performed separately. **B**, spectrum of mutations identified in *EGFR*. 27 lung tumor specimens contained multiple mutations in *EGFR*. Adapted from Meador et al. *Clin Cancer Res* 2014.

uses the numbering system of the mature protein, following cleavage of the signal peptide [78]. The former (nascent protein numbering system) will be used throughout this text in reference to specific amino acids.

There are eleven known human ErbB ligands, which demonstrate varying selectivity for specific ErbB family members. The seven ligands that bind EGFR are epidermal growth factor (EGF), epigen (EPG), transforming growth factor- $\alpha$  (TGF- $\alpha$ ), amphiregulin (AR), betacellulin (BTC), heparin-binding EGF-like growth factor (HB-EGF), and epiregulin (EPR). The latter three also bind to ErbB4, in addition to neuregulin-3 and -4 (Nrg-3/4). Erb3/HER3 binds neuregulin-1 and -2 (Nrg-1/2). There are no known ligands for ErbB2/HER2 [78, 80].

Ligand binding to the extracellular domain of EGFR induces a conformational change that releases the receptor into the extended, active conformation, enabling homo- or hetero-dimerization with another ErbB receptor [79]. Though ErbB2/HER2 has no known ligand, it is the preferred dimerization partner of all ErbBs [81]. In total, including various isoforms of each of the receptors and all eleven possible ligands, there are 614 possible combinations of ligand-receptor ErbB complexes [78]. Given the importance of ErbB signaling in development and epithelial homeostasis, the amount, location, and stability of these receptors and ligands are tightly regulated within the cell.

Following asymmetric dimer formation (N-lobe to C-lobe of the kinase domains), trans-phosphorylation of tyrosine residues in the cytoplasmic domain creates docking sites for initiating of downstream signaling [78, 79]. Two major signaling pathways downstream of EGFR activation are mitogen-associated protein kinase (MAPK)

signaling and phosphoinositide 3-kinase (PI3K)/AKT signaling, which are broadly responsible for proliferation and survival of the cell, respectively [78, 80].

### ***Lung adenocarcinoma-associated EGFR mutations***

The first EGFR TKI developed for treatment of NSCLC, gefitinib, was originally developed based on the premise that EGFR is expressed more abundantly in lung cancer tissue as compared to surrounding lung parenchyma [80]. However, early clinical trials testing gefitinib in patients with lung adenocarcinoma revealed low (~10-20%) objective response rates, and responses were not associated with levels of EGFR expression as assessed by immunohistochemistry [82, 83]. These clinical data suggested that EGFR expression alone was not a sufficient biomarker of response to EGFR TKIs, and that there existed some as-yet undefined molecular mechanism of sensitivity of lung adenocarcinomas to EGFR inhibition.

In 2004, somatic activating mutations were identified in the kinase domain of EGFR in a subset of lung adenocarcinomas [18-20]. These mutations are associated with sensitivity to small molecule kinase inhibitors of EGFR, while lung cancers with wild-type EGFR do not display the same sensitivity [18-20]. This observation explained the heterogeneity of responses seen in the unselected population of lung adenocarcinomas, and it allowed for more precise definition of molecular markers of sensitivity to EGFR TKIs in lung cancer. At the time of their discovery, these mutations made EGFR the first 'targetable' genomic driver in lung cancer.

These activating mutations in the EGFR kinase domain occur most frequently in lung tumors of younger, often female, patients and never-smokers [18-20]. Consistent with observed clinical responses to EGFR TKIs in individuals of East Asian descent, *EGFR* activating mutations have also been observed more commonly (up to 35% of lung tumors) in this demographic [84-86]. The average frequency of *EGFR* mutations identified in lung cancer patients of non-East Asian descent is about 10%.

Among *EGFR*-mutant lung adenocarcinomas, the most common EGFR activating mutation identified is a multinucleotide deletion or combined insertion/deletion (indel) in exon 19 of the EGFR kinase domain ( $EGFR^{19DEL}$ ), occurring in roughly 50% of *EGFR*-mutant lung tumors (**Fig. 1A-B, Fig. 2B**) [79, 87]. This in-frame deletion results in the loss of at least four consecutive, conserved amino acids, L747-A750 (LREA) in close proximity to amino acid K745, which is critical for ATP binding [18-20, 88]. Most commonly 15 base pairs in length, multiple variations of this deletion have been identified in lung adenocarcinomas. The second most common *EGFR* activating mutation is a point mutation in codon 858 in exon 21 (2573T>G;  $EGFR^{L858R}$ ), substituting arginine for leucine [79, 87]. This substitution occurs in the activation loop of EGFR, adjacent to the highly conserved DFG motif [18-20, 89].

Both  $EGFR^{19DEL}$  and  $EGFR^{L858R}$  result in constitutive, ligand-independent induction of EGFR kinase activity and oncogenic transformation of the lung cancer cell in which they occur [79].  $EGFR^{19DEL}$  and  $EGFR^{L858R}$  are typically treated the same clinically, as they confer comparable sensitivity to most EGFR TKIs in patients. However, a recent retrospective analysis of two phase III clinical trials indicated that afatinib extended overall survival rates for patients whose tumors harbored  $EGFR^{19DEL}$ ,

but not EGFR<sup>L858R</sup>, further suggesting biological differences between these two activating mutations [90]. There also exists preclinical data indicating subtle differences between these two mutant forms of EGFR. Specifically, EGFR<sup>L858R</sup> has been associated with higher levels of baseline auto-phosphorylation of the receptor and greater sensitivity to EGFR tyrosine kinase inhibitors, as compared to EGFR<sup>19DEL</sup> [18]. It has also been shown that EGFR<sup>L858R</sup> requires dimerization for signaling (similar to wild-type EGFR), whereas EGFR<sup>19DEL</sup> does not [91]. Finally, in dox-inducible genetically engineered mouse models, mice harboring the EGFR<sup>L858R</sup> transgene develop tumors more quickly than those harboring the EGFR<sup>19DEL</sup> transgene [92].

Other mutations in *EGFR* exons 18-21 have been identified as recurrent, but less frequent, in lung adenocarcinoma. Substitution mutations in codon 719 (exon 18) and codon 861 (exon 21) occur in approximately 3% and 2% of *EGFR*-mutant lung cancers, respectively, and confer sensitivity to EGFR TKIs [20, 79, 93-95]. In-frame, 6-amino acid insertions in exon 19 have also been identified in 1% of *EGFR*-mutant lung cancers and confer sensitivity to EGFR TKIs [51]. Interestingly, several different multinucleotide insertions have been identified in exon 20 and result in different sensitivities to EGFR TKIs. Exon 20 insertions occurring between amino acids 767-774 are found in 4-9% of *EGFR*-mutant lung cancers and confer primary resistance to all known EGFR TKIs [79, 96, 97]. However, the specific insertion of amino acids FQEA between A763 and Y764 of EGFR exon 20 has been shown in preclinical models to confer increased sensitivity to EGFR TKIs [52].

### ***First-generation anti-EGFR therapies***

After seminal discoveries in the 1980s implicating *EGFR* as a human oncogene and elucidating its function as a receptor tyrosine kinase, the race was on to develop targeted inhibitors of EGFR signaling [98]. Gefitinib, the first EGFR tyrosine kinase inhibitor (TKI) to be approved for clinical use, was developed as a small molecule inhibitor of wild-type EGFR [84, 98, 99] (**Table 3**). Approved first in Japan in 2002, gefitinib gained conditional FDA approval in 2003, which was ultimately revoked after a failed phase III trial in an unselected patient population. Erlotinib, another first-generation EGFR TKI, was concomitantly developed and was FDA-approved the following year, in 2004 [84, 98, 100]. This approval was based on a study also in an unselected patient population, but the benefit was a mere 2 months in overall survival. As described in the previous section, it was discovered shortly thereafter that the small subset of patients with such impressive responses and long-term benefit actually harbored activating mutations in the kinase domain of *EGFR* in their tumors [18-20].

Both gefitinib and erlotinib are reversible, aniline-quinazoline inhibitors that bind the EGFR kinase domain [99, 100]. Originally believed to bind EGFR exclusively in the open, active conformation, additional studies in recent years have raised the question of whether these type I kinase inhibitors are also capable of binding the inactive conformation of EGFR [101, 102]. When bound to wild-type EGFR, they inhibit ligand-induced EGFR autophosphorylation and attenuate downstream signaling responsible for proliferation and survival of the cell [99, 100].

Following the initial 2004 discovery that *EGFR*-mutant NSCLCs were exquisitely

**Table 3. List of EGFR TKIs currently approved or in clinical development.**

	Drug name	Target(s)	Reversible/irreversible
1 <sup>st</sup> generation	Gefitinib	EGFR	Reversible
	Erlotinib	EGFR	Reversible
	Icotinib	EGFR	Reversible
2 <sup>nd</sup> generation	Afatinib	EGFR/HER2	Irreversible
	Dacomitinib	Pan-ErbB	Irreversible
	Neratinib	EGFR/HER2	Irreversible
3 <sup>rd</sup> generation	AZD9291	mutEGFR	Irreversible
	Rocelitinib	mutEGFR	Irreversible
	ASP8273	mutEGFR	Irreversible
	EGF816	mutEGFR	Irreversible
	HM61713	mutEGFR	Irreversible
	AP26113	mutEGFR/ALK	Reversible

mutEGFR = EGFR<sup>L858R</sup>, EGFR<sup>T90M</sup>, EGFR<sup>L858R/T90M</sup>

Adapted from Yu, HA et al, Clin Cancer Res, 2014 [103]

sensitive to erlotinib and gefitinib, multiple prospective clinical trials were initiated to test the efficacy of EGFR targeted therapy versus standard chemotherapy in this patient population. Between 2004-2009, objective response rates in patients treated with erlotinib or gefitinib monotherapy increased from 8-9% in unselected NSCLC to 55-90% in patients selected on the basis of molecular testing for EGFR mutations prior to treatment [44, 45, 84-86, 104-109]. This series of trials provided the necessary data to the oncology community to conclude that mutational testing, rather than fluorescence *in situ* hybridization (FISH) or immunohistochemistry (IHC) for EGFR, was the most sensitive and specific method for clinical identification of tumors sensitive to EGFR TKIs. In 2009, two randomized phase III clinical trials provided definitive evidence proving the superiority of EGFR TKIs over standard chemotherapy regimens in patients prospectively genotyped for EGFR mutation status, supporting their use as first-line therapy for EGFR-mutant lung cancer [44, 45].

In addition to EGFR TKIs, monoclonal antibodies targeting EGFR have also been developed for treatment of human cancers. One such antibody, cetuximab, is a human-murine chimeric IgG1 monoclonal antibody that binds to the extracellular domain III of EGFR. Cetuximab blocks ligand binding to EGFR and prevents the receptor from adopting the extended conformational state necessary for dimerization [110, 111]. Cetuximab has been shown to be effective for multiple solid tumors, including colorectal and head and neck cancers [112-115]. Early clinical trials demonstrated some efficacy for cetuximab in lung cancer when combined with chemotherapy [116, 117], and preclinical studies have demonstrated efficacy of cetuximab monotherapy in a mouse model of lung cancer harboring EGFR<sup>L858R</sup>, but not EGFR<sup>19DEL</sup> [118]. However, studies

in a panel of *EGFR*-mutant cell lines did not demonstrate *in vitro* sensitivity to cetuximab, nor has sensitivity to monotherapy cetuximab ever been correlated to *EGFR* mutations in human lung tumors [119].

### ***Acquired resistance to first-generation EGFR TKIs***

Despite the encouraging clinical responses seen with erlotinib and gefitinib, *EGFR*-mutant tumors virtually always develop resistance within about 12 months of initiation of treatment [44, 120, 121]. In order to develop subsequent therapeutic options for patients, many studies in the past decade have been focused on elucidating mechanisms of this resistance [2, 4]. Broadly speaking, these resistance mechanisms can be divided in to two large categories: *EGFR*-dependent mechanisms and *EGFR*-independent mechanisms.

By far the most common mechanism of resistance to erlotinib and gefitinib (~60%) is a second-site mutation in *EGFR* that results in a change from threonine to methionine in codon 790 (*EGFR*<sup>T790M</sup>) [122-125] (**Figure 3**). This substitution occurs as a result of a mutation from C→T at nucleotide 2,369 in exon 20 of the kinase domain of *EGFR* [122]. Analogous mutations in the fusion kinase *BCR-ABL* confer resistance to imatinib and dasatinib in chronic myelogenous leukemia (CML), demonstrating that second-site mutations at this 'gatekeeper' site are a conserved mechanism of resistance to TKIs [126, 127]. Similar to *BCR-ABL* T315I, *EGFR*<sup>T790M</sup> was originally believed to mediate resistance primarily by interfering with drug binding to the receptor, without inhibiting catalytic activity [122, 128, 129]. However, subsequent studies

revealed that another major mechanism of resistance is that the T790M substitution restores ATP affinity to the receptor, such that first-generation, ATP-competitive EGFR TKIs become less potent inhibitors [130]. Of note, *EGFR* amplification has been identified in a small subset of TKI-resistant tumors, both in the presence and absence of EGFR<sup>T790M</sup> [4, 124].

While EGFR<sup>T790M</sup> was originally discovered as a somatic resistance mutation in tumors treated with first-generation EGFR TKIs, it has also been identified in the germ line. Case reports have described families in which multiple members harbor germline EGFR<sup>T790M</sup> mutations and develop NSCLC [131, 132]. Some of these tumors harbored additional EGFR kinase mutations, but several harbored EGFR<sup>T790M</sup> as the sole EGFR alteration. Preclinical studies have shown that EGFR<sup>T790M</sup> is sufficient to produce tumors in transgenic mouse models, suggesting that this mutation is oncogenic even without an accompanying EGFR<sup>L858R</sup> or EGFR<sup>19DEL</sup> alteration [133].

In addition to second-site mutations in EGFR, activation of 'bypass' signaling of several other RTKs has been associated with resistance to first generation EGFR TKIs. Amplification of *HER2* or *MET* tyrosine kinase has been seen in approximately 12% and 5% of erlotinib- or gefitinib-resistant tumors, respectively [2, 4, 61, 103, 134-137]. Activation of the *AXL* tyrosine kinase has also been shown in models of resistance to EGFR TKIs, and a recent study demonstrated increased *AXL* expression in 5 of 26 gefitinib-resistant tumors [6, 138].

Acquired activating mutations in *BRAF* and *PIK3CA*, as well as loss of RAS

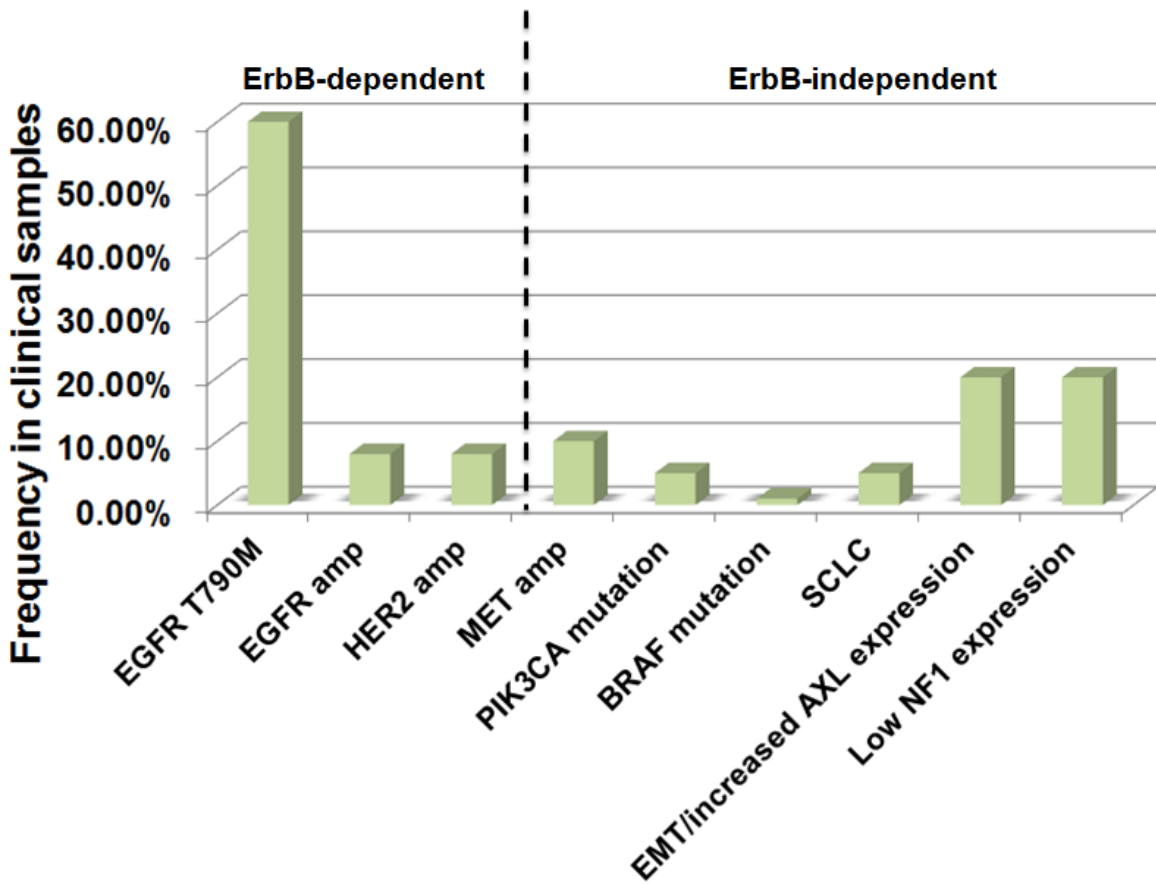


**Figure 3. Frequency of resistance mechanisms identified in clinical samples of acquired resistance to gefitinib or erlotinib.**

Frequencies of mechanisms of resistance identified in gefitinib- or erlotinib-resistant *EGFR*-mutant lung tumors. While typically mutually exclusive, these resistance mechanisms have been found to be co-occurring in some patients with TKI resistance. These frequencies represent estimates, as they are combined from multiple different studies. Compiled from refs [2-6].

negative regulator *NF1*, have also all been observed at lower frequencies in tumors with acquired resistance to first-generation EGFR TKIs [4, 5, 137]. Finally, histological changes have been associated with acquired resistance to EGFR TKIs. Specifically, a small subset of erlotinib- and gefitinib-resistant *EGFR*-mutant NSCLC tumors acquire either a SCLC morphology or an EMT-like phenotype. Attempts to therapeutically inhibit these different EGFR-independent mechanisms of resistance to erlotinib and gefitinib have been met with varied success [103].

### ***Second-generation EGFR TKIs and antibody+TKI combinations***

Given that the majority of erlotinib- and gefitinib-resistant lung tumors harbor EGFR<sup>T790M</sup>, extensive efforts have been directed towards developing additional anti-EGFR therapies that can overcome EGFR<sup>T790M</sup>-mediated resistance. The earliest efforts to target EGFR<sup>T790M</sup> were the development of second-generation, irreversible EGFR/HER2 TKIs such as afatinib, neratinib, and dacomitinib (**Table 3**). Similar to erlotinib and gefitinib, these second-generation EGFR TKIs are also anilino-quinazoline small molecule inhibitors, but they form a covalent bond with cysteine 797 in the kinase domain of EGFR [139-141].

Preclinical studies demonstrated that, in addition to inhibiting wild-type and L858R/19DEL EGFR with similar potency as erlotinib and gefitinib, afatinib can inhibit EGFR<sup>T790M</sup> *in vitro* with 100-fold potency relative to these first-generation TKIs [141]. Unfortunately, afatinib cannot achieve sufficient plasma concentrations to effectively inhibit EGFR<sup>T790M</sup> *in vivo*, due to dose-limiting toxicities associated with inhibition of wild-

type EGFR [128, 142]. In the LUX-Lung 1 trial conducted in patients who previously progressed on erlotinib or gefitinib, afatinib achieved a 7% objective response rate, but there was no improvement in overall survival in the afatinib arm compared to placebo [143]. However, given its potency against tumors harboring EGFR<sup>L858R</sup> and EGFR<sup>19DEL</sup>, afatinib was eventually approved as first-line therapy for *EGFR*-mutant lung cancer following a phase III trial that demonstrated improved PFS for afatinib compared to the combination of cisplatin and pemetrexed [49].

Afatinib would ultimately prove to have efficacy against EGFR<sup>T790M</sup>-positive *EGFR*-mutant lung cancer, but only when used in combination with an anti-EGFR antibody. In 2009, preclinical studies demonstrated increased expression of EGFR ligands epiregulin and amphiregulin in the context of EGFR<sup>T790M</sup>-mediated acquired resistance to first-generation EGFR TKIs [118]. The combination of afatinib (EGFR/HER2 TKI) with cetuximab (EGFR mAb) was subsequently shown to induce tumor shrinkage in mouse models of *EGFR*-mutant lung cancer harboring EGFR<sup>T790M</sup>. The afatinib + cetuximab combination effectively diminished total and phosphorylated EGFR in this model [118]. Based on these data, a Phase IB/II clinical trial was initiated testing the combination of afatinib + cetuximab in patients with acquired resistance to first-generation EGFR TKIs.

The combination of afatinib + cetuximab achieved a 29% response rate and median PFS of 4.7 months in tumors that had previously progressed on erlotinib or gefitinib [144]. This was the first anti-EGFR therapy that demonstrated clinical efficacy in the context of acquired resistance to first-generation EGFR TKIs. Interestingly, in the clinic, afatinib + cetuximab was equally effective in resistant tumors with or without

EGFR<sup>T790M</sup>. This suggests that a cohort of tumors have acquired an ErbB-dependent, non-EGFR<sup>T790M</sup> mechanism of resistance to first-generation EGFR TKIs.

One potential explanation for the response to afatinib + cetuximab in tumors lacking EGFR<sup>T790M</sup> is that these tumors harbor *EGFR* amplification, as has been previously reported in resistance to first-generation EGFR TKIs [4]. Another possible molecular explanation for these responses is *HER2* amplification, because *HER2* amplification has been detected in a subset of erlotinib/gefitinib-resistant tumors (typically mutually exclusive with EGFR<sup>T790M</sup>), and afatinib is known to inhibit HER2 signaling [136, 141]. Interestingly, the combination of cetuximab + erlotinib did not produce anti-tumor responses in preclinical models, indicating that an irreversible EGFR TKI and/or broader ErbB inhibition is necessary for this combination therapy [118]. Collectively, these data suggest an as-yet undefined, synergistic mechanism of the afatinib + cetuximab combination therapy.

Unfortunately, acquired resistance to afatinib + cetuximab has also emerged. While the full spectrum of resistance mechanisms to this combination therapy remains unknown, one early study demonstrated that, in a subset of cases, activation of mTORC1 signaling by genomic alterations in *TSC1* and *NF2* may play a role [145]. This study further showed that combination with mTORC1 inhibitor rapamycin can potentially overcome acquired resistance to afatinib + cetuximab in preclinical models.

### ***Mutant-selective third-generation EGFR TKIs***

Efforts by multiple academic and pharmaceutical teams have also led to the development of third-generation, or ‘mutant-selective’ EGFR TKIs that were specifically designed to inhibit the EGFR<sup>T790M</sup> receptor (**Table 3**). In contrast to the first- and second-generation EGFR TKIs, these inhibitors are wild-type sparing, meaning that they inhibit EGFR<sup>L858R</sup>, EGFR<sup>19DEL</sup>, and EGFR<sup>T790M</sup> but have no efficacy against wild-type EGFR. The first mutant-selective EGFR TKI to be developed was WZ4002, a pyrimidine-based inhibitor that binds covalently to C797 in the kinase domain of EGFR [146]. This compound demonstrated proof-of-principle increased potency (30 to 100-fold) against EGFR<sup>T790M</sup> and decreased potency (100-fold) against wild-type EGFR [146]. However, it never reached clinical development.

Mutant-selective EGFR TKIs currently in clinical development include AZD9291, rociletinib (CO-1686), AP26113, HM61713, EGF816, and ASP8273, the first two being the current leading molecules [103]. In a phase I-II dose finding clinical trial of patients who previously progressed on first- or second-generation EGFR TKIs, rociletinib achieved a 59% objective response rate and 93% disease control rate (defined as either partial/complete response or stable disease) [54]. Interestingly, the response rate among patients with T790M-negative tumors was 29%, and the disease control rate was 59%. Of note, 80% of patients harboring T790M-negative tumors that responded to rociletinib were taking other EGFR TKIs until immediately (3 days) before starting on study, so a retreatment effect is an unlikely explanation for this T790M-negative response [54]. The most prominent side effect of rociletinib is hyperglycemia, which is thought to occur via off-target effects on IGF-1R by a metabolite.

AZD9291 has also shown promise in early clinical trials. In a phase I study of patients who progressed on previous EGFR TKIs, AZD9291 achieved a 55% objective response rate and 83% disease control rate overall. In patients with tumors harboring EGFR<sup>T790M</sup>, a response rate of 61% and disease control rate of 95% was observed [55]. As with rociletinib, a small percentage (21%; 11% on EGFR TKI therapy immediately prior) of tumors without EGFR<sup>T790M</sup> also responded to AZD9291. Issues regarding sensitivity of EGFR<sup>T790M</sup> detection and intra-tumoral heterogeneity are potential explanations for these T790M-negative responses seen with both rociletinib and AZD9291, but the true underlying mechanism of this observation remains unknown [55].

Rociletinib is structurally similar to WZ4002. Specific commonalities include a similar positioning of the electrophilic group that forms a bond with C797 as well as the presence of a pyrimidine 5-substituent [147, 148]. By contrast, although AZD9291 also binds covalently to EGFR C797, it is an architecturally and pharmacologically distinct molecule. Among other differences between the two classes of molecules, AZD9291 possesses an electrophilic group positioned on the pyrimidine C-2 substituent ring, and there is no substituent at the pyrimidine 5-position [147].

Both rociletinib and AZD9291 are not only effective against the most common lung cancer-associated EGFR mutations (EGFR<sup>T790M</sup>, EGFR<sup>19DEL</sup>, EGFR<sup>L858R</sup>), they have also demonstrated *in vitro* efficacy against rarer activating EGFR mutations, such as EGFR<sup>G719S</sup>, EGFR<sup>L861Q</sup>, and in-frame exon 19 insertions [147, 149]. Unlike rociletinib, AZD9291 does not demonstrate 'off-target' activity against IGF-1R, but the prominent AZD9291 metabolite, AZD5104, does have modest inhibitory effects against wild-type EGFR and HER2 [147].

As predicted by their preclinical profiles, these mutant-selective inhibitors have been shown to induce milder side effects attributed to inhibition of wild-type EGFR in non-cancerous cells [54, 55]. As a result, they are prime candidates for combination therapies that are much less tolerable with first- and second-generation EGFR TKIs. Phase I trials are currently ongoing to test safety and preliminary efficacy of AZD9291 in combination with MEDI4736 (anti-PD-L1 antibody), AZD6094 (MET inhibitor), and selumetinib (MEK inhibitor; NCT02143466). Finally, because of their potency against EGFR<sup>19DEL</sup> and EGFR<sup>L858R</sup> even in the absence of EGFR<sup>T790M</sup>, AZD9291 and rociletinib are now being tested in the first-line setting to treat *EGFR*-mutant lung cancer (NCT02296125, NCT02186301). It remains to be seen whether progression-free survival will be extended relative to first- or second-generation EGFR TKIs with the use of mutant selective, third-generation TKIs.

Unfortunately, as we have seen with other generations of EGFR TKIs, acquired resistance is already emerging for these mutant-selective EGFR TKIs. Early studies utilizing WZ4002 revealed *MAPK1* amplification, loss of negative regulators of ERK1/2 signaling such as *DUSP6*, and activation of IGF-1R signaling as mechanisms of resistance to this non-clinical compound [150, 151]. At the time these studies were initiated, *in vitro* resistance to CO-1686 had been shown to be associated with acquisition of an EMT phenotype as well as increased *AKT3* expression, and there was no data describing mechanisms of resistance to AZD9291 [149].

## Purpose of these studies

The development of small molecule EGFR kinase inhibitors has revolutionized treatment of *EGFR*-mutant lung cancer in the last decade. Unfortunately, durable responses longer than one year are rarely seen. There are now multiple first-generation (reversible), second-generation (irreversible) and third-generation (irreversible, mutant-selective) EGFR TKIs either approved or in clinical development. Mechanisms of resistance to these inhibitors have proven to be heterogeneous, but a significant percentage tumors resistant to first-generation EGFR TKIs display sustained EGFR dependence. Given this pattern of sustained ‘addiction’ to EGFR signaling, it is possible that patients could derive significant clinical benefit from sequential treatment with multiple different EGFR TKIs, if given in the correct order.

Discerning the optimal sequence of anti-EGFR therapy in lung cancer patients with *EGFR*-mutant tumors will ultimately require clinical investigation. However, a great deal of discovery work can be accomplished in the laboratory in order to inform clinical trial design. In fact, we and others have shown in the last decade that preclinical modeling of resistance mechanisms to EGFR TKIs using cell lines, xenografts, and transgenic mouse models can predict clinical resistance mechanisms in patients with *EGFR*-mutant lung cancer. By discerning these resistance mechanisms, we can develop an understanding of how to designate subsequent therapies that are appropriate and have rational basis.

In these dissertation studies, we used *in vitro* and *in vivo* preclinical modeling of multiple scenarios of sequential drug resistance in an attempt to further discern the

appropriate sequence of treatment with first-, second- and third-generation EGFR TKIs. We sought a greater understanding of the mechanisms of resistance to each of these EGFR TKIs, including the degree of heterogeneity in resistance mechanisms, the circumstances under which resistance is associated with sustained EGFR dependence, and/or at what point rewiring of this ‘oncogene addiction’ results in a more EGFR-independent tumor. While such questions will require many more years of work to answer in full, the dissertation studies described here were designed to contribute to the collective understanding of optimal treatment of EGFR-mutant lung cancer. Developing a more precise understanding of the proper sequence of treatment with EGFR TKIs will allow for patients to achieve maximal benefit from available therapies, in an era in which treatment resistance remains the greatest clinical barrier.

Specifically, we first performed whole-genome/exome sequencing on multiple pairs of erlotinib/afatinib-sensitive and –resistant isogenic paired cell lines, in order to assess the full spectrum of DNA alterations associated with resistance. We found very few additional putative ‘driver’ mutations, but we did identify significant genome-wide copy number changes associated with erlotinib/afatinib resistance in these cell lines, in addition to previously identified resistance mechanisms, such as EGFR<sup>T790M</sup>, *MET* amp and EMT (Chapter II). To our knowledge, this was the first comprehensive genomic analysis of paired isogenic EGFR TKI-sensitive versus –resistant cell lines. We then demonstrated that EGFR<sup>T790M</sup>-positive models of resistance to erlotinib or afatinib are more sensitive to growth inhibition by AZD9291 than by afatinib + cetuximab. However, AZD9291 resistance confers cross-resistance to afatinib + cetuximab, whereas xenografts resistant to afatinib + cetuximab are subsequently sensitive to AZD9291.

This suggests one potential treatment sequence of: erlotinib/afatinib→afatinib + cetuximab→AZD9291 (Chapter III). We subsequently analyzed *in vitro* and *in vivo* models of AZD9291 resistance and found RAS/MAPK pathway dysregulation and sensitivity to MEK inhibition with small-molecule inhibitor selumetinib (Chapter IV). Finally, utilizing *in vitro* and *in vivo* models of acquired resistance to AZD9291 + selumetinib, we found that resistance to combined EGFR/MEK inhibition can in some cases be associated with increased ERK phosphorylation and sensitivity to ERK inhibitor, SCH772984, or alternative MEK inhibitor, trametinib (Chapter V).

While the optimal sequence of targeted therapies in *EGFR*-mutant lung cancer can ultimately only be determined clinically, these preclinical studies provide a framework for rational trial design. In addition, this model serves as a paradigm for approaching treatment of other oncogene-addicted cancers for which multiple targeted therapies are available or in development.

**Chapter II: Next-generation sequencing of paired tyrosine kinase inhibitor-sensitive and -resistant EGFR mutant lung cancer cell lines identifies spectrum of DNA changes associated with drug resistance.**

Adapted from: Peilin Jia, Hailing Jin, **Catherine B. Meador**, Kadoaki Ohashi, Lin Liu, Valentina Pirazzoli, Kimberly B. Dahlman, Katerina Politi, Franziska Michor, Zhongming Zhao, and William Pao. (2013) Next-generation sequencing of paired tyrosine kinase inhibitor-sensitive and –resistant EGFR mutant lung cancer cell lines identifies spectrum of DNA changes associated with drug resistance. *Genome Res* 23(9):1434-45.

**Significance**

At the time this work was initiated, next-generation sequencing (NGS) was a relatively new technology, and whole-genome or whole-exome sequencing was not easily accessible, even on a research basis. The rapidity with which NGS technologies have advanced in recent years is evidenced by the fact that both research and clinical samples are now routinely analyzed on NGS-based platforms, and turnaround time from sequencing to data interpretation is vastly shorter than it was a few years ago. When the work from this chapter was published, it was the first comprehensive, genome-wide sequencing analysis performed on isogenic pairs of drug-sensitive and –resistant cell lines to identify the spectrum of DNA changes associated with drug resistance in EGFR mutant lung cancer.

## Introduction

Over the past several decades, somatic mutations in genes encoding kinases have become associated with increased sensitivity of different solid tumors to kinase inhibitors. Examples include the gene products of specific “driver oncogenes” including *EGFR*, *ALK*, *BRAF*, and *KIT*, which are effectively targeted with gefitinib/erlotinib [45, 108], crizotinib [152], vemurafenib [153], and imatinib [154], in lung cancer (*EGFR*, *ALK*), melanoma (*BRAF*), and gastrointestinal stromal tumors (*KIT*), respectively. Unfortunately, virtually all patients with metastatic cancer eventually develop disease progression, limiting the effectiveness of these agents. Common mechanisms of acquired resistance include the development of second-site gene mutations (e.g., “gatekeeper mutations”) that alter binding of drug to target and re-activation of the original oncogene-driven kinase signaling pathway through the up-regulation of alternative kinases. For example, in patients with *EGFR* mutant lung adenocarcinomas harboring drug-sensitive mutations (deletions in exon 19 or the L858R point mutation in exon 21), tumor cells in more than half develop a second-site *EGFR* T790M mutation [122, 123], while 5%–10% acquire *MET* amplification [134, 135]. Occasionally, changes in tumor histology have also been observed, with tumor cells displaying features of small-cell lung cancer or epithelial–mesenchymal transition (EMT) [4].

A common laboratory method used to model acquired resistance involves the development of isogenic pairs of drug-sensitive and drug-resistant human tumor cell lines. Parental drug-sensitive cells are cultured in stepwise fashion with increasing concentrations of drug until cells emerge that are 50-fold to 100-fold less sensitive to

growth inhibition. Cells are initially treated with a drug concentration at which 30% of the cells are growth inhibited or killed (GI30), and when cells resume normal growth patterns, the drug concentration is increased [137, 155]. In *EGFR* mutant lung cancer, this type of modeling using *EGFR* tyrosine kinase inhibitors (TKIs) has reliably identified clinically relevant resistance mechanisms such as *EGFR* T790M, *MET* amplification, and EMT [137, 155]. To date, the full spectrum of DNA mutations and copy number changes associated with such resistance mechanisms remains to be determined.

Next-generation sequencing (NGS) technologies augmented with bioinformatics analyses provide powerful approaches to screen for genome-wide genetic alterations in matched samples to identify various types of mutations associated with drug resistance. In a recent study, RNA sequencing (RNA-seq) was applied to detect mutations in drug-resistant clones developed from parental cell lines [156]. To our knowledge, the use of genome-wide DNA sequencing to compare drug-sensitive and drug-resistant cell lines has not yet been reported. Here, we used whole-genome sequencing (WGS) or whole-exome sequencing (WES) and bioinformatics analysis to characterize mutational changes associated with four populations of parental *EGFR* mutant drug-sensitive lines and five corresponding drug-resistant lines that were already known to harbor *EGFR*T790M mutations, *MET* amplification, or EMT, respectively (**Figure 4**). These studies illustrate the power of NGS technologies to uncover genome-wide changes associated with drug resistance.

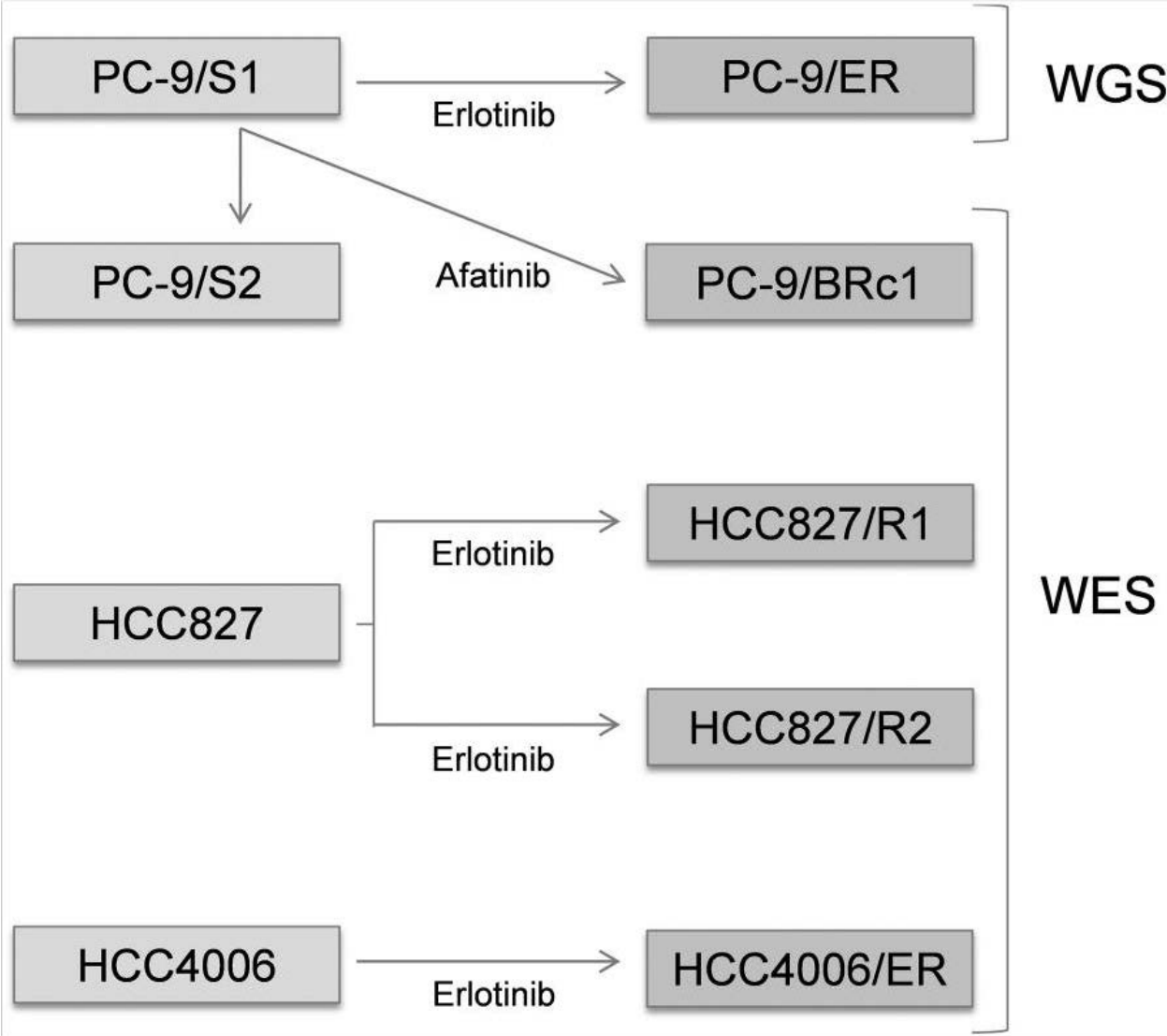


**Figure 4. Description of cell lines examined.**

(TKI) Tyrosine kinase inhibitor; (WGS) whole-genome sequencing; (WES) whole-exome sequencing. Cell lines in the left boxes are drug-sensitive, while those in the right boxes are drug-resistant. PC-9/S2, PC-9/ER, and PC-9/BRc1 were derived from PC-9/S1 cells; HCC827/R1 and HCC827/R2 were derived from HCC827 cells; HCC4006/ER were derived from HCC4006 cells. Comparisons between PC-9/S1 and PC-9/S2, PC-9/S1 and PC-9/ER, PC-9/S1 and PC-9/BRc1, HCC827 and HCC827/R1, HCC827 and HCC827/R2, and HCC4006 and HCC4006/ER were performed as detailed in the text.

## Results

### ***Spectrum of genetic alterations associated with isogenic pairs of drug-sensitive and drug-resistant cells***

#### *PC-9/S1 versus PC-9/ER (T790M)*

PC-9/S1 parental cells are known to harbor a drug-sensitive *EGFR* exon 19 deletion, while polyclonal PC-9/ER cells, developed after long-term culture in the EGFR TKI erlotinib, contain a second-site *EGFR* T790M mutation (**Figure 4**) [155]. PC-9/ER cells display sensitivity to the T790M-specific inhibitor WZ4002 [146], suggesting that they remain dependent on EGFR signaling for survival (**Appendix Figure 23**). To determine the full spectrum of mutations associated with erlotinib sensitivity and resistance, we performed WGS on genomic DNA from both lines. We denote this parental cell line sequenced by WGS as PC-9/S1, to distinguish it from a second set of parental cells (PC-9/S2) sequenced by WES after multiple passages in culture in the absence of TKI selection (see next section and **Figure 4**). For PC-9/S1 cells, a total of  $128.3 \times 10^9$  bases were covered by short reads (100 bp, paired-end), with an average of 42.3x coverage of the human genome, and for PC-9/ER cells,  $148.7 \times 10^9$  bases of short reads were obtained, with an average of 49.0x coverage (**Table 4**). These sequence reads covered ~92.0% bases of the human reference genome (hg19) by at least one read and ~87.2% bases by a depth of at least 20x. We then compared data from the resistant and parental lines to identify mutations that occurred at >20% allele frequency that were unique to each cell population. As expected, both parental and resistant cells were found to harbor the same *EGFR* exon 19 deletion (c.2235\_2249del,

p.E746\_A750del, at chr7: 55242465–55242479), while only the resistant cells harbored *EGFR* T790M (c.C2369T, p.T790M, at chr7: 55249071).

Using a set of optimized filtering criteria for high prediction accuracy (**Appendix Figure 24**), we identified a total of 7060 novel single nucleotide variants (SNVs) and 7442 small insertions/deletions (indels) that were unique to PC-9/ER versus parental PC-9/S1 cells. Thirty-three SNVs (including 19 missense, three stop-gain, and 11 synonymous SNVs) and 11 indels were predicted to occur in exonic regions (**Table 5**). We chose for validation by direct sequencing the predicted exonic SNVs/indels that did not fail our manual review (see Methods) and were amenable to primer design. All selected SNVs ( $n = 15$ , 100%) and 86% of selected indels ( $n = 7$ ) for validation were verified to be present only in PC-9/ER cell DNA by direct sequencing (**Table 6**; **Appendix Table 12**). In the reverse comparison, nine and four predicted exonic SNVs and deletions, respectively, were unique to PC-9/S1 parental cells (**Table 5**); all selected SNVs ( $n = 4$ ) and 50% of indels ( $n = 2$ ) were validated (**Figure 5**; **Tables 6,7**). These data indicate that in this isogenic pair of cells, exonic mutations are both acquired and lost during the selection process for resistance, with more mutations being acquired than lost. We next applied the software tool Control-FREEC [157, 158] to detect CNVs uniquely aberrant in PC-9/ER cells compared with PC-9/S1 parental cells. While many small amplified/deleted regions were detected across the genome, there were three large blocks of amplifications (spanning >1 Mb) involving chromosomes 5, 7, and 22 (**Appendix Figure 25**; **Appendix Table 13**). The 5p15.1–5p15.2 locus overlapped with a region we previously reported in tumor samples from patients with *EGFR* mutant lung cancer and acquired resistance to EGFR TKIs [134]; the region spans ~3.7 Mb and

encompasses cancer genes collected from the Cancer Gene Census (CGC) database [159] such as *ANKH*, *CTNND2*, *DNAH5*, *FAM105A*, *FAM105B*, and *TRIO*. The locus 7p11.2–7p13 involves *EGFR*, the amplification of which has been frequently reported in patients with acquired resistance [124]. The third locus, which is at 22q12.3–22q13.1, spans ~3.2 Mb and involves many genes including the CGC cancer gene *MYH9*. Large blocks of deletions were detected in 2q32–2q34, 7q31.1–7q35, 10p11.21–10p15.3, 22q11.21, and Xp21.1 (**Appendix Table 13**). Loss of copy number in these loci involved multiple CGC genes such as *IDH1*, *MET*, *SMO*, and *BRAF*. Taken together with the SNV/indel data, these analyses show that more genes were affected by copy number changes than exonic SNVs/indels during the development of drug resistance.

#### *PC-9/S2 versus PC-9/BRc1 (T790M)*

Polyclonal PC-9 parental cells were treated with a different EGFR TKI, afatinib, and used to select for a T790M-harboring resistant line, PC-9/BRc1, which was derived from a single-cell clone [155]. Through WES, we compared the exomes in PC-9/BRc1 and PC-9/S2 cells (**Figure 4; see below**). We obtained  $8.4 \times 10^9$  bases of short reads (74-bp paired-end) for PC-9/S2 cells with an average of 232.6× coverage, and  $7.8 \times 10^9$  bases of short reads for PC-9/BRc1 (216.7× coverage). These sequence reads covered ~99.0% of bases of the targeted regions (NimbleGen SeqCap EZ Exome Library kit v2) by at least one read and ~94.7% of bases by a depth of at least 20× (**Table 4**). A total of 88 SNVs and three

**Table 4 Summary of data derived from next-generation sequencing of 9 EGFR mutant cell lines**

	WGS		WES						
	PC-9/S1	PC-9/ER	PC-9/S2	PC-9/BRc1	HCC827	HCC827/R1	HCC827/R2	HCC4006	HCC4006/ER
# bases sequenced	128.3×10 <sup>9</sup>	148.7×10 <sup>9</sup>	8.4×10 <sup>9</sup>	7.8×10 <sup>9</sup>	4.6×10 <sup>9</sup>	5.4×10 <sup>9</sup>	4.3×10 <sup>9</sup>	4.3×10 <sup>9</sup>	5.3×10 <sup>9</sup>
Coverage (x)	42.3	49.0	232.6	216.7	119.4	139.7	110.8	109.9	137.3
Covered fraction (% , ≥1)	92.0	92.0	99.0	98.9	99.1	99.2	98.9	99.0	99.2
Callable fraction (% , ≥20)	86.7	87.7	94.7	94.7	87.8	88.4	86.5	85.5	88.6

WGS: whole genome sequencing. WES: whole exome sequencing.

**Table 5. Summary of single nucleotide variants (SNVs) and small insertions/deletions (indels) unique to each cell line**

	PC-9	PC-9	PC-9	PC-9	HCC827		HCC827	HCC827	HCC4006	HCC4006
	/S1	/ER	/S2	/BRc1	vs. R1	vs. R2	/R1	/R2		/ER
SNVs										
Missense	7	19	20	61	5	1	12	19	14	13
Stop-gain		3	1	7			1		2	
Synonymous	2	11	6	20	3		3	7	4	7
Indels										
Frameshift deletion	1	1		1			1			2
Frameshift insertion		1		1			1	1		
Nonframeshift deletion	3	9		1						

**Table 6. Summary of validation studies on putative SNVs and indels**

	PC-9	PC-9	PC-9	PC-9	HCC827		HCC827	HCC827	HCC4006	HCC4006	Summary		
	/S1	/ER	/S2	/BRc1	vs. R1	vs. R2	/R1	/R2		/ER	All	P	R
<i>SNVs</i>													
# Predicted	7	22	21	68	5	1	13	19	16	13	185	50	135
# selected for validation	4	15	3	11	4	0	12	15	10	9	83	21	62
# validated	4	15	3	11	4		8	15	2	9	71	13	58
Validation rate (%)	100	100	100	100	100		67	100	20	100	85.54	61.90	93.55
<i>Indels</i>													
# predicted	4	11	0	3	0	0	2	1	0	2	23	4	19
# selected for validation	2	7					1	0		2	12	2	10
# validated	1	6					0			2	9	1	8
Validation rate (%)	50	86					0			100	75	50	80

P – parental; R – resistant.

**Table 7. List of validated SNVs and indels in parental cell lines**

Gene	Chr.*	Position (bp)	RefSeq	Nucleotide change	Amino change	acid	Tumor variant freq.
<b>PC-9/S1 vs. PC-9/ER, SNVs</b>							
<i>ADCY10</i>	1	167793927	NM_018417	c.A3917T	p.K1306M		20.37%
			NM_001167749	c.A3458T	p.K1153M		
<i>SLC39A10</i>	2	196545280	NM_001127257	c.C514T	p.H172Y		36.07%
			NM_020342	c.C514T	p.H172Y		
<i>VWDE</i>	7	12420170	NM_001135924	c.C731T	p.T244I		34.88%
<i>UBE3B</i>	12	109921713	NM_130466	c.A209G	p.K70R		23.91%
			NM_183415	c.A209G	p.K70R		
<i>C1GALT1<sup>#</sup></i>	7	7278411	NM_020156	c.T746G	p.I249S		18.03%
<i>ANK3<sup>#</sup></i>	10	61844931	NM_001149	c.C1231G	p.Q411E		19.61%
<b>PC-9/S1 vs. PC-9/ER, indels</b>							
<i>CUBN</i>	10	16960732-16960741	NM_001081	c.6880_6889del	p.2294_2297del		27.50%
<b>PC-9/S2 vs. PC-9/BRc1, SNVs</b>							
<i>SPEN</i>	1	16258538	NM_015001	c.G5803C	p.E1935Q,		29.63%
<i>GRIK2</i>	6	102516283	NM_021956	c.T2624G	p.L875X,		25.55%
<i>HIRIP3</i>	16	30004831	NM_003609	c.G1456C	p.E486Q,		25.97%
<b>HCC827, SNVs</b>							
<i>SPZ1</i>	5	79616573	NM_032567	c.C539A	p.A180D		27.59%
<i>TRIM36</i>	5	114506855	NM_001017397	c.C128T	p.T43I		31.15%
<i>HARS2</i>	5	140075201	NM_012208	c.A508G	p.R170G		23.32%
<i>PPARGC1B</i>	5	149221858	NM_001172698	c.G2617T	p.D873Y		27.47%
			NM_001172699	c.G2542T	p.D848Y		
			NM_133263	c.G2734T	p.D912Y		
<b>HCC4006, SNVs</b>							
<i>TESK2</i>	1	45887454	NM_007170	c.C287A	p.A96E,		23.38%
<i>CPA5</i>	7	130008410	NM_001127442	c.T1198G	p.W400G		28.70%
			NM_080385	c.T1283G	p.M428R		
			NM_001127441	c.T1283G	p.M428R		

Genes with multiple transcripts were displayed in more than one row. Position is based on human reference genome (hg19).

\*Chr.: chromosome.

<sup>#</sup>These genes were missed by our bioinformatics filtering criteria but were recovered by manual check and confirmed by Sanger sequencing.

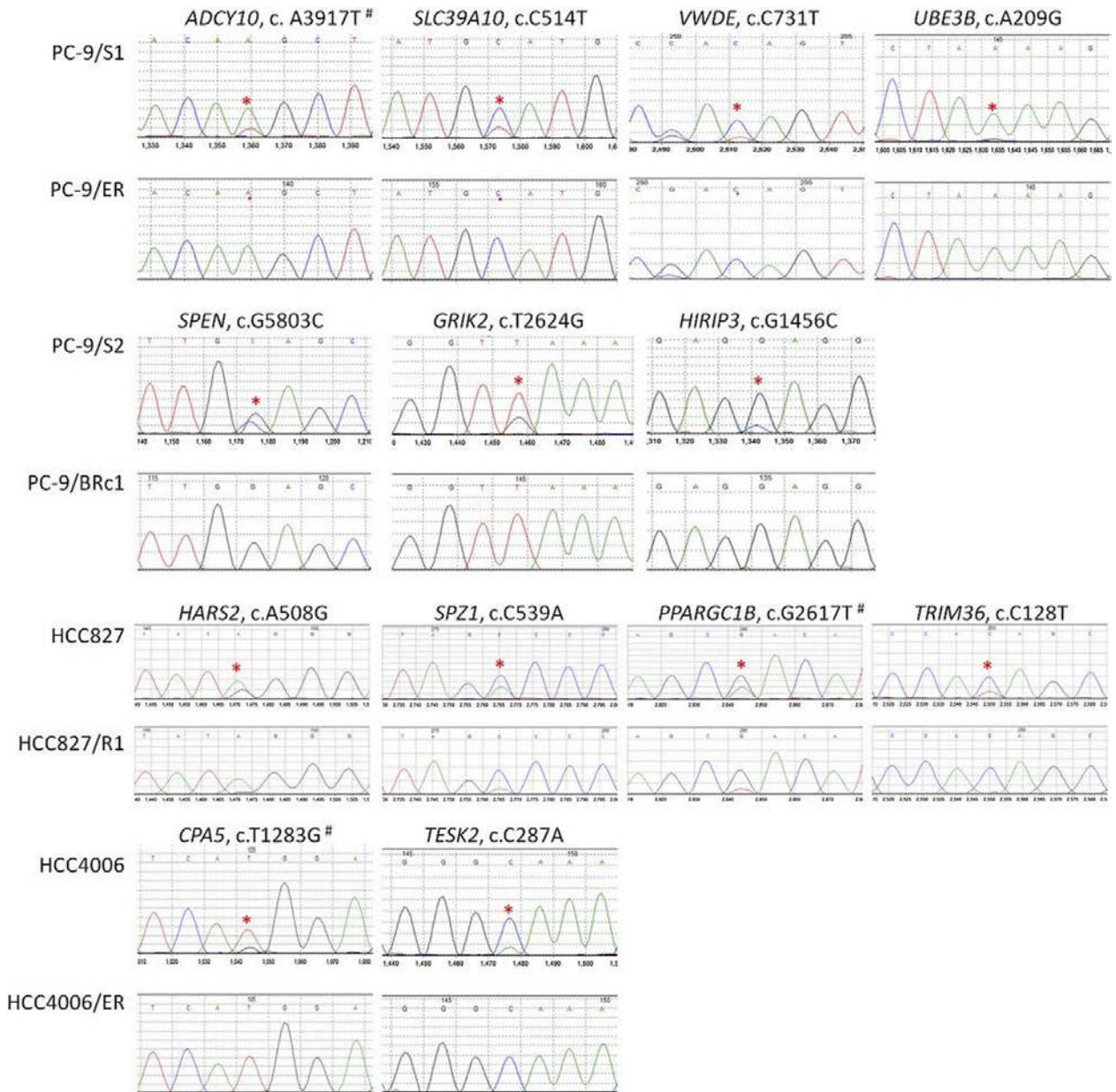


**Figure 5. Sanger sequencing chromatograms of mutations “lost” in drug-resistant cell lines compared with matched drug-sensitive cell lines.**

For each panel, the mutation marked by a red asterisk is shown in the sensitive line (top) and resistant line (bottom). (#) The mutation occurs in multiple transcripts with different nucleotide positions and/or amino acid positions. Detailed information is available in **Table 7**.

indels were detected in exonic regions that were unique to PC-9/BRc1 cells, while 27 SNVs were unique to PC-9/S2 (**Table 5**). For validation, we selected mutations likely to have high functional impact (e.g., those indicated as “probably damaging” by PolyPhen-2 software) [160]. All of the selected SNVs (11 for PC-9/BRc1 and three for PC-9/S2) were validated (**Tables 6, 7; Appendix Table 14**). Thus, again, we predicted more coding SNVs/indels in the resistant cell population compared with the parental cells. A greater number of changes may have been observed in PC-9/BRc1 cells than PC-9/ER cells, since the former were derived from a single cell clone, while the latter were polyclonal.

CNV detection using WES data can be variable, since interpretations can be affected by the non-uniform nature of exome capture reactions [161]. We therefore applied two software tools, VarScan 2 [162] and ExomeCNV [163], to determine the CNVs in PC-9/BRc1 cells. To get more reliable results, we focused only on the regions detected by both tools. When using VarScan 2, we selected regions with >1000 bp and log ratios >0.25 or <-0.25. For ExomeCNV, we selected regions with >1000 bp with abnormal copy numbers (e.g., ≠2) (**Appendix Figure 26; Appendix Table 15**). Large amplified regions encompassing CGC genes included 1p36.21–1p36.33 (*CAMTA1, PRDM16, RPL22, TNFRSF14*), 3q13.13–3q27.3 (*BCL6, EIF4A2, ETV5, FOXL2, GATA2, GMPS, MECOM, MLF1, PIK3CA, RPN1, SOX2, WWTR1*), and 21p11.1–21q22.3 (*ERG, OLIG2, RUNX1, TMPRSS2, U2AF1*) among others. PC-9/BRc1 cells also had regions of copy number loss, affecting cancer-related genes such as *ABI1, GATA3, KIF5B, KLF6*, and *MLLT10* on 10p11.1–10p15.3, *AKT1* on 14q32.33, and *MYH9* and *PDGFB* on 22q12.3–22q13.1. More details are provided

in Supplemental Table S4. Collectively, similar to PC-9/ER cells, we predicted that PC-9/BRc1 cells harbored more copy number changes than SNVs and indels when compared with their parental cell counterparts.

#### *PC-9/S1 versus PC-9/S2*

To determine whether the DNA changes associated with acquired resistance in PC-9/ER and PC-9/BRc1 cells were random or due to drug selection, we compared the profiles of the two parental cell populations, PC-9/S1 and PC-9/S2. These cells were passaged about six to eight times (1.5 mo) in media without drug selection (**Figure 4**). Using the same pipeline for paired samples and our standard cutoff of >20% mutation allele frequency for a called mutation, we did not find any coding SNVs/indels that uniquely occurred in either cell line, even allowing for differences in sequencing coverage (42.3x for PC-9/S1 and 232.6x for PC-9/S2 cells). Thus, the SNVs detected in the resistant cell lines were likely due to drug treatment and did not arise from the normal culturing process. We did not compare CNV differences because the significantly different depth of coverage provided by WGS and WES would strongly affect the CNV calling.

#### *HCC827 versus HCC827/R1 (EGFR T790M) and HCC827/R2 (MET amplification)*

We used WES to characterize the spectrum of mutations associated with a different set of isogenic pairs of cell lines. HCC827 cells, harboring an exon 19 deletion, are sensitive to erlotinib; drug selection in vitro led to two polyclonal resistant lines: HCC827/R1, which harbor the T790M mutation and lack *MET* amplification, and HCC827/R2, which lack T790M and

display *MET* amplification [137]. HCC827/R1 but not HCC827/R2 cells further display sensitivity to the T790M-specific TKI, WZ4002 (**Appendix Figure 27**); conversely, HCC827/R2 but not HCC827/R1 cells display sensitivity to a *MET* TKI, SGX-532 [137] (data not shown). Details of the sequencing data are listed in **Tables 4-6**. As expected, all three lines harbored the same *EGFR* exon 19 deletion (c.2235\_2249del, p.E746\_A750del, at chr7: 55242465–55242479). In HCC827/R1 cells, the *EGFR* T790M point mutation (c.C2369T) was found manually at low allele frequency (7%), while HCC827/R2 cells did not contain any alleles with T790M.

We detected 16 exonic SNVs (12 missense, one stop-gain, and three synonymous) and two indels (**Table 5**) that were unique to HCC827/R1 cells compared with parental cells. Conversely, eight SNVs were found only in parental cells. In HCC827/R2 cells, 26 SNVs (19 missense and seven synonymous), and one indel (**Table 5**) were predicted to be unique, while only one SNV was detected as significant in the parental line (**Table 5**). Validation rates are shown in **Table 6**, and the validated SNVs/indels are shown in **Appendix Tables 16 and 18** for HCC827/R1 and HCC827/R2, respectively. Thus, as in PC-9 cells, HCC827 resistant cells harbored more genetic changes than parental cells.

We applied the same pipeline as in PC-9/BRc1 to detect CNVs for HCC827/R1 and for HCC827/R2, both of which were compared with HCC827 parental cells. In HCC827/R1, large amplifications were found in chromosomes 7 and 18, where the cancer genes *BRAF* (7q34) and *BCL2* (18q21.33–18q22.1) are located, respectively (**Appendix Figure 28**). We also found an amplified region on 21p11.1–21q22.3 of unknown significance (**Appendix Table 17**). Regions with fewer copies compared with parental cells were found in 5p11–5q35.3 (involving

the CGC gene *PDGFRB*), 7p11.2–7p12.1 (involving the gene *EGFR*), and 12p12.2–12p13.33.

In HCC827/R2, amplifications were mainly detected in 5p15.2–5p15.33, 7q21.3–7q31.1, and 18q11.2 (**Appendix Figure 29; Appendix Table 19**). On chromosome 7, there was a 6-Mb block encompassing *MET* (**Figure 6; Appendix Figure 29**); this gene was known to be amplified by fluorescent in situ hybridization (FISH) [137]. Interestingly, in the HCC827/R1 cell line, the same region displayed a different pattern: We found a sharp low-level peak spanning only ~1.9 Mb (**Figure 6; Appendix Figure 28**). Consistent with these data, HCC827/R1 cells did not display *MET* amplification by FISH [137]. We specifically examined the amplified regions in both HCC827/R1 and R2 cells and found that the amplicons in both covered all *MET* coding regions. In HCC827/R1, the amplified region was predicted to have a low copy number, while in HCC827/R2, the amplified region was large and with a high copy number (**Figure 6; Appendix Figure 28**).

To validate these CNV changes further and to examine whether there were other structural variants that may affect *MET*, we conducted RNA-seq of these three cell lines and systematically searched for gene fusion events involving *MET* using FusionMap [164]. We did not find any evidence for structural variations involving *MET*. We also examined exon-level and transcript-level expression intensities as measured by the fragments per kilobase of transcript per million fragments mapped (FPKM) algorithm. We found that all exons of *MET* were expressed in all three cell lines, with the highest expression in HCC827/R2 cells. Previous studies have shown that some lung adenocarcinomas harbor mutations in *MET* that result in skipping of exon 14 [165]. Analysis of our RNA-seq data

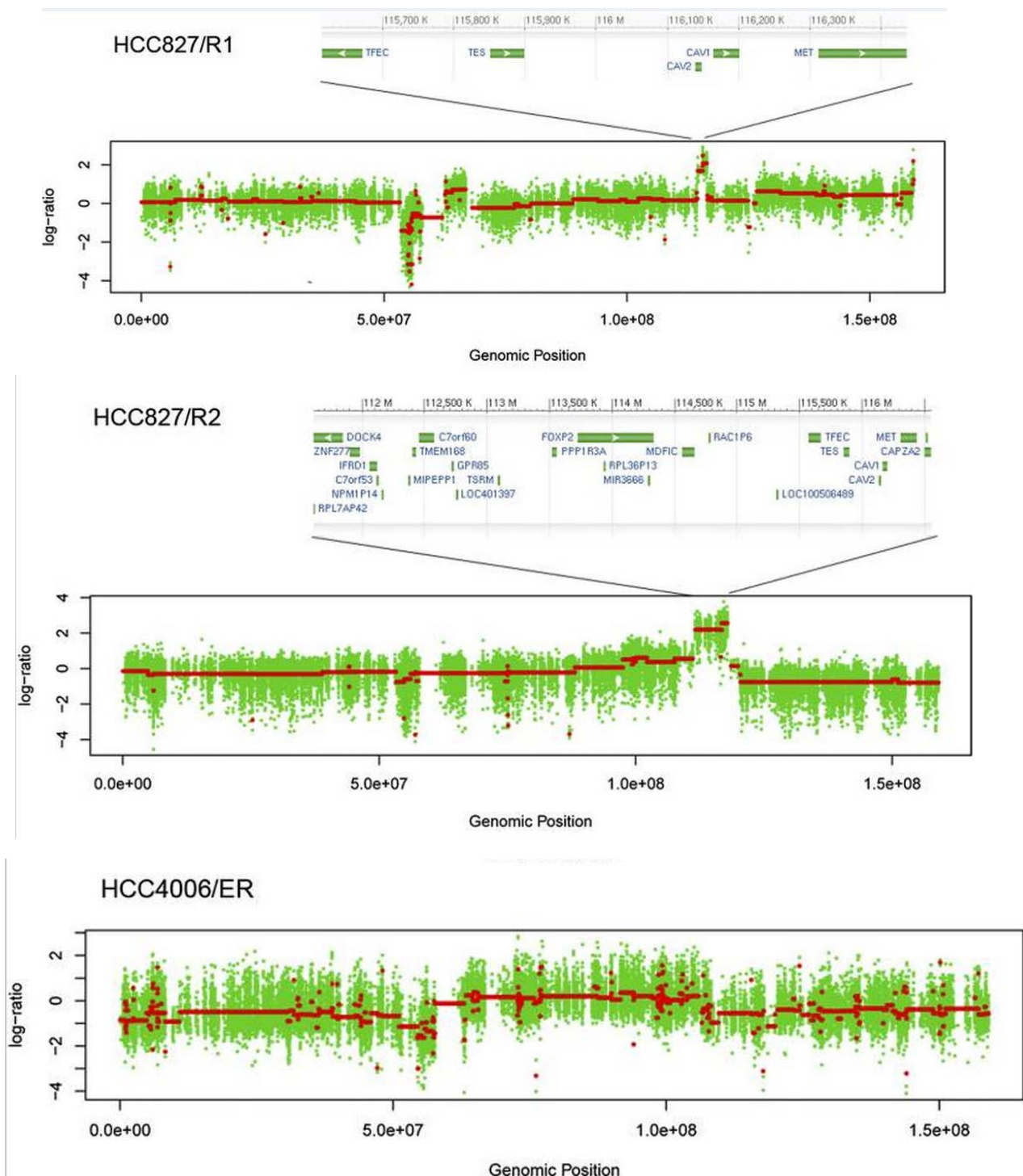


**Figure 6. Copy number variation (CNV) regions on chromosome 7 for HCC827/R1, HCC827/R2, and HCC4006/ER cells.**

(X-axis) Genomic position; (y-axis) log<sub>2</sub> ratio of CNVs in resistant versus sensitive cells. Red lines indicate the segments. The size of the MET amplicon is different in HCC827/R1 and HCC827/R2 cells. See text for details.

indicated no evidence for exon skipping. Collectively, these data show that *MET* is amplified and expressed at different levels in HCC827/R1 and HCC827/R2 cells, with the highest amplification/expression in HCC827/R2 cells

#### *HCC4006 versus HCC4006/ER cells (EMT)*

We next used WES to identify mutations associated with HCC4006 parental and polyclonal resistant cells, the latter of which developed features consistent with EMT (i.e., loss of E-cadherin, increased expression of vimentin, and spindle-like morphology) [137]. Both cell lines harbored the same known *EGFR* mutation (i.e., 9-bp nonframeshift deletion [c.2239\_2247del, p.747\_749del, at chr7: 55242469–55242477] coupled with c.G2248C, p.A750P, chr7: 55242478). Neither harbored the T790M mutation as expected, and HCC4006/ER cells are resistant to the T790M-specific TKI, WZ4002 (**Appendix Figure 30**). We found 20 exonic SNVs (13 missense and seven synonymous SNVs) and two frameshift deletions unique to HCC4006/ER cells (**Table 5**), most of which were validated (**Table 6**; **Appendix Table 20**). In contrast, 20 SNVs (14 missense, two stop-gain, and four synonymous SNVs) were predicted to be unique to parental cells; two of 10 coding SNVs were confirmed by direct sequencing (**Table 7**). Similar to our observations in the other resistant cell lines, more mutations were “selected for” during drug treatment, while fewer mutations were “selected against.”

Our CNV analysis revealed that compared with parental cells, HCC4006/ER cells displayed a large number of duplications/deletions across the whole genome (**Appendix Figure 31**). Surprisingly, the number of CNV gains and losses were at least 10-fold greater than that seen in the other cell line comparisons (**Table 8**). Although the numbers of regional gains/losses might be

significantly affected by the size of CNVs and the segmentation methods adopted by different software tools, the observed trend of many more aberrant CNVs in HCC4006/ER was clearly supported by the actual depth of coverage at CNV regions, regardless of software tools (data not shown). The most significantly altered region involved a deletion on chromosome 11, spanning 7.7 Mb in 11p13–11p12 and encompassing the cancer genes *WT1* and *LMO2*.

### ***Sample relatedness***

To quantitatively assess genetic relationships between parental/resistant cell line pairs, we adapted the genetic concept of measuring relatedness between individuals based on their shared genetic information. We hypothesized that even though each cell line displayed unique mutations, truly matched parental and resistant cell line samples should share more common SNVs than with unmatched lines. To test this, we computed pairwise identity-by-state (IBS) [166] based on the called SNVs for all pairs of cell lines formed by any two of the nine cell lines, regardless of whether they were matched or unmatched. As expected, the four PC-9-related cell lines, the three HCC827-related cell lines, and the two HCC4006-related cell lines each grouped together (**Figure 7**), while all the other pairs did not. These data support the notion that even though each line acquired mutations during drug selection, cell lines generated from the same parental cell line remained more closely related to each other than to the other lines. Moreover, the data internally confirm that the samples were not contaminated with each other throughout the process of drug selection and sequencing.

**Table 8. Summary of copy number variation (CNV) regions identified in whole-exome sequencing (WES) samples using two software tools.**

Cell line	Control-FREEC		VarScan2-pipeline		ExomeCNV <sup>§</sup>	
	Gain	Loss	Gain	Loss	Gain	Loss
PC-9/ER	377	76				
PC-9/BRC1			104 (76 <sup>*</sup> )	272 (141)	135 (117)	55 (49)
HCC827/R1			114 (57)	294 (95)	158 (133)	47 (12)
HCC827/R2			17 (15)	128 (24)	77 (50)	67 (31)
HCC4006/ER			1934 (1420)	1630 (1059)	1364 (1078)	298 (225)

Whole genome sequencing data were analyzed by Control-FREEC and whole exome sequencing data were analyzed by VarScan 2 and ExomeCNV.

<sup>§</sup> The reported regions are those whose copy number >2 or < 2 and targeted base pairs ≥ 1000.

<sup>\*</sup> The numbers in parentheses are the counts of regions called by both software tools.

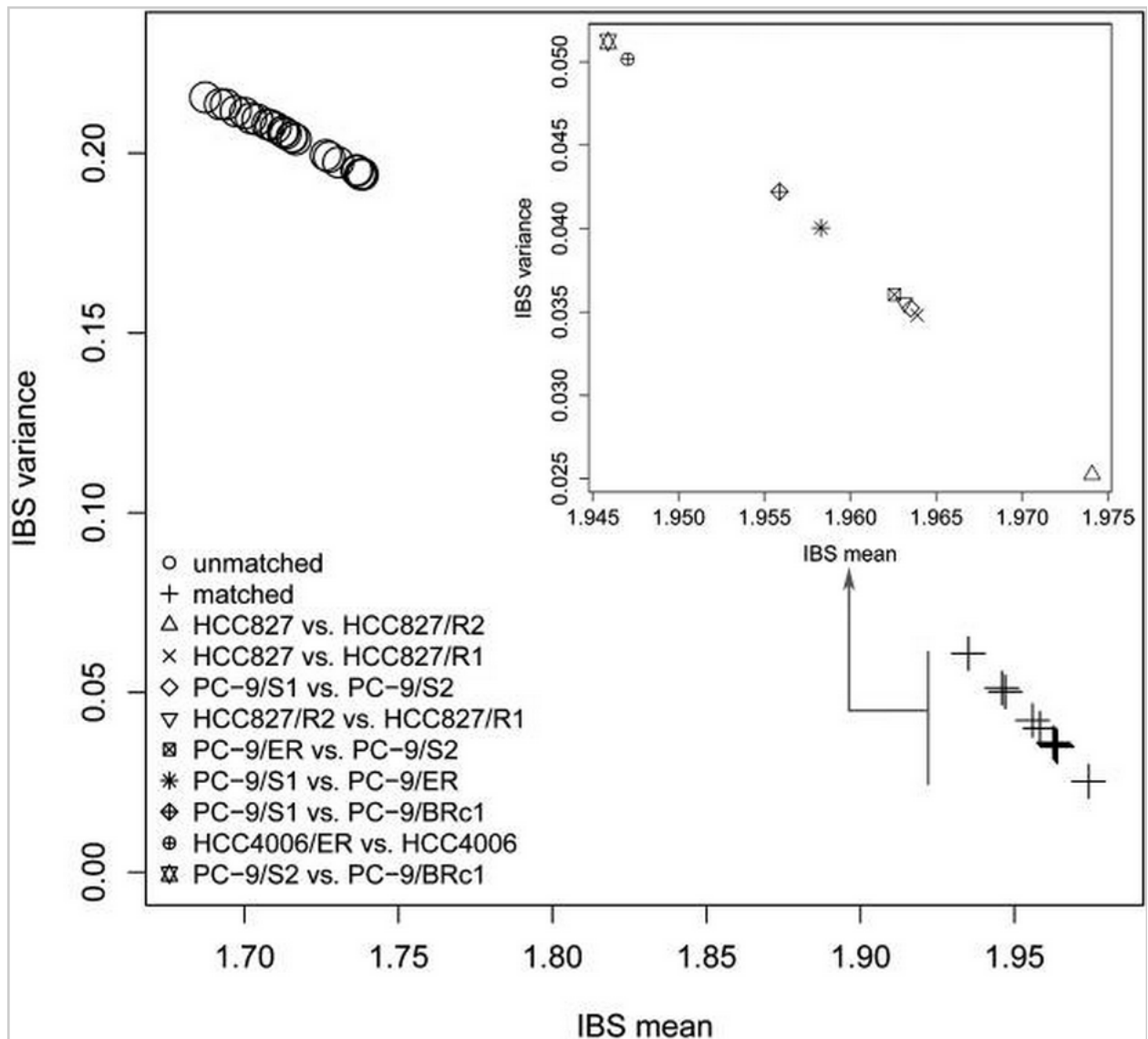


**Figure 7. Pairwise comparison of samples.**

Identity-by-state (IBS) analysis was applied to compute the shared alleles for each pair of cell lines, with the mean on the x-axis and the variance on the y-axis. On the main panel, each point represents a pair of cell lines, regardless of whether they were matched (denoted by +) or not (denoted by a circle dot). In the internal panel, the truly matched sensitive- resistant pairs were enlarged to show the details.

## ***Mutation patterns***

We compared mutation patterns in each of the cell lines (**Figure 8**). In both PC-9/ER and PC-9/BRC1 resistant cells, the most prevalent mutations were C:G → T:A transitions, followed by C:G → A:T transversions. C:G → T:A transitions are predominantly seen in lung cancers from never/light smokers, while C:G → A:T transversions are more predominant in smokers [167]. Similar data were obtained for HCC827/R1, HCC827/R2, and HCC4006/ER cells, although the numbers of mutations were low. The transition over transversion ratio (Ti/Tv) was 2.01 for both PC-9/S1 and PC-9/ER cells (WGS) and varied slightly for each pair of WES samples (HCC827: 2.42, HCC827/R1: 2.37, HCC827/R2: 2.46, HCC4006: 2.51, and HCC4006/ER: 2.40). Since there was not much difference in the Ti/Tv ratios among the drug-sensitive and drug-resistant lines, we could not discern whether TKI treatment selected for certain types of mutations over others.

We then investigated these SNVs in greater detail to identify any genome-wide patterns of their location. For the exome mutations, we surveyed the following genomic features: GC content [168], DNA replication timing [169], presence of lamina-associated domains [170], chromosome banding [171], and recombination rate [172]. We found that there were no mutations in repeat elements [173] and CpG islands [174]. The distribution of GC content at a resolution of 200 bp around each SNV did not display a different pattern compared with the genome-wide background, with mean GC content of 0.4. For chromosome banding, recombination rate, DNA replication timing, and lamina-associated domains, we did not detect any significant enrichment. For instance,

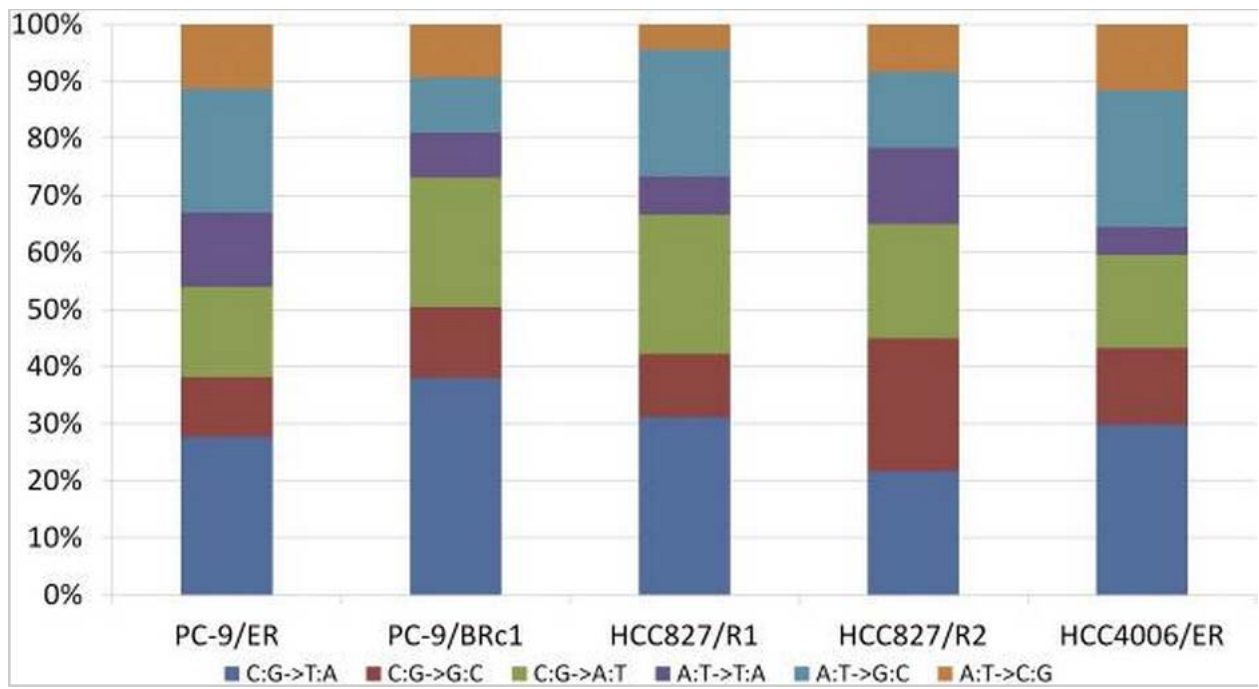
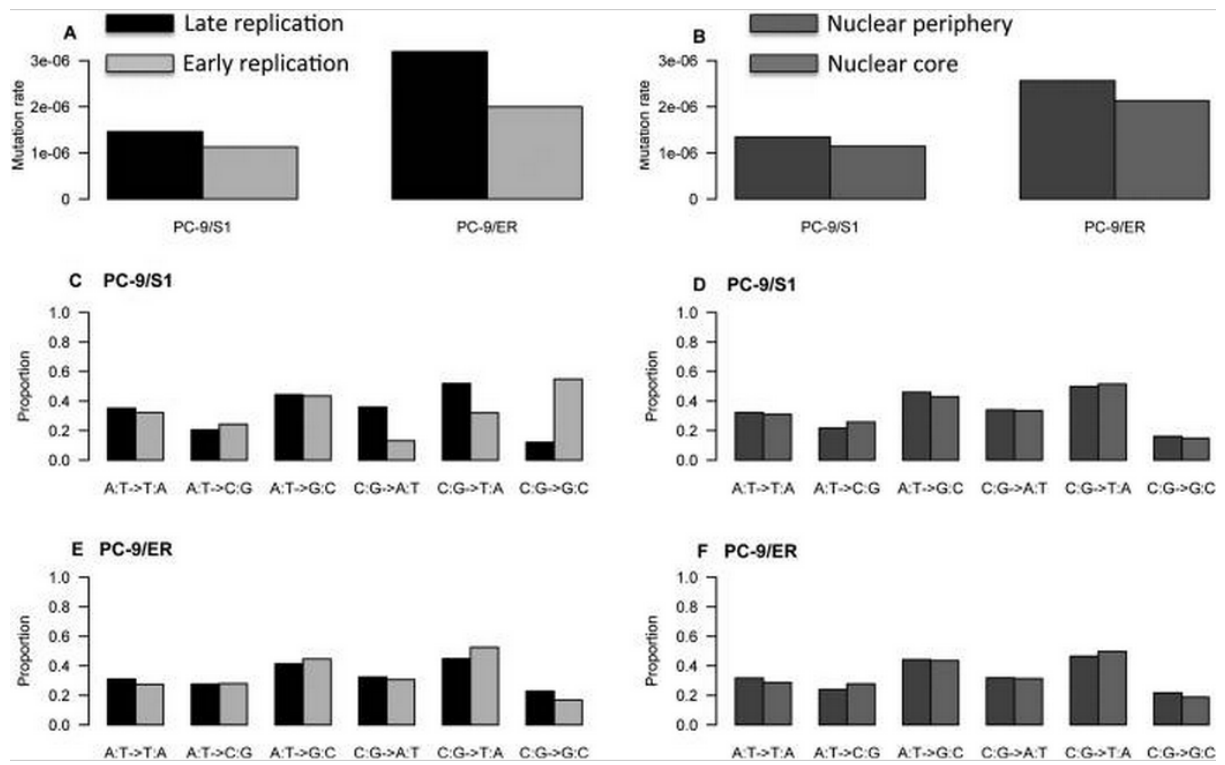


Figure 8. Patterns of mutations that uniquely occurred in each resistant cell line.

almost half of the SNVs were located in “gneg” regions, while the other half resided in “gpos” regions (i.e., recognized stain values from Giemsa stains). We next surveyed whether the SNVs were preferentially located in specific regions within genes, for instance, the C or N terminus. We found an excess of these mutations located in the 5'-UTR regions of genes (**Appendix Table 21**). This observation might be due to the limited number of SNVs available and will be confirmed in future studies.

We then performed similar analyses for the WGS data of PC-9/ER and PC-9/S1 cells. We overlaid the SNVs with information on DNA replication timing and lamina-associated domains (**Figure 9**). We found that there was a higher frequency of SNVs in “constant late” replication timing zones as compared with “constant early” replication timing zones ( $\chi^2$  *P*-value <  $10^{-5}$ ). These replication timing zones were identified based on consistency in the patterns across eight different cell types [169]. These findings are consistent with previous data showing an enrichment of mutation frequencies in late replication domains across multiple different cell types [175]. We further identified an enrichment of SNV frequencies in genomic regions harboring lamina-associated domains compared with the remainder of the nucleus ( $\chi^2$  *P*-value <  $10^{-5}$ ).

Finally, in each case, we examined the mutation signatures, i.e., the six different types of nucleotide substitutions that might arise (AT|TA, AT|CG, AT|GC, CG|AT, CG|TA, and CG|GC) (**Figure 9**). The mutation signatures stratified by lamina-associated domains were quite similar in the two samples, with a correlation of 0.98, whereas the correlation of mutation transversion patterns stratified by DNA replication timing was less similar, with a correlation of only 0.27.



**Figure 9. Patterns of SNV frequencies (A, B) and signatures (C-F) across different stratifications of genomic material.**

### ***Mutations shared across resistant cells***

We compared data from all the resistant lines to determine if there were mutations shared by cells regardless of the known mechanisms of acquired resistance (i.e., *EGFR* T790M, *MET*, or *EMT*). While *EGFR* T790M mutations were found as expected in three of five resistant lines (PC-9/ER, PC-9/BRc1, HCC827/R1) (**Table 9**), surprisingly, only one gene was observed to be mutated in more than one line. *LRP1B* mutations were found in two cell lines, with three mutations in PC-9/BRc1 and one in HCC827/R1 cells.

Among CNV changes across drug-resistant cell lines, chromosome 7 harbored the most frequent co-occurring regions. Amplified regions on 7q around *MET* in HCC827/R1 and HCC827/R2 overlapped with each other as discussed above (**Figure 6**). Changes in regions on 7p, especially involving *EGFR*, were also observed; e.g., amplification in PC-9/ER (**Appendix Table 13**) and amplification/deletion in HCC827/R1 (**Appendix Table 17**). Adjacent regions on 5p, which have been frequently reported in lung cancer samples [134, 176], were detected both in PC-9/ER (**Appendix Table 14**) and HCC827/R2 cells (**Appendix Table 19**).

### ***Driver gene specification***

Finally, to determine whether there were other potential driver genes, we systematically searched for non-silent SNVs/indels located in kinase genes, especially those that might impact the three key phosphorylation residues; i.e., serine, threonine, and tyrosine. We assessed the functional impact of SNVs using PolyPhen-2 [160] and SIFT [177] algorithms, which predict damage to protein

**Table 9. List of genetic alterations associated with drug-resistance for each cell line**

<b>Cell line</b>	<b>Known mechanisms</b>	<b>Nucleotide change</b>	<b>Amino acid change</b>	<b>Validated by experiments</b>	<b>Detected by NGS</b>
PC-9/ER	<i>EGFR</i>	c.C2369T	p.T790M	Direct sequencing	Yes
PC-9/BRC1	<i>EGFR</i>	c.C2369T	p.T790M	Direct sequencing	Yes
HCC827/R1	<i>EGFR</i>	c.C2369T	p.T790M	Direct sequencing	No <sup>#</sup>
HCC827/R2	<i>MET</i>	Amplification	n/a	FISH <sup>*</sup>	Yes
HCC4006/ER	EMT	n/a	n/a	Immunoblotting	n/a

<sup>\*</sup>FISH: fluorescent *in situ* hybridization. <sup>#</sup>The proportion of reads supporting the mutant allele was 7%, which failed the filter criterion of 20% in the VarScan 2 pipeline.

function or structure based on amino acid conservation and structural features. A total of six kinase genes were found to harbor non-silent SNVs/indels occurring in six cell lines (**Appendix Table 22**). Among them, only three variants were located within kinase domains; C2369T (T790M) in *EGFR* in PC-9/ER, PC-9/BRc1, and HCC827/R1 cells, A1491T (E497D) in *HIPK3* in HCC827/R2 cells, and C287A (A96E) in *TESK2* in HCC4006 cells (**Appendix Figure 32**). Both the C2369T (T790M) mutation in *EGFR* and the A1491T (E497D) mutation in *HIPK3* are predicted to be “deleterious” (SIFT score < 0.05 or PolyPhen-2  $\geq$  0.5), while C287A (A96E) in *TESK2* occurred in parental cells and is predicted to be “benign.” However, only the C2369T (T790M) mutation in *EGFR* impacts phosphorylation sites. Put together, these results suggest that the T790M in *EGFR* is the most likely mutation affecting drug resistance in the cells in which it was detected.

## Discussion

In the past decade, multiple new targeted therapies have shown remarkable anti-tumor activity in genetically defined “oncogene-addicted” cancers [45, 46, 152-154]. However, acquired resistance remains a significant obstacle limiting the survival of patients with metastatic disease. Many mechanisms have been identified, but comprehensive genomic profiles of resistant tumor cells have not yet been established. Here, we used a model system of “oncogene addiction”—isogenic pairs of drug-sensitive and drug-resistant *EGFR* mutant lung cancer cells—and next-generation sequencing to characterize genome-wide changes associated with the acquisition of drug resistance in vitro. Importantly, the study of these *EGFR* mutant cells has already identified mechanisms of resistance

found in human patient samples (i.e., secondary *EGFR* mutations, *MET* amplification, and EMT) [137, 155], suggesting that additional genetic changes identified are likely to have clinical relevance as well. To our knowledge, this is the first comprehensive analysis using WGS or WES of isogenic pairs of drug-sensitive and drug-resistant cell lines.

Comparing resistant cells with their matched parental counterparts, we identified 18–91 coding SNVs/indels that were acquired and 1–27 that were lost during drug treatment. While the secondary *EGFR* T790M mutation was found appropriately in the two resistant lines known to harbor this mutation, very few exonic SNVs/indels were shared across resistant lines, and many of the additional mutations identified did not have obvious biological significance. Analysis of mutation spectra across parental cells sequenced at different times and the resistant cells treated with either erlotinib or afatinib suggest that the SNVs/indels that were acquired or lost were due to drug selection, not just random mutation during in vitro culturing. These data illustrate five important principles. First, WGS/WES can be used to detect resistance mechanisms in isogenic pairs of lines. Second, the number of exonic SNVs/indels that differ among isogenic pairs of lines is relatively low (magnitude of only  $10^2$ ). Third, additional biological studies are needed to determine if many mutations are just “passengers” or, indeed, contribute to gain of fitness in the acquisition of acquired resistance. Fourth, analysis of the Ti/Tv ratios in treated cells suggested that TKI treatment does not significantly alter the ratio of transition/transversion mutations induced in cells. Finally, by extrapolating the findings from cell lines to human tumors, the acquisition of resistance may be unique in each individual patient and even within individual tumors within patients.

When investigating genome-wide patterns of these SNVs, we identified some interesting trends. For instance, we found that the SNVs were enriched in 5' UTRs within protein-coding genes as compared with 3' UTRs based on exome sequencing data. When investigating WGS data, we found that there was a significant difference in SNV frequency as well as the mutation signatures in genomic material with late replication timing as well as those containing nuclear lamina-associated domains. These data suggest that certain areas of the genome might be more prone to accumulation of SNVs.

Surprisingly, we observed more CNV changes than SNV/indel changes across all resistant lines, and the one line that had an EMT phenotype displayed significantly higher levels of CNV changes than the other lines with acquired resistance. These observations suggest that CNV changes may play a larger role than previously appreciated in the acquisition of drug resistance and again highlight that resistance may be heterogeneous in the context of different tumor cell backgrounds.

This study has some limitations. For example, WGS was performed on one isogenic pair of lines, while WES was used for the remaining pairs. WGS enables detection of all types of possible mutations, including SNVs, indels, CNVs, and structural variants (SVs), while WES has limited ability to identify SVs. However, WES generally delivers higher coverage than WGS (>100x vs. ~40x; Illumina HiSeq 2000 platform), which allows for greater power in discovering SNVs/indels that have low allele frequency in a cell population. Here, to enable comparison of WGS and WES data, we focused on detecting SNVs/indels with >20% allele frequency. Furthermore, for most of the cell lines, we did not perform whole

transcriptome sequencing, which could enable the detection of changes at the RNA level, such as alternative splicing, gene-fusion events, etc. [178]. In future studies, we plan to explore the significance of mutations that occur at both DNA (e.g., lower allele frequency) and RNA levels (e.g., transcriptional level).

A second limitation involves the use of WES data to call CNVs. While CNV detection using WGS data has been successfully applied in cancer [179-181], WES data have only recently been proven to be practically workable. Since WES data are vulnerable to various biases such as GC content, target capture reactions, and non-uniform data distribution, caution should still be taken when detecting CNV changes from WES data. Because the false discovery rate in CNV calls can be high, especially in whole-exome sequencing data, we applied two computational tools for CNV detection and focused on the consistent regions called by both tools to improve data quality. Note that amplification of the entire *MET* gene in HCC827/R2 and in HCC827/R1 was detected by both tools, providing evidence of the quality of the CNV changes we detected.

A third limitation involves the various cell lines examined. All of the parental lines were derived from polyclonal populations, and only the PC-9/BRC1 resistant line was derived from a single-cell clone. To determine if the identified SNVs/indels coexist in all or only some of the resistant cells, we would need to perform single-cell sequencing from multiple clonally derived cell populations. In addition, the PC-9/S1 and PC-9/S2 control cells were just two splits from starting polyclonal population of cells grown separately for ~1.5 mo, making them a less compelling control than if we had examined cells cultured for longer periods of

time in the absence of drug selection. These issues can be addressed in future studies.

In summary, these results demonstrate a framework for studying the evolution of drug-related genetic variants over time and provide the first genome-wide spectrum of mutations associated with the development of cellular drug resistance in an oncogene-addicted cancer. In future studies, we plan to use this framework to examine the effect of different types and doses of targeted therapies on the evolution of drug resistance and to extend these analyses to mechanisms of acquired resistance to cytotoxic chemotherapies and radiation.

## **Materials and methods**

### ***Cell culture***

*EGFR*-mutant TKI-sensitive parental cell lines PC-9, HCC827, and HCC4006 were cultured in erlotinib or afatinib following well-established TKI dose-escalation protocols to develop PC-9/ER, PC-9/BRc1, HCC827/R1, HCC827/R2, and HCC4006/ER cells [137, 155]. Details of cell culture conditions and treatments were described in [137].

### ***Next-generation sequencing***

DNAs were extracted from each cell line using a DNeasy kit (Qiagen). PC-9/S1 and PC-9/ER DNA samples were submitted for whole-genome sequencing on an Illumina Genome Analyzer IIx platform. Whole-exome sequencing of PC-

9/S2 and PC-9/BRc1 samples was conducted on an Illumina HiSeq 2000 platform using the NimbleGen SeqCap EZ Exome Library kit v2. HCC827, HCC827/R1, HCC827/R2, HCC4006, and HCC4006/ER DNA samples were submitted for whole-exome sequencing on an Illumina HiSeq 2000 platform using the Agilent SureSelect 38-Mb Kit.

### ***Read mapping and alignment***

Quality-control analysis of sequence reads was performed using FastQC software (FastQC; <http://www.bioinformatics.babraham.ac.uk/projects/fastqc/>). Reads that failed to pass quality control were removed from further analysis. We mapped the reads of each sample to the human reference genome (hg19) using BWA (version 0.5.9-r16) [182]. Local realignment was performed around small indels using the Genome Analysis Toolkit (GATK) [183]. The base quality scores initially reported by Illumina platform were recalibrated based on covariates of the read group, the reported base quality score, the machine cycle, and the combination of the base and its ahead base. After post-alignment refinement and removal of duplicate reads, we called somatic variants using VarScan 2 [162]. The pipeline is shown in Appendix Figure A2.2.

### ***Detection of unique variants***

To search for cell-line-specific variants, we performed the following comparisons: (1) PC-9/S1 unique variants compared with PC-9/ER, (2) PC-9/ER unique variants compared with PC-9/S1, (3) PC-9/S2 unique variants compared

with PC-9/BRc1, (4) PC-9/BRc1 unique variants compared with PC-9/S2, (5) PC-9/S1 unique variants compared with PC-9/S2, (6) PC-9/S2 unique variants compared with PC-9/S1, (7) HCC827 unique variants compared with HCC827/R1, (8) HCC827 unique variants compared with HCC827/R2, (9) HCC827/R1 unique variants compared with HCC827, (10) HCC827/R2 unique variants compared with HCC827, (11) HCC4006 unique variants compared with HCC4006/ER, and (12) HCC4006/ER unique variants compared with HCC4006. In each case, the VarScan 2 “somatic” model was executed designating the targeted cell line as “tumor” and the cell line to be compared as “normal.”

To select high-confidence SNVs, we started with the somatic SNVs classified as “high confidence” by VarScan 2 and performed the following filtering: (1) at least 15 supporting reads in the tumor sample at the position; (2) at least five reads supporting the mutation allele; (3) supporting reads for the mutation allele in both the forward and reverse strands; (4) somatic  $P$ -values  $< 0.05$ ; (5) the average base quality for variant-supporting reads was  $>20$ ; and (6) if there were three SNVs within a 10-bp window, all of them were removed. We further removed SNVs that occurred in dbSNP build 131 or the 1000 Genomes Project data set and denoted what remained as novel “somatic” SNVs [184]. The functional impact of non-silent SNVs was assessed using the PolyPhen-2 [160] and SIFT [177] algorithms, which predict the effects on protein functions based on the degree of amino acid conservation and structural information. For high-confidence indels, we implemented similar filtering criteria as for SNVs.

### ***Copy number variations (CNVs)***

WGS data and WES data could behave differently in that WES data are more vulnerable to system biases such as the exome capture reaction. We therefore applied different analysis pipelines to detect CNVs in these two data types. For WGS samples, we detected CNVs using the software tool Control-FREEC [157, 158] with all default parameters. For CNVs in WES data, due to the non-uniform nature of the exome capture reaction, we applied two software tools and focused on the consensus calls by both tools in order to obtain high-confidence results. We first executed the “copynumber” function in VarScan 2 in the four resistant cell lines versus their respective parental cell lines, i.e., (1) PC-9/BRc1 versus PC-9/S2, (2) HCC827/R1 versus HCC827, (3) HCC827/R2 versus HCC827, and (4) HCC4006/ER versus HCC4006. The uniquely mapped reads (e.g., through SAMtools view -q 1) were used for this analysis. To adjust the potential biases introduced by different sample depth, we included a data ratio computed based on the uniquely mapped reads and the read length in the normal and tumor samples following the instruction of VarScan 2. The candidate CNV regions were filtered using the “copyCaller” option of VarScan 2 and then smoothed and segmented by the DNACopy package (Seshan VE, Olshen A. Cited August 2012. DNACopy: DNA copy number data analysis. R package version 1.24.20) from the Bioconductor project [185]. Secondly, we applied the R package ExomeCNV [163] to detect CNVs from the WES samples. ExomeCNV takes the targeted intervals as units and determines a log ratio for each interval based on the mapped reads in a pair of matched samples.

### ***Direct dideoxynucleotide-based sequencing***

Parental or TKI-resistant specific SNPs and short indels were validated by direct sequencing. Cell line DNAs were used as template for PCR amplification. M13-tagged gene-specific primers were designed using Primer3 software [186]. Sequence chromatograms were analyzed using Mutation Surveyor software (SoftGenetics, LLC) and manual inspection.

### ***Sample relatedness***

To assess the correlations among samples, we adopted the calculation of pairwise identity-by-state (IBS) [166] based on the called SNVs. For the nine cell lines sequenced in this study, we iteratively compared any two of them, regardless of whether they were matched or unmatched. This resulted in  $9 \times 8/2 = 36$  pairs of cell lines. For each pair, we first obtained the overlapping positions where a SNV is reported in both cell lines and calculated the number of shared alleles at each position. The average value and standard deviation (SD) of the number of shared alleles for all positions were calculated for each pair of cell lines, which were then used to assess the correlations among samples. A higher average number and a lower scale of SD of the shared alleles indicate that the two cell lines share more identical SNVs and, thus, are more likely related to each other than to others.

### ***RNA-seq data analysis***

Total RNAs were extracted from HCC827, HCC827/R1, and HCC827/R2 cell lines using a Qiagen RNeasy mini kit. The Illumina Tru-Seq RNA sample prep kit was used for library preparation. Then, RNA sequencing was performed in the

Vanderbilt Technologies for Advanced Genomics (VANTAGE) core. Paired-end reads with 50 bp in length were generated by an Illumina HiSeq 2500 and were initially mapped to the human reference genome and human transcriptome using the software TopHat v2.0.8 [187]. We used FusionMap [164] to search for potential gene fusion events that might be involved in *MET*. Gene expression levels were measured by the fragments per kilobase of transcript per million fragments mapped (FPKM) algorithm [188].

## Chapter III: Optimizing the sequence of anti-EGFR targeted therapy in EGFR-mutant lung cancer

Adapted from: **Catherine B. Meador**, Hailing Jin, Elisa de Stanchina, Caroline A. Nebhan, Valentina Pirazzoli, Lu Wang, Pengcheng Lu, Huy Vuong, Katherine E. Hutchinson, Peilin Jia, Xi Chen, Rosana Eisenberg, Marc Ladanyi, Katerina Politi, Zhongming Zhao, Christine M. Lovly, Darren A. E. Cross, and William Pao. (2014) Optimizing the sequence of anti-EGFR targeted therapy in EGFR-mutant lung cancer. *Mol Cancer Ther* 14(2):542-52.

### Introduction

Activating mutations in the tyrosine kinase domain of the EGF receptor (EGFR) are found in 10-35% of lung adenocarcinomas, the predominant subtype of non-small cell lung cancer (NSCLC) [18-20]. Such mutations, which occur most commonly either as small in-frame deletions in exon 19 (19del) or point mutations in exon 21 (L858R), confer sensitivity to the first- and second-generation EGFR tyrosine kinase inhibitors (TKIs) gefitinib, erlotinib, and afatinib [18-20, 44-49].

While multiple lines of anti-EGFR therapies have been developed to treat EGFR-mutant tumors, acquired resistance (AR) to these regimens remains a major clinical obstacle. Metastatic EGFR-mutant lung cancers treated with erlotinib or gefitinib in the first-line setting develop into resistant tumors within 9-16 months [3]. In over 50% of cases, acquired resistance to erlotinib or gefitinib involves emergence of a second-site EGFR mutation substituting threonine for methionine at position 790 in exon 20 (T790M) [122, 123]. Other rarer mechanisms include amplification of the genes encoding the MET and ERBB2 kinases, mutations in *BRAF* or *PIK3CA* [3, 134-136], reduced expression of the RAS GTPase

neurofibromin (encoded by the gene *NF1*) [5], and activation of the AXL kinase [6]. Histologic changes such as epithelial-to-mesenchymal transition (EMT) and development of small-cell lung cancer (SCLC) features have also been detected in a small subset of tumors from patients with AR to first-generation TKIs [4, 6, 189].

We previously showed that dual inhibition of EGFR with the second-generation TKI afatinib and the anti-EGFR antibody cetuximab induces tumor regression of T790M+ transgenic mouse lung tumors, overcoming a model of primary AR to erlotinib and gefitinib. The addition of cetuximab to afatinib results in simultaneous depletion of phospho- and total EGFR [118]. In a subsequent phase Ib clinical trial of afatinib + cetuximab, a 29% response rate was observed in patients with AR to gefitinib or erlotinib, regardless of T790M status [144]. Thus, a substantial fraction of EGFR-mutant tumors remain dependent on the EGFR signaling axis for survival even after AR to first-generation TKIs. Unfortunately, resistance to afatinib + cetuximab has already been observed in patients. For example, activation of mTORC1 signaling may confer resistance to afatinib + cetuximab in some tumors [145]; however, a complete understanding of the spectrum of resistance mechanisms to afatinib + cetuximab is currently lacking.

Third-generation mutant-specific EGFR TKIs, such as AZD9291, CO-1686, and HM61713, have also shown activity in patients with T790M+ AR to gefitinib or erlotinib [190-192]. These agents are designed to specifically inhibit mutant EGFR (i.e., 19del-, L858R-, and/or T790M+), sparing the wild-type receptor [193]. As these new compounds become widely available for clinical use, patients will be treated with multiple lines of EGFR-targeted therapies with increasing frequency. For example, a patient with EGFR-mutant lung cancer may receive erlotinib or afatinib as first line therapy, with the assumption that when progressive disease

develops, the resistant tumor will still be sensitive to other EGFR-targeted therapies such as afatinib + cetuximab or AZD9291. If mutant-specific TKIs become available in the first line setting, whether tumor cells with acquired resistance to such inhibitors will be more aggressive or even responsive to subsequent anti-EGFR treatment remains unknown. In summary, the effect of sequential treatment with various anti-EGFR agents on tumor evolution and drug resistance in EGFR-mutant lung cancer remains to be determined. Data demonstrating the optimal sequence of these therapies is needed in order to inform clinical decision-making. Here, we model resistance to anti-EGFR treatments in EGFR mutant lung cancer cell lines in order to further elucidate mechanisms of sensitivity and resistance of tumors to each of the available anti-EGFR therapies. Importantly, previous work from our lab and others has demonstrated that cell line modeling is highly predictive of resistance mechanisms seen in patients, validating use of this preclinical approach [137, 155].

## Results

### ***AZD9291 versus afatinib + cetuximab in T790M+ cell lines***

Clinical data demonstrate efficacy of both AZD9291 and afatinib + cetuximab in the T790M+ second-line setting (i.e., AR to erlotinib/gefitinib/afatinib), but the relative potency of these therapies is unknown. Here, we utilized a panel of T790M+ cell lines (**Table 10, Appendix Figure 33**) to compare directly the growth-inhibitory and signaling effects of afatinib + cetuximab versus AZD9291 in T790M+ disease. In prior studies, we had derived multiple erlotinib- and afatinib-resistant EGFR mutant cell lines by well-established *in vitro* dose-escalation

protocols [155]. Here, we also present data from a novel T790M+ cell line (VP-2) derived directly *ex vivo* from the pleural fluid of a patient with EGFR-mutant (19del) lung adenocarcinoma and AR to erlotinib (**Appendix Figure 34A, Materials and methods**). VP-2 cells demonstrated amplification of the *EGFR* locus by fluorescence *in-situ* hybridization (FISH), were resistant to growth inhibition by erlotinib and afatinib, and retained sensitivity to AZD9291 (**Appendix Figure 34B-D**). Consistent with sensitivity to AZD9291, VP-2 cells did not display amplification of *MET* by array comparative genomic hybridization (aCGH).

We treated at clinically relevant doses (i.e., at concentrations at or below the  $C_{max}$  as determined by phase I clinical trial data) T790M+ cell lines VP-2, PC-9/ERc1, PC-9/BRc1, HCC827/R1 (all 19del; T790M), and H1975 (L858R; T790M) with either afatinib + cetuximab [50nM; 5 $\mu$ g/mL] or AZD9291 [50nM]. Both afatinib + cetuximab and AZD9291 inhibited proliferation of T790M+ cells in long-term (10-day) growth inhibition assays, but AZD9291 induced more growth inhibition than afatinib + cetuximab (**Figure 10A, Appendix Figure 34E**). Consistent with these findings, analysis of cell lysates showed that both therapies decreased phospho-EGFR and downstream pathways involving phospho-ERK and phospho-AKT at both 6h and 24h, confirming and extending previously published data (**Figure 10B, Appendix Figure 34F**) [118, 136, 193]. Both afatinib + cetuximab and AZD9291 also induced expression of the pro-apoptotic BCL-2 family member BIM, which is required for apoptosis induced by EGFR TKIs in EGFR-mutant cells (**Figure 10B**) [194]. Collectively, these data confirm the activity of both afatinib + cetuximab and

**Table 10. Drug-sensitive and –resistant cell lines used in this study.**

TKI resistance status	Name and EGFR genotype
<b>TKI-naïve</b>	
<b>Parental EGFR-mutant</b>	PC-9 (19del)
	HCC827 (19del)
<b>First-line (primary) AR</b>	
<b>Erlotinib/afatinib-resistant</b>	VP-2 (19del + T)
	PC-9/ERc1 (19del + T)
	PC-9/BRc1 (19del + T)
	HCC827/R1 (19del + T)
	PC-9/BRc1/V4 (19del + T)
	PC-9/BRc1/V5 (19del + T)
	PC-9/BRc1/V7 (19del + T)
	H1975 (L+T)
<b>AZD9291-resistant</b>	PC-9/AZR (19del)
<b>Second-line (secondary) AR</b>	
<b>AZD9291-resistant</b>	PC-9/ERc1/AZR (19del + T)
	HCC827/R1/AZR* (19del)
	H1975/AZR (L+T)
<b>A+C-resistant</b>	PC-9/BRc1/A+CR3
	PC-9/BRc1/A+CR5**
	PC-9/BRc1/A+CR6
	PC-9/BRc1/A+CR7
	PC-9/BRc1/A+CR8
	PC-9/BRc1/A+CR9**

*TKI-naïve:* PC-9 and HCC827 cells are parental EGFR-mutant cell lines sensitive to all EGFR TKIs. *First-line (primary) AR:* VP-2 is a novel cell line derived from a pleural effusion of a patient harboring a lung adenocarcinoma with T790M+ acquired resistance to erlotinib and afatinib (see materials and methods for details). PC-9/ERc1 and PC-9/BRc1 are T790M+ clonal cell lines derived from PC-9 cells with *in vitro* acquired resistance to erlotinib and afatinib (BIBW2992), respectively. HCC827/R1 is a T790M+, erlotinib-resistant cell line derived from HCC827 cells.

Parental H1975 cells harbor both the EGFR TKI-sensitizing L858R mutation and the T790M resistance mutation and are erlotinib-resistant *in vitro*. PC-9/BRc1/V4, -5, and -7 cells were derived from vehicle-treated PC-9/BRc1 xenografts and serve as controls for cells with second-line A+C resistance. PC-9/AZR cells are derived from PC-9 cells with *in vitro* acquired resistance to AZD9291. *Second-line (secondary) AR*: PC-9/ERc1/AZR, HCC827/R1/AZR, and H1975/AZR cells were derived from PC-9/ERc1, HCC827/R1, and H1975 cells, respectively, with *in vitro* acquired resistance to AZD9291. PC-9/BRc1/A+CR3, -5, -6, -7, -8, and -9 cells were derived from six different PC-9/BRc1 xenografts treated with long-term A+C. 19del, EGFR exon19 deletion; L, EGFR L858R point mutation; T, T790M; AR, acquired resistance. \*HCC827/R1/AZR cells were derived from polyclonal HCC827/R1 (19del+T790M) cells but lost T790M with acquired resistance to AZD9291 \*\*PC-9/BRc1/A+CR5 and -9 xenografts were not used as models of A+C resistance because they were derived from xenografts that were either collected while mice were off drug (PC-9/BRc1/A+CR9) or that re-responded and were not resistant to A+C *in vivo* at the time of collection (PC-9/BRc1/A+CR5).

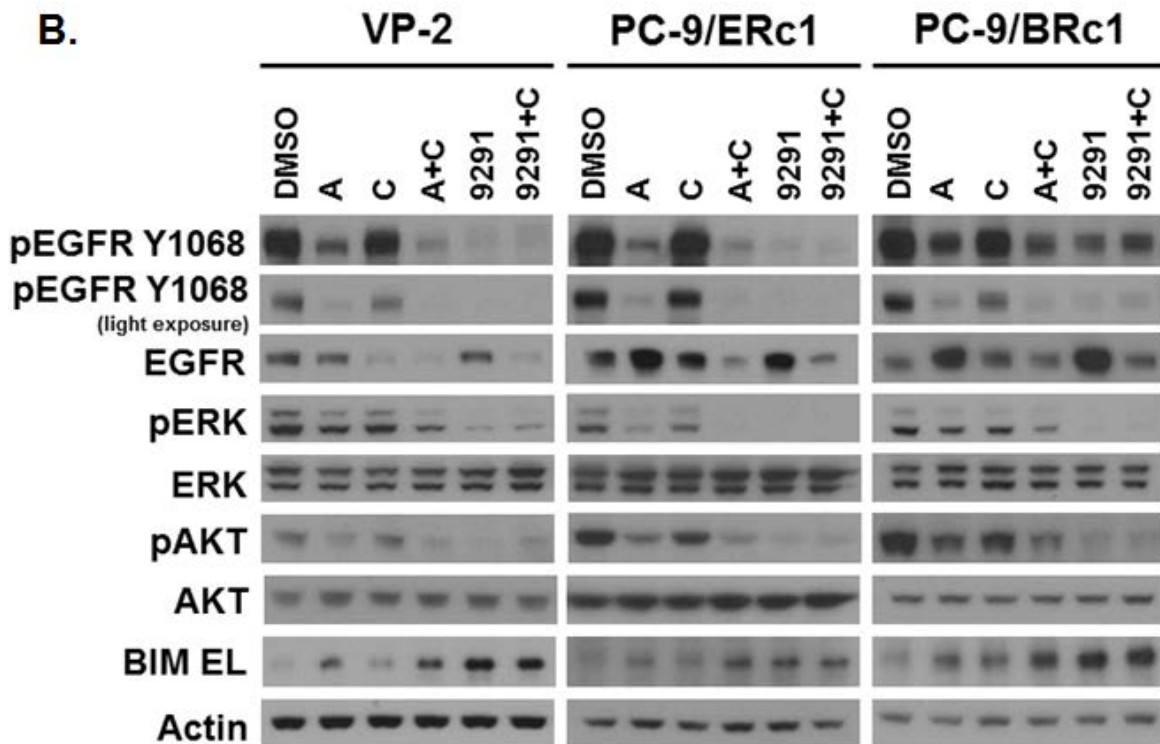
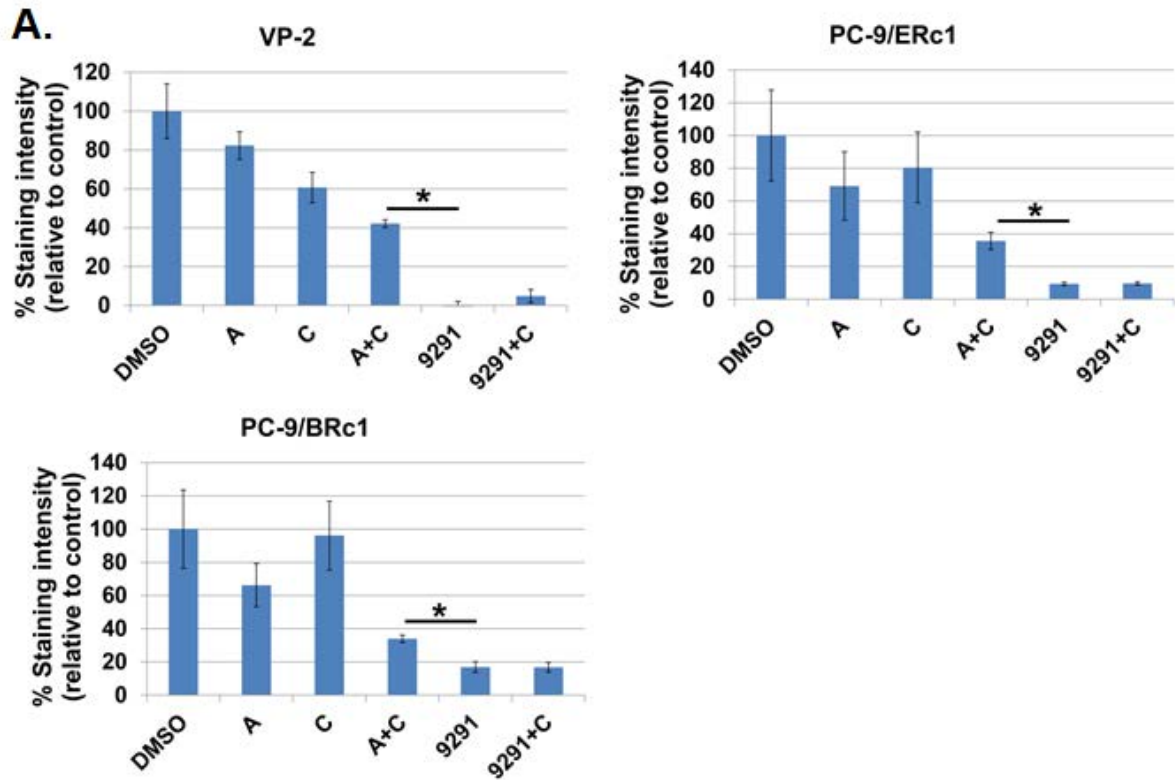


Figure 10. Afatinib plus cetuximab (A+C) versus AZD9291 in T790M+ cell lines.

**A**, Quantification of crystal violet staining of VP-2, PC-9/ERc1, and PC-9/BRc1 cells treated in triplicate with DMSO, afatinib (A) [50nM], cetuximab (C) [5µg/mL], afatinib + cetuximab (A+C), AZD9291 (9291) [50nM], or AZD9291 + cetuximab (9291+C) for 10 days. Data are expressed as mean ± standard deviation of triplicate measurements; \*p<0.10 for AZD9291 vs. A+C. **B**, Immunoblotting of cell lysates from VP-2, PC-9/ERc1, and PC-9/BRc1 treated for 24 hours with DMSO, afatinib (A) [50nM], cetuximab (C) [5µg/mL], A+C, AZD9291 (9291) [50nM], or AZD9291 + cetuximab (9291+C) show the effect of each treatment on phospho-EGFR, phospho-ERK, phospho-AKT and BIM EL induction.

AZD9291 in our models of T790M+ acquired resistance to EGFR TKIs and further suggest that AZD9291 may be a more potent inhibitor in this setting.

It remains unknown whether AZD9291 + cetuximab will have any clinical utility as a combination therapy for EGFR-mutant lung cancer. In order to discern the effects of combining AZD9291 with cetuximab versus treating with AZD9291 alone, we evaluated the signaling and growth inhibitory effects of this combination in the assays described above. While AZD9291 + cetuximab did cause a greater decrease in total EGFR expression, this did not lead to any additive growth-inhibitory or differential downstream signaling effects in our T790M+ cell line models of erlotinib/afatinib resistance, even using various doses of either drug (**Fig. 10A-B, Appendix Figure 34G**).

#### ***Derivation of afatinib + cetuximab-resistant cell lines***

We next sought to test whether AZD9291 could overcome resistance to afatinib + cetuximab. Therefore, we derived new afatinib + cetuximab-resistant cell lines by subjecting xenografts of PC-9/BRc1 cells (19del; T790M) to long-term treatment with afatinib + cetuximab until tumors began to grow in the presence of drug (**Fig. 11A-B**). Re-derived cell lines from the afatinib + cetuximab-treated xenografts showed increased EGFR protein expression (**Appendix Figure 35A**) and persistent levels of *EGFR* amplification by fluorescence *in situ* hybridization (FISH) relative to vehicle-treated controls (**Appendix Figure 35B**). Phospho-RTK arrays of baseline signaling in two representative afatinib + cetuximab-resistant cell lines revealed sustained phospho-EGFR but no increased activation of

additional RTKs that would suggest ‘bypass’ signaling as a mechanism of resistance (**Appendix Figure 35C**). Notably, we also did not see increased phospho-S6 in our afatinib + cetuximab-resistant cell lines (**Appendix Figure 35A**), suggesting that the mechanism of resistance in this model is not due to increased mTOR pathway activity, as previously characterized in separate experiments [145]. H&E staining of afatinib + cetuximab-resistant tumors did not show features of SCLC morphology, a known mechanism of resistance to first- and second-generation EGFR TKIs (**Appendix Figure 35D**). A combination of amplicon-based targeted next-generation sequencing (NGS; NCBI SRA Accession ID: SRP049301) and cDNA-based dideoxynucleotide sequencing did not detect any additional mutations in *KRAS*, *PIK3CA*, *BRAF*, or *EGFR*, *ERBB2*, *ERBB3*, or *ERBB4*. Thus, afatinib + cetuximab-resistant lines demonstrated increased EGFR protein without evidence of alternative known resistance mechanisms, suggesting that they might still be dependent on the EGFR signaling axis for survival.

### **AZD9291 overcomes afatinib + cetuximab resistance**

Having derived afatinib + cetuximab-resistant cell lines, we tested their sensitivity to clinically relevant concentrations of AZD9291 in standard growth inhibition assays. We chose PC-9/BRc1/A+CR6 and PC-9/BRc1/A+CR7 cells for further characterization, because they developed the most resistance to afatinib + cetuximab *in vivo* (**Figure 11B**). In soft agar assays, both PC-9/BRc1/A+CR6 and PC-9/BRc1/A+CR7 cells were resistant to growth inhibition by afatinib + cetuximab relative to PC-9/BRc1/V7 vehicle control, but colony formation of all cell lines was significantly inhibited in the presence of AZD9291 (**Figure 11C**). Consistent with

the growth inhibition data, immunoblotting of cell lysates demonstrated less inhibition of phospho-EGFR, phospho- extracellular signal-regulated kinase (phospho-ERK), and phospho-protein kinase B (phospho-PKB/AKT) in afatinib + cetuximab-resistant cells than afatinib + cetuximab-sensitive PC-9/BRc1/V7 cells upon treatment with afatinib + cetuximab; however, AZD9291 diminished EGFR and downstream signaling in both control and afatinib + cetuximab-resistant cell lines (**Figure 11D**). Thus, AZD9291 appears to overcome resistance to afatinib + cetuximab in these cell lines *in vitro*. As in erlotinib/afatinib resistant cell lines, addition of cetuximab to AZD9291 induced a slightly greater decrease in total EGFR by immunoblotting but no significant change in growth inhibition as compared to AZD9291 alone in afatinib + cetuximab-resistant cell lines (**Figure 11C-D**).

To confirm our findings *in vivo*, we re-implanted our original xenograft-derived cell lines subcutaneously into nude mice and measured changes in tumor volume following treatment with AZD9291. Consistent with the *in vitro* results, parental PC-9/BRc1 and PC-9/BRc1/V7 cells displayed tumor regression following 1 week of treatment with both afatinib + cetuximab and AZD9291, but only AZD9291 induced shrinkage of afatinib + cetuximab-resistant PC-9/BRc1/A+CR6 and PC-9/BRc1/A+CR7 xenografts (**Figure 11E**). Taken together with our *in vitro* growth inhibition and signaling data, these findings strongly suggest that these preclinical models of afatinib + cetuximab resistance maintain reliance on EGFR signaling for survival and that AZD9291 may have clinical efficacy in some settings of afatinib + cetuximab resistance.

### ***Afatinib + cetuximab does not overcome AZD9291 resistance***

In order to test whether A+C could overcome resistance to AZD9291, we generated four AZD9291-resistant cell lines using well-established TKI dose-escalation protocols [128, 135, 155, 195] (**Table 10, Appendix Figure 33**). PC-9/AZR cells were derived from TKI-sensitive PC-9 parental cells, mimicking first-line resistance to AZD9291. Three other AZD9291-resistant cell lines (PC-9/ERc1/AZR, HCC827/R1/AZR, H1975/AZR) were derived from T790M+ erlotinib-resistant 'parental' cell lines, modeling the clinical setting of second-line resistance to AZD9291. After long-term culture in TKI, AZD9291-resistant PC-9, PC-9/ERc1, HCC827/R1, and H1975 cells acquired the ability to grow in drug concentrations >100 fold (1 $\mu$ M) the initial IC<sub>50</sub> (median inhibitory concentration) of the parental cells resistant to first- and second- generation EGFR TKIs erlotinib and afatinib (**Figure 12A; Appendix Figure 36A**). A combination of amplicon-based targeted NGS (NCBI SRA Accession ID: SRP049329) and cDNA-based dideoxynucleotide sequencing did not detect any acquired mutations in *KRAS*, *PIK3CA*, *BRAF*, or *EGFR*, *ERBB2*, *ERBB3*, or *ERBB4* in the setting of AZD9291 resistance; specifically, we did not observe any mutations at Cys797 in EGFR, the site at which AZD9291 makes a covalent bond with EGFR.

In long-term colony formation and growth inhibition assays, all AZD9291-resistant cell lines were resistant to growth inhibition by both AZD9291 and afatinib + cetuximab as compared to parental (i.e., AZD9291-sensitive) controls (**Fig. 12B Appendix Figure 36B**). Furthermore, immunoblotting of cell lysates from AZD9291-resistant cells treated with AZD9291 for 6 hours showed inhibition of phospho-EGFR

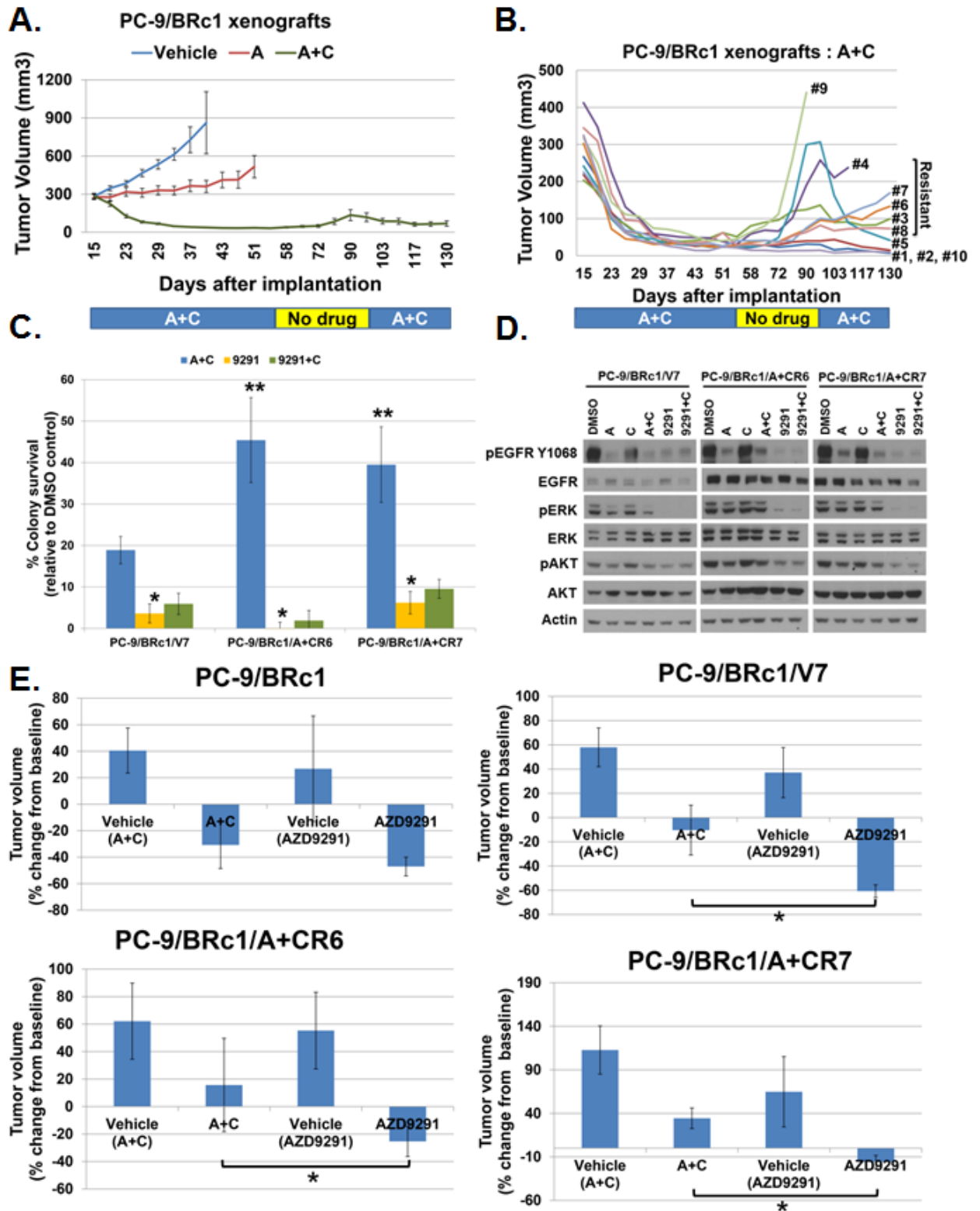


Figure 11. Afatinib plus cetuximab (A+C)-resistant cell lines are sensitive to growth inhibition by AZD9291.

**A**, To derive A+C-resistant lines, mice bearing PC-9/BRC1 xenografts were treated long-term with either vehicle, afatinib (A) [25 mg/kg p.o.], or A+C [25mg/kg p.o.; 50mg/kg i.p.]. Data are expressed as mean  $\pm$  standard deviation of tumor volumes calculated twice weekly for 10 mice/group. Treatment was withdrawn for days 56-94 to allow tumor re-growth before re-initiation of treatment on day 95. **B**, Xenograft data of A+C-treated mice from A are plotted as individual tumor curves. Tumors that grew in the presence of drug were deemed resistant (#3, 4, 6, 7 and 8); cell lines were derived from all tumors from which sufficient tissue could be obtained at the point of experiment termination (#3, 5, 6, 7, 8, and 9). **C**, Quantification of soft agar assays of xenograft-derived A+C-resistant cell lines PC-9/BRC1/A+CR6 and PC-9/BRC1/A+CR7 vs. A+C-sensitive vehicle control cell line PC-9/BRC1/V7 treated for 10 days with either DMSO, A+C [50nM; 5 $\mu$ g/mL], AZD9291 (9291) [50nM], or AZD9291 + cetuximab (9291+C). Data are expressed as mean  $\pm$  standard deviation of hexuplicate data; \* $p$ <0.05 for AZD9291 vs. A+C; \*\* $p$ <0.05 for A+C in PC-9/BRC1/A+CR6 and PC-9/BRC1/A+CR7 vs. PC-9/BRC1/V7. **D**, Immunoblotting of lysates from PC-9/BRC1/V7, PC-9/BRC1/A+CR6, and PC-9/BRC1/A+CR7 cells treated for 6 hours with DMSO, afatinib (A) [50nM], cetuximab (C) [5 $\mu$ g/mL], A+C, AZD9291 (9291) [50nM], or AZD9291 + cetuximab (9291+C) demonstrate that A+C-resistant cells PC-9/BRC1/A+CR6 and PC-9/BRC1/A+CR7 cells are relatively resistant to inhibition of phospho-EGFR, phospho-ERK, and phospho-AKT compared to PC-9/BRC1/V7 cells upon treatment with A+C, but AZD9291 inhibits phospho-EGFR and downstream signaling in both A+C-sensitive and A+C-resistant cell lines. **E**, Xenograft-derived A+C-resistant PC-9/BRC1/A+CR6 and PC-9/BRC1/A+CR7 cells, xenograft-derived A+C-sensitive PC-9/BRC1/V7 cells, and parental PC-9/BRC1 cells were re-implanted as xenografts in immunodeficient mice and treated for one week with either A+C [25mg/kg p.o.; 50mg/kg i.p.], AZD9291 [10mg/kg p.o.], or respective vehicle controls. Tumor volumes were calculated from twice-weekly caliper measurements, and data are plotted as percentage tumor growth or shrinkage relative to baseline. Data are expressed as mean  $\pm$  standard deviation of measurements from five mice. \* $p$ <0.05 for AZD9291 vs. A+C.

but sustained phosphorylation of ERK and AKT (**Figure 12C**). The dissociation between phospho-EGFR and phospho-ERK/AKT inhibition in this setting further suggests an EGFR-independent mechanism of resistance to AZD9291. More extensive characterization of these cell lines is ongoing; however, in collaboration with the AstraZeneca project team, we have found that AZD9291-resistant cells often display activation of the MAPK pathway [1]. Consistent with these data, addition of a MEK inhibitor (AZD6244) partially re-sensitized our AZD9291-resistant cells to inhibition of colony formation by AZD9291 (**Appendix Figure 36D**). Addition of cetuximab to AZD9291 diminished total EGFR protein levels in AZD9291-resistant cells but did not increase growth inhibition relative to AZD9291 alone (**Figure 12B-C**). Collectively, these studies suggest that resistance to AZD9291 may be mediated by EGFR-independent mechanisms that confer cross-resistance to subsequent anti-EGFR therapies.

## **Discussion**

Patients with metastatic EGFR mutant lung cancer experience dramatic and prolonged benefit from treatment with EGFR TKIs such as gefitinib and erlotinib. Unfortunately, resistance occurs in most cases, with more than half of patients acquiring a second-site T790M mutation. Recently, studies with newer generations of anti-EGFR treatments such as afatinib + cetuximab and AZD9291 confirm that some tumors maintain dependence on EGFR signaling even in the setting of disease progression. The optimal sequence of anti-EGFR therapy is now unknown, but preclinical modeling of AR to targeted therapies has proven to

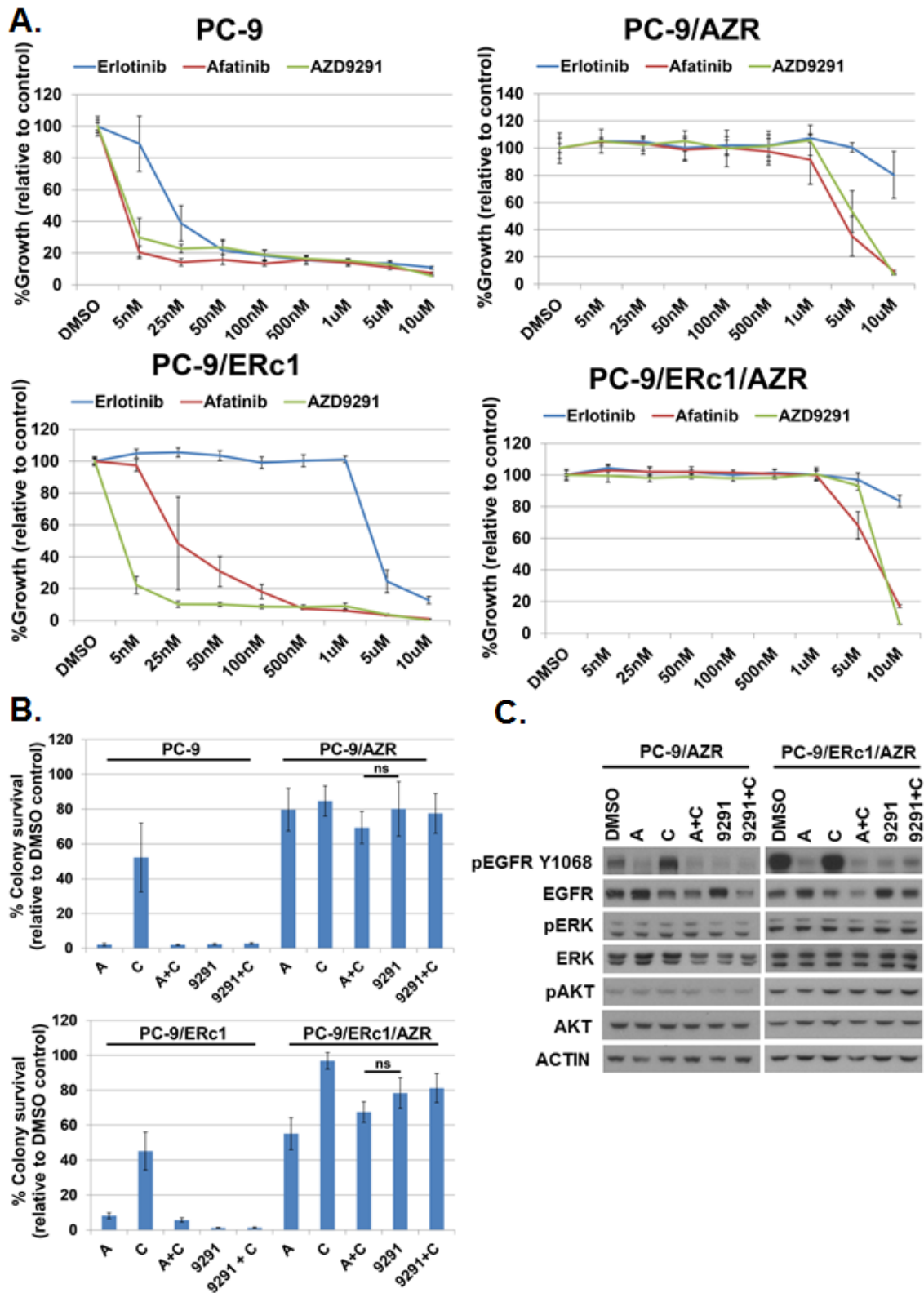


Figure 12. AZD9291-resistant cell lines are resistant to growth inhibition by A+C.

**A**, Cell growth-inhibition assays demonstrate the resistance of PC-9/AZR and PC-9/ERc1/AZR cells to AZD9291, relative to isogenic parental controls PC-9 and PC-9/ERc1, respectively. AZD9291 resistance also confers robust cross-resistance to first- and second-generation EGFR TKIs erlotinib and afatinib. Data are expressed as a percentage of DMSO control and plotted as mean  $\pm$  standard deviation of hexuplicate data. **B**, Quantification of soft agar assays of PC-9, PC-9/AZR, PC-9/ERc1, and PC-9/ERc1/AZR cells treated for 10 days with either DMSO, afatinib (A), cetuximab (C), A+C [50nM; 5 $\mu$ g/mL], AZD9291 (9291) [50nM], or AZD9291 + cetuximab (9291+C). Data are expressed as mean  $\pm$  standard deviation of hexuplicate data; ns= non-significant at  $p=0.05$  for AZD9291 vs. A+C. **C**, Immunoblotting of lysates from PC-9/AZR and PC-9/ERc1/AZR cells treated for 6 hours with DMSO, afatinib (A) [50nM], cetuximab (C) [5 $\mu$ g/mL], A+C, AZD9291 (9291) [50nM], or AZD9291 + cetuximab (9291+C) demonstrate that AZD9291 can still inhibit phospho-EGFR but not downstream phospho-ERK or phospho-AKT in AZD9291-resistant cells.

be an effective strategy for predicting clinical outcomes. Here, we used existing and new cell line models of resistance to first-, second- and third- generation anti-EGFR therapies *in vitro* and *in vivo* in order to determine rationally a treatment sequence that may confer maximal duration of clinical benefit before development of acquired resistance to all available anti-EGFR therapies.

*First-line EGFR targeted therapy:* Erlotinib, gefitinib, and afatinib are approved for treatment of EGFR-mutant lung tumors in the first-line setting. In addition, preclinical data suggest that AZD9291 could be highly effective in the first-line setting [118, 193, 196], and a trial testing AZD9291 in TKI-naïve patients is underway. However, the question of whether use of AZD9291 in the first-line setting will extend PFS for patients compared to erlotinib, gefitinib, or afatinib alone remains to be determined clinically. Furthermore, it is unclear at this point whether tumors that develop resistance to mutant-specific TKIs in the first-line setting will demonstrate a more aggressive phenotype than erlotinib/gefitinib/afatinib-resistant tumors, or whether they will respond to subsequent anti-EGFR therapies.

*Second-line EGFR targeted therapy:* Early clinical trial data demonstrate that both afatinib + cetuximab and AZD9291 can effectively overcome AR to first- and second-generation EGFR TKIs [144, 190], which we recapitulate in our preclinical models. We further show that while addition of cetuximab to AZD9291 does induce a slightly greater decrease in levels of total EGFR compared to AZD9291 alone, the combination does not provide added growth-inhibitory effect *in vitro*. This suggests that, at the doses tested, AZD9291 is sufficiently potent as monotherapy to inhibit EGFR T790M signaling below the threshold needed for

inhibition of cell growth. However, it is still possible that the combination, through dual targeting of the receptor, could possibly have some increased efficacy in patients and may warrant further investigation clinically in the future.

*Third-line EGFR targeted therapy:* We show that secondary resistance to afatinib + cetuximab may be mediated in some cases by EGFR-dependent mechanisms that can be overcome by AZD9291. Addition of cetuximab to AZD9291 did not appear to confer any added benefit in the setting of afatinib + cetuximab resistance. Currently, we do not know how frequently such EGFR dependence will occur. In separate work, we have shown that other models of afatinib + cetuximab resistance (derived under different conditions and protocols than the models presented here) are characterized by activation of mTORC1 signaling [145]. These data are consistent with the notion that disease progression is due to heterogeneous mechanisms in patients. Ongoing analysis of patients' tumors with acquired resistance to afatinib + cetuximab will shed further light on the proportion of afatinib + cetuximab-resistant tumors that retain sensitivity to subsequent anti-EGFR therapies.

In preclinical models of acquired resistance to AZD9291, cells appear to have bypassed EGFR signaling alone for survival. In the presence of drug, they display sustained activation of downstream signaling, despite decreased phospho-EGFR. Consistent with these findings, in contrast to afatinib + cetuximab resistance, our models of resistance to AZD9291 displayed cross-resistance to all other anti-EGFR therapies in both the first- and second-line setting. Thus, one potential scenario for cases of T790M+ resistance involves afatinib + cetuximab

followed by AZD9291 but not vice versa. Confirmation of these findings will require clinical trials testing different treatment sequences.

Previous work by others has implicated increased activation of the mitogen-activated protein kinase 1 (MAPK1)/ERK signaling pathway as a mechanism of acquired resistance to WZ4002, a similar mutant-specific EGFR TKI that never reached clinical development [150]. These authors showed that WZ4002 in combination with a MAP-ERK kinase (MEK) inhibitor was sufficient to overcome WZ4002 resistance. Similarly, our ongoing studies of AZD9291 resistance mechanisms implicate MAPK pathway dysregulation (Eberlein et al, manuscript under review), with potential re-sensitization through combined EGFR and MEK inhibition. Clinical testing of such findings will further inform sequential treatment regimens with these therapies.

This study addresses critical and timely questions for patients with EGFR-mutant lung cancer but may also be applicable to oncogene-driven tumor types in general. *In vitro* preclinical studies in chronic myelogenous leukemia (CML) have shown that the order and concentration of treatment with dasatinib or nilotinib following imatinib resistance has an effect both on the specific resistance mutations that emerge in the target fusion kinase BCR-ABL and on the sensitivity to subsequent targeted therapies [197]. Similarly, recent studies indicate that metastatic prostate cancer with acquired resistance to first-generation anti-androgens maintain reliance on androgen receptor signaling for survival [198] and are sensitive to subsequent therapy with second-generation anti-androgens such as enzalutamide. However, enzalutamide resistance can be mediated by 'bypass' induction of the glucocorticoid receptor, suggesting that enzalutamide-resistant

tumors have escaped dependence on the androgen receptor for survival and that subsequent anti-androgen therapies may be ineffective for such patients [199]. Together with our findings in EGFR mutant lung cancer, the studies in CML and prostate cancer highlight the fact that as multiple lines of targeted therapies are utilized with increasing frequency in the clinic, a thorough understanding of the molecular determinants of sensitivity and resistance of tumors to sequential treatment will be critical in order to maximize benefit to patients.

## **Materials and methods**

### ***Cell lines***

All cell lines utilized in these studies were authenticated via routine genotyping for known EGFR kinase mutations. Cell lines were kept in continuous culture for no more than 8 weeks and were routinely tested for mycoplasma contamination to ensure accuracy of experimental data. Cells were cultured in RPMI + L-glutamine (Corning) and supplemented with 10% heat-inactivated fetal bovine serum (Atlanta Biologicals) and 1% penicillin/streptomycin (Corning) and grown in a humidified incubator with 5% CO<sub>2</sub> at 37C. EGFR-mutant cell lines PC-9, HCC827, and H1975 have been maintained in the Pao laboratory since 2004. Isogenic resistant cell lines were derived in the lab as described previously and in this manuscript [155]. Briefly, parental cells were cultured with increasing concentrations of TKI starting at the IC<sub>30</sub>. All resistant cells were maintained in drug, and TKI was refreshed every 72 hours.

### ***Derivation of VP-2 cell line***

VP-2 cells were derived from a 70 year-old male never smoker patient who first received 2 cycles of carboplatin/paclitaxel/bevacizumab chemotherapy before starting on erlotinib. He experienced a partial response on erlotinib, with acquired resistance occurring after 18 months. He then received one month of afatinib, with no response, at which time he developed a large pleural effusion which was tapped. Pleural fluid was obtained with informed consent on an IRB-approved protocol (THO-0547). After pelleting the cells and washing 3x in sterile PBS, red blood cells were lysed in ACK buffer (Lonza INC, Allendale, NJ). After lysis, the remaining cell pellet was washed 3x in sterile PBS. The remaining mixture of cells was then distributed into 10cm dishes. Cells were cultured in RPMI supplemented with 10% heat inactivated fetal bovine serum and penicillin-streptomycin as described above. The medium was changed every 1-3 days for approximately 3 months. To verify that the established cell line (named VP-2) harbored EGFR mutations, we performed direct sequencing.

### ***Immunoblotting***

Resistant cells were removed from drug selection 72 hours before immunoblotting experiments. Cells were washed on ice with cold PBS and lysed in radioimmunoprecipitation (RIPA) buffer (250mM Tris-HCl pH 7.5, 75mM NaCl, 1% NP-40/IGEPAL, 0.1% sodium dodecyl sulfate) supplemented with complete protease inhibitor cocktail (Roche), 40mM sodium fluoride, 1mM sodium orthovanadate, and 1  $\mu$ M okadaic acid. Lysates were subjected to SDS-PAGE (4-12% gels) followed by immunoblotting with the indicated antibodies and detection

by Western Lightning ECL reagent (Perkin-Elmer). The following antibodies were obtained from Cell Signaling Technologies: phospho-ERK (T202/Y204; 1:1000; #9101), ERK (1:1000, #9102), phospho-AKT (S473; 1:500; #9271), AKT (1:1000; #9272), phospho-S6 (S240/244; 1:1000; #2215), S6 (1:1000; #2217), BIM (1:1000; #2819), HRP-conjugated anti-mouse (1:3000; #7076), and HRP-conjugated anti-rabbit (1:3000; #7074). Phospho-EGFR antibody was obtained from Abcam (Y1068; 1:1000; #EP774Y), EGFR from BD Transduction Laboratories (1:500; #610017), and actin from Sigma-Aldrich (1:3000; #A2066). Phospho-RTK arrays were purchased from R&D Systems (#ARY001B), and assays were run on cells maintained in 10% FBS using the manufacturer's protocol.

### ***Xenograft studies***

Nude mice (*nu/nu*; Harlan Laboratories) used for *in vivo* studies were cared for in accordance with guidelines approved by the Memorial Sloan-Kettering Cancer Center (MSKCC) Institutional Animal Care and Use Committee and Research Animal Resource Center (New York, NY). Eight-week-old female mice were injected s.c. with 10 million PC-9/BRc1, PC-9/BRc1/V7, PC-9/BRc1/A+CR6, and PC-9/BRc1/A+CR7 cells. When tumors reached approximately 150mm<sup>3</sup>, animals were randomized to receive vehicle, the combination of afatinib [25 mg/kg p.o. qd] and cetuximab [50mg/kg i.p. twice per week], or AZD9291 [5mg/kg or 10mg/kg p.o. qd], as indicated. Mice were observed daily for signs of morbidity/mortality. Tumors were measured twice weekly using calipers, and volume was calculated using the formula: length x width<sup>2</sup> x 0.52. Body weight was

also assessed twice weekly. Tumor samples were collected within 8 hours of the last treatment. Portions of each extracted tumor were preserved in 4% paraformaldehyde, flash-frozen in liquid nitrogen, or minced and placed fresh into culture medium for derivation of cell lines.

### ***Soft agar assays***

Colony formation of PC-9, PC-9/AZR, PC-9/ERc1, and PC-9/ERc1/AZR cells was assessed using the CytoSelect 96-Well *In Vitro* Tumor Sensitivity Assay (Soft Agar Colony Formation) kit purchased from Cell BioLabs, Inc. (# CBA-150), according to the manufacturer's protocol. Briefly 50  $\mu$ L of base agar matrix was dispensed into each well of a 96-well tissue culture plate. 5,000 cells in 75  $\mu$ L of cell suspension agar matrix were dispensed into each well, and 50  $\mu$ L of culture medium was added to each well, containing various drugs as indicated. Fresh medium with drugs was added every 72 hours. After 10 days of incubation, the matrix was solubilized, and MTT reagent was added to each well. The absorbance was measured on a SpectraMax fluorometer at 570nm.

### ***Histology***

Xenograft tumors were fixed in 4% paraformaldehyde (PFA) overnight at room temperature, placed in 70% ethanol and sent to Histoserv, Inc. for paraffin embedding and sectioning. 5 $\mu$ m sections were used for hematoxylin and eosin (H&E) staining.

### ***Growth inhibition assays***

Short-term (72h) cellular growth inhibition was measured with CellTiter Blue Reagent (Promega, #G8081) according to the manufacturer's instructions using cells plated in hexuplicate at a density of 3,000 cells per well. Fluorescence was measured on a SpectraMax fluorometer, and growth inhibition was calculated as percentage of vehicle-treated wells. For longer-term cellular growth inhibition assays, 3,000 cells/well were plated in 24-well plates and treated with indicated drug combinations. Media and inhibitors were refreshed every 72 hours, and cells were grown for 10 days or until confluence in untreated wells. Cells were fixed and stained in 20% methanol with .025% crystal violet and washed with water. Dried plates were imaged and staining intensity quantified on the LI-COR Odyssey.

### ***FISH Analysis***

Cells were grown in RPMI 1640 with 10% FBS to ~70% confluence, then harvested and fixed in crayon fixative (methanol:acetic acid = 3:1) for FISH analysis. FISH analysis was performed using the EGFR/CEP7 dual-color probe set from Abbott Molecular and following the protocol from Vysis/Abbott Molecular with a few modifications. In brief, the probe targeting EGFR gene was labeled with SpectrumOrange (red), and chromosome 7 centromere probe (CEP7) was labeled with SpectrumGreen (green); nuclei were counterstained with DAPI (blue). FISH signal scoring and capture were performed by Fluorescence microscope (Zeiss)

coupled with ISIS FISH Imaging System (Metasystems). Two hundred interphase cells showing optimum hybridization signals were scored.

### ***EGFR cDNA sequencing***

Total RNA was extracted from TKI-sensitive and resistant cell lines using the RNeasy mini kit (Qiagen, Germantown, MD). *EGFR* cDNA was generated via SuperScript III one-step RT-PCR system with platinum Taq DNA polymerase (Invitrogen, Carlsbad, CA). Gene-specific primers (GSPs), *EGFR*-cDNA-F (5'-CCCCTGACTCCGTCCAGTAT -3') and *EGFR*-cDNA-R (5'-TGGCTAGTCGGTGTAACGT-3') were used in the system to amplify the entire *EGFR* cDNA. To sequence through the whole fragment, several other primers were also designed for dideoxynucleotide sequencing, ***EGFR-cDNA-w1-F*** (5'-GCAGTGACTTTCTCAGCAACA -3'), ***EGFR-cDNA-w2-F*** (5'-GAAATCATACGCGGCAGGAC -3'), ***EGFR-cDNA-w3-F*** (5'-TGGAGCCTCTTACACCCAGT -3'), and ***EGFR-cDNA-w4-F*** (5'-ATAGTCGCCCAAAGTTCCGT -3').

### ***Amplicon-based targeted next-generation sequencing***

Using Illumina's online Design Studio, we generated amplicon probes for use with the Illumina MiSeq platform against all exons of selected genes allowing an extension of 25 bases into the introns on either side of each exon. Amplicon probes were designed not to avoid common single-nucleotide polymorphic (SNP) regions, because some somatic SNPs are often included in genomic SNP

databases (for example, EGFR c.2369C>T, p.T790M in lung cancers resistant to first-line EGFR therapy is deposited in the dbSNP database, SNP ID: rs121434569) but are still important for biological function.

### ***Next-generation sequencing analysis***

Raw paired-end sequencing reads in FASTQ files were evaluated for quality using the FastQC tool v1.10.1 (<http://www.bioinformatics.bbsrc.ac.uk/projects/fastqc/>) and aligned to the human reference genome (UCSC hg19) using BWA-MEM algorithm v0.7.8 [200] with default parameters. Duplicated reads were removed using Picard MarkDuplicates tool v1.88 (<http://picard.sourceforge.net>). Next, to improve SNP and indel detection, the aligned reads were improved using the local realignment and base quality score recalibration procedure following the GATK (v2.5-2) Best Practices recommendations [201, 202]. The analysis-ready reads from a pair of drug-resistant versus sensitive cell lines were then used to call mutations unique to resistant cell lines using MuTect v1.1.4 [203] with default parameters. All SNVs passed the default filters of MuTect and SNVs flagged for clustered read position filter were included in our final list of MuTect calls. A variant was preserved if <2 reads supported the variant allele in the normal sample, its average base quality was > 30, it was not a strand bias artifact, and its log-odd score calculated by MuTect was > 6.3. We removed known SNPs included in dbSNP build 137 [204]. Variant annotation was performed using ANNOVAR tool (v2013-5-9) [205].

### ***Statistical analysis***

Quantification of crystal violet assays, soft agar assays, and xenograft data are presented as means  $\pm$  SD. The Wilcoxon rank sum test was used for (pairwise) group comparisons. All p values are nominal, without adjusting for the study-wise type I error rate. All analyses are conducted using R software version 3.0. unless indicated specifically.

## **Chapter IV: Acquired resistance to mutant-selective EGFR inhibitor AZD9291 is associated with increased dependence on RAS signaling in preclinical models**

Adapted from: Catherine A. Eberlein, Daniel Stetson, Aleksandra A. Markovets, Katherine J. Al Kadhimi, Zhongwu Lai, Paul R. Fisher, **Catherine B. Meador**, Paula Spitzler, Eiki Ichihara, Sarah J. Ross, Miika J. Ahdesmaki, Ambar Ahmed, Laura E. Ratcliffe, Elizabeth L. Christey O'Brien, Claire H. Barnes, Henry Brown, Paul D. Smith, Jonathan R. Dry, Garry Beran, Kenneth S. Thress, Brian Dougherty, William Pao and Darren A. E. Cross. (2015) Acquired resistance to mutant-selective EGFR inhibitor AZD9291 is associated with increased dependence on RAS signaling in preclinical models. *Cancer Res* [epub] April 13.

### **Introduction**

Tumors containing activating epidermal growth factor receptor mutations (EGFRm) (e.g. deletion in exon 19 or an L858R point mutation) account for about 20% of advanced non-small-cell lung cancer (NSCLC) [206]. Although these mutations also sensitize EGFR to inhibition by the established tyrosine kinase inhibitor (TKI) therapies erlotinib and gefitinib [84], almost all tumors will develop acquired resistance to these TKIs within 9-15 months [44, 48]. In approximately 60% of cases, this acquired resistance is associated with an additional T790M mutation in EGFR [2, 4, 122]. As there are currently no treatments approved for patients with these tumors [49, 207] new EGFR TKIs such as AZD9291, WZ4002 and CO-1686 are being developed which inhibit both EGFRm and T790M mutations in preclinical models [146, 149, 193]. AZD9291 and CO-1686 have also shown promising Phase 1 activity in patients with T790M advanced NSCLC who have progressed while on prior therapy with an EGFR-TKI [147, 149]. These new

TKIs may also provide treatment options in the TKI-naive setting for patients with advanced EGFRm NSCLC. However, despite the potential improvements from therapy with these TKIs, experience with targeted agents suggest that resistance to these drugs may also emerge and potentially limit their effectiveness. Therefore identification of resistance mechanisms is important to drive new therapeutic strategies for treating drug resistance in patients. *In vitro*, EGFRm cells chronically exposed to escalating doses of gefitinib or erlotinib acquire clinically relevant resistance mechanisms [208, 209], and subsequent studies have identified a range of further potential resistance mechanisms [150, 210-214]. Although the clinical importance of many of these mechanisms remains to be determined, trying to predict acquired resistance, especially to new emerging agents such as AZD9291, is a critical area of research. To date, resistance mechanisms have typically been determined from single clonal lines selected from resistant populations of cancer cells and therefore may represent only a small percentage of the original cancer cell population. Since human NSCLC samples are heterogeneous [215-217] and tumors are likely to derive acquired resistance through multiple mechanisms, we postulated that it may be better to take a population approach to understanding the diversity and interplay of resistance mechanisms. We studied multiple cell populations resistant to gefitinib, afatinib, WZ4002 or AZD9291 to identify predominant mechanisms of resistance and to investigate signaling pathways activated by various resistance mechanisms.

## Results

### ***Generation of EGFR mutant cell populations resistant to AZD9291 and other EGFR TKIs***

To carry out a broad investigation into acquired resistance to EGFR inhibitors, we generated in parallel multiple EGFRm (PC9; Ex19del. chosen as a validated cell line for modeling EGFR inhibitor resistance [155]) and EGFRm/T790M (PC9 derivatives and NCI-H1975; L858R/ T790M) cell populations with induced resistance to gefitinib, afatinib, WZ4002 or AZD9291, using either a dose escalation method or by culturing the cells in a single dose of AZD9291 (**Appendix Table 23**).

### ***Resistance to AZD9291 and other EGFR TKIs is often associated with increased sensitivity to MEK inhibition***

To investigate whether the survival of resistant populations was through activation of alternative signaling pathways that circumvent EGFR dependency, we used a diverse panel of small molecule inhibitors representing key signaling pathways or emerging resistance mechanisms (**Appendix Table 24**). The ability of each agent, in the presence of originating EGFR TKI, to inhibit cell growth was measured using an in vitro phenotypic assay, and IC<sub>50</sub> values determined following 72 hours treatment (**Table 11; Appendix Table 25**). It was striking that 13 of 28 PC9 resistant populations and 2 of 4 NCI-H1975 resistant populations were greater than 5 times more sensitive to the MEK inhibitor selumetinib in combination with the originating EGFR inhibitor, when compared to the

corresponding parental cells treated with selumetinib. We therefore focused subsequent studies on understanding mechanisms of selumetinib sensitivity in these populations. To confirm that increased selumetinib sensitivity was related to RAS-MAPK pathway inhibition, phosphorylation levels of ERK1/2 and MEK1/2 were analyzed by immunoblotting PC9 parental and resistant populations grown in the presence of EGFR inhibitor and treated with increasing concentrations of selumetinib. Resistance to selumetinib in the PC9, PC9 GR\_4 and PC9 GR\_5 cells was associated with a strong induction of phosphorylated MEK and weaker inhibition of ERK phosphorylation when compared to the effects of selumetinib in the sensitive cell populations, PC9 GR\_2 and PC9 AZDR\_4 (**Figure 13A**). The dependency of EGFR resistant cell populations on RAS-MAPK activity was further analyzed using PC9 WZR\_1 cells which showed > 5 fold increased sensitivity to selumetinib (**Table 11**). Consistent with PC9 GR\_2 and AZDR\_4 populations, WZR\_1 cells maintained in presence of WZ4002 demonstrated expected inhibition of phosphorylated EGFR, and phosphorylated ERK (**Figure 13Bi**) and growth inhibition (**Figure 13C**) were highly sensitive to selumetinib treatment. In contrast, WZR\_1 cells that had been cultured in the absence of WZ4002 displayed an EGFR and selumetinib ERK sensitivity profile similar to that seen in PC9 parental cells, namely, weak inhibition of ERK phosphorylation and strong induction of pMEK (**Figure 13A, Figure 13Bii**) with associated growth inhibition refractory to selumetinib (**Figure 13C**). The strong increase in levels of phosphorylated MEK1/2 in response to selumetinib treatment in the resistant compared to the sensitive populations (**Figure 13A, Figure 13Bi**) suggests a difference in pathway activity upstream of MEK between sensitive and resistant populations in response to relief of negative feedback loops upon MEK inhibition.

Table 11. IC<sub>50</sub> (μM) values from cell growth inhibition assays comparing compound sensitivity between parental and resistant cell populations.

Cell population	Genetic alterations detected within resistant populations	selumetinib (MEK1/2)	AZD9291 (EGFR)
PC9		6.95 (±2.5)	0.008 (±0.002)
PC9 GR_1	EGFR T790M / KRAS gain (2.44 fold)	7.24 (±3.2)	1.12 (±0.5)
PC9 GR_2	NRAS E63K	0.62 (±0.3)	2.8 (±0.4)
PC9 GR_3	EGFR T790M	6.2 (±3.6)	0.18 (±0.2)
PC9 GR_4	EGFR T790M	7.32 (±2.3)	0.02 (±0.01)
PC9 GR_5	EGFR T790M	8.77 (±1.5)	0.14 (±0.06)
PC9 GR_6	EGFR T790M	7.44 (±2.6)	0.005 (±0.001)
PC9 GR_7	EGFR T790M	3.7 (±0.99)	0.002 (±0.002)
PC9 GR_8	EGFR T790M / KRAS gain (2.82 fold)	2.48 (±1.4)	2.40 (±0.97)
PC9 AR_1	KRAS gain (4.62 fold)	2.7 (±0.23)	2.41 (±0.5)
PC9 AR_4	EGFR T790M	1.63 (±1.1)	0.73 (±0.3)
PC9 AR_6	NRAS gain (2.08 fold)	0.89 (±0.6)	2.4 (±0.5)
PC9 WZR_1	NRAS Q61K	0.23 (±0.04)	1.99 (±0.03)
PC9 WZR_3	KRAS gain (1.4 fold)	0.22 (±0.1)	1.65 (±0.5)
PC9 AZDR_1	NRAS gain (1.32 fold) / MAPK1 gain / CRKL gain	0.25 (±0.06)	2.3 (±0.9)
PC9 AZDR_2	NRAS G12V	1.4 (±0.9)	3.69 (±1.2)
PC9 AZDR_3	MAPK1 gain / CRKL gain	2.38 (±0.9)	1.94 (±0.5)
PC9 AZDR_4	ND	0.19 (±0.1)	2.48 (±1.1)
PC9 AZDR_5	NRAS E63K	0.17 (±0.05)	2.14 (±0.06)
PC9 AZDR_6	NRAS E63K	0.11 (±0.03)	1.6 (±0.02)
PC9 AZDR_7	NRAS G12R	0.14 (±0.03)	2.63 (±0.3)
PC9 GR_1_AZDR_1	EGFR T790M / KRAS gain (2.64 fold)	3.6 (±0.7)	2.4 (±0.95)
PC9 GR_1_AZDR_2	KRAS gain (2.5 fold)	6.7 (±1.4)	2.7 (±1.2)
PC9 GR_1_AZDR_3	EGFR T790M / KRAS gain (2.15 fold)	3.4 (±0.5)	2.4 (±0.7)
PC9 GR_1_AZDR_4	EGFR T790M / KRAS gain (2.45 fold)	3.6 (±2.6)	2.6 (±0.9)
PC9 GR_6_AZDR_1	ND	0.28 (±0.2)	1.35 (±0.05)
PC9 GR_6_AZDR_2	NRAS gain (1.27 fold)	0.54 (±0.3)	2.24 (±0.6)
PC9 GR_6_AZDR_3	NRAS gain (1.88 fold)	0.13 (±0.06)	1.48 (±0.3)
PC9 GR_6_AZDR_4	ND	0.73 (±0.5)	1.74 (±0.8)
NCI-H1975	EGFR T790M	4.94 (±3)	0.016 (±0.01)
NCI-H1975 AZDR_1	EGFR T790M	0.024 (±0.003)	2.52 (±0.4)
NCI-H1975 AZDR_2	EGFR T790M	0.15 (±0.1)	2.21 (±0.2)
NCI-H1975 AZDR_3	EGFR T790M	>10	3.04 (±0.4)
NCI-H1975 AZDR_4	EGFR T790M / NRAS Q61K	5.46 (±3.7)	2.67 (±0.7)

represents cell lines which are at least 5 fold more sensitive to selumetinib than in the relevant parental cell line.

represents cell lines which are at least 5 fold less sensitive to AZD9291 than in the relevant parental cell line.

Cells were treated with dose titrations of indicated inhibitors alone for parental cells and in the presence of original EGFR inhibitor for resistant populations. IC<sub>50</sub> values represent an average of at least 2 independent experiments. Errors are standard deviation. Additional compound data is shown in **Appendix Table25**. DNA from resistant populations was analysed for gene mutation and/or gene copy number across a panel of cancer associated genes. Data represents genetic alterations detected in the resistant populations. Fold gain is indicated in brackets for *NRAS* and *KRAS*. ND = Non detected



**A-B**, Cells cultured in the presence or absence of originating EGFR inhibitor as indicated were dosed with titrations of selumetinib for 6 hours. Lysates were analysed by immunoblotting. Data is representative of 2 separate experiments. **C**, WZR\_1 cells cultured in the absence of WZ4002 prior to the experiment were treated with titrations of selumetinib over 96 hours with no added WZ4002, 0.03  $\mu$ M or 0.3  $\mu$ M WZ4002. Data is representative of two separate experiments.

### ***Comparison of genetic alterations across multiple populations of EGFRm or EGFRm/T790M cells resistant to AZD9291 and other EGFR TKIs***

In order to investigate the molecular drivers of EGFR TKI resistance we analyzed DNA samples prepared from parental and a selection of 32 resistant populations (**Appendix Table 23**) for the presence of gene mutations and/or copy number changes across a panel of cancer associated genes using multiple assay platforms. The genetic modifications detected and associated allele frequencies for PC9 and NCI-H1975 populations are summarized in Table 11 and (**Appendix Figure 37**). Each mutation detected was confirmed across at least 2 different assay platforms (**Appendix Table 26**). Across the PC9 populations, 7/8 gefitinib- and 2/3 afatinib-resistant populations had detectable T790M mutations, whereas none of the populations resistant to the WZ4002 or AZD9291 had acquired a detectable T790M mutation (**Table 11**). The T790M gefitinib-resistant populations mostly showed sensitivity to AZD9291, with dose response curves indicating almost all cells in populations PC9 GR\_4, 6 and 7 were sensitive to AZD9291 (**Appendix Figure 38Ai**). However, less than 50% of cells in populations PC9 GR\_1 (T790M, KRAS gain 5.43 fold), PC9 GR\_3 (T790M) and PC9 GR\_5 (T790M) were sensitive to growth inhibition by AZD9291 (**Appendix Figure 38Aii**), suggesting these populations contained heterogeneous resistant mechanisms. The IC<sub>50</sub> values across all AZD9291-sensitive cells were similar (**Appendix Figure 38B**). Although T790M was detected within the PC9 GR\_8 (T790M, KRAS gain 7.06 fold) population, these cells showed no sensitivity to AZD9291 (**Appendix Figure 38Aiii**), suggesting that the entire population contained resistant clones. This observation of heterogeneous mechanisms of

resistance to gefitinib within populations is consistent with the clinical setting, supporting use of this population approach for understanding resistance dynamics. Notably, PC9 resistant cell populations lacking detectable T790M frequently displayed increased sensitivity to selumetinib in combination with EGFR inhibition. In selumetinib-sensitive EGFRm/T790M populations with induced resistance to EGFR inhibitors, no additional EGFR mutations were detected. This suggests that RAS/MAPK signaling was important for driving resistance in the absence of EGFR signaling (**Table 11**). Interestingly, a number of different NRAS alterations were observed in PC9 populations resistant to AZD9291, gefitinib and WZ4002, and NCI-H1975 cells resistant to AZD9291 (**Table 11**). Notably, we observed a novel non-canonical E63K mutation in NRAS in the only gefitinib-resistant T790M-negative PC9 population and in two AZD9291-resistant PC9 populations (**Table 11; Appendix Figure 39**). This novel NRAS mutation occurs within the functional domain at a sequence position parallel to somatic mutations observed in both KRAS [218] and HRAS [219]. We also identified functionally activating NRAS G12V and G12R mutations in 2 different AZD9291-resistant PC9 populations (**Table 11**). This is the first identification of G12V NRAS in the context of NSCLC. In addition to gene mutations, copy number gains of MAPK1, CRKL, NRAS and KRAS were detected across the resistant populations (**Table 11**), with the gain of NRAS and KRAS resulting in increased protein levels (**Appendix Figure 40**). Of particular interest, KRAS gain was observed in the T790M PC9\_GR\_1 population that was partially sensitive to AZD9291 (**Table 11**), suggesting KRAS contributes to the heterogeneous mechanisms of resistance to gefitinib within this population. Indeed, 4 separate AZD9291-resistant populations of PC9 GR\_1 cells were subsequently generated and KRAS gain was retained within each resistant

population (**Table 11**). Interestingly, although T790M was still present in populations PC9 GR1\_AZDR\_1, 3 and 4, T790M was no longer detectable in PC9 GR1\_AZDR\_2 cells.

### ***Modifications of RAS genes can drive resistance to EGFR inhibition***

As NRAS mutations were detected in 7 of the resistant populations and were frequently associated with selumetinib sensitivity, its role in resistance was further investigated. Basal levels of active NRAS were lower in parental PC9 cells compared to resistant PC9 populations in which an E63K, G12V, (**Figure 14A**) E63K or Q61K (**Appendix Figure 40**) NRAS mutation had been detected. Treatment of parental PC9 cells with 160nM AZD9291 decreased levels of phosphorylated EGFR and active NRAS. In contrast, in mutant NRAS cells, a decrease in phosphorylated EGFR was not associated with corresponding decrease in active NRAS, suggesting constitutive activation of NRAS disconnected from EGFR in these cells (**Figure 14A; Appendix Figure 41A**). In transient exogenous expression in PC9 cells, WT and mutant NRAS variants were activating (**Appendix Figure 41Bi,ii**) and prevented cell growth inhibition by either AZD9291 or gefitinib compared to control transfected cells (**Figure 14B**). Increased resistance to growth inhibition by AZD9291 was also observed in additional parental EGFRm cell lines similarly transfected with WT and activating mutant NRAS variants (**Appendix Figure 41C**). Knockdown of NRAS in cell populations with 3 separate siRNAs, but not KRAS, for 72 hours resulted in a significant decrease in phosphorylated ERK in the resistant populations harboring NRAS mutations, but to a lesser extent in the PC9 parental cells (**Figure 14C**).

Moreover, knockdown of NRAS but not KRAS was associated with inhibition of proliferation only in the NRAS mutant populations (**Figure 14D**). These data indicate that activating NRAS mutations including the novel E63K NRAS are sufficient to drive resistance to EGFR inhibition. Similarly knockdown of NRAS in the presence of AZD9291 caused a significant decrease in cell growth of PC9 GR\_6 AZDR\_2 (NRAS gain 2.4 fold) and PC9 GR\_6 AZDR 3 (NRAS gain 3.68 fold) populations (data not shown). As KRAS gain was detected within 8 resistant populations (**Table 11**), we determined whether this could similarly drive resistance. Knockdown of KRAS in PC9 parental cells had no effect on cell growth or levels of phosphorylated ERK (**Figure 14C**), whereas KRAS knockdown in PC9 AR\_1 (KRAS gain 24.6 fold), in the presence of afatinib, caused a significant decrease in both phosphorylated ERK levels after 48 hours (**Figure 15A**) and proliferation over 72 hours (**Figure 15B**). Interestingly, knockdown of KRAS in the PC9 GR\_1 (T790M and KRAS gain 5.43 fold) population, had no effect on cell proliferation alone or when treated in combination with gefitinib (**Figure 15C**). However a significant decrease in cell growth was observed when KRAS knockdown was combined with AZD9291 treatment (**Figure 15C**). Consistent with this, knockdown of KRAS in the presence of AZD9291 resulted in complete inhibition of phosphorylated ERK, but not in case of gefitinib (**Figure 15D**). These observations suggest that KRAS and T790M are both important for driving resistance in the PC9 GR\_1 population. Interestingly, we noted that a 2.64 fold gain of KRAS, as detected in WZR\_3 cells, was associated with increased sensitivity to selumetinib, but cell populations with KRAS gains of between 4.44 and 24.6 fold were insensitive to selumetinib (**Table 11**), suggesting a threshold effect of KRAS expression. Indeed, partial knockdown of KRAS for 48 hours in

AR\_1 cells (KRAS gain 24.6 fold) with afatinib re-sensitized them to selumetinib inhibition as revealed by decreased phosphorylated ERK, FRA1 and p90RSK levels compared to cells similarly treated with control siRNA (**Figure 15E**). Moreover partial knockdown of KRAS followed by treatment with selumetinib resulted in significantly greater inhibition of cell growth compared to cells treated with control siRNA (**Figure 15G**). By contrast, no significant increase in inhibition of MAPK pathway or cell growth was observed with partial knockdown of KRAS followed by selumetinib treatment in WZR\_3 cells (KRAS gain 2.64 fold) cultured in the presence of WZ4002 (**Figure 15F, 15H**). Interestingly selumetinib inhibition of MEK1/2 in AR\_1 cells resulted in enhanced pMEK1/2 levels compared to that observed in selumetinib sensitive WZR\_3 cells (**Figure 15E, 15F**). Collectively, this data is consistent with previous reports in which KRAS amplification in colon cells drives high levels of pathway output and ERK dependent negative feedback, relief of which upon MEK inhibition drives relative insensitivity to MEK inhibitors [133]. Similarly, we observed that enhanced exogenous expression of wild-type NRAS in PC9 AR\_6 cells (NRAS 4.23 fold gain) reduced the effectiveness of selumetinib treatment on phosphorylated ERK and growth inhibition compared to PC9 AR\_6 cells treated with control DNA (data not shown).

***In vitro a combination of AZD9291 with selumetinib delays or prevents resistance emerging in EGFRm and EGFRm/T790M cells***

Since the data had indicated that RAS-MAPK activation was a frequent mechanism of AZD9291 and other EGFR TKI resistance, we tested whether treatment with a combination of AZD9291 and selumetinib could delay or prevent

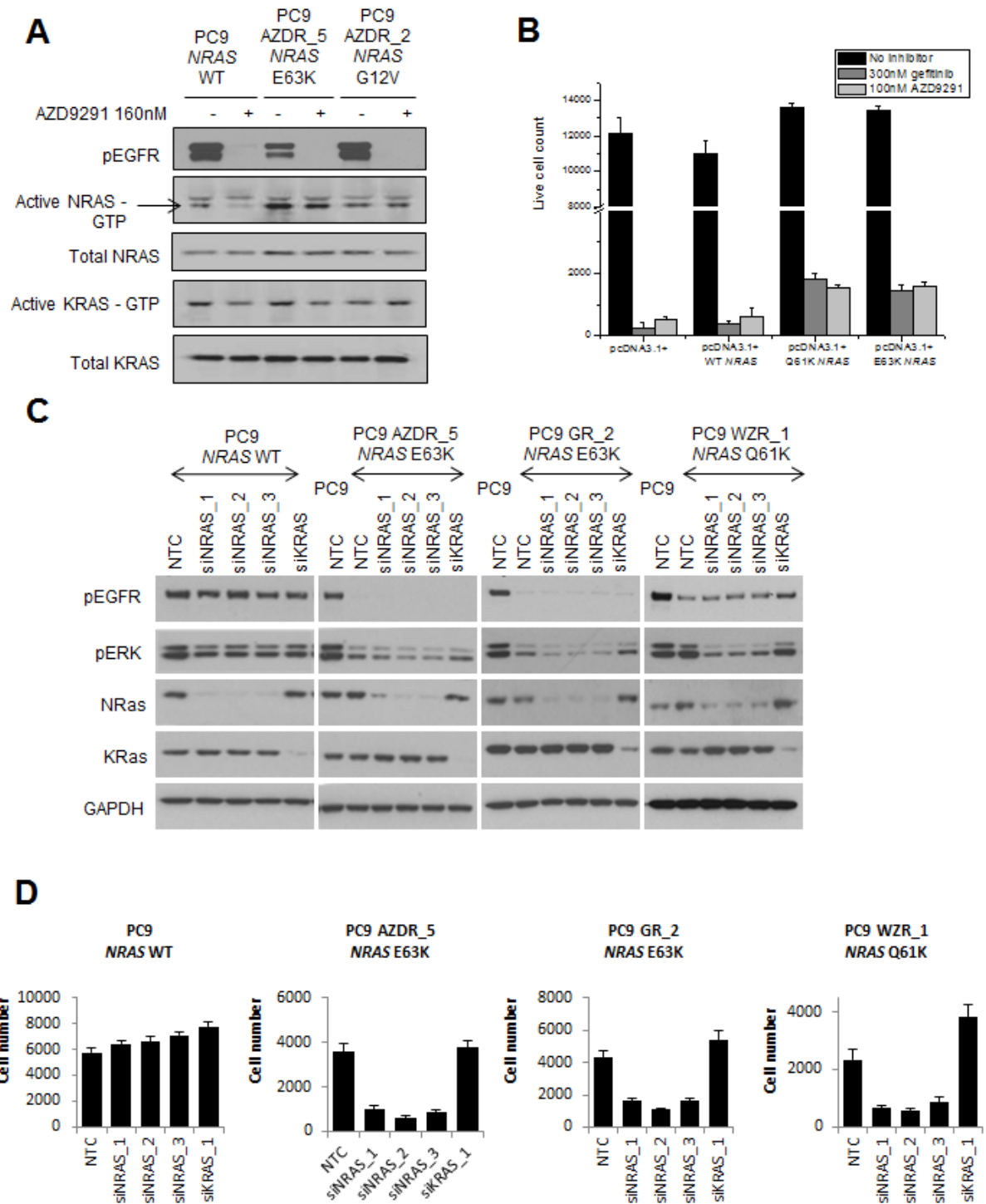


**Figure 14.** Determining the functional role of NRAS modifications in acquired resistance to EGFR inhibitors.

**A**, Resistant populations were cultured in media without EGFR inhibitor for 5 days prior to carrying out the assay. Lysates were prepared from parental and resistant cells serum starved overnight and treated for 6 hours +/- 160nM AZD9291. RAS activity was measured using RAS GTPase-specific pulldown assays. **B**, PC9 cells transfected with NRAS and control pcDNA 3.1+ constructs for 48 hours were treated with 100nM AZD9291 or 300nM gefitinib for a further 96 hours. Live cell number was determined by nuclei count. The data is representative of three separate experiments. Error bars are standard deviation. **C**, Resistant populations were cultured in media supplemented with EGFR inhibitor for all siRNA experiments. Lysates from cells treated with 20nM NTC, NRAS or KRAS siRNA for 48 hours were analyzed by immunoblotting. **D**, Cells treated for 72 hours with 20nM NTC, NRAS or KRAS siRNA were fixed and cell number determined by nuclei count. Data is representative of 3 replicate experiments. Error bars are standard deviation.

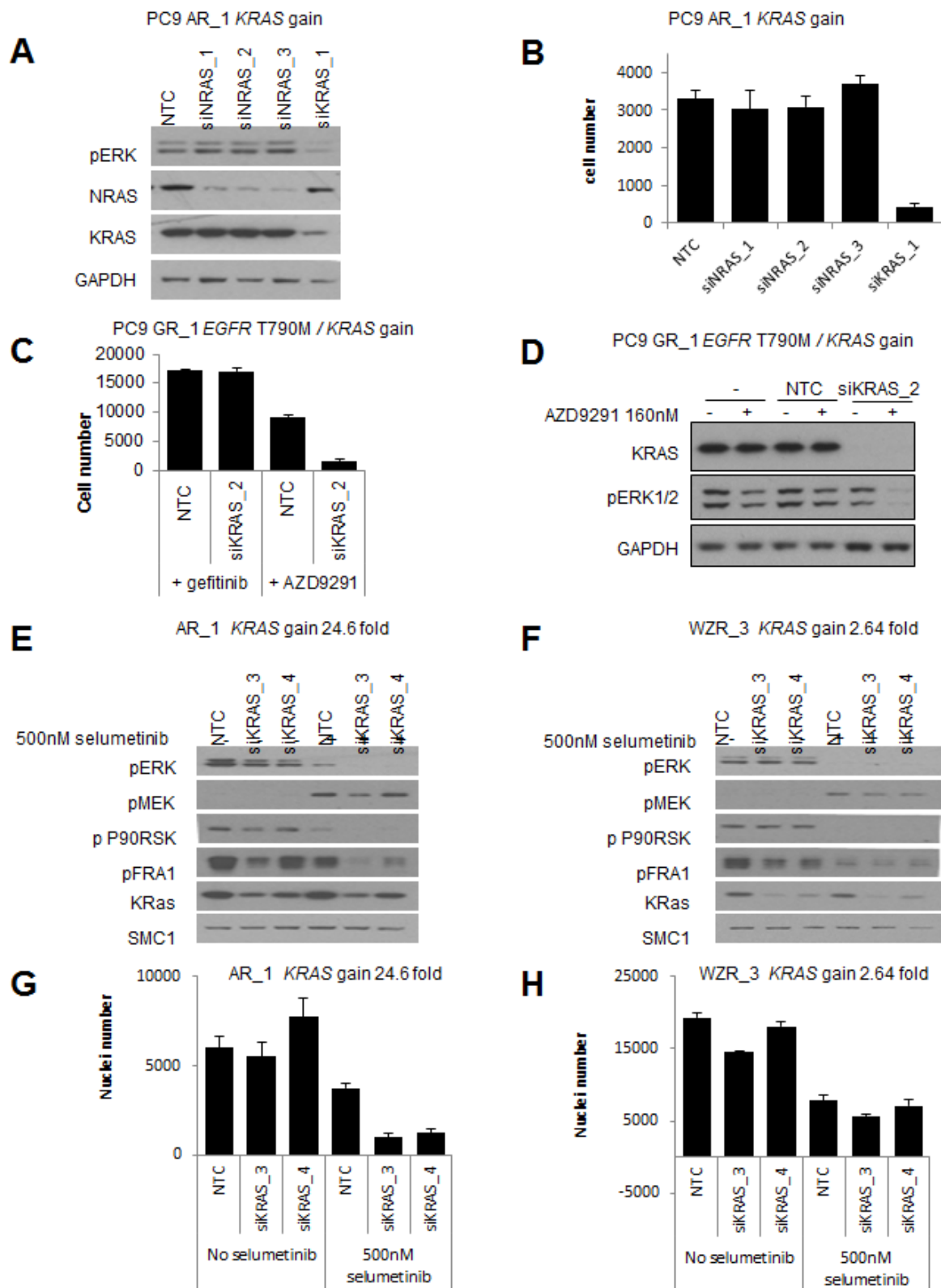


**Figure 15.** Determining the functional role of KRAS gain in acquired resistance to EGFR inhibitors.

**A**, Immunoblotting of PC9 AR\_1 (KRAS gain) cells grown in 1.5 $\mu$ M afatinib transfected with 20nM of NRAS, KRAS or control siRNA for 48 hours. **B**, PC9 AR\_1 (KRAS gain) cells grown in 1.5 $\mu$ M afatinib treated for 96 hours with 20nM of NRAS, KRAS or control siRNA. Cell number was determined by nuclei count. **C**, PC9 GR\_1 (EGFR T790M / KRAS gain) cells grown in 1.5 $\mu$ M gefitinib were transfected with 20nM of KRAS or control siRNA +/- 160nM AZD9291. After 4 days cell number was determined by nuclei count. Data shown is representative data. Error bars are standard deviation. **D**, Immunoblotting of PC9 GR\_1 cells, grown in media containing gefitinib, transfected with 20nM of KRAS or NTC siRNA for 5 days and then treated with 160nM of AZD9291 for 2 hours. **E**, Immunoblotting of PC9 AR\_1 (KRAS gain) cells grown in 1.5 $\mu$ M afatinib and **F**, WZR\_3 (KRAS gain) cells grown in 1.5 $\mu$ M WZ4002 transfected with 20nM of KRAS or control siRNA for 48 hours and then treated for 4 hours +/- 500nM selumetinib. **G**, PC9 AR\_1 (KRAS gain) cells grown in 1.5 $\mu$ M afatinib and (H) WZR\_3 (KRAS gain) cells grown in 1.5 $\mu$ M WZ4002 treated for 96 hours with 20nM of KRAS or control siRNA +/- 500 nM selumetinib. Cell number was determined by nuclei count.

the emergence of resistance in these settings. PC9 (EGFR<sup>m</sup>) cells were treated with 160nM AZD9291 or 100nM selumetinib alone or in combination. Selumetinib alone did not inhibit proliferation of PC9 cells (**Figure 16A**). Whereas resistant PC9 cells began to emerge after 34 days treatment with AZD9291, no resistant cells were observed over a similar time with a combination of AZD9291 and selumetinib (**Figure 16A**). To investigate the combination in the EGFR<sup>m</sup>/T790M setting, NCI-H1975 cells were treated with 160nM AZD9291 or 100nM selumetinib alone or in combination. Treatment with 100nM selumetinib alone did not inhibit proliferation of NCI-H1975 cells (**Figure 16B**). Treatment with AZD9291 initially slowed the rate of proliferation, however a small resistant population had emerged following 17 days of treatment (**Figure 16B**). Treatment with a combination of AZD9291 + selumetinib significantly delayed outgrowth of resistant cells compared to AZD9291 alone (**Figure 16B**). Similarly a combination of AZD9291 + selumetinib prevented emergence of resistance in 2 other cell lines, HCC827 (EGFR Ex19del) and NCI-H820 (EGFR Ex19del/T790M<sup>+</sup>/METamp) (**Appendix Figure 42A, B**). To further explore the EGFR<sup>m</sup>/T790M setting, PC9 GR<sub>1</sub> cells (T790M and KRAS gain) were treated with a combination of AZD9291 + selumetinib. Following treatment an increase in pro-apoptotic markers, cleaved PARP and BIM, and a decrease in anti-apoptotic Bcl-xL was observed together with a more profound effect on phosphorylated ERK levels than either agent alone (**Figure 16C**). Moreover the combined effect of inhibition of ERK signaling and apoptotic pathway was associated with a greater decrease in cell number over 12 days compared to either inhibitor alone (**Figure 16D**). Although combination of AZD9291 + selumetinib did not increase apoptotic markers in NCI-H1975 (**Figure 16E**), a profound anti-proliferative effect was observed following 12 days treatment

with the combination compared to each agent alone (**Figure 16F**). Overall these *in vitro* studies indicated that combining AZD9291 + selumetinib leads to more profound mechanistic and phenotypic inhibition of cells.

***In vivo a combination of AZD9291 + selumetinib caused regression of AZD9291 resistant tumors in transgenic models***

Finally, we tested the concept that MEK pathway inhibition could circumvent resistance to AZD9291 using *in vivo* mouse tumor models that develop lung adenocarcinomas driven by EGFR L858R + T790M or EGFR L858R [133] and are highly sensitive to inhibition by AZD9291 [147]. Animals with EGFR L858R + T790M transgenic tumors were chronically treated with 5 mg/kg/day AZD9291 and showed initial tumor regression followed by progressive disease after 3 months treatment (**Figure 17A**). Animals were subsequently treated with AZD9291 in combination with 5 mg/kg twice daily of selumetinib. Remarkably, resistant tumors in 3/6 animals showed a profound response to the combination, showing strong regression after 1-2 months of combination treatment (**Figure 17A**). Tumor regression was not observed when tumor-bearing EGFR L858R + T790M mice were treated with selumetinib alone for 1-2 weeks (**Figure 17B**). Similarly, an animal bearing an EGFR L858R tumor showed progression after 3 months of AZD9291 treatment, which regressed following combination of AZD9291 + selumetinib (**Figure 17C**). These data provide compelling *in vivo* evidence to support RAS-MAPK signaling dependency as an important resistance mechanism to AZD9291.

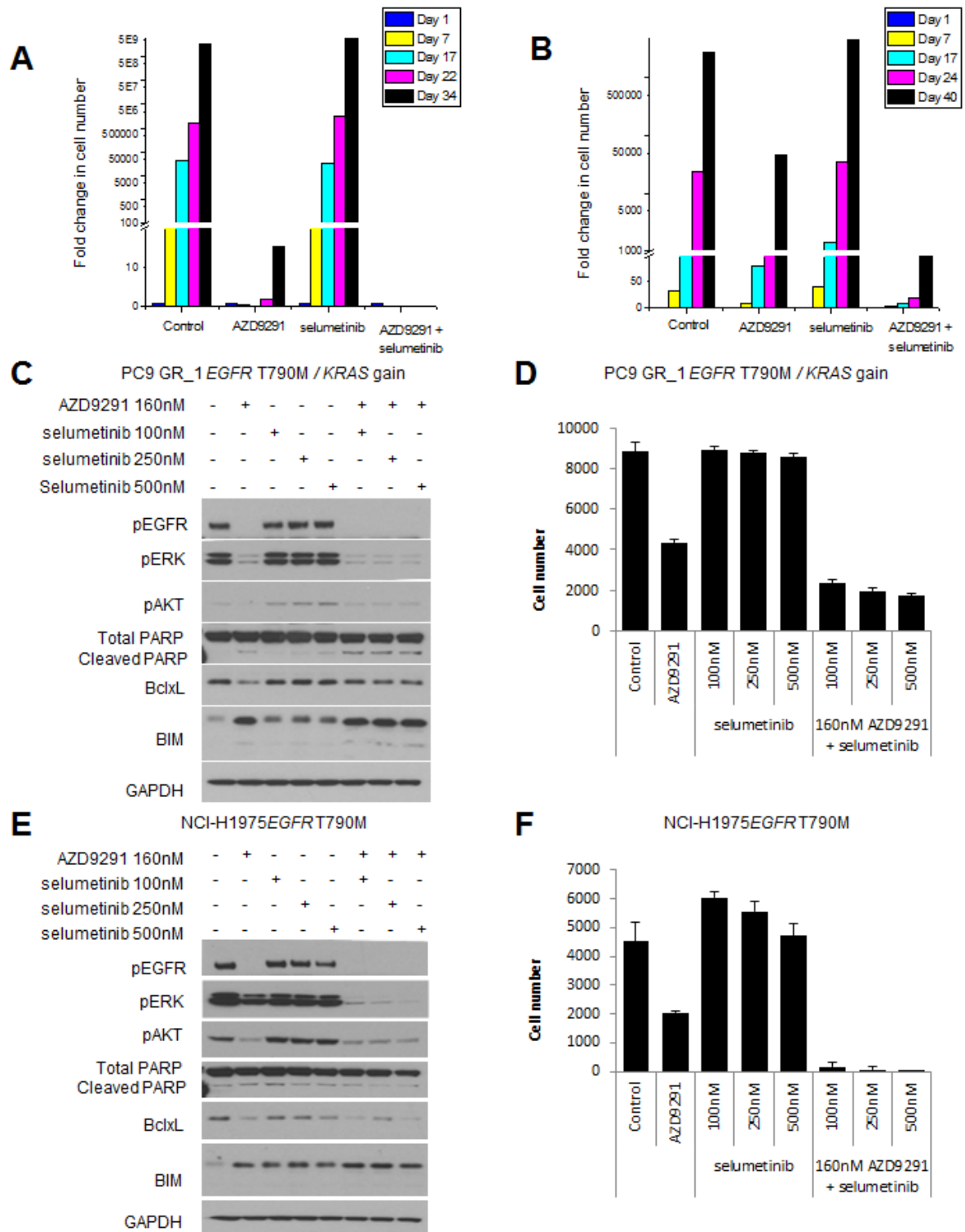
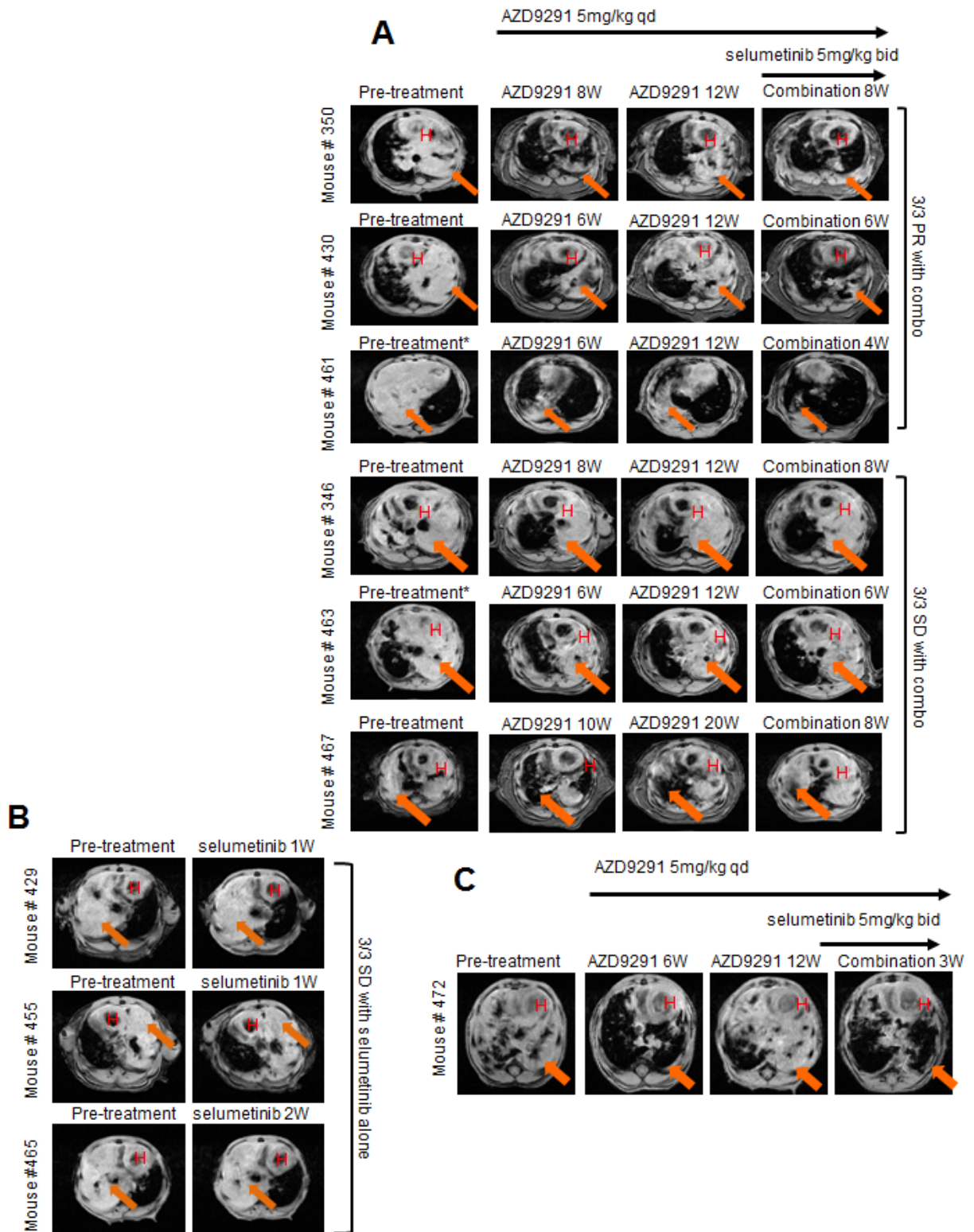


Figure 16. In vitro combination of AZD9291 with selumetinib induces more profound phenotype inhibition.

**A**, PC9 and **B**, NCI-H1975 cells were chronically treated for 34 days with DMSO, AZD9291, selumetinib or a combination of AZD9291 with selumetinib. Fold increase in cell number was monitored over time. Lysates from PC9 GR\_1 **C**, or NCI-H1975 **D**, cells treated with AZD9291 and selumetinib alone or in combination for 48 hours were analysed by immunoblotting. PC9 GR\_1 **E**, or NCI-H1975 **F**, cells were treated over 12 days with AZD9291 and selumetinib alone or in combination. Cells were fixed and cell number determined from nuclei count. Error bars represent standard deviation.



**Figure 17.** In vivo combination of AZD9291 and selumetinib can overcome acquired resistance to AZD9291 in mutant EGFR transgenic models of lung cancer.

**A**, MR images of lungs from tumor-bearing EGFR<sup>L858R</sup> + T790M transgenic mice pretreatment, after treatment with AZD9291 for 6-20 weeks (W) until progressive disease, and subsequently with the combination of AZD9291/selumetinib for 4-8 weeks. **B**, MR images of lung from tumor-bearing EGFR<sup>L858R</sup> + T790M mice pre- and post-treatment with selumetinib for 1-2 weeks (1W/2W). Combo, AZD9291/selumetinib; H, heart; arrow denotes tumor. **C**, MR images of lung from a tumor-bearing EGFR<sup>L858R</sup> transgenic mouse pretreatment, after treatment with AZD9291 for 6-12 weeks (W) until disease progression, and subsequently with the combination of AZD9291/selumetinib for 3 weeks (3W). \*Pretreatment images for mouse #461 and #463 were obtained after these mice received 4 weeks of low dose (1-2.5mg/kg) AZD9291 with no response, before being switched to 5mg/kg dosing.

### ***Basal levels of RAS-MAPK pathway components do not predict MEK inhibitor sensitivity across resistant populations***

We also explored whether the activity status of RAS-MAPK pathway could identify tumors that would benefit from combination of EGFR TKI with selumetinib. Unexpectedly, immunoblotting from parental and resistant populations revealed little correlation between basal ERK phosphorylation levels and selumetinib sensitivity (**Appendix Figure 40**). Consistent with this data, analysis of phosphorylated and total protein levels using a Reverse Phase Protein Array (RPPA), showed basal levels of phosphorylated ERK were not indicative of selumetinib sensitivity (**Appendix Table 23; Appendix Table 27**; see also Supplementary Table 5 from [1]). In conjunction with this, sensitivity to MEK inhibition was not consistently correlated with levels of other phosphorylated or total proteins known to be involved in RAS-MAPK signaling (**Appendix Table 27**; see also Supplementary Table 5 from [1]).

### **Discussion**

Significant advances in our understanding of acquired resistance to EGFR targeted drugs in EGFRm NSCLC, including but not limited to identification of T790M, MET or HER2 amplification and PIK3CA mutants [4], is helping towards the development of new rational treatment strategies to potentially prolong patient benefit such as AZD9291 and CO-1686 which target T790M. However, a large proportion of EGFR inhibitor acquired resistance remains unexplained, and it is

anticipated that cells will also find alternative mechanisms to circumvent inhibition by new agents such as AZD9291 and CO-1686.

We have used a novel approach by directly comparing resistance mechanisms across 32 populations with acquired resistance to different EGFR TKIs, and provide the first pre-clinical in-depth analysis of AZD9291 acquired resistance. We took a population approach to try to better emulate the heterogeneity of resistance that occurs in advanced tumors due to competing pressures on both selection of existing clones and gain of new alterations.

A key finding is identification of certain NRAS mutations or NRAS gain as the most frequently detected genetic modifications able to drive resistance to AZD9291. Although previous *in vitro* data has similarly identified an NRAS Q61K mutation in acquired resistance to gefitinib or erlotinib [137, 220], this is the first report of an NRAS activating mutation conferring acquired resistance to other EGFR inhibitors such as AZD9291. Furthermore this is the first report of the novel NRAS E63K mutation, and together with NRAS G12V, the first report of these NRAS mutations associated with EGFRm NSCLC. The high incidence of NRAS modifications was somewhat surprising in light of recent clinical data in which common NRAS mutations were not detected in lung cancers with acquired resistance to gefitinib or erlotinib [2, 137]. However, genetic alterations in NRAS have been associated with resistance to EGFR agents in other disease settings such as colorectal cancer [221, 222], raising the hypothesis that NRAS aberrations may become important in lung cancer too. Copy number changes were not analyzed in the previous studies, therefore the clinical relevance of NRAS copy number gain in lung cancer remains unknown. Using more extensive DNA

analysis a role for NRAS activation in EGFR TKI resistant EGFRm NSCLC may eventually emerge, and furthermore may only become more apparent as newer agents become established in clinical practice.

Despite the clinical prevalence of specific NRAS molecular alterations being unclear, it was notable how activation of RAS-MAPK signaling independent of EGFR activity was a common biological theme, although the precise molecular nature driving resistance remains unclear for a number of populations. Others have reported alternative mechanisms of resistance to EGFR TKIs associated with increased dependency on RAS-MAPK signaling including loss of NF1, CRKL amplification and EMT [5, 220, 223, 224]. In addition, amplification of MAPK1 was reported as a resistance mechanism to WZ4002 [150] and has been observed in PC9 AZD9291 resistant populations in the current study. Taken together, these studies suggest that activation of RAS-MAPK signaling independent of EGFR could be a frequent resistance mechanism for the TKIs currently in development, with multiple different aberrations converging on RAS-MAPK signaling. This mirrors other disease areas, where resistance mechanisms to EGFR targeting result in RAS-MAPK pathway activation by various mechanisms e.g. mutations in KRAS, NRAS and BRAF in colorectal cancer [221, 222] or over expression of RAS family in head and neck cancer [225] are associated with cetuximab resistance. Moreover, data presented here and by others [5, 150] support use of MEK inhibitors such as selumetinib in combination with new EGFR TKIs to overcome such acquired resistance mechanisms or potentially in earlier treatment as part of prevention strategies. Interestingly, our data support that this combination may provide benefit in both T790M and EGFRm TKI-naïve settings.

In addition to increased sensitivity to selumetinib across a number of the resistant populations, we also observed increased sensitivity to the Aurora kinase B inhibitor AZD1152-HQPA, in combination with AZD9291, in all of the AZD9291 resistant NCIH1975 populations compared to the parental cells (**Appendix Table 25**). This is consistent with recent reports [226] and is worthy of further investigation. Overall, the emerging pre-clinical evidence presented here supports a picture whereby during chronic exposure to AZD9291, competing selection pressures are likely to influence which clones within a heterogeneous population ultimately become dominant. This could also involve T790M clones becoming less prevalent within a tumor as other resistance clones become more dominant. Moreover, data from ourselves and others provide a compelling rationale for combining inhibitors of the RAS-MAPK signaling such as selumetinib with AZD9291 across EGFRm settings in NSCLC, to tackle RAS-MAPK as a potentially important escape mechanism within such clones. A key challenge will be to develop effective patient selection strategies to identify those patients who may benefit from such a combination. Emerging data suggest that multiple genetic and non-genetic alterations, including certain NRAS modifications reported here, could occur that converge on activating the RAS-MAPK pathway, and therefore it is possible that a broad biomarker platform will need to be established. It is important that measuring basal phosphorylation levels of ERK is unlikely to be sufficient to determine dependence on RAS-MAPK signaling or sensitivity to MEK inhibitors [227], thus more sophisticated predictive biomarker strategies will need to be developed. Future studies will determine how clinically prevalent these pre-clinical mechanisms will be, but these pre-clinical observations provide important insights to focus clinical translation efforts.

## **Materials and methods**

### ***Cell lines, cell culture and compound reagents***

All AstraZeneca cell lines were authenticated by short-tandem repeat analysis (STR). PC9 cells (obtained 2011, STR tested May 2013) were from Akiko Hiraide, Preclinical Sciences R&D AZ Japan. NCI-H1975 (CRL-5908, obtained 2004, STR tested Nov 2012), NCI-H820 (HTB-181, obtained 2011, STR tested Jan 2013) and HCC827 (CRL-2868, obtained 2012, STR tested Oct 2012) cells were obtained from ATCC. HCC-2279 (K72279, obtained 2013, STR tested Mar 2013) cells were obtained from KCLB. Cells were cultured in RPMI containing 10% FCS with 2 mmol/L glutamine, supplemented with EGFR inhibitor for resistant cell populations. Selumetinib, gefitinib, afatinib, WZ4002, BMS-536924, AZD5363, AZD2014, AZD8055, GDC-0941, AZD4547, AZD1152-HQPA and AZD9291 were synthesized according to published methods. AZ\_6592, AZ\_0012, AZ\_1902 and AZ\_9424 in house compounds (AstraZeneca).

### ***In vitro cell assays***

Phenotypic cell assays, immunoblotting and RAS activation assays were carried out as previously described [137, 147] and detailed in Supplementary Methods (Appendix 4 Materials and Methods). Cells were transfected using Lipofectamine RNAiMAX reagent, Invitrogen (Paisley, UK), FuGENE 6 Transfection Reagent, Promega (Madison, USA) or by electroporation, MaxCyte. siRNA and DNA constructs are detailed in Supplementary Methods (Appendix 4 Materials and Methods).

### ***Genetic analysis***

SnaPshot mutation analysis was carried out as previously described [68]. Targeted and whole exome sequencing (WES) were performed on MiSeq and HiSeq platforms, Illumina; Ion Torrent PGM platform, Life Technologies and by Sanger di-deoxy sequencing. Comparative genomic hybridization was performed using SurePrint G3 Human CGH microarrays, Agilent Technologies (Santa Clara, USA). Sequence data processing, mutation detection and gene copy number assessment were carried out as described in Supplementary Material (Appendix 4 Materials and Methods). Data is accessible in NCBI's Sequence Read Archive accession number SRP044079 and NCBI's Gene Expression Omnibus (GEO) accession number GSE59239.

### ***Transgenic mouse studies and MRI***

In vivo experiments were carried out as previously described using both EGFRL858R+T790M and EGFRL858R transgenic models [147]. Details are included in Supplementary Methods (Appendix 4 Materials and Methods).

## Chapter V: Mechanisms of resistance to combined EGFR/MEK inhibition in *EGFR*-mutant non-small cell lung cancer

Adapted from: **Catherine B. Meador**, Eiki Ichihara, Robert McEwen, Pengcheng Lu, Xi Chen, Cath Eberlein, Darren A. E. Cross, Christine M. Lovly, and William Pao. Mechanisms of resistance to combined EGFR/MEK inhibition in *EGFR*-mutant non-small cell lung cancer. *Manuscript in preparation*.

### Introduction

Approximately 10-35% of non-small cell lung cancers (NSCLCs) harbor activating mutations in the kinase domain of the epidermal growth factor receptor (EGFR) [18-20]. Since the discovery of these mutations in 2004, EGFR tyrosine kinase inhibitors (TKIs), such as gefitinib, erlotinib, and afatinib have demonstrated impressive efficacy against *EGFR*-mutant lung cancers and have led to significant improvements in survival rates for patients with this disease [44, 45, 49].

While these earlier generations of EGFR TKIs were originally designed to inhibit the wild-type receptor, third generation mutant-selective EGFR TKIs such as AZD9291, rociletinib, and others have recently been designed to specifically inhibit lung cancer-associated mutant forms of EGFR. These newer inhibitors are highly potent and decrease off-target inhibition of wild-type EGFR in normal tissues [147, 149]. AZD9291 and rociletinib have demonstrated objective response rates of 55% and 59%, respectively, in phase I/II trials, and they are currently being tested in the first line setting (NCT02296125) [54, 55].

Despite these successes, drug resistance remains the greatest barrier to treatment of *EGFR*-mutant lung cancer. Acquired resistance to first- and second-generation *EGFR* TKIs virtually always occurs within about 12 months and is most commonly associated with a second-site T790M substitution mutation in the kinase domain of *EGFR* [122-124, 134]. Activation of bypass signaling pathways as well as histologic changes have also been associated with resistance to first- and second-generation *EGFR* TKIs [2, 4]. While it remains to be seen whether resistance will occur as quickly or as frequently when mutant-selective inhibitors are used in the first-line setting, cases of acquired resistance to AZD9291 have already been documented clinically [228].

We previously demonstrated that acquired resistance to AZD9291 is associated with increased dependence on RAS signaling in preclinical models [1]. We subsequently showed that the combination of AZD9291 plus a MEK1/2 inhibitor, selumetinib, may delay or overcome acquired resistance to AZD9291 monotherapy in some cases [1]. Notably, it has also been shown that ERK reactivation occurs following short-term treatment with single-agent mutant-selective *EGFR* TKIs [229]. Based on these and other data, the combination of AZD9291 + selumetinib is now being investigated in a clinical trial (NCT02143466). Unfortunately, we know from previous experience with targeted therapies that acquired resistance to this combination therapy in *EGFR*-mutant lung cancer is likely to occur eventually. We sought to anticipate therapeutic escape mechanisms by developing and analyzing preclinical models of resistance to AZD9291 + selumetinib.

## Results

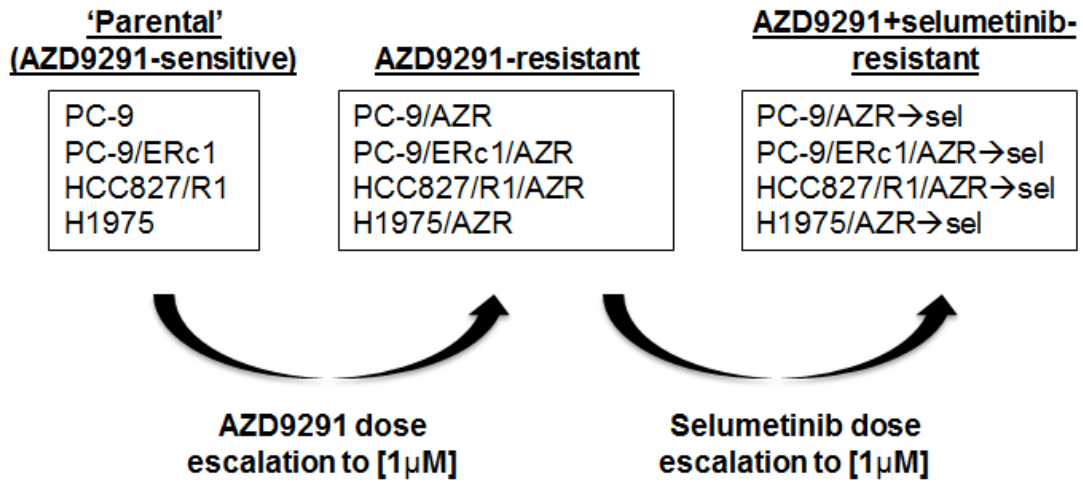
### ***Establishing models of resistance to AZD9291 + selumetinib***

We previously generated four AZD9291-resistant cell lines from *EGFR*-mutant 'parental' lung adenocarcinoma cell lines (either TKI-naïve or erlotinib-resistant cell lines) and found that all four populations of resistant cells maintained sensitivity to combination treatment with AZD9291 + selumetinib [230]. Following well-established dose escalation protocols, we subsequently added selumetinib to our *in vitro* culture conditions until we derived cell lines to be resistant to the combination of AZD9291 + selumetinib (**Figure 18A and Materials and Methods**) [155].

Sequential derivations of drug-resistant cells for each *EGFR*-mutant cell line led to a trio of isogenic cell populations: 1. The 'parental' cell line (either TKI-naïve or erlotinib-resistant: PC-9, PC-9/ERc1, HCC827/R1, and H1975); 2. the AZD9291-resistant cell line (PC-9/AZR, PC-9/ERc1/AZR, HCC827/R1/AZR, and H1975/AZR); and 3. The AZD9291 + selumetinib-resistant cell line (PC-9/AZR→sel, PC-9/ERc1/AZR→sel, HCC827/R1/AZR→sel, H1975/AZR→sel) (**Figure 18B, Appendix Figure 43**).

Immunoblotting of EGFR and downstream signaling pathways revealed an increase in phospho-ERK and/or phospho-AKT in the setting of resistance to the combination of AZD9291 + selumetinib (**Appendix Figure 44**). Since it has been reported that resistance to targeted therapies in *EGFR*-mutant lung cancer can occur via bypass signaling by other receptor tyrosine kinases (RTKs), we performed phospho-RTK arrays in order to test whether such bypass signaling

A.



B.

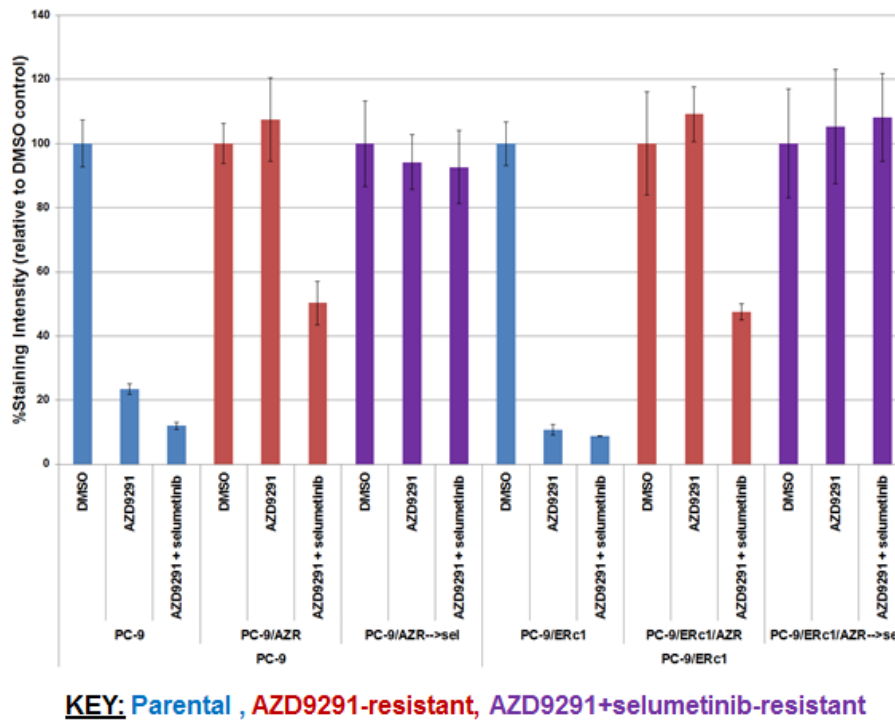


Figure 18. *In vitro* modeling of resistance to AZD9291 + selumetinib.

**A**, Derivation of AZD9291+selumetinib-resistant cells. 'Parental' TKI-sensitive (PC-9) or erlotinib-resistant (PC-9/ERc1, HCC827/R1, and H1975) cells were exposed to increasing concentrations of AZD9291 to the point of resistance at [1  $\mu$ M] AZD9291. AZD9291-resistant cells were then exposed to increasing concentrations of selumetinib to the point of resistance at [1  $\mu$ M] selumetinib (see materials and methods). **B**, Crystal violet assays demonstrate acquired resistance to AZD9291+selumetinib in the combination-resistant cells (PC-9/AZR $\rightarrow$ sel and PC-9/ERc1/AZR $\rightarrow$ sel), as compared to their isogenic parental (PC-9 and PC-9/ERc1) and AZD9291-resistant (PC-9/AZR and PC-9/ERc1/AZR) counterparts. Cells were treated for 10 days with either AZD9291 [50nM], selumetinib [500nM], or the combination. Cells were fixed and stained with crystal violet. Staining intensity was measured to determine relative cell growth, and data are shown as a percentage of DMSO-treated cells. Error bars indicate one standard deviation. Data shown are representative of three independent experiments.

mechanisms were responsible for sustaining downstream activation of phospho-ERK and phospho-AKT in this setting. While we observed a slight increase in phospho-MET and phospho-IGF-1R in two of the AZD9291 + selumetinib-resistant cell lines relative to their parental and AZD9291-resistant counterparts, these cell lines did not demonstrate sensitivity to the MET inhibitor, crizotinib, or the IGF-1R inhibitor, linsitinib (OSI-906; data not shown).

### ***AZD9291+selumetinib-resistant cells are sensitive to ERK inhibition***

Given the dramatic increase in phospho-ERK present in the AZD9291 + selumetinib-resistant cell lines, we next tested whether these cell lines were sensitive to an ERK inhibitor, SCH772984. In 10-day growth inhibition assays, we found that two of four of our AZD9291 + selumetinib-resistant cell lines, PC-9/AZR→sel and PC-9/ERc1/AZR→sel, were sensitive to SCH772984 alone (although not as sensitive as PC-9 parental cells to AZD9291 alone; **Figure 19A, Appendix Figure Figure 45**). These data further support our hypothesis that in some cases, *EGFR*-mutant lung cancer cell lines may retain dependence on downstream RAS/RAF/MEK/ERK signaling for survival, despite having acquired resistance to vertical EGFR/MEK inhibition. This result also indicates that, not surprisingly, there exists some heterogeneity in the mechanism(s) of resistance to AZD9291 + selumetinib, as demonstrated by the fact that two of the combination-resistant cell lines did not display sensitivity to ERK inhibition.

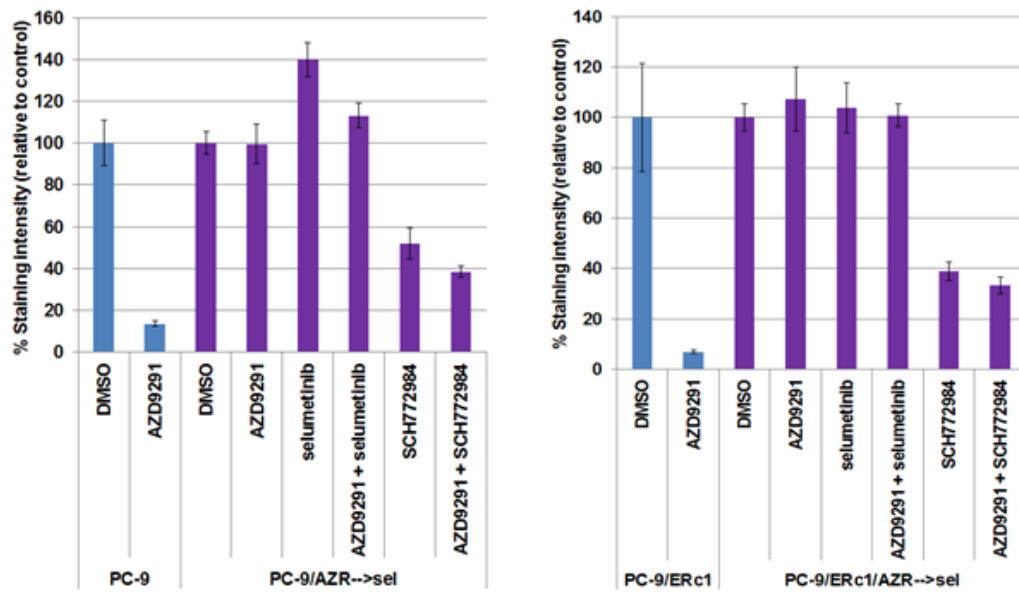
We then performed immunoblotting of PC-9/AZR→sel and PC-9/ERc1/AZR→sel cell lines following 48 hours of treatment with AZD9291,

selumetinib, SCH772984, or the respective combinations. Consistent with the phenotypic data demonstrating sensitivity to ERK inhibition, the AZD9291 + selumetinib-resistant cell lines showed increased expression of pro-apoptotic BCL-2 family member, BIM, in response to treatment with SCH772984 (**Figure 19B**). In addition, the AZD9291 + selumetinib-resistant cell lines harbored increased phospho-MEK, which, similar to increased phospho-ERK signal, was not affected by the addition of AZD9291 (**Figure 19B**). By contrast, AZD9291 treatment did inhibit phosphorylation of EGFR in these cells (data not shown). Taken together, these data suggest that resistance to AZD9291 + selumetinib may be the result of activation of signaling downstream of EGFR but upstream of ERK. According to this model, AZD9291 + selumetinib-resistant cells may have acquired (a) mechanism(s) of increased RAS/RAF/MEK activation that overcomes the ability of selumetinib to inhibit cell growth but confers sensitivity of the cells to ERK inhibition.

***AZD9291+selumetinib-resistant cells are sensitive to alternative MEK inhibitor, trametinib***

There are multiple MEK1/2 inhibitors approved or in clinical development, each of which harbors a distinct profile in terms of potency, specificity, and mechanism of action. For example, even comparing selumetinib to other allosteric, non-competitive MEK1/2 inhibitors such as trametinib, there exist important differences regarding the respective effects of these molecules on MEK activation and signaling. For example, trametinib more potently inhibits RAF-mediated MEK

**A.**



**KEY:** Parental , AZD9291+selumetinib-resistant

**B.**

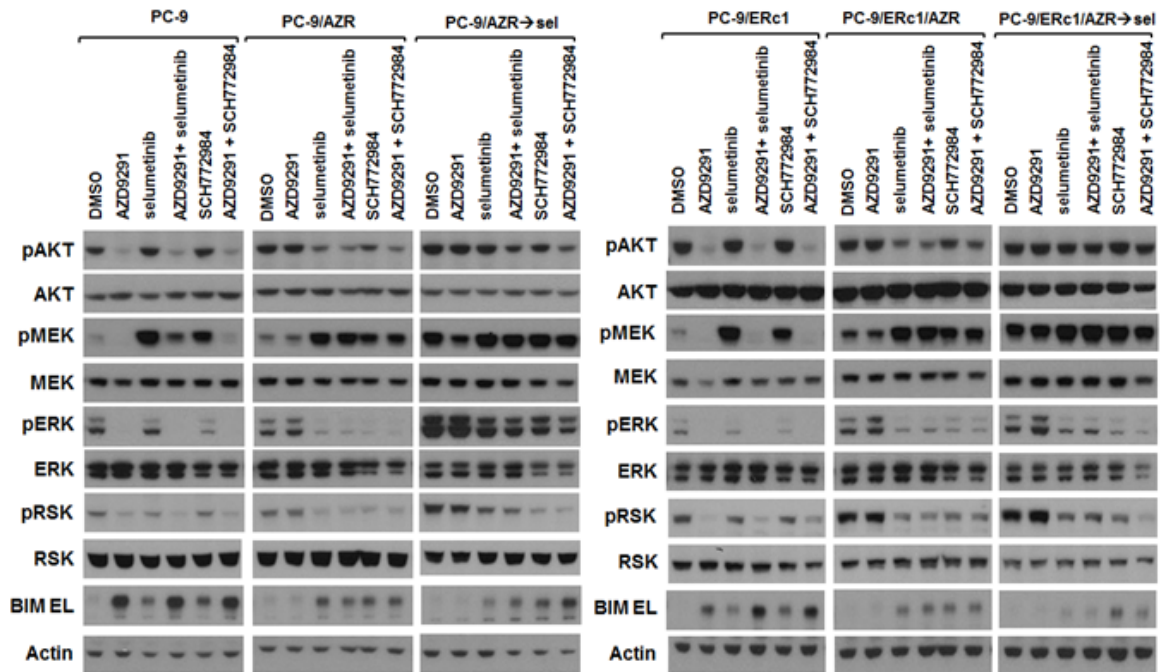


Figure 19. AZD9291+selumetinib-resistant cells are sensitive to ERK inhibition.

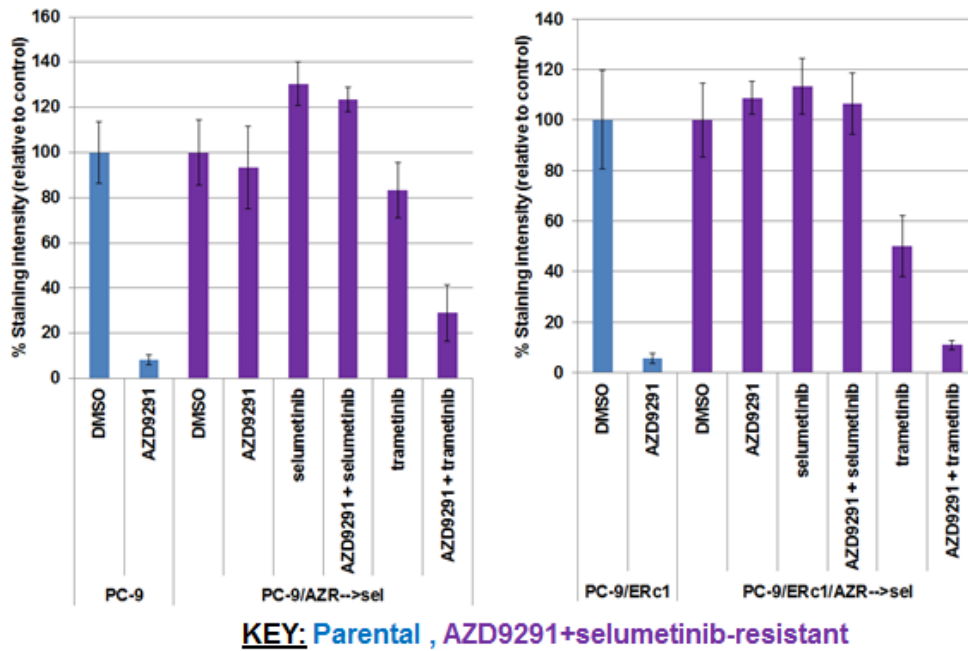
**A**, Crystal violet assays demonstrate growth inhibition of AZD9291+selumetinib-resistant cells (PC-9/AZR→sel and PC-9/ERc1/AZR→sel) by ERK inhibitor SCH772984. Cells were treated for 10 days with either AZD9291 [50nM], selumetinib [500nM], SCH772984 [500nM], or combinations thereof. Cells were fixed and stained with crystal violet. Staining intensity was measured to determine relative cell growth, and data are shown as a percentage of DMSO-treated cells. Error bars indicate one standard deviation. **B**, Immunoblotting of parental (PC-9, PC-9/ERc1), AZD9291-resistant (PC-9/AZR, PC-9/ERc1/AZR), and AZD9291+selumetinib-resistant (PC-9/AZR→sel, PC-9/ERc1/AZR→sel) cells reveals increased baseline phospho-MEK and phospho-ERK in AZD9291+selumetinib-resistant cells. Cells were treated for 48 hours with either AZD9291 [50nM], selumetinib [500nM], SCH772984 [500nM], or combinations thereof. ERK inhibitor SCH772984 inhibits phospho-ERK and phospho-RSK while inducing BIM, a pro-apoptotic BCL-2 family member, in AZD9291+selumetinib-resistant cells. Note that lysates within each set of isogenic cell lines were run on the same gel and have been separated in figure for clarity of presentation only. Data shown are representative of three independent experiments.

phosphorylation at serine 217, decreasing the extent of feedback reactivation of MEK and causing more profound pathway inhibition as compared to other MEK inhibitors, including selumetinib [231, 232]. Given these data, combined with the observation of increased baseline phospho-MEK in addition to phospho-ERK in our models of AZD9291 + selumetinib resistance, we hypothesized that resistance to selumetinib may not necessarily confer cross-resistance to other MEK inhibitors in the setting of *EGFR*-mutant lung cancer.

In order to test this hypothesis, we evaluated the sensitivity of our AZD9291 + selumetinib-resistant cell lines to trametinib in a long-term growth inhibition assay. We found that the same two AZD9291 + selumetinib-resistant cell lines that were sensitive to SCH772984 also displayed sensitivity to trametinib (**Figure 20A, Appendix Figure 46**). However, unlike SCH772984, which works well as monotherapy in this context, trametinib induces greater growth inhibition in combination with AZD9291 than alone.

Similar to the SCH772984 data, immunoblotting following 48 hours of treatment with trametinib +/- AZD9291 revealed inhibition of phospho-ERK and increased expression of BCL-2 (**Figure 20B**). It is worth noting, however, that phospho-ERK is not always completely inhibited by treatment with SCH772984 or trametinib. This may be partially explained by feedback reactivation of ERK during the 48 hour treatment window. However, these signaling data are also consistent with the fact that growth inhibition of the resistant cells by SCH772984 and/or trametinib does not ever reach the degree of growth inhibition by AZD9291 in parental *EGFR*-mutant cells (**Figure 19A, Figure 20A**), suggesting that there may be other factors contributing to the resistant phenotype.

**A.**



**B.**

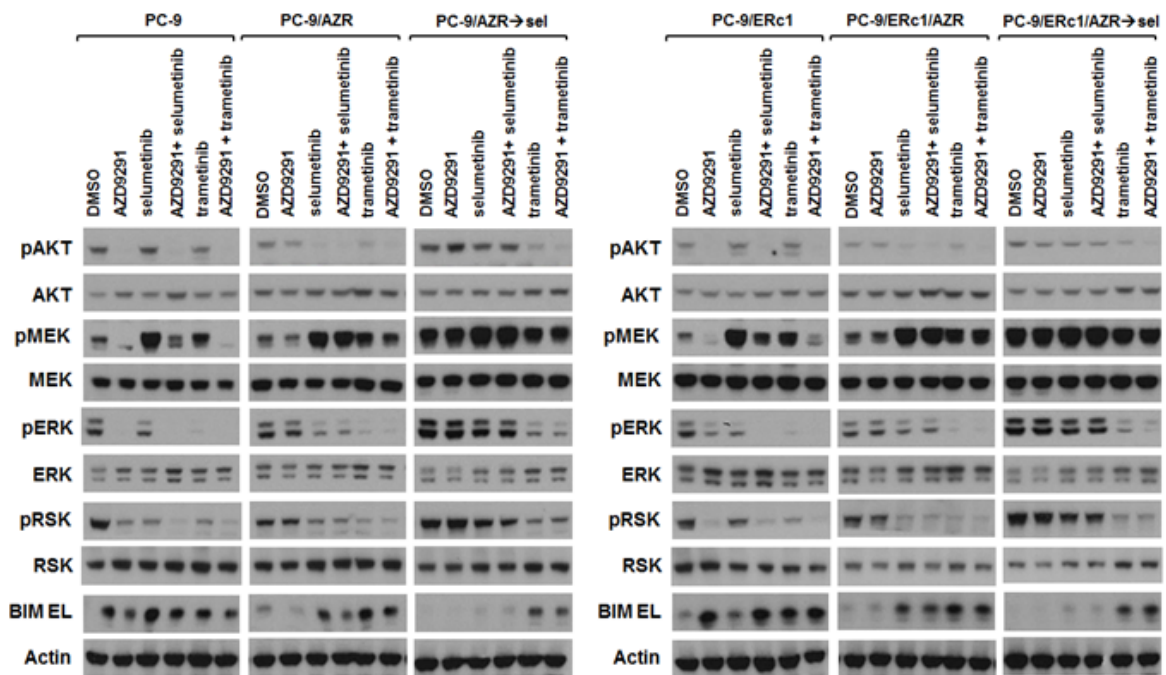


Figure 20. AZD9291+selumetinib-resistant cells are sensitive to alternative MEK inhibitor, trametinib.

**A,** Crystal violet assays demonstrate growth inhibition of AZD9291+selumetinib-resistant cells (PC-9/AZR→sel and PC-9/ERc1/AZR→sel) by MEK inhibitor, trametinib. Cells were treated for 10 days with either AZD9291 [50nM], selumetinib [500nM], trametinib [50nM], or combinations thereof. Cells were fixed and stained with crystal violet. Staining intensity was measured to determine relative cell growth, and data are shown as a percentage of DMSO-treated cells. Error bars indicate one standard deviation.

**B,** Immunoblotting of parental (PC-9, PC-9/ERc1), AZD9291-resistant (PC-9/AZR, PC-9/ERc1/AZR), and AZD9291+selumetinib-resistant (PC-9/AZR→sel, PC-9/ERc1/AZR→sel) cells reveals increased baseline phospho-MEK and phospho-ERK in AZD9291+selumetinib-resistant cells. Cells were treated for 48 hours with either AZD9291 [50nM], selumetinib [500nM], trametinib [50nM], or combinations thereof. MEK inhibitor trametinib inhibits phospho-ERK and phospho-RSK while inducing BIM, a pro-apoptotic BCL-2 family member, in AZD9291+selumetinib-resistant cells. Note that lysates within each set of isogenic cell lines were run on the same gel and have been separated in figure for clarity of presentation only. Data shown are representative of three independent experiments.

### ***Increased RAS-GTP in AZD9291+selumetinib-resistant cells***

In order to further discern the mechanism of this increased activation of RAS/RAF/MEK signaling in the setting of AZD9291 + selumetinib resistance, we tested the level of activated RAS (RAS-GTP) in our AZD9291 + selumetinib-resistant cell lines that demonstrated this phenotype. Interestingly, RAS-GTP levels were increased in PC-9/AZR→sel and PC-9/ERc1/AZR→sel cells relative to the corresponding isogenic parental and AZD9291-resistant cells (**Figure 21**). RAS-GTP levels in AZD9291 + selumetinib-resistant cells were not affected by 24 hours of treatment with AZD9291. These data support a model of EGFR-independent RAS activation that results in increased downstream RAF→MEK→ERK signaling.

Notably, Sanger sequencing of genomic DNA from our AZD9291 + selumetinib resistant cell lines did not reveal acquired mutations in exons 2 and 3 of *KRAS*, *NRAS*, *HRAS*, and *MEK1* as well as exons 11 and 15 of *BRAF*, which have been previously reported in both treatment-naïve and drug-resistant lung adenocarcinoma and melanoma. We also did not find evidence of genomic amplification of *KRAS*, *NRAS*, or *HRAS* or loss of *DUSP4* or *DUSP6* expression in these cell lines (data not shown). Further studies are needed to determine the mechanism(s) of increase activation of RAS, MEK, and ERK, and their relative contribution to AZD9291 + selumetinib resistance in this context.

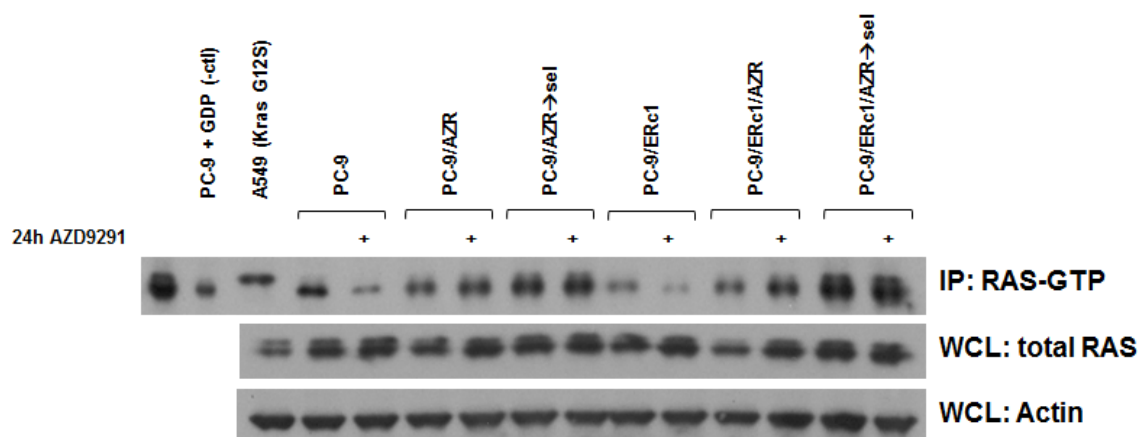


**Figure 21. AZD9291+selumetinib-resistant cells demonstrate increased RAS activation.**

AZD9291+selumetinib-resistant cells display higher levels of RAS-GTP than isogenic paired parental or AZD9291-resistant cells. Active RAS (RAS-GTP) was detected using the Active RAS Pull-down and Detection Kit from Thermo Scientific. Parental (PC-9, PC-9/ERc1), AZD9291-resistant (PC-9/AZR, PC-9/ERc1/AZR), and AZD9291+selumetinib-resistant (PC-9/AZR→sel, PC-9/ERc1/AZR→sel) cells were treated for 24 hours with either DMSO or AZD9291 [50nM]. Immunoblotting on RAS-GTP pull-down and whole cell lysates (WCL) was performed to show relative levels of active and total RAS. Data shown are representative of two independent experiments.

## Discussion

In these studies, we modeled acquired resistance to AZD9291 + selumetinib in a panel of *EGFR*-mutant lung cancer cell lines in order to discern potential mechanisms of resistance to this combination therapy. We describe two potential methods for overcoming acquired resistance to AZD9291 + selumetinib: treatment with ERK inhibitor, SCH772984, and/or treatment with an alternative MEK inhibitor, trametinib. Our data are suggestive of phenotypic heterogeneity, as we show that only two of four AZD9291 + selumetinib-resistant cell lines are sensitive to SCH772984 and trametinib (PC-9/AZR→sel and PC-9/ERc1/AZR→sel).

The underlying mechanisms of resistance to AZD9291 + selumetinib and subsequent sensitivity to ERK and/or MEK inhibition remain to be fully elucidated; however, our data suggest a few avenues for further study. Both of our AZD9291 + selumetinib-resistant cell lines that remain sensitive to trametinib and SCH772984 display increased active (GTP-bound) RAS as well as higher levels of phosphorylated MEK and phosphorylated ERK at baseline (as compared to their isogenic parental and AZD9291-resistance counterparts). The RAS/RAF/MEK/ERK signaling pathway is regulated at every level by numerous different molecules, such as RAS guanine nucleotide exchange factors (GEFs), GTPase activating proteins (GAPs), dual specificity phosphatases (DUSPs), among many others. While we did not observe loss of DUSP4 or DUSP6 expression in our AZD9291 + selumetinib-resistant cell lines, more work is needed to rule out dysregulation of other RAS/RAF/MEK/ERK negative regulators as a mechanisms of resistance to combined EGFR/MEK inhibition in our preclinical

models. Validation and analysis of whole-exome sequencing data from our AZD9291 + selumetinib-resistant cell lines is currently ongoing and may provide potential genomic mechanisms explaining the phenotypes described herein.

Ultimately, our *in vitro* findings will need to be validated in human tumor samples with acquired resistance to AZD9291 + selumetinib. By combining these types of mechanistic studies with *ex vivo* analysis of human samples, we can develop a more precise understanding of what mediates resistance to different combinations of EGFR and MEK inhibitors in the clinic. In this way, similar to the way in which we have approached treatment of *EGFR*-mutant lung cancer during the past decade, we can begin to discern whether there is an opportunity for sequential application of MEK/ERK inhibitors in combination with EGFR inhibitors in the treatment of *EGFR*-mutant lung cancer.

## **Materials and methods**

### ***Cell lines***

All cell lines utilized in these studies were authenticated via routine genotyping for known EGFR kinase mutations. Cell lines were kept in continuous culture for no more than 8 weeks and were routinely tested for mycoplasma contamination to ensure accuracy of experimental data. Cells were cultured in RPMI + L-glutamine (Corning) and supplemented with 10% heat-inactivated fetal bovine serum (Atlanta Biologicals) and 1% penicillin/streptomycin (Corning) and grown in a humidified incubator with 5% CO<sub>2</sub> at 37C. Isogenic resistant cell lines were derived in the lab as described previously and in this manuscript [155].

Briefly, parental cells were cultured with increasing concentrations of TKI starting at the IC<sub>30</sub> until the resulting cell populations were resistant to growth inhibition at [1 µM] drug concentrations. All resistant cells were maintained in drug, and TKI was refreshed every 72 hours.

### ***Immunoblotting***

Resistant cells were removed from drug selection 72 hours before immunoblotting experiments. Cells were washed on ice with cold PBS and lysed in radioimmunoprecipitation (RIPA) buffer (250mM Tris-HCl pH 7.5, 75mM NaCl, 1% NP-40/IGEPAL, 0.1% sodium dodecyl sulfate) supplemented with complete protease inhibitor cocktail (Roche), 40mM sodium fluoride, 1mM sodium orthovanadate, and 1µM okadaic acid. Lysates were subjected to SDS-PAGE (4-12% gels) followed by immunoblotting with the indicated antibodies and detection by Western Lightning ECL reagent (Perkin-Elmer). The following antibodies were obtained from Cell Signaling Technologies: phospho-ERK (T202/Y204; 1:1000; #9101), ERK (1:1000, #9102), phospho-AKT (S473; 1:500; #9271), AKT (1:1000; #9272), BIM (1:1000; #2819), phospho-SRC (Y416; 1:1000; #2101), SRC (1:1000; #2108), phospho-FAK (Y397; 1:1000; #D20B1), FAK (1:1000; #3285), phospho-MEK1/2 (S217/221: 1:1000; #9154), MEK1/2 (1:1000; #9126), phospho-RSK (S380; 1:1000; #11989), RSK (1:1000; #9355), HRP-conjugated anti-mouse (1:3000; #7076), and HRP-conjugated anti-rabbit (1:3000; #7074). Phospho-EGFR antibody was obtained from Abcam (Y1068; 1:1000; #EP774Y), EGFR from BD Transduction Laboratories (1:500; #610017), and actin from Sigma-Aldrich (1:3000; #A2066).

### ***RAS-GTP pull down***

To detect RAS-GTP levels, we used the Active RAS Pull-Down and Detection Kit from ThermoScientific (#16117). Following 24 hours of treatment with [50nM] AZD9291 or [100nM] dasatinib, as indicated, cell lysates were harvested and resuspended in 300uL of the kit's Lysis/Binding/Wash buffer supplemented with protease and phosphatase inhibitors as described in the previous section ("Immunoblotting"). Lysates were quantified by BCA Assay (ThermoScientific #23225). *In vitro* GTPγS and GDP treatment, and the active RAS precipitation were performed as per manufacturer's instructions. Active (pulldown) and total (WCL) RAS was detected using the anti-RAS antibody provided with the kit as per manufacturer's instructions.

### ***Growth inhibition assays***

3,000 cells/well were plated in 24-well plates and treated with indicated drug combinations. Media and inhibitors were refreshed every 72 hours, and cells were grown for 10 days or until confluence in untreated wells. Cells were fixed and stained in 20% methanol with .025% crystal violet and washed with water. Dried plates were imaged and staining intensity quantified on the LI-COR Odyssey.

## Chapter VI: Conclusions and Future Directions

### Summary of findings

Clinical and preclinical data have collectively elucidated several potential sequences of treatment with targeted therapies in *EGFR*-mutant lung cancer. A simplified schematic of these treatment sequences is presented in **Figure 22**. Of note, this schematic does not provide an exhaustive list of scenarios and/or available targeted therapies; rather, it is intended as an illustration of the findings presented in this manuscript and clinical data pertinent to these specific findings.

At the time of this writing, upon diagnosis with *EGFR*-mutant lung cancer, a patient will either receive an approved first- or second-generation EGFR TKI (such as erlotinib, gefitinib, or afatinib; **scenarios #1 and #2**) or be enrolled in a clinical trial testing a mutant selective EGFR TKI, such as AZD9291 (**scenario #3**). Of note, we have shown in preclinical models that the combination of afatinib + cetuximab may delay acquired resistance relative to single-agent erlotinib or afatinib and therefore may also be useful in the first line setting (Pirazzoli et al., *submitted*; **scenario #4**). A randomized phase II/III clinical trial is currently ongoing testing afatinib + cetuximab versus afatinib alone in treatment-naïve patients with advanced stage *EGFR*-mutant lung cancer (NCT02438722).

Unfortunately, we know that acquired resistance to each of these anti-EGFR therapies will likely occur. The majority of tumors with resistance to first- or second-

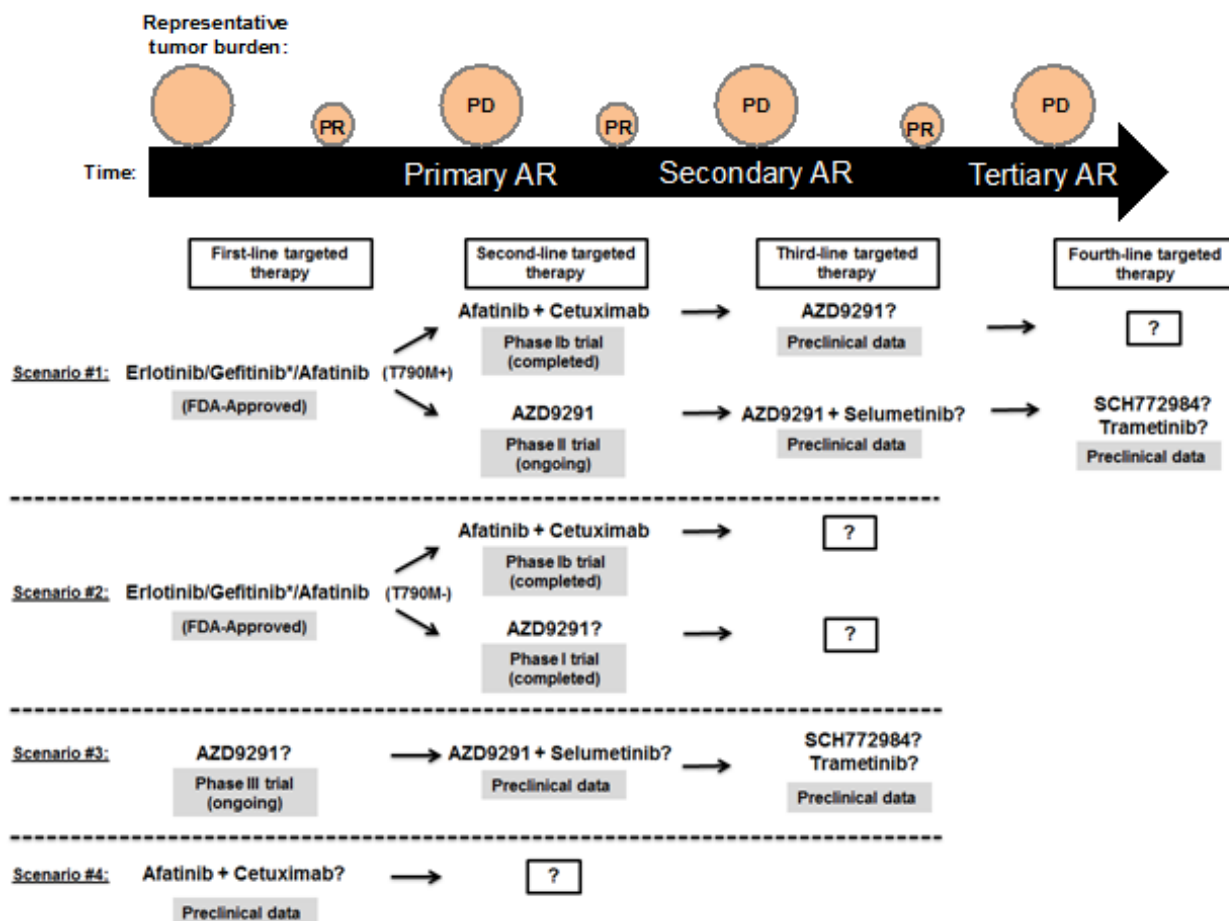


**Figure 22. Potential sequential application of targeted therapies in EGFR-mutant lung cancer.**

Erlotinib, gefitinib, and afatinib are approved for treatment of EGFR-mutant lung tumors in the first-line setting. Preclinical and early clinical trial data demonstrate that both afatinib plus cetuximab and AZD9291 can overcome T790M+ AR to first- and second-generation EGFR TKIs in some cases (scenario #1). Phase Ib trial data also demonstrate that afatinib plus cetuximab can similarly overcome T790M- AR to first- and second-generation EGFR TKIs, but AZD9291 has shown significantly less efficacy in T790M- tumors as compared to T790M+ tumors (scenario #2). Treatment strategies for patients whose tumors harbor other (i.e. EGFR-independent) mechanisms of resistance to first- and second-generation EGFR TKIs are not represented in this schema. AZD9291 is currently being tested in the first-line setting (scenario #3), and preclinical data suggest that afatinib plus cetuximab may also be useful as a first-line therapy (scenario #4). Preclinical data suggest that AZD9291 can overcome acquired resistance to afatinib plus cetuximab in cell line models harboring T790M (scenario #1; Chapter III). In some cases, preclinical models of resistance to AZD9291 are sensitive to inhibition by AZD9291 plus MEK1/2 inhibitor selumetinib (scenarios #1 and #3; Chapters III and IV), and subsequent resistance to the combination of AZD9291 + selumetinib may be overcome by the ERK inhibitor, SCH772984 or an alternative MEK inhibitor, trametinib (scenarios #1 and #3; Chapter V).

generation EGFR TKIs will acquire a second mutation in the kinase domain of EGFR, T790M (**scenario #1**). Clinical trial data have now demonstrated that tumors harboring T790M upon acquired resistance to first- or second-generation EGFR TKIs ('T790M-positive') may respond to the combination of afatinib + cetuximab (29% ORR) or mutant-selective EGFR TKIs such as AZD9291 (61% ORR; **scenario #1**). Herein, we have shown in preclinical models that, following secondary acquired resistance to afatinib + cetuximab, T790M-positive tumors may still be sensitive to third-line treatment with AZD9291 (**scenario #1; Chapter III**). Interestingly, the converse is not true. Rather, our models of acquired resistance to AZD9291 demonstrate cross-resistance to other anti-EGFR therapies, including afatinib + cetuximab (**scenario #1; Chapter III**)

Another subset of tumors resistant to first- or second-generation EGFR TKIs will respond to subsequent EGFR targeted therapies, even though they lack the secondary T790M mutation (**scenario #2**). In fact, clinical trial data have shown that response to second-line afatinib + cetuximab is T790M-independent (29% ORR), and a small subset of T790M-negative tumors (11-21%) responded to second-line AZD9291. Biomarkers of sensitivity to subsequent anti-EGFR therapies in the setting of T790M-negative resistance to first- and second-generation EGFR TKIs remain to be elucidated.

Yet another subset of tumors with resistance to first- or second-generation EGFR TKIs will harbor molecular or phenotypic changes that render them TKI-resistant in an EGFR-independent manner (**Figure 3**). In some cases, when the resistance mechanism is identified, rational therapeutic strategies targeting 'bypass' signaling pathways may have some efficacy in overcoming acquired

resistance [103]. These scenarios involving EGFR-independent mechanisms of resistance are not represented in **Figure 22**.

Our models of acquired resistance to AZD9291, in both the first- and second-line setting, demonstrated cross-resistance to other anti-EGFR targeted therapies. AZD9291-resistant cell lines and mouse tumors were sensitive to subsequent treatment with AZD9291 plus a MEK1/2 inhibitor, selumetinib (**scenarios #1, #3; Chapters III and IV**); however, long-term treatment with AZD9291 + selumetinib ultimately resulted in resistance to this combination. Our preliminary data suggest that tumors with resistance to AZD9291 + selumetinib may be sensitive to treatment with ERK inhibitors (SCH772984), or alternative MEK inhibitors, such as trametinib (**scenarios #1 and #3; Chapter V**).

## **Future directions**

### ***T790M-negative, EGFR-dependent resistance to first-generation EGFR TKIs***

As mentioned in the previous section, 20-30% of patients with T790M-negative acquired resistance to first- and second-generation EGFR TKIs such as erlotinib and gefitinib respond to subsequent anti-EGFR targeted therapies such as AZD9291, rociletinib, and afatinib plus cetuximab. This was initially a surprising observation, given that these therapies were specifically designed to overcome T790M-mediated resistance. It is possible that this finding can be explained by lack of detection of T790M (biopsy of a different lesion, technical limitations, etc.), but it is also possible that these clinical data truly reveal a cohort of tumors that

sustain reliance on EGFR signaling in the absence of T790M. As such, further work is needed to discern the potential mechanism of this resistance.

In order to discern EGFR-dependent, T790M-negative mechanisms of resistance to first- and second-generation EGFR TKIs, we have developed 8 EGFR-mutant lung adenocarcinoma cell lines with sustained T790M-negative resistance to first- and second-generation EGFR TKIs erlotinib and afatinib. While none of our T790M-negative models of erlotinib and afatinib resistance yet display significant sensitivity to anti-EGFR therapies, we continue to seek such *in vitro* models in order to recapitulate the responses seen in the clinic. In addition, tumors with T790M-negative acquired resistance to erlotinib/ gefitinib that were subsequently treated with afatinib + cetuximab are undergoing molecular analysis via the MSK-IMPACT assay at Memorial Sloan Kettering Cancer Center. This testing will provide genomic sequencing data on 341 cancer-related genes and will hopefully provide us with more accurate methods of assessing which tumors are likely to respond to subsequent anti-EGFR therapies after progressing on first- and second-generation EGFR TKIs. An alternative approach to learning more about the biology of T790M-negative resistance would be to develop novel cell lines or patient-derived xenografts (PDXs) from tumor samples genotyped as T790M-negative at the time of erlotinib/afatinib-resistance. In addition to genomics profiling, derivation of these types of models would allow for more extensive assessment of phenotype, including signaling and cell viability experiments [226].

### ***Heterogeneity in mechanisms of resistance to first-generation EGFR TKIs***

As available technologies for molecular analysis of tumor tissue improve, we are gaining a greater understanding of the genomic intratumoral heterogeneity that exists in solid tumors. This phenomenon also holds true following acquired resistance to EGFR TKIs. In other words, while the most common mechanisms of resistance to first-generation EGFR TKIs often occur in a mutually exclusive manner, there is increasing evidence of these alterations co-occurring within one tumor [2]. Notably, even in cell line models of acquired resistance to first- and second-generation EGFR TKIs, potentially functional genomic changes of unknown significance have been observed to occur in the same pool of resistant cells in which known driver mutations were also observed (**Chapter II**).

This degree of heterogeneity requires us to move toward a more nuanced, combinatorial approach to treatment with targeted therapies. For example, the allele frequency of the T790M mutation in an *EGFR*-mutant tumor with acquired resistance to erlotinib, gefitinib, or afatinib may give some insight into the clonality of the resistant tumor. If additional targetable resistance mechanisms can be identified within the tumor, this finding would suggest some utility for combination therapies with a mutant-selective EGFR TKI (such as AZD9291) plus additional targeted agents. These mutant selective inhibitors are well suited for inclusion in combination therapeutic regimens, given their relatively mild side effect profiles.

Ideally, routine molecular analyses of tumor specimens on more comprehensive analysis platforms can serve as a hypothesis-generating tool for *in vitro* mechanistic work. While significant efforts are being made to increase the frequency of biopsies obtained for therapeutic molecular analysis of resistant tumors, such biopsies are not without risk. In addition, tumor sampling is inherently

biased, and it has been shown to underestimate the genomic heterogeneity present within a given tumor [233, 234]. In reality, current methods for detecting the presence and molecular nature of acquired resistance are not sufficiently sensitive to enable dynamic monitoring of tumor heterogeneity in response to therapy. Encouragingly, however, recent studies have begun to demonstrate the feasibility of analysis of cell-free plasma DNA (cfDNA) to successfully detect and subsequently monitor heterogeneous mechanisms of resistance to anti-epidermal growth factor receptor (EGFR) targeted therapies in non-small cell lung cancer (NSCLC) [228, 235].

In addition to genomic-level heterogeneity, analysis of signaling and phenotypic heterogeneity is becoming more feasible, thanks to complementary technologies allowing capture and analysis of circulating tumor cells (CTCs) [236]. Ultimately, the combination of genomic and phenotypic data from a 'liquid biopsy' or single-cell analysis of multiple metastatic lesions would enable a greater degree of precision in selecting targeted therapies for heterogeneous tumors.

### ***Mechanisms of resistance to AZD9291***

A primary goal of the work presented in this manuscript was elucidating mechanisms of resistance to mutant-specific EGFR TKI AZD9291. In our studies, we demonstrated that dysregulation of MAP kinase signaling may confer resistance to mutant-selective EGFR TKI AZD9291. However, AZD9291-resistant tumors have only recently emerged in the clinic, and previous experience indicates that there will likely be multiple distinct mechanisms by which tumor cells achieve

this resistance. It was recently reported that a substitution mutation resulting in a change from cysteine to serine in EGFR codon 797 (the binding site of AZD9291; C797S) has been observed in AZD9291-resistant tumors [228]. It was also reported that cell lines with the C797S mutation in EGFR but lacking the T790M mutation are resistant to AZD9291, but maintain sensitivity to first- and second-generation EGFR TKIs [237]. Given that EGFR C797S has now been identified in AZD9291-resistant tumors by multiple different groups, it is surprising that this mutation has not yet emerged *in vitro*. It is possible that it will emerge with time, as more cell line models of AZD9291 resistance are developed. However, it is also possible that there is something specific about the *in vivo* setting that selects for this resistance mutation, i.e., metabolites of AZD9291.

More work is needed to determine the full spectrum of resistance mechanisms to AZD9291 and other mutant-selective EGFR TKIs. Whole-exome sequencing of AZD9291-resistant cell lines in our lab demonstrated acquired mutations in a genes such as *FCGBP*, *KCNE4*, *NRG1*, *RASGRF1*, *TGFB3*, *DVL2*, *PPFIA3*, whose protein products have a diverse range of normal functions in the cell. Follow-up studies discerning whether these alterations are functional in this context and sufficient to confer resistance to AZD9291 will improve our ability to discern relevant resistance mechanisms in patients.

### ***Mechanisms of resistance to AZD9291 + selumetinib***

Finally, given our findings that AZD9291 + selumetinib can overcome resistance to AZD9291, and given the fact that the combination of AZD9291 +

selumetinib is currently being tested in the clinic, we sought to anticipate potential mechanisms of resistance to this combination. We found that some *EGFR*-mutant cell lines resistant to AZD9291 + selumetinib maintained sensitivity to an ERK inhibitor, SCH772984, and an alternative MEK inhibitor, trametinib. While these observations are compelling, more work is needed to elucidate fully the mechanisms of these sensitivities. Notably, previous work in our lab has demonstrated that increased phospho-SRC is associated with reactivation of phospho-ERK following AZD9291 treatment in parental, TKI-sensitive *EGFR*-mutant lung cancer cell lines (Eiki Ichihara, personal communication) and that dasatinib can in some cases inhibit growth of AZD9291 + selumetinib-resistant cells. Analysis of whole-exome sequencing data from each of our AZD9291 + selumetinib-resistant cell lines is ongoing, and may provide some mechanistic information to explain the phenotypes we have observed.

Of 23 evaluable patients who have been enrolled to date in a clinical trial testing the combination of AZD9291 + selumetinib (NCT02143466) [238], 9 patients have experienced a partial response to therapy. Unfortunately for these patients, we anticipate that acquired resistance to AZD9291 + selumetinib is likely to occur eventually. If that happens, correlation of our preclinical findings to patient tumors could potentially inform subsequent, rational treatment strategies for patients with acquired resistance to this combination therapy.

### ***Immune microenvironment of solid tumors***

The significant heterogeneity of many solid tumors and consistent evolution of resistance to targeted therapies suggest that new approaches may be needed to achieve complete eradication of disease. In addition to targeting the genomic dysregulation that often drives resistance to therapy, another potential therapeutic opportunity lies in modulation of the tumors' interaction with the immune system. The importance of the immune system in the body's natural defense against cancer has been well established, and tumor cells have evolved creative mechanisms for 'hiding' from attack by the immune system [239]. Therefore, disrupting these mechanisms and/or increasing the immunogenicity of the tumor present potentially promising therapeutic opportunities. One example of therapeutic exploitation of this phenomenon is the recent development of immune checkpoint inhibitors, which are showing significant promise in the treatment of solid tumors [240]. As we develop a more extensive understanding of the specific ways in which tumor cells modulate themselves and their surrounding environment to escape identification and eradication by the immune system, we may be able to develop creative and potentially effective new therapies for genomically heterogeneous tumors.

## **Conclusion**

The past decade has seen dramatic improvement in outcomes for patients with *EGFR*-mutant lung cancer. These improved outcomes are the result of the identification of biomarkers of sensitivity to targeted therapies and subsequent rapid development of therapeutic agents for this purpose. However, there is much work still to be done. Significant extension of progression-free and overall survival

is meaningful and encouraging, but we have not yet reached the point of a cure. For *EGFR*-mutant lung cancer, the next steps in targeted therapy depend largely on what we can learn from ongoing clinical trials of mutant-selective, third-generation EGFR TKIs. As with previous generations of EGFR TKIs, we seek to learn whether there are differences in efficacy and/or mechanisms of resistance among all of the available third-generation EGFR TKIs. Over time, we will learn whether mechanisms of resistance to these third-generation inhibitors are more commonly EGFR-dependent or EGFR-independent, giving us insight into the relative need for fourth or fifth generation EGFR TKIs versus better inhibitors of downstream effector pathways.

In addition to kinase-directed targeted therapies, another major breakthrough in the field of solid tumor oncology has been the recent success of immune checkpoint inhibitors in solid tumors, including lung cancer. In the case of *EGFR*-mutant lung cancer, for which we already have multiple available, highly effective targeted therapies, one of the primary scientific challenges will be to discern whether combination of TKIs with immunotherapies will improve patient outcomes. While immune checkpoint inhibitors will hopefully demonstrate broad efficacy across tumor types, more data are needed to stratify tumors based on their likelihood of response. The ultimately goal is to develop rational strategies for use of these therapies in the clinic, rather than distributing them to unselected populations.

Continued scientific discovery, combined with improving clinical infrastructure for mutational testing and administration of appropriate targeted agents, is launching us into a new area of 'precision medicine' in oncology. Our

arsenal of targeted therapies is growing along with our understanding of the genomic complexity and signaling plasticity of solid tumors. As we gain insight into the clonal evolution of tumors in response to targeted therapy, the greatest challenge that we ultimately face is discerning the most appropriate combinations and dosing strategies of these therapeutic agents. In the long run, our ability to design these rational combinations and appropriate sequences of treatment will dictate the next phase of forward progress in cancer therapy, hopefully making drug-resistant disease a thing of the past.

## Appendix

### Supplementary information for Chapter I

No supplementary materials, methods, tables or figures accompany this chapter.

## Supplementary information for Chapter II

No supplementary material and methods accompany this chapter.

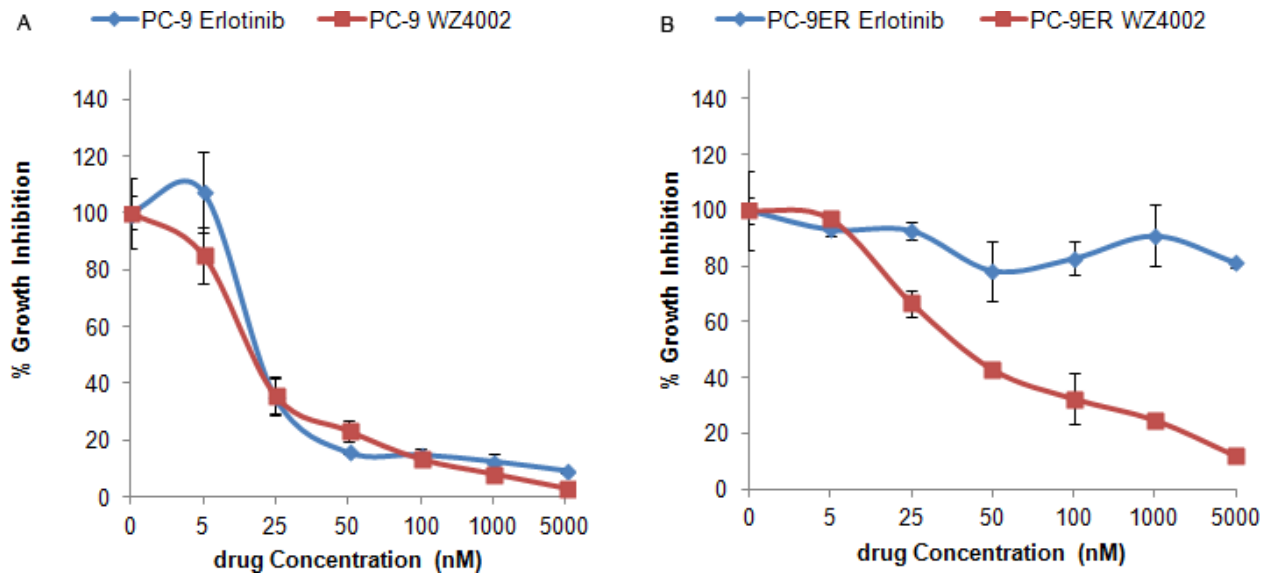


**Figure 23. Effect of erlotinib and WZ4002 (T790M-specific small molecule) on the growth of PC-9 (A) and PC-9/ER cells (B).**

The data suggest that PC-9/ER still depend upon EGFR signaling for survival.

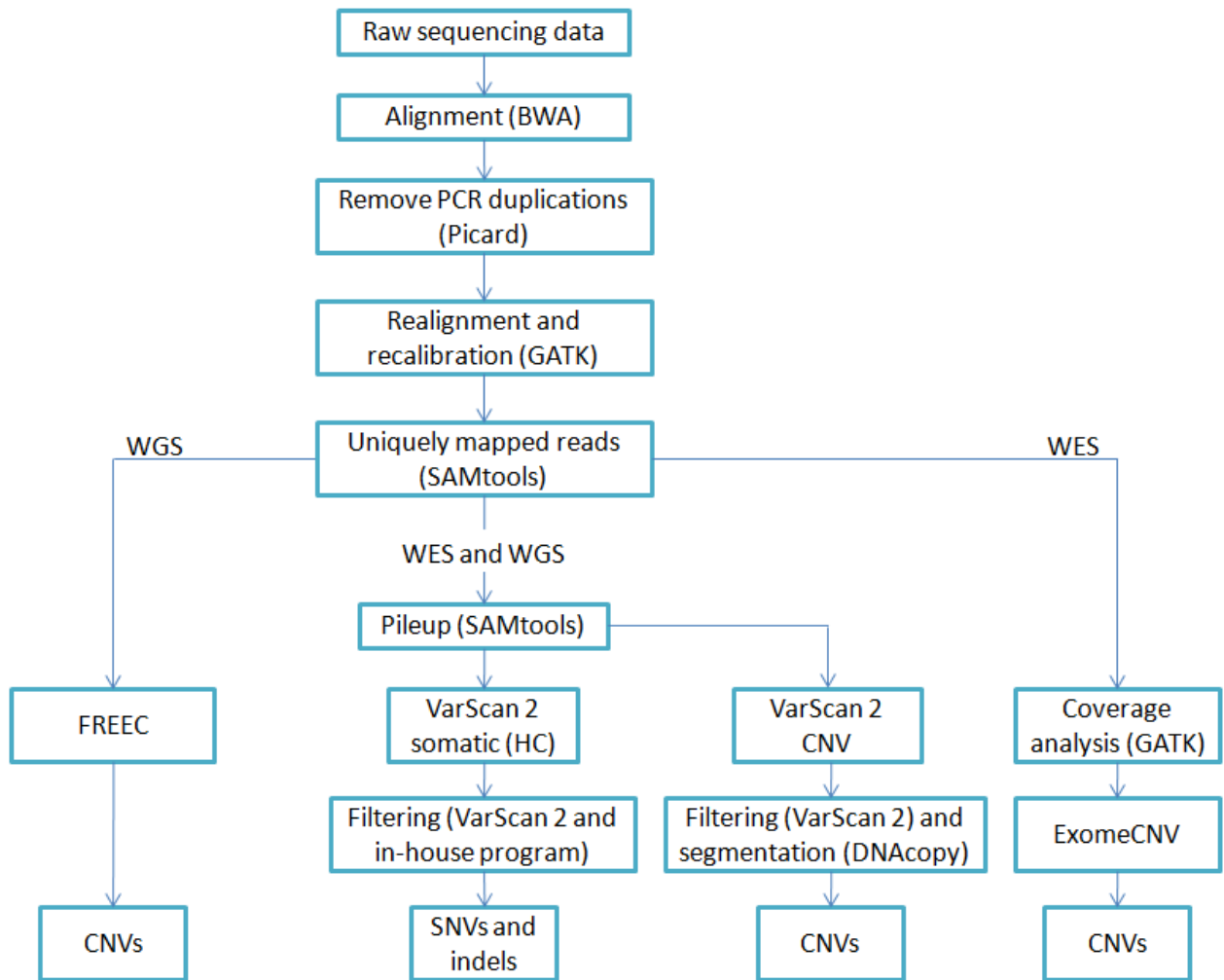


**Figure 24. Analysis pipeline.**

The process to call SNVs and small insertions and deletions (indels) was the same for whole genome sequencing (WGS) and whole exome sequencing (WES) data but was different for calling copy number variations. HC: high confidence.

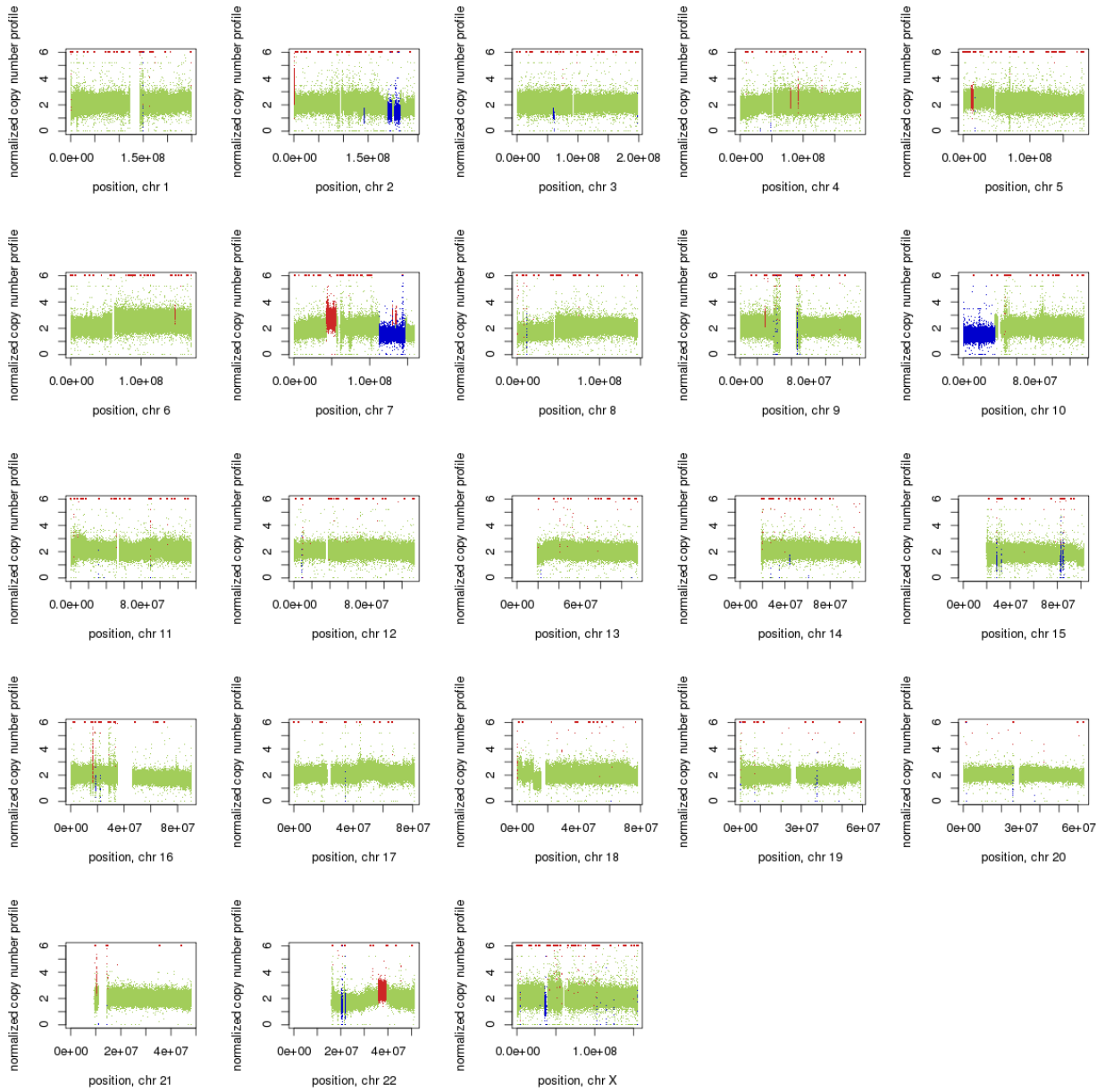


**Figure 25. Copy number variation (CNV) changes in PC-9/ER compared to PC-9/S1 by Control-FREEC.**

Red: CNV gain; blue: CNV loss; green: no change.

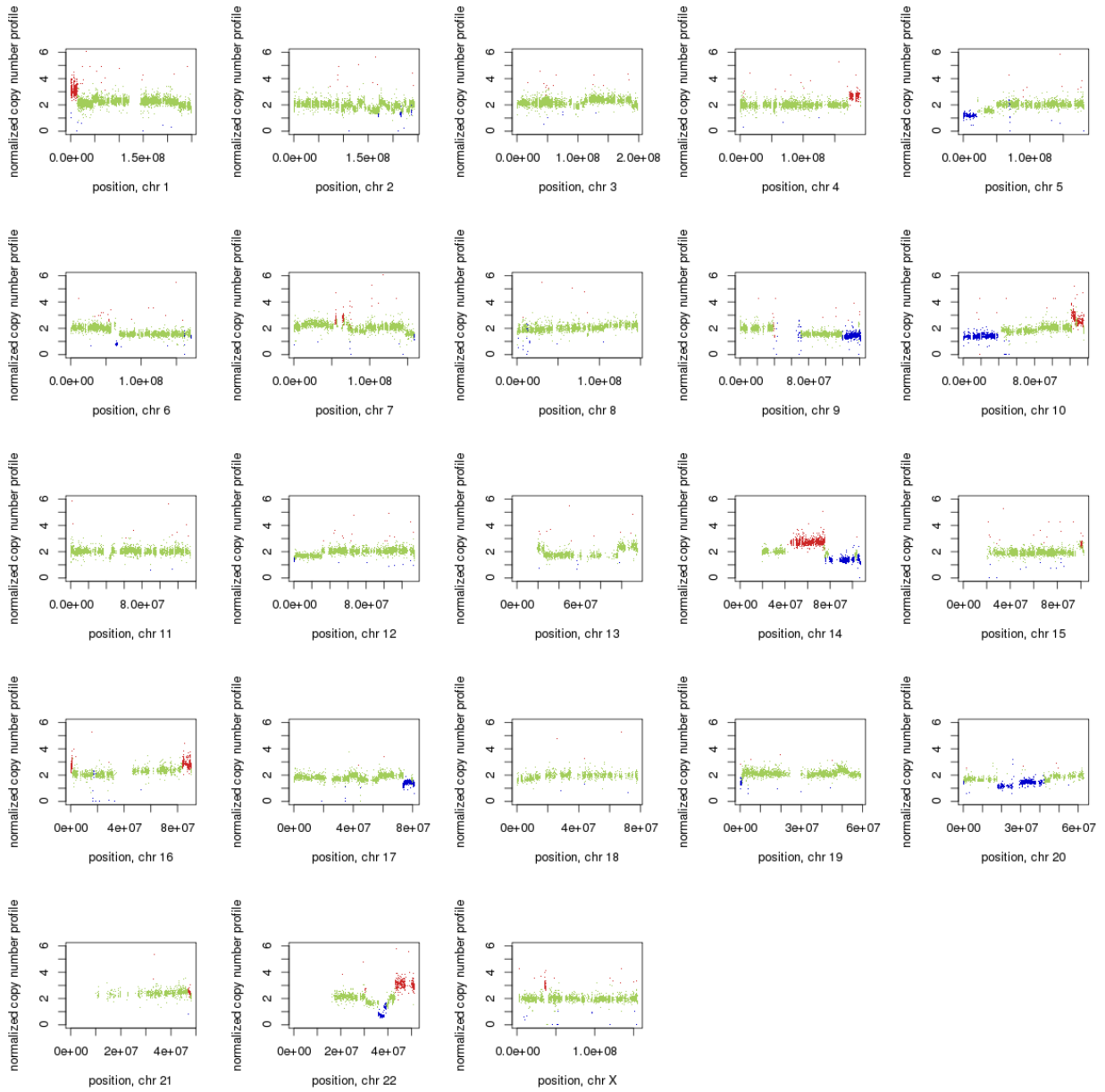


**Figure 26. Copy number variation (CNV) changes in PC-9/BRc1 compared to PC-9/S2.**

Red: CNV gain; blue: CNV loss; green: no change.

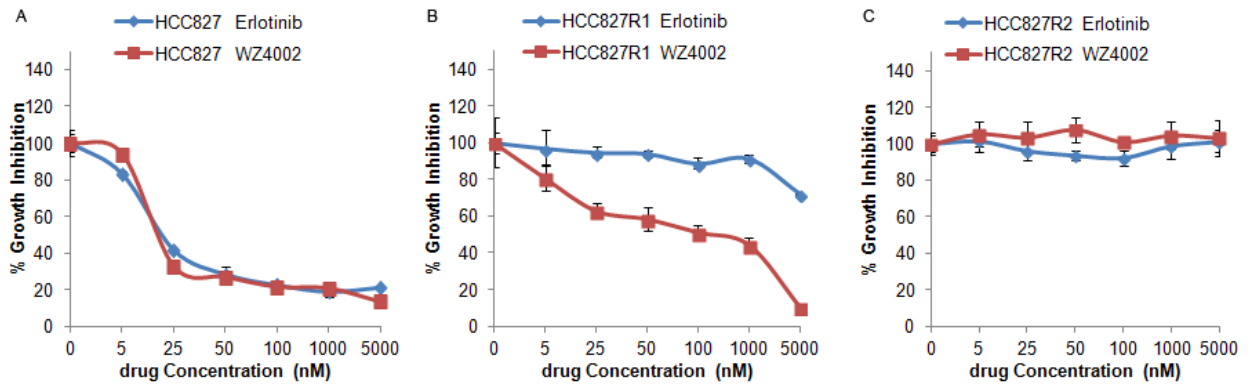


**Figure 27. Effect of erlotinib and WZ4002 (T790M-specific small molecule) on the growth of HCC827 (A), HCC827/R1 (B), and HCC827/R2 (C) cells.**

The data suggest that HCC827/R1 but not HCC827/R2 cells still depend upon EGFR signaling for survival.

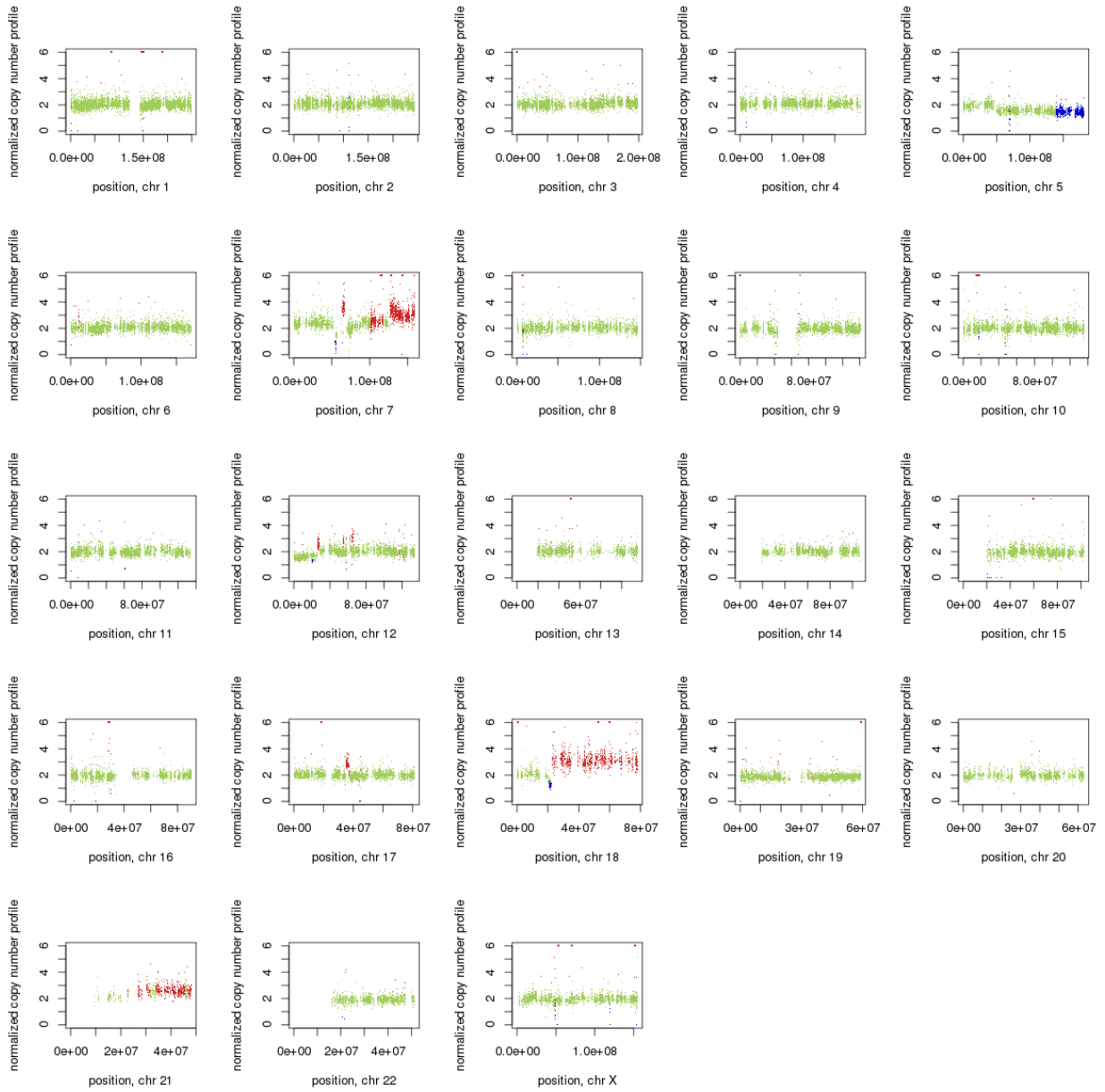


**Figure 28. Copy number variation (CNV) changes in HCC827/R1 compared to HCC827.**

Red: CNV gain; blue: CNV loss; green: no change.

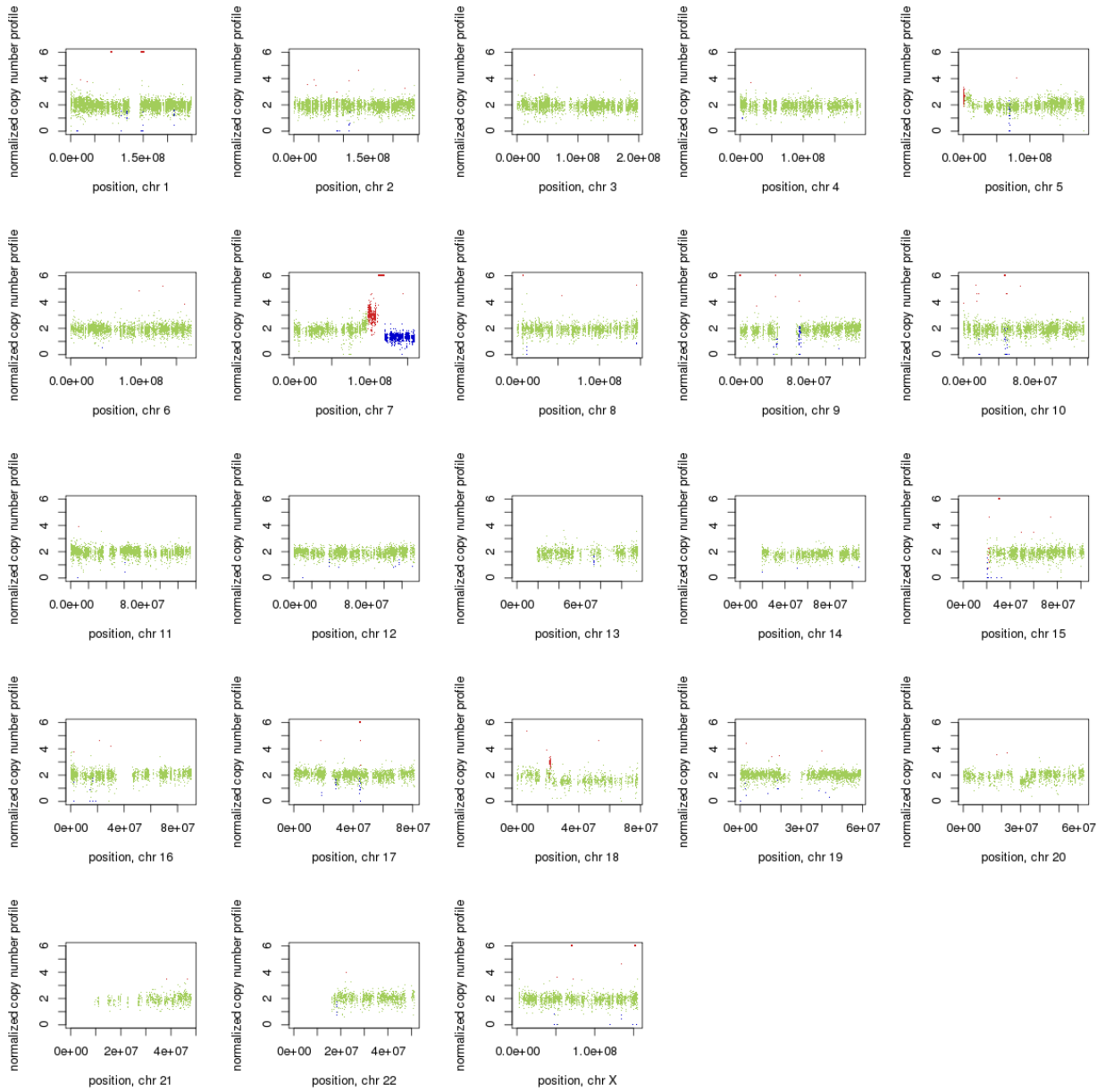


**Figure 29. Copy number variation (CNV) changes in HCC827/R2 compared to HCC827.**

Red: CNV gain; blue: CNV loss; green: no change

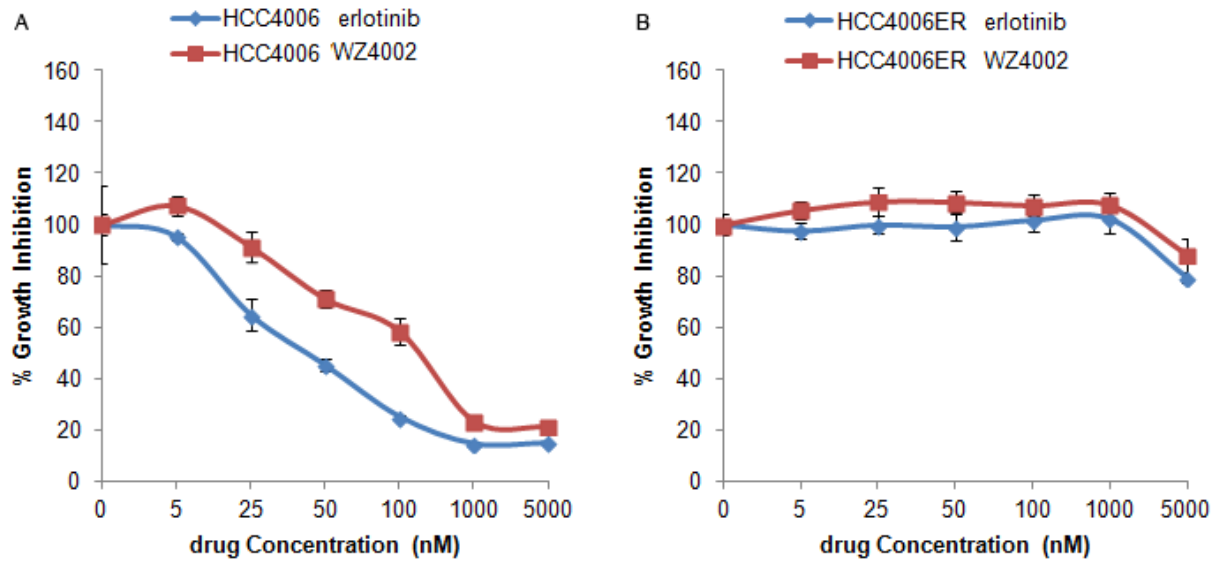
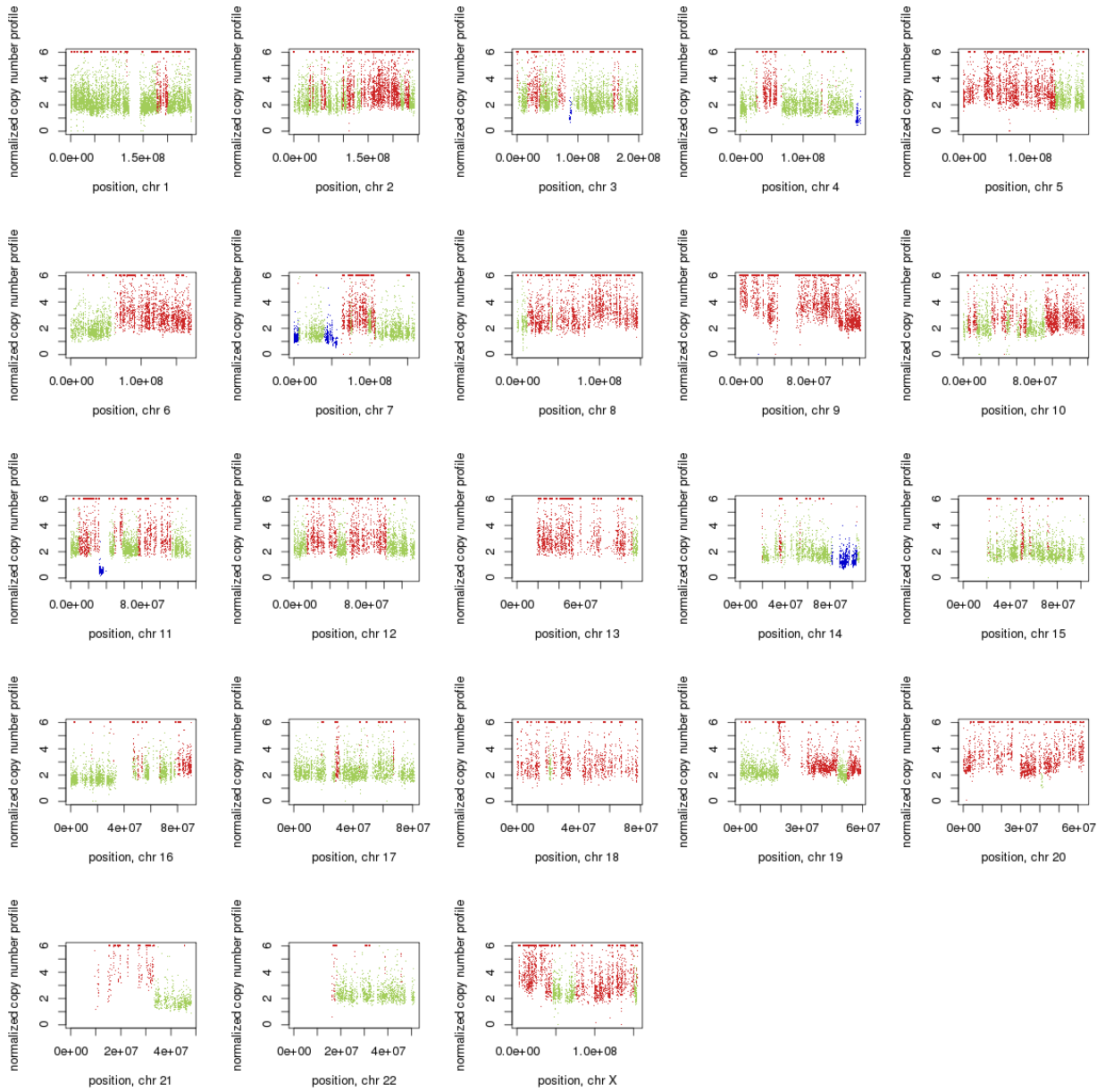


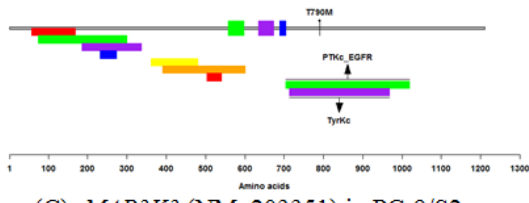
Figure 30. Effect of erlotinib and WZ4002 (T790M-specific small molecule) on the growth of HCC4006 (A) and HCC4006/ER (B) cells.



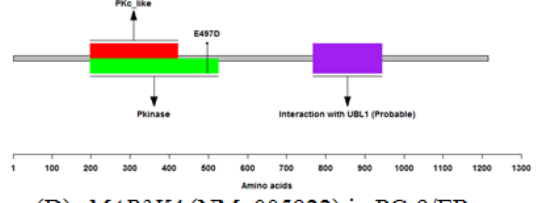
**Figure 31. Copy number variation (CNV) changes in HCC4006/ER compared to HCC4006.**

Red: CNV gain; blue: CNV loss; green: no change.

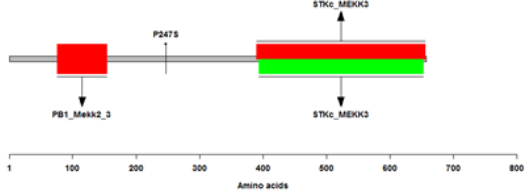
(A). *EGFR* (NM\_005228) in PC-9/ER, PC-9/BRc1 and HCC827/R1(validated)



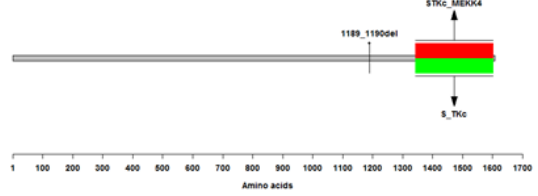
(B). *HIPK3* (NM\_005734) in HCC827/R2 (validated)



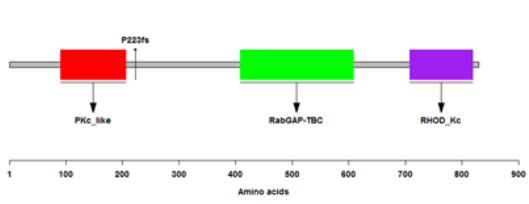
(C). *MAP3K3* (NM\_203351) in PC-9/S2



(D). *MAP3K4* (NM\_005922) in PC-9/ER



(E). *TBCK* (NM\_033115) in HCC827/R1



(F). *TESK2* (NM\_007170) in HCC4006 (validated)

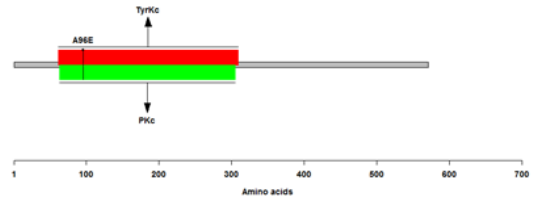


**Figure 32. Illustration of location of mutations in kinase genes detected in the cell lines.**

Table 12 List of validated SNVs and indels in PC-9/ER cells.

Gene	Chr. *	Position (bp)	RefSeq	Nucleotide change	Amino acid change	Tumor var freq **
<u>SNVs</u>						
<i>KIF17</i>	1	20998644	NM_020816	c.C2509T	p.Q837X	41.38%
			NM_0011228 19	c.C2509T	p.Q837X	
<i>GPR61</i>	1	110085927	NM_031936	c.C283T	p.P95S	43.75%
<i>PKP4</i>	2	159477811	NM_0010054 76	c.G481C	p.G161R	50%
			NM_003628	c.G481C	p.G161R	
<i>SRGAP 3</i>	3	9032400	NM_0010331 17	c.C2610A	p.S870R	58.82%
<i>ZNF445</i>	3	44489533	NM_014850	c.C2682A	p.S894R	42.42%
<i>ATP8A1</i>	4	42551076	NM_181489	c.G1630A	p.D544N	20.83%
			NM_006095	c.G1606C	p.G536R	
			NM_0011055 29	c.G1561C	p.G521R	
<i>AFAP1L 1</i>	5	148702274	NM_152406	c.G1804A	p.A602T	27.27%
			NM_0011463 37	c.G1804A	p.A602T	
<b><i>EGFR</i></b>	<b>7</b>	<b>55249071</b>	<b>NM_005228</b>	<b>c.C2369T</b>	<b>p.T790M</b>	<b>21.92%</b>
<i>LIN7C</i>	11	27528284	NM_018362	c.G16T	p.E6X	26.67%
<i>SF1</i>	11	64535163	NM_201997	c.C1222T	p.H408Y	21.62%
			NM_201998	c.C1222T	p.H408Y	
			NM_201995	c.C1222T	p.H408Y	
			NM_0011780 30	c.C1597T	p.H533Y	
			NM_0011780 31	c.C1144T	p.H382Y	
<i>BIRC3</i>	11	102195950	NM_004630	c.C1222T	p.H408Y	
			NM_182962	c.A710T	p.N237I	25.84%
			NM_001165	c.A710T	p.N237I	
<i>CPNE8</i>	12	39161493	NM_153634	c.C519A	p.D173E	42.11%
<i>GNPTG</i>	16	1412518	NM_032520	c.G592T	p.E198X	36.67%
<i>PDILT</i>	16	20387492	NM_174924	c.G441C	p.W147C	34.04%
<i>AOC2</i>	17	40997679	NM_009590	c.G1036C	p.V346L	25%
			NM_001158	c.G1036C	p.V346L	
<i>TSGA10 #</i>	2	99720494	NM_182911	c.G547A	p.A183T	27.78%
			NM_025244	c.G547A	p.A183T	
<i>FRAS1#</i>	4	79238630	NM_0011661 33	c.A1928T	p.E643V	59.09%
			NM_025074	c.A1928T	p.E643V	
<i>SEC24D #</i>	4	119738478	NM_014822	c.C338G	p.S113C	41.46%
<i>ATP2A1 #</i>	16	28914722	NM_004320	c.G2941A	p.D981N	46.15%
			NM_173201	c.G2941A	p.D981N	
<i>GRIN3B #</i>	19	1003585	NM_138690	c.G883T	p.D295Y	55.56%
<u>Indels</u>						
<i>ZNF385 B</i>	2	180383295- 180383297	NM_0011133 98	c.159_161del	p.53_54del	20.75%
			NM_152520	c.465_467del	p.155_156del	
			NM_0011133	c.237_239del	p.79_80del	

			97				
<i>ACACA</i>	17	35601597-35601602	NM_198834	c.2644_2649del	p.882_883del	34.55%	
			NM_198838	c.2299_2304del	p.767_768del		
			NM_198837	c.2359_2364del	p.787_788del		
			NM_198839	c.2533_2538del	p.845_846del		
			NM_198836	c.2533_2538del	p.845_846del		
<i>FAM122C</i>	X	133941611-133941611	NM_001170780	c.91delT	p.L31fs	38.60%	
<i>LRCH2</i>	X	114391202-114391204	NM_020871	c.1490_1492del	p.497_498del	33.33%	
<i>TBC1D8B</i>	X	106069294-106069314	NM_017752	c.862_882del	p.288_294del	52.63%	
			NM_198881	c.862_882del	p.288_294del		
<i>ZNF793</i>	19	38028414-38028414	NM_001013659	c.854_855insT	p.C285fs	20.75%	

Chr.: chromosomes. Var freq: variant frequency. # These genes are missed by our stringent filtering criteria but were confirmed by Sanger resequencing.

**Table 13. CNV regions in PC-9/ER**

<b>Cytoband</b>	<b>Start (Mb)</b>	<b>End (Mb)</b>	<b>Copy number</b>	<b>Size (Mb)</b>	<b>CGC* genes</b>
<i>Amplification</i>					
2p25.3	0	0.79	3-4	0.79	
5p15.1-p15.2	11.53	15.28	3	3.74	
7p11.2-p13	43.36	55.33	3	11.97	<i>EGFR, IKZF1</i>
7q32.3	130.50	130.63	3	0.13	
22q12.3-q13.1	35.99	39.24	3	3.25	<i>MYH9</i>
<i>Deletion</i>					
2q22.1	141.73	142.17	1	0.44	
2q32	189.12	197.88	1	8.76	<i>PMS1</i>
2q34	202.75	214.48	1	11.73	<i>CREB1, IDH1</i>
7q31.1-q32.3	112.95	130.5	1	17.55	<i>MET</i>
7q32.3-q33	130.63	133.53	1	2.9	
7q33-q35	134.71	146.79	1	12.07	<i>BRAF, CREB3L2, KIAA1549</i>
9q13	66.93	67.04	1	0.11	
10p14-p15.3	0.00	11.77	1	11.77	
10p11.21-p12.32	11.77	35.58	1	23.81	<i>ABI1, MLLT10, KIF5B</i>
15q25.2	82.89	83.02	1	0.13	
22q11.21	20.34	20.49	1	0.15	
Xp11.4-p21.1	35.38	38.4	1	3.02	

\*CGC: Cancer Gene Census.

**Table 14. List of validated SNVs in cell line PC-9/BRc1**

<b>Gene</b>	<b>Chr. *</b>	<b>Position (bp)</b>	<b>RefSeq</b>	<b>Nucleotide change</b>	<b>Amino change</b>	<b>acid</b>	<b>Tumor var freq **</b>
<i>LRP1B</i>	2	141214142	NM_018557	c.G9845T	p.G3282V,		37.77%
<i>LRP1B</i>	2	141459727	NM_018557	c.C6285A	p.Y2095X,		28.71%
<i>LRP1B</i>	2	141660570	NM_018557	c.G3685T	p.E1229X,		40.13%
<i>RFX6</i>	6	117240392	NM_173560	c.A1115T	p.K372I,		26.43%
<i>AHI1</i>	6	135644437	NM_00113483 1	c.C3191T	p.A1064V,AHI1		59.26%
			NM_00113483 0	c.C3191T	p.A1064V,AHI1		
			NM_017651	c.C3191T	p.A1064V,		
<i>EGFR</i>	7	55249071	NM_005228	c.C2369T	p.T790M,		33.24%
<i>MLL2</i>	12	49434397	NM_003482	c.C7156T	p.R2386W,		37.74%
<i>PCDH9</i>	13	67800964	NM_203487	c.C1609T	p.R537X,PCDH9		20%
			NM_020403	c.C1609T	p.R537X,		
<i>CDH24</i>	14	23524547	NM_144985	c.G217A	p.D73N,CDH24		35.34%
			NM_022478	c.G217A	p.D73N,		
<i>HIRA</i>	22	19343811	NM_003325	c.G2397T	p.W799C,		60.66%
<i>ATRX</i>	X	76875965	NM_000489	c.C5170A	p.L1724I,ATRX		41.67%
			NM_138270	c.C5056A	p.L1686I,		

Chr.: chromosomes. \*\* Var freq: variant frequency.

**Table 15. CNV regions in PC-9/BRc1**

<b>Cytoband</b>	<b>Start (Mb)</b>	<b>End (Mb)</b>	<b>Copy number</b>	<b>Size (Mb)</b>	<b>CGC* genes</b>
<i>Amplification</i>					
1p36.21-p36.33	0.75	13.93	4.78	13.19	<i>CAMTA1, PRDM16, RPL22, TNFRSF14, BCL6, EIF4A2, ETV5, FOXL2, GATA2, GMPS, MECOM, MLF1, PIK3CA, RPN1, SOX2, WWTR1</i>
3q13.13-q27.3	111.26	187.45	3.00	76.19	
4q33-q35.2	172.74	190.86	3.33	18.13	
7q11.21-q11.22	64.25	71.28		7.02	<i>SBDS</i>
10q26.11-q26.3	121.54	134.92	3.89	13.38	<i>FGFR2</i>
13q32.1-q34	96.41	99.08	3	2.67	
14q21.2-q24.3	42.37	75.47	3.68	33.10	
15q26.2-q26.3	96.87	101.87	3.00	5.00	
16q23.3-q24.3	83.38	90.03	3.92	6.65	<i>CBFA2T3, FANCA</i>
19q13.32-q13.41	47.71	52.73	3.00	5.02	<i>KLK2, PPP2R1A</i>
21p11.1-q22.3	9.91	48.08	3.33	38.18	<i>ERG, OLIG2, RUNX1, TMPRSS2, U2AF1</i>
22q13.2-q13.33	43.09	51.19	4.40	8.10	
Xp21.1	35.82	37.67	4.50	1.85	
<i>Deletion</i>					
2q22.2-q31.1	142.57	171.40	1.00	28.83	
2q33.1	197.89	202.74	1.00	4.85	<i>SF3B1</i>
2q34-q35	214.73	217.06	1.00	2.33	<i>ATIC</i>
2q36.3-q37.1	227.66	233.43	1.00	5.77	
2q37.2	236.79	237.03	1.00	0.24	
3q11.2	96.53	96.96	1.00	0.43	
4q12	53.46	54.55	1.00	1.08	<i>FIP1L1</i>
5p14.3-p15.33	0.14	20.31	1.00	20.16	
5p12-p14.3	21.98	45.65	1.00	23.67	<i>IL7R, LIFR</i>
6p25.3	0.11	0.29	1.00	0.19	
6q12	64.29	66.21	1.00	1.92	
6q12-q27	69.35	170.89	1.00	101.54	<i>ECT2L, EZR, FGFR10P, FOXO3, GOPC, MLLT4, MYB, PRDM1, ROS1, TNFAIP3, EZH2, MLL3, MNX1</i>
7q35-q36.3	147.08	158.94	1.00	11.86	
8q21.13-q21.2	85.44	86.09	1.00	0.65	
9p11.1-q34.3	40.70	141.11	1.00	100.42	<i>ABL1, BRD3, FANCC, GNAQ, NUP214, OMD, PTCH1, RALGDS, SYK, TSC1, XPA, ABI1, GATA3, KIF5B, KLF6, MLLT10, EXT2</i>
10p11.1-p15.3	0.09	38.69	1.00	38.59	
11p11.2-p12	36.68	45.31	1.00	8.63	
11q13.4	74.55	74.65	1.00	0.11	
12p13.33	0.18	1.92	1.00	1.74	<i>ERC1, KDM5A</i>
14q24.3-q32.33	76.09	107.28	1.00	31.19	<i>BCL11B, DICER1, GOLGA5, TCL1A, TRIP11, TSHR, AKT1, ASPSCR1, CANT1, RNF213, SEPT9, SRSF2</i>
17q25.1-q25.3	73.66	81.05	1.00	7.39	
18p11.32	0.16	0.63	1.00	0.46	
19p13.3	0.07	1.13	1.00	1.06	
20p13	0.07	0.37	1.00	0.30	
20p11.1- q13.12	17.92	45.36	1.00	27.44	<i>ASXL1, MAFB, TOP1, SDC4</i>
22q12.3-q13.1	36.00	40.07	1.00	4.06	<i>MYH9, PDGFB</i>

CGC: Cancer Gene Census.

**Table 16. List of validated SNVs in cell line HCC827/R1**

<b>Gene</b>	<b>Chr. *</b>	<b>Position (bp)</b>	<b>RefSeq</b>	<b>Nucleotide change</b>	<b>Amino acid change</b>	<b>Tumor var freq **</b>
<i>C1orf87</i>	1	60476121	NM_152377	c.A1135T	p.N379Y	23.59%
<i>TTC13</i>	1	231067615	NM_024525	c.G992A	p.G331D	20.75%
			NM_001122835	c.G833A	p.G278D	
<i>LRP1B</i>	2	141093341	NM_018557	c.G11959A	p.D3987N	25.88%
<i>ADCY5</i>	3	123044280	NM_183357	c.G1977A	p.M659I	20%
			NM_001199642	c.G927A	p.M309I	
<i>CPEB2</i>	4	15009978	NM_182485	c.A1961G	p.Q654R	25%
			NM_001177382	c.A1961G	p.Q654R	
<i>TLR2</i>	4	154625931	NM_003264	c.G1872A	p.W624X	30.19%
<i>NOS3</i>	7	150693625	NM_001160110	c.A404G	p.Y135C	38.46%
			NM_000603	c.A404G	p.Y135C	
			NM_001160109	c.A404G	p.Y135C	
			NM_001160111	c.A404G	p.Y135C	
<i>MYH1</i>	17	10411873	NM_005963	c.G1704T	p.K568N	20.30%
<i>SFRP1</i> <sup>#</sup>	8	41122998	NM_003012	c.G633A	p.M211I	29.03%

Chr.: chromosomes.

\*\*Var freq: variant frequency.

# These genes were missed by our stringent filtering criteria but were confirmed by Sanger resequencing.

**Table 17. CNV regions in HCC827/R1**

<b>Cytoband</b>	<b>Start (Mb)</b>	<b>End (Mb)</b>	<b>Copy number</b>	<b>Size (Mb)</b>	<b>CGC* genes</b>
<i>Amplification</i>					
7p12.1-p22.3	0.54	51.26	3	50.72	<i>CARD11, ETV1, HNRNPA2B1, HOXA11, HOXA13, HOXA9, IKZF1, PMS2</i>
7q11.21	62.9 1	158.94	3.80	82.11	<i>SBDS, AKAP9, CDK6, MET, SMO, CREB3L2, KIAA1549, BRAF, EZH2, MLL3, MNX1</i>
12q13.13	54.7 4	54.89	3	0.16	
17q12	35.3 1	37.12	3.88	1.14	<i>LASP1, MLLT6</i>
18p11.22	8.83	9.20	4	0.37	
18q11.2-q23	22.8 0	78.01	4.076	55.20	<i>SS18, ZNF521, MALT1, SMAD4, BCL2, KDSR</i>
21p11.1-q22.3	9.59	45.92	3.5	36.33	<i>ERG, OLIG2, RUNX1, TMPRSS2, U2AF1</i>
<i>Deletion</i>					
11q12.1	57.1 9	57.32	1	0.13	
12p12.2-p13.33	0.07	20.83	1	20.76	<i>CCND2, ERC1, ETV6, KDM5A, ZNF384</i>
17q21.2	39.1 5	39.43	1	0.28	
18q11.2	21.1 0	22.06	1	0.96	
2q11.2	97.5 1	97.69	1	0.18	
5p11-q35.3	0.14	180.69	1	180.5 5	<i>ACSL6, AFF4, APC, ARHGAP26, CD74, EBF1, IL6ST, IL7R, ITK, LIFR, NPM1, NSD1, PDGFRB, PIK3R1, RANBP17, TLX3</i>
7p11.2-p12.1	51.2 9	57.52	1	6.24	<i>EGFR</i>
8p11.21-p11.22	38.9 5	40.53	4	1.58	

CGC: Cancer Gene Census.

**Table 18. List of validated SNVs in cell line HCC827/R2**

Gene	Chr. *	Position (bp)	RefSeq	Nucleotide change	Amino change	acid	Tumo r var freq **
<i>PPM1B</i>	2	44428427	NM_0010335 57	c.A89C	p.Q30P		26.27 %
			NM_002706	c.A89C	p.Q30P		
			NM_0010335 56	c.A89C	p.Q30P		
			NM_177968	c.A89C	p.Q30P		
<i>PIKFYV E</i>	2	209218871	NM_015040	c.G6094T	p.V2032F		26.42 %
<i>COL4A3</i>	2	228172569	NM_000091	c.C4396G	p.P1466A		25.22 %
<i>PRUNE2</i>	9	79469101	NM_015225	c.G60T	p.K20N		30%
<i>IPPK</i>	9	95397576	NM_022755	c.G931C	p.E311Q		24.44 %
<i>HIPK3</i>	11	33360958	NM_005734	c.A1491T	p.E497D		45.97 %
			NM_0010482 00	c.A1491T	p.E497D		
<i>DNAH9</i>	17	11872719	NM_004662	c.T2272A	p.Y758N		20.35 %
			NM_001372	c.T13336A	p.Y4446N		
<i>MYO15A</i>	17	18058678	NM_016239	c.C8391G	p.I2797M		28.21 %
<i>ITGA3</i>	17	48151895	NM_002204	c.C1466T	p.S489F		21.98 %
			NM_005501	c.C1466T	p.S489F		
<i>C19orf57</i>	19	14000422	NM_024323	c.C1247T	p.T416I		22.73 %
<i>ZNF573</i>	19	38230827	NM_152360	c.A390T	p.K130N		48.09 %
			NM_0011726 92	c.A300T	p.K100N		
			NM_0011726 89	c.A300T	p.K100N		
			NM_0011726 91	c.A558T	p.K186N		
			NM_0011726 90	c.A564T	p.K188N		
<i>AIFM3</i>	22	21331162	NM_0010180 60	c.G1153C	p.E385Q		51.56 %
			NM_0011462 88	c.G1171C	p.E391Q		
			NM_144704	c.G1153C	p.E385Q		
<i>DDX3X</i>	X	41205842	NM_001356	c.C1582T	p.R528C		43.03 %
			NM_0011934 17	c.C1534T	p.R512C		
			NM_0011934 16	c.C1582T	p.R528C		
<i>IL1RAPL 2</i>	X	105011627	NM_017416	c.G2034T	p.E678D		30.29 %
<i>F9</i>	X	138642963	NM_000133	c.G787C	p.V263L		30.27 %

---

<i>SLC36A</i>	5	150718671	NM_181776	c.C475G	p.L159V	18.06
2 <sup>#</sup>						%

---

Chr.: chromosomes.

\*\*Var freq: variant frequency.

# These genes were missed by our stringent filtering criteria but were confirmed by Sanger resequencing.

**Table 19. CNV regions (>100kb) in HCC827/R2**

<b>Cytoband</b>	<b>Start (Mb)</b>	<b>End (Mb)</b>	<b>Copy number</b>	<b>Size (Mb)</b>	<b>CGC* genes</b>
<i>Amplification</i>					
5p15.2-p15.33	0.14	11.73	3	11.59	
7q21.3-q31.1	97.49	108.16	4.45	10.67	
7q31.1-q31.31	111.85	117.88	5	6.03	<i>MET</i>
18q11.2	21.21	21.78	3.83	0.56	
<i>Deletion</i>					
1p22.1	93.65	93.83	1	0.17	
1p13.2	115.40	115.54	1	0.14	
1q32.3	213.25	213.44	1	0.19	
7p14.3	32.11	32.86	1	0.75	
7q31.31-q36.3	119.91	158.94	1	39.02	<i>BRAF, CREB3L2, EZH2, KIAA1549, MLL3, MNX1, SMO</i>
9p22.3	15.27	15.68	1	0.41	<i>PSIP1</i>
9p22.2	17.23	17.76	1	0.54	
18q11.2-q23	21.86	77.96	1	56.10	<i>BCL2, KDSR, MALT1, SMAD4, SS18, ZNF521</i>
20q11.21-q11.22	29.62	32.44	1	2.82	<i>ASXL1</i>
20q11.22-q11.23	34.00	35.18	1	1.18	

\*CGC: Cancer Gene Census.

**Table 20. List of validated SNVs in cell line HCC4006/ER**

<b>Gene</b>	<b>Chr.*</b>	<b>Position (bp)</b>	<b>RefSeq</b>	<b>Nucleotide change</b>	<b>Amino acid change</b>	<b>Tumor var freq**</b>
<i>APOB</i>	2	21233340	NM_000384	c.C6400A	p.Q2134K	32.81%
<i>GABRB2</i>	5	160837999	NM_000813	c.A523C	p.T175P	20.22%
			NM_021911	c.A523C	p.T175P	
<i>MDN1</i>	6	90428335	NM_014611	c.A6333G	p.I2111M	31.12%
<i>RUNDC3B</i>	7	87445550	NM_138290	c.C1249A	p.Q417K	25.40%
			NM_001134406	c.C1051A	p.Q351K	
			NM_001134405	c.C1198A	p.Q400K	
<i>OPRK1</i>	8	54147411	NM_000912	c.T518G	p.L173W	31.51%
<i>DNAJB5</i>	9	34996685	NM_012266	c.A635G	p.H212R	21.57%
			NM_001135004	c.A737G	p.H246R	
			NM_001135005	c.A851G	p.H284R,	
<i>MON2</i>	12	62926233	NM_015026	c.C1416A	p.D472E	30.95%
<i>CCDC33</i>	15	74627461	NM_182791	c.G1052C	p.G351A	24.32%
<i>ITSN1</i>	21	35258716	NM_003024	c.G4969A	p.E1657K	60%

\*Chr.: chromosomes.

\*\*Var freq: variant frequency.

**Table 21. Distribution of SNVs in 5' versus 3' UTRs and within the gene body across the different cell lines.**

	<b>5'-UTR</b>	<b>3'-UTR</b>	<b>Gene body*</b>
PC-9/S1	3	2	4
PC-9/ER	8	2	23
PC-9/S2	6	3	18
PC-9/BRc1	10	3	76
HCC827 vs. HCC827/R1	2	0	6
HCC827/R1	1	1	10
HCC827/R2	4	1	21
HCC4006	3	0	9
HCC4006/ER	1	3	16

\*We excluded those SNVs that failed in experimental validation. Therefore the numbers here may not match exactly to those listed in Table 2. Gene body indicates all the regions in a gene excluding the 5'- and 3'-UTRs.

**Table 22. Summary of kinase genes harboring non-silent SNVs/indels in each cell line.**

	PC-9 /S1	PC-9 /ER	PC-9 /S2	PC-9 /BRc1	HCC827		HCC827 /R1	HCC827 /R2	HCC4006	HCC4006 /ER
					vs. R1	vs. R2				
By SNV	0	<i>EGFR</i> *	<i>MAP3K3</i>	<i>EGFR</i> *	0	0	0	<i>HIPK3</i>	<i>TESK2</i>	0
By indel	0	<i>MAP3K4</i>	0	0	0	0	<i>TBCK</i>	0	0	0

\*Mutations involved in phosphorylation sites.

## Supplementary information for Chapter III

No supplementary materials, methods or tables accompany this chapter.

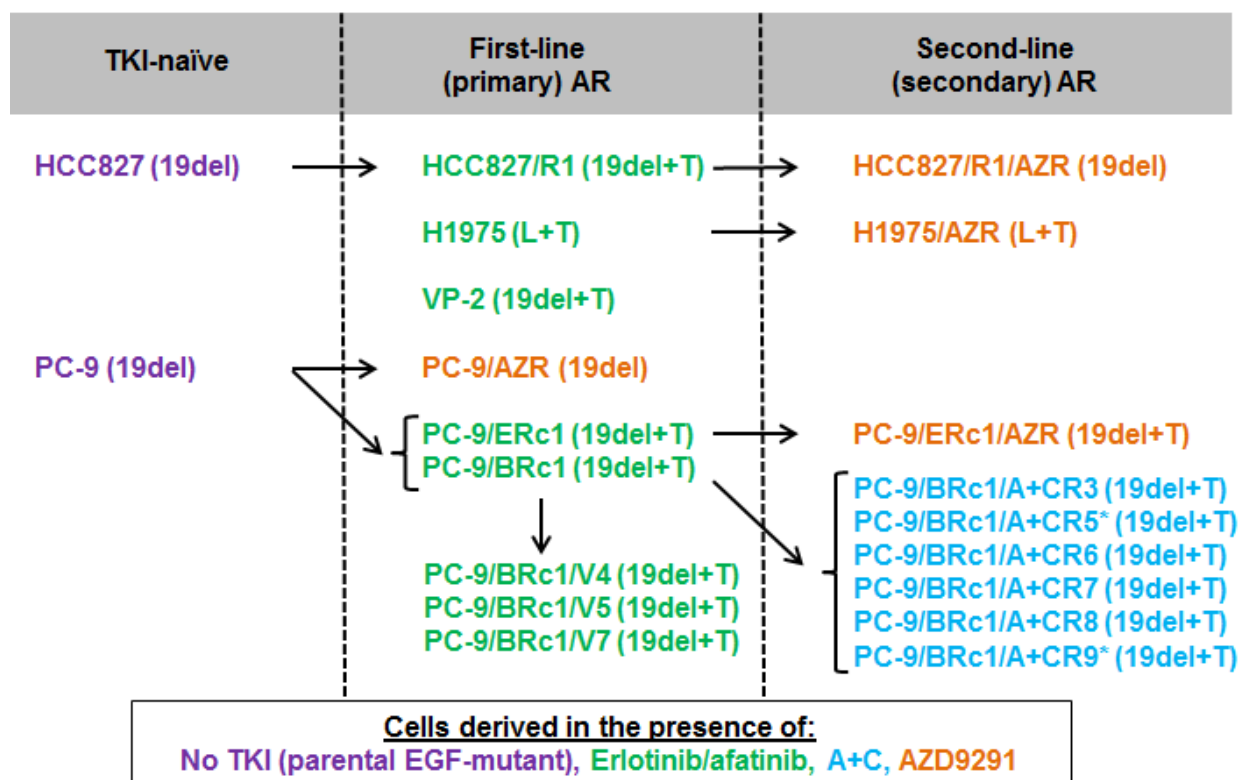


**Figure 33. Schematic of derivation 'lineages' for drug-sensitive and –resistant cell lines used in this study.**

HCC817/R1 cells were derived from HCC827 parental cells, and HCC827/R1/AZR cells were derived from HCC827/R1 cells. H1975/AZR cells were derived from H1975 cells. PC-9/AZR, PC-9/ERc1, and PC-9/BRc1 cells were derived from PC-9 parental cells. PC-9/ERc1/AZR cells were derived from PC-9/ERc1 cells. PC-9/BRc1/A+C and PC-9/BRc1/V cells were derived from PC-9/BRc1 cells in the presence or absence of A+C, respectively. Cell line names are color coded indicating the most recent EGFR inhibitor to which they were derived to be resistant. See Table 1 for additional information regarding derivation methods and genotype details.

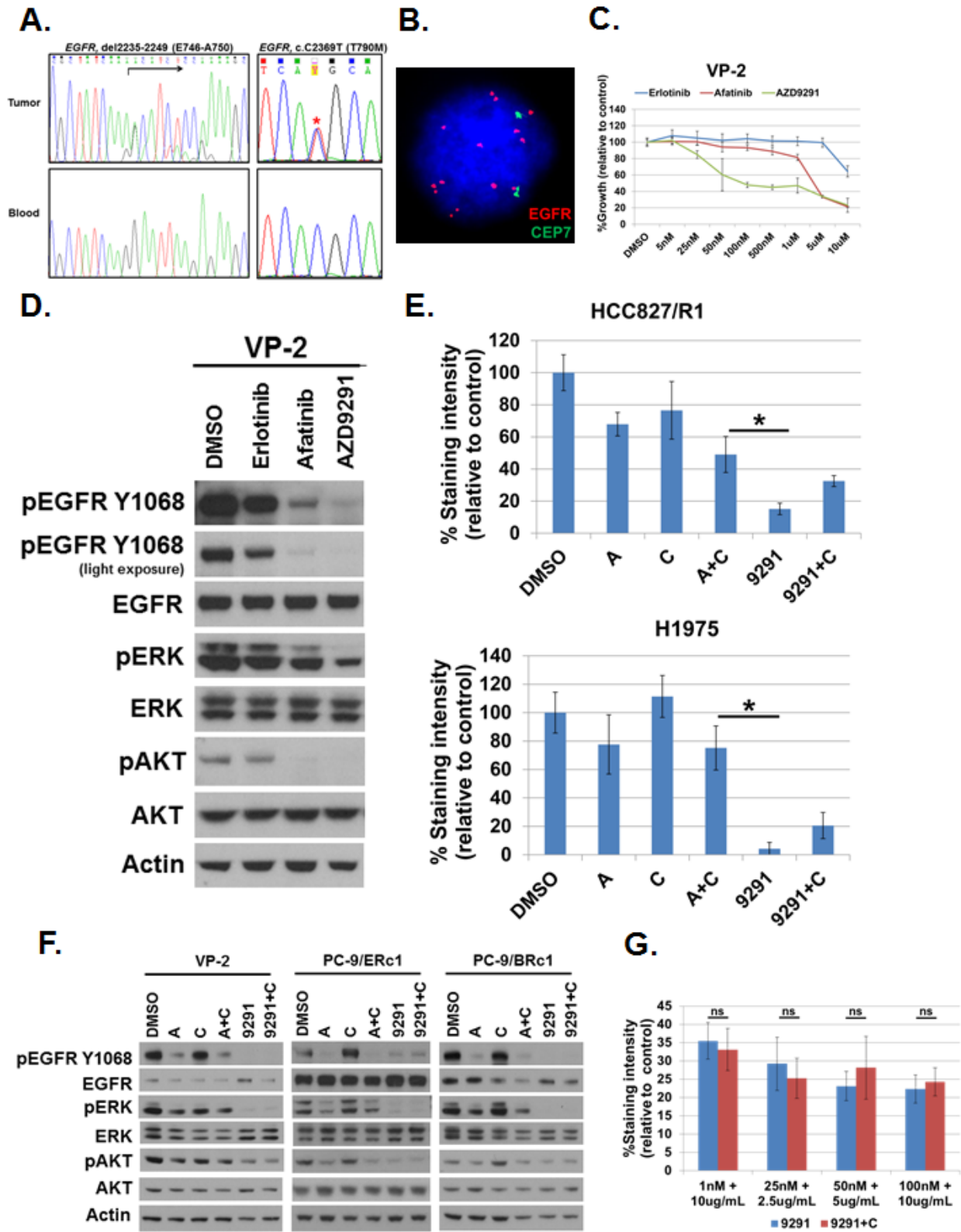
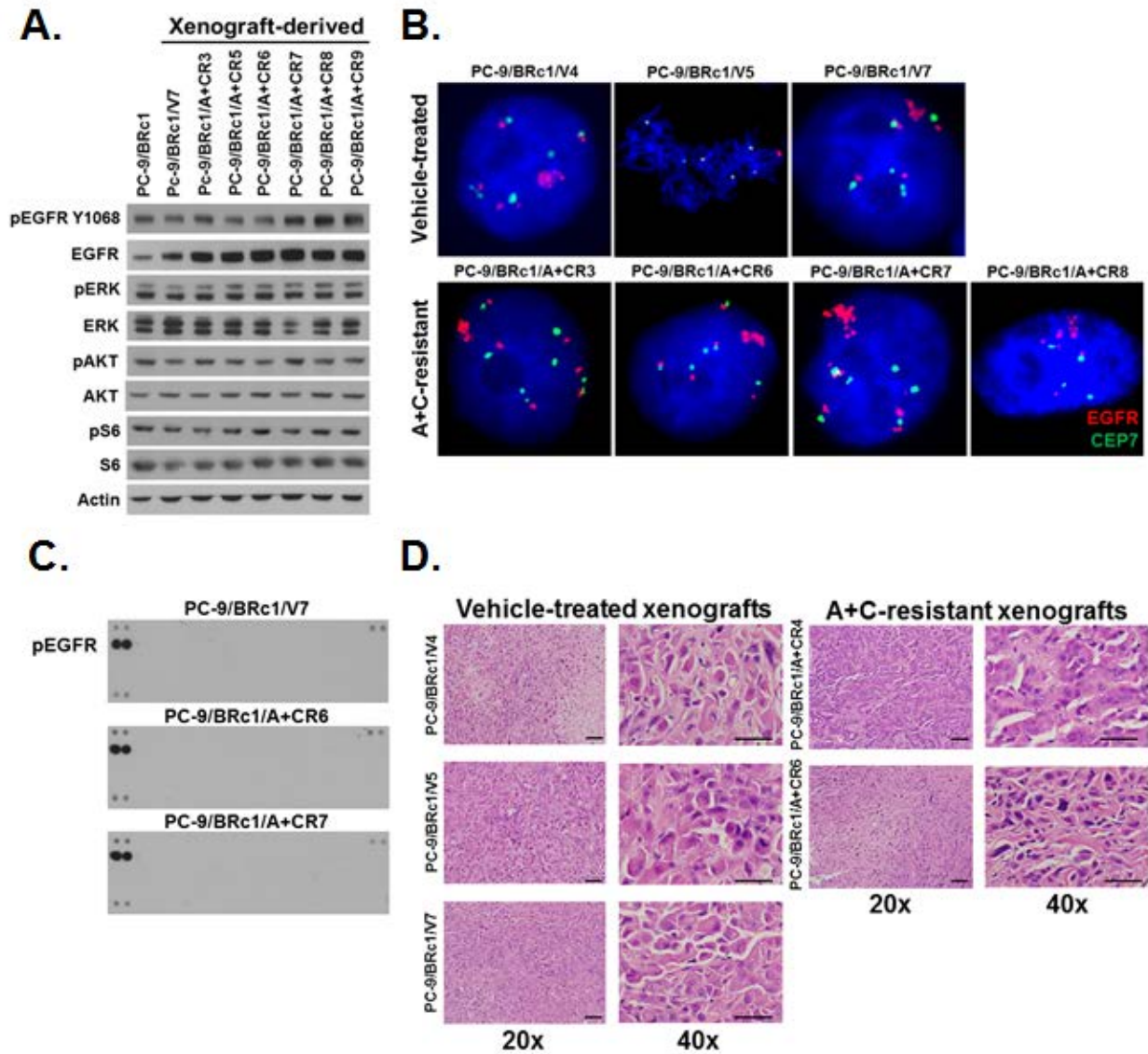


Figure 34. Characterization of T790M+ cell lines.

**A**, Forward sequence tracings from EGFR exons 19 (left) and 20 (right) demonstrating somatic EGFR 19del and EGFR T790M mutations in VP-2 cells. **B**, EGFR fluorescence *in situ* hybridization (FISH) of VP-2 cells. Nuclei show multiple clustered *EGFR* signals (red) and 4 chromosome 17 centromere signals (green), indicating *EGFR* amplification. **C**, Cell growth-inhibition assays demonstrate the resistance of VP-2 cells to erlotinib and afatinib and the sensitivity to growth inhibition by AZD9291. Data are expressed as a percentage of DMSO control and plotted as mean  $\pm$  standard deviation of hexuplicate data. **D**, Immunoblotting of lysates from VP-2 cells treated for 6 hours with DMSO, erlotinib [500nM], afatinib [50nM], or AZD9291 [50nM] demonstrate that AZD9291 is the most potent inhibitor of both phospho-EGFR and downstream signaling in VP-2 cells. **E**, Quantification of crystal violet staining of H1975 and HCC827/R1 cells treated for 10 days in triplicate with DMSO, afatinib (A) [50nM], cetuximab (C) [5ug/mL], afatinib + cetuximab (A+C), AZD9291 (9291) [50nM], or AZD9291 + cetuximab (9291+C). Data are expressed as mean  $\pm$  standard deviation of triplicate measurements; \* $p < 0.10$  for AZD9291 vs. A+C. **F**, Immunoblotting of cell lysates from VP-2, PC-9/ERc1, and PC-9/BRc1 treated for 6 hours with DMSO, afatinib (A) [50nM], cetuximab (C) [5ug/mL], A+C, AZD9291 (9291) [50nM], or AZD9291 + cetuximab (9291+C) show the effect of A+C and AZD9291 on phospho-EGFR, phospho-ERK, and phospho-AKT. **G**, Quantification of crystal violet staining of PC-9/BRc1 cells treated for 10 days in triplicate with increasing doses of AZD9291 alone (9291) or AZD9291 + cetuximab (9291+C), as indicated. Concentrations of AZD9291 are listed in [nM]; concentrations of cetuximab are listed in [ug/mL]. Data are expressed as mean  $\pm$  standard deviation of triplicate measurements; ns = non-significant at  $p = 0.05$  for AZD9291 vs. AZD9291 + cetuximab at all doses tested.



**Figure 35. Characterization of A+C-resistant cell lines.**

**A**, Immunoblotting of lysates from PC-9/BRC1, PC-9/BRC1/V7, and PC-9/BRC1/A+CR3, -5, -6, -7, -8, and -9 cells shows increased EGFR expression but no increase in total or phospho- ERK, AKT, or S6 in the A+C-resistant cell lines **B**, Fluorescence *in-situ* hybridization (FISH) analysis of vehicle control PC-9/BRC1/V4, -5, and -7 versus A+C-resistant PC-9/BRC1/A+CR3, -6, -7 and -8 cells show sustained, but not increased, amplification of the *EGFR* locus in the setting of A+C resistance. The tumor nuclei show 4-5 individual signals as well as one big cluster of signals for *EGFR* (red) and 5-6 signals for the centromere of chromosome 17 (green), indicating *EGFR* amplification. **C**, Phospho-RTK arrays of A+C-sensitive PC-9/BRC1/V7 cells versus A+C-resistant PC-9/BRC1/A+CR6 and -7 cells shows no increased phosphorylation of other 'bypass' (i.e. non-EGFR) receptor tyrosine kinases in A+C-resistant cells at baseline. **D**, H&E staining of A+C-resistant xenograft tumors compared to vehicle-treated controls demonstrate a lack of histological differences that could account for A+C resistance; bar, 50 $\mu$ m.

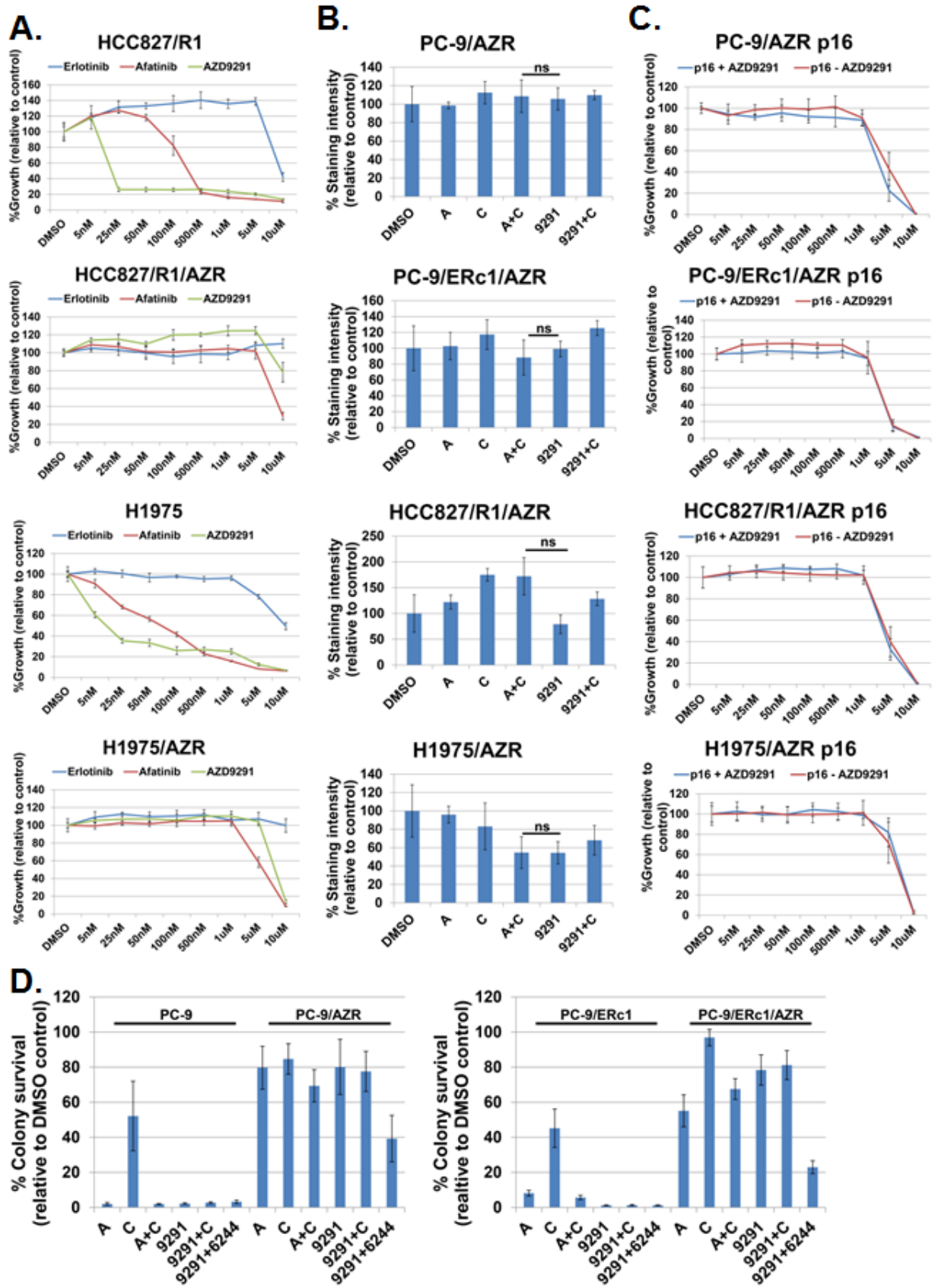


Figure 36. Characterization of AZD9291-resistant cell lines.

**A**, Cell growth-inhibition assays demonstrate the resistance of HCC827/R1/AZR and H1975/AZR cells to AZD9291, relative to isogenic parental controls HCC827/R1 and H1975, respectively. AZD9291 resistance also confers robust cross-resistance to first- and second-generation EGFR TKIs erlotinib and afatinib. Data are expressed as a percentage of DMSO control and plotted as mean  $\pm$  standard deviation of hexuplicate data. **B**, Quantification of crystal violet staining of PC-9/AZR, PC-9/ERc1/AZR, HCC827/R1/AZR, and H1975/AZR cells treated in triplicate with DMSO, afatinib (A) [50nM], cetuximab (C) [5ug/mL], afatinib + cetuximab (A+C), AZD9291 (9291) [50nM], or AZD9291 + cetuximab (9291+C) for 10 days. Data are expressed as mean  $\pm$  standard deviation of triplicate measurements; ns= non-significant at  $p=0.05$  for AZD9291 vs. A+C. **C**, Cell growth-inhibition assays demonstrate the sustained resistance of PC-9/AZR, PC-9/ERc1/AZR, HCC827/R1/AZR, and H1975/AZR cells to AZD9291 following 16 passages in the absence of drug; p16, passage  $16 \pm [1\mu\text{M}]$  AZD9291. **D**, Quantification of soft agar assays of PC-9, PC-9/AZR, PC-9/ERc1, and PC-9/ERc1/AZR cells treated for 10 days with either DMSO, afatinib (A), cetuximab (C), A+C [50nM; 5ug/mL], AZD9291 (9291) [50nM], AZD9291 + cetuximab (9291+C), or AZD9291 + AZD6244 [500nM] (9291+6244). Some data are the same as shown in Fig. 3B, with the addition here of AZD6244 data to demonstrate moderate sensitivity of AZD9291-resistant cell lines to dual EGFR + MEK inhibition.

## Supplementary information for Chapter IV

### Materials and Methods

#### *Generation of EGFR inhibitor resistant cell populations*

PC9, PC9 GR\_6 or NCI-H1975 cells were used to generate EGFR inhibitor resistant cell populations using a dose escalation method as previously described [193]. Populations resistant to a single concentration of 160nM AZD9291 were prepared as above with continual culturing of the cells in the indicated concentration of inhibitor until a resistant population reached 80% confluency.

#### *Cell survival assay*

Cellular Sytox proliferation assays were performed as previously described [241] and detailed in Supplementary material. Origin software was used to interpolate IC<sub>50</sub> values. Briefly, cells were plated into 384 well cell culture microplates at 1000 cells per well in 70µl of RPMI media containing 10% fetal calf serum, 2mM L-glutamine and supplemented with originating EGFR inhibitor for resistant cell populations. The cells were allowed to attach overnight at 37°C, 5% CO<sub>2</sub>. The following day titrations of test compound were added to the assay plates using an Echo Liquid Handler, Labcyte (California, USA) and the treated cells incubated for a further 72 hours at 37°C, 5% CO<sub>2</sub>. Each compound was tested as an 11 point dose response with a top concentration of 10µM and 1 in 3 dilutions. For resistant populations test compound was added in combination with the originating EGFR

inhibitor in the growth media. Following 72 hours incubation of the compound treated plates, 5µl of 2µM SYTOX Green Nucleic Acid Stain, Life Technologies (Paisley, UK) was added per well and the plates incubated at room temperature for one hour. The number of fluorescent cells per well was measured on the Acumen TTP LabTech Ltd. (Melbourn, UK) this number representing the dead cell count. 10µl of 0.25% Saponin Sigma (Dorset, UK) was added per well and the plates incubated over night at room temperature. The total number of fluorescent cells per well was acquired on the Acumen. The number of dead cells was subtracted from the total number of cells and the live cell number plotted to determine EC<sub>50</sub> values.

### ***Immunoblotting***

Immunoblotting was performed using standard SDS-PAGE procedures as previously described and detailed in Supplementary information. In brief, cells were lysed on ice with RIPA buffer Thermofisher Scientific Inc. (Rockford, IL, USA) supplemented with PhosSTOP Phosphatase Inhibitor Cocktail Tablets and cComplete Protease Inhibitor Cocktail Tablets, Roche (Basel, Switzerland). Total proteins were separated on 4–12% Bis-tris gels, Invitrogen (Paisley, UK) and transferred to immunoblotting membranes. Membranes were blocked in 5% (w/v) non-fat milk or 5% (w/v) bovine serum albumin (BSA) in phosphate buffered saline + Tween 20 (PBST) (3.2 mM Na<sub>2</sub>HPO<sub>4</sub>, 0.5 mM KH<sub>2</sub>PO<sub>4</sub>, 1.3 mM KCl, 135 mM NaCl, 0.05% Tween 20, pH 7.4) and then probed with the respective primary antibodies overnight at 4°C. After washing and incubation with secondary antibodies, detected proteins were visualized using the horseradish peroxidase

Western Lightning substrate according to the manufacturer's instructions (Perkin Elmer). Antibodies used for western blot; phospho-ERK (T202/Y204; cat.# 9101), ERK (cat.#9102), phospho-AKT (S473; cat.#9271), phospho-EGFR(Y1068 cat.#2234), EGFR (cat. #2232), Bim (cat.#2933), BclxL (cat.#2762), PARP/Cleaved PARP (cat.#9542), phospho-MEK1/2 (S217/221; cat.# 9154), Phospho-p90RSK (Thr573; cat.#9346, GAPDH (cat.#5174), Phospho-FRA1 (Ser265), Anti-rabbit IgG, HRP-linked Antibody (cat.#7074); Anti-mouse IgG, HRP-linked Antibody (cat.#7072) Cell Signaling Technologies (Danvers, MA, USA): Nras sc-31 Santa Cruz Biotechnology, Inc. (Dallas, Texas USA);, Kras LS-C175665 Lifespan Biosciences Inc. (Seattle WA, USA)

### ***RPPA analysis***

Cell lysates were prepared in Tissue Protein Extraction Reagent (Pierce cat.#78510) supplemented with protease and phosphatase inhibitors. Phosphorylated and total protein levels were determined using a Reverse Phase Protein Array platform by Theranostics Health (Rockville, MA, USA).

### ***RAS activation assay***

Parental and resistant cells were serum starved overnight and supplemented with 160nM of AZD9291 for 6hrs. RAS activity was measured using the RAS-binding domain of RAF-1 to pulldown active RAS according to the manufacturers protocol (Thermo Scientific Cat#16117). Following separation by SDS PAGE, proteins were transferred to membranes which were probed with an anti-NRAS antibody (Santa Cruz).

### ***RNA interference constructs***

ON-TARGETplus siRNA constructs non-target control (NTC) (D-001810-10), siNRAS\_1 (J-003919-05), siNRAS\_2 (J-003919-06), siNRAS\_3 (J-003919-07), siKRAS\_1 (J-005069-10), siKRAS\_3 (J-005069-08) and siKRAS\_4 (J-005069-11) were purchased from Dharmacon (Lafayette, CO USA); siKRAS\_2 SAS1\_Hs01\_002025580 Sigma (Dorset, UK).

### ***DNA expression constructs***

pcDNA 3.1+ control; pcDNA 3.1+ / NRAS E63K; pcDNA 3.1+ / NRAS Wild Type; pcDNA 3.1+ / NRAS Q61K plasmids (Life Technologies Ltd. Paisley, UK). For exogenous expression over 12 days DNA constructs were transfected into EGFRm cell lines using a 1:3 DNA:Fugene ratio. 48 hours following initial transfection the media was exchanged for media supplemented with 160nM AZD9291. Repeat transfections were carried out every 96 hours over a period of 12 days whilst the cells were maintained in the presence of 160nM AZD9291. The cells were fixed in 100% ethanol and nuclei stained with 1 µg/ml Hoechst 33342 for 30 min. The cells were washed in PBS and imaged on the Cellomics Arrayscan. Cell number was determined using a cell count algorithm. For 96 hour expression MaxCyte transfection technology was used to electroporate the PC9 cells. PC9 cells were passaged the day before the transfection. On the day of the transfection cells were harvested and resuspended at  $9 \times 10^7$  cells per 600 µl MaxCyte buffer. 100 µl of cell suspension was transferred to a MaxCyte cuvette

and the cells electroporated with 20 µg DNA construct. Following electroporation the cells for each condition were transferred to a 6 well plate and incubated at 37°C for 30 minutes after which they were seeded in a 6 well plate at  $4 \times 10^5$  cells per well. Following overnight incubation the cells were harvested and replated in 384 well plate at 1000 cells/well. The next day the cells were dosed with titrations of either AZD9291 or gefitinib and the plates incubated for a further 96 hours. A live cell number was determined using sytox green nuclei stain as described above and plotted to determine EC<sub>50</sub> values.

### ***DNA preparation***

Parental and resistant cells were cultured to 80% confluency in T75 flasks. Cells were harvested and pelleted at 1000 rpm for 5 minutes. Cell pellets were frozen at -80°C until DNA isolation was performed. The Allprep DNA/RNA/miRNA Universal kit, Qiagen Ltd, (Crawley,UK), was used to prepare DNA following the manufacturers protocol.

### ***Sequencing***

Purified DNA was enriched for all exons of the 20 genes from the Qiagen GeneRead Lung panel or for all exomes using the Agilent SureSelect exome panel. Libraries were prepared and indexed using manufacturer's instructions. Illumina's NGS MiSeq or HiSeq sequencing platforms were used to generate sequencing data. Raw sequencing reads were aligned to the human reference genome hg19 using the BWA mem aligner (v0.7.4) [182] with the following

parameters: -P -c 20. Mapped reads were subject to local realignment around indels using IndelRealigner after RealignerTargetCreator from the Genome Analysis Tool Kit (v2.5.2) [201]. Orthogonal validation of the *NRAS* E63K variant was performed by sequencing using the Life Technologies Ion Torrent PGM platform and Sanger di-deoxy sequencing.

***Mutation detection and gene copy number assessment from sequencing data.***

Aligned sequences were analyzed for Single Nucleotide Variants (SNVs) and indels using in-house developed variant calling algorithm the *VarDict* (manuscript in preparation) designed for ultra-deep targeted sequencing data with the capability to call SNVs and indels in a single step. High quality variants were obtained after filtering out false positives calls based on sequencing base quality (mean phred score > 25) and mapping quality (mean mapping quality score > 20), allele frequency (AF > 1%), variant's location within a read (more than 5 nt from the end of the read), strand bias, and a variant's depth of coverage (more than 5 reads supporting a variant). The variants were annotated using snpEff and snpSift [242, 243] that included dbSNP 138, clinical SNP, as well as COSMIC (v68). The candidate mutations were obtained after filtering out dbSNP variants (but retaining clinically relevant SNPs), and those with predicted low effect mutations, such as silent mutations and mutations in UTR, intron, and intergenic regions. Finally, mutations were further filtered using SNPeffect database (<http://snpeffect.switchlab.org/>) [244] as COSMIC mutations might still contain common polymorphic SNPs that are not pathogenic. The *Seq2C* algorithm

(manuscript in preparation) was applied for the analysis of gene amplifications and deletions from targeted sequencing data using three step normalization. The median number of mapped reads in the cohort of samples was used to adjust the uneven distribution of reads in sequencing experiment and the medians of adjusted coverage for each gene were used to normalize the uneven gene yields due to GC-content or other systematic bias. The log<sub>2</sub>Ratio was calculated by dividing the normalized gene coverage by the median coverage of all genes in the sample. Genes with log<sub>2</sub>Ratio value less than -1.0 were considered deleted; genes with log<sub>2</sub>Ratio value greater than 1.0 were considered gain of copy number. All gain of copy number values quoted within the text are log<sub>2</sub>ratio values converted to fold change relative to parental cells.

### ***Comparative Genomic Hybridization***

Comparative genomic hybridization was performed using the Agilent SurePrint G3 Human CGH 2x400K microarrays (Agilent Technologies, Santa Clara, CA, USA) according to manufacturer's suggested protocol. Raw data were processed using Agilent's Feature Extraction software v10.7.3.1. **The** feature extraction files were loaded, processed and visualized in Nexus Copy Number v7 (BioDiscovery, Inc., El Segundo, CA, USA). Oligonucleotide probes were mapped to the genes according to the NCBI37/hg19 assembly. Segmentation of aCGH data was done using BioDiscovery's SNPRang Segmentation algorithm with minimum of three probes per a segment. The cut-off for a gene copy number gain was defined as log<sub>2</sub>Ratio value greater than 1.0 and for loss as log<sub>2</sub>Ratio value less than -1.0.

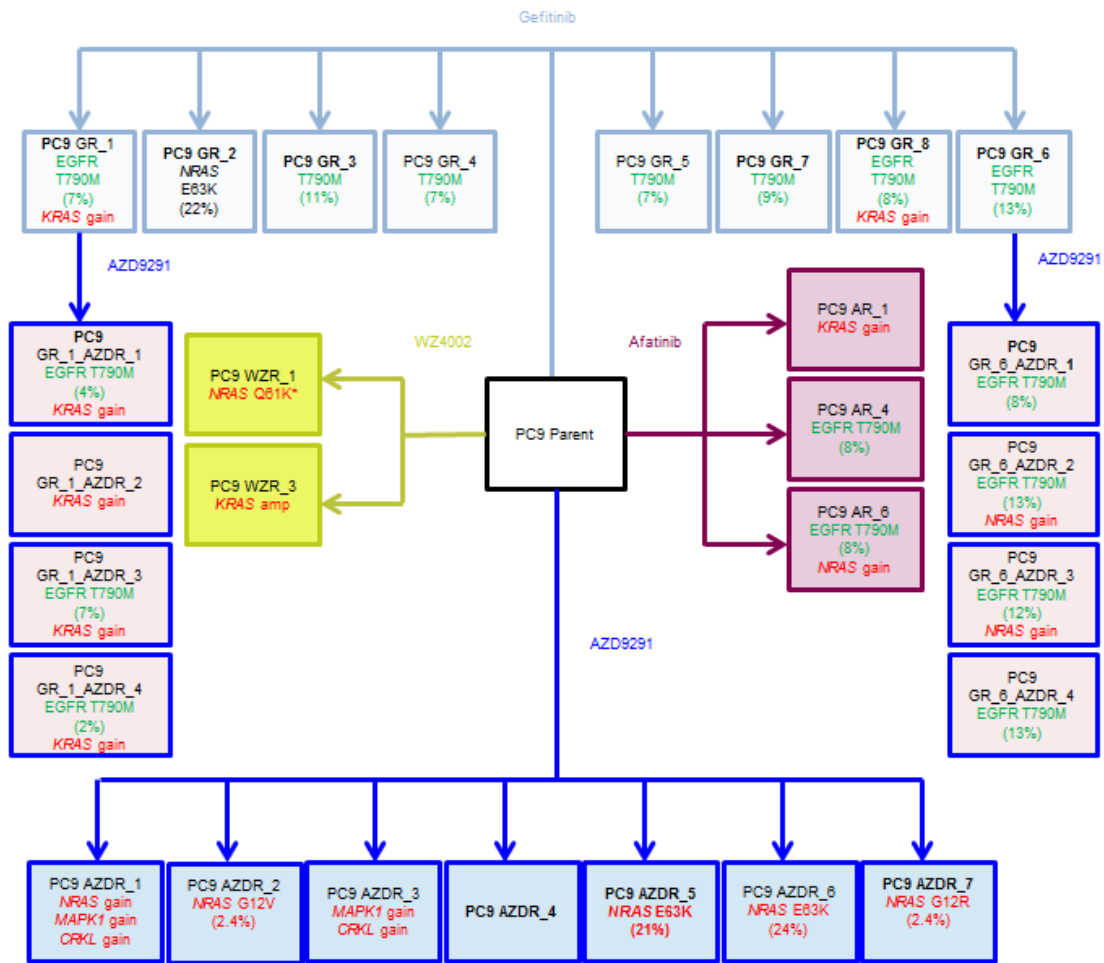
### ***Transgenic Mouse Studies***

All animals were kept in pathogen-free housing under guidelines approved by the Vanderbilt University Medical Center Institutional Care and Use Committee. The generation of EGFR<sup>L858R+T790M</sup> and EGFR<sup>L858R</sup> mice was previously described [133]. Doxycycline was administered by feeding mice with doxycycline-impregnated food pellets (625ppm; Harlan-Teklad). AZD9291 and selumetinib was suspended in 0.5% w/v HPMC (hydroxyl propyl methyl cellulose) in deionized water and administered via oral gavage once or twice daily, respectively, at the dose of 5mg/kg. Mice were imaged every 2-4 weeks at the Vanderbilt University Institute of Imaging Science.

### ***MRI***

All procedures were approved by Vanderbilt's Institutional Animal Care and Usage Committee. Mice were anesthetized via inhalation of 2%/98% isoflurane/oxygen and maintained under anesthesia throughout the course of the experiment. Animals were secured in a prone position in a 38-mm inner diameter radiofrequency (RF) coil and placed in a Varian 7T horizontal bore imaging system Varian Inc. (Palo Alto, CA, USA) for data collection. A constant body temperature of 37°C was maintained using heated air flow. Prior to treatment, mice were scanned to confirm the presence of growing lung nodules. Image acquisition and lung tumour volume measurements were performed as described previously [147].

**A**



**B**

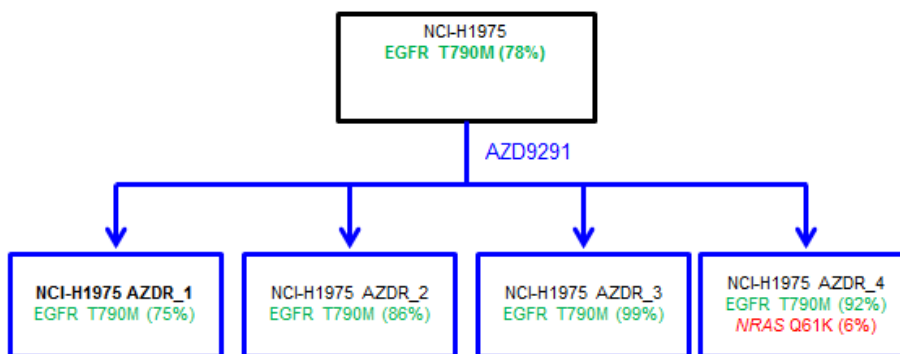
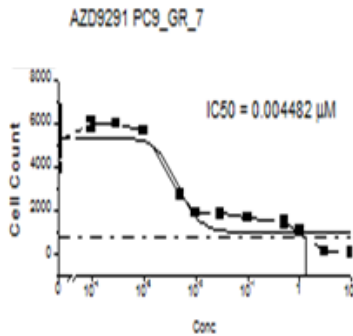
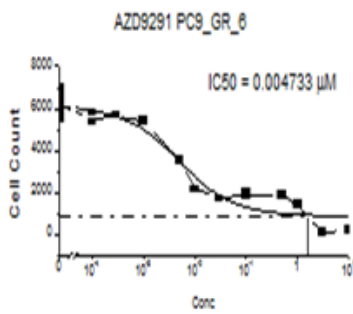
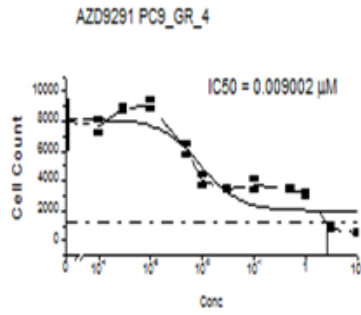


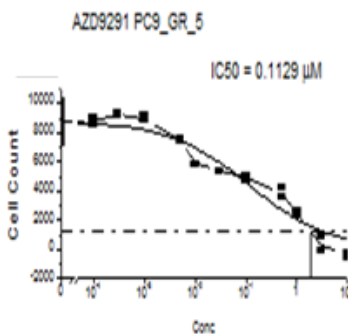
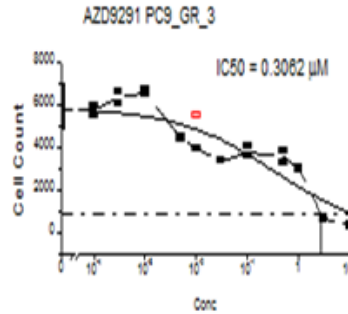
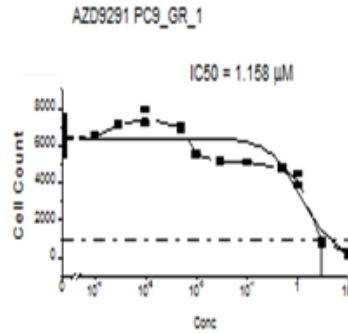
**Figure 37. Comparison of genetic alterations across multiple populations resistant to AZD9291 and other EGFR TKIs**

(A) Genetic alterations detected in DNA from 28 separate PC9 resistant populations Allele frequencies are shown. (B) Genetic alterations detected in DNA from 4 separate NCI-H1975 resistant populations. Allele frequencies are shown.

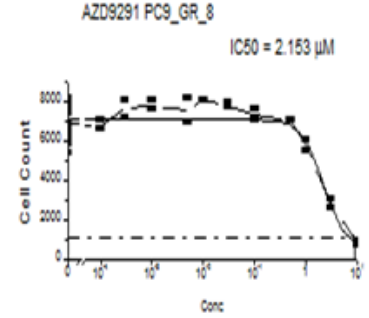
**A (i) PC9\_GR T790M+ populations with a full response to AZD9291**



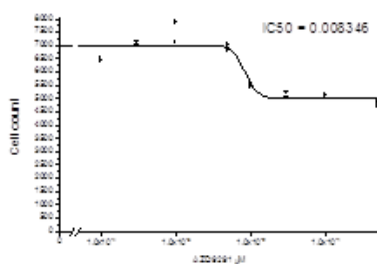
**(ii) PC9\_GR T790M+ populations with a partial response to AZD9291**



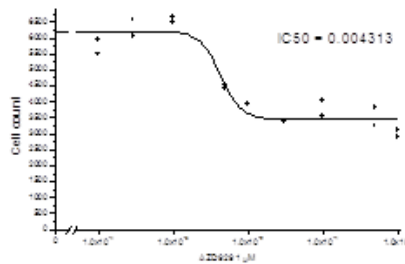
**(iii) PC9\_GR T790M+ population with no response to AZD9291**



**B AZD9291 PC9\_GR\_1 partial response**



**AZD9291 PC9\_GR\_3 partial response**



**AZD9291 PC9\_GR\_5 partial response**

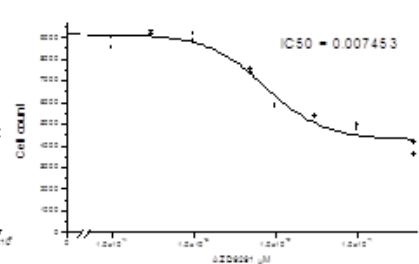


**Figure 38. Treatment of resistant populations with AZD9291.**

PC9 gefitinib resistant T790M+ populations were treated with a dose response of AZD9291 and dose response curves plotted to determine IC<sub>50</sub> values. **(A)** Representative dose response curves indicate varying sensitivity of the cells within the populations to AZD9291 (i) less than 50% of the cells are sensitive to AZD9291 growth inhibition; (ii) almost all of the cells are sensitive to AZD9291 growth inhibition; (iii) none of the cells are sensitive to AZD9291 growth inhibition. **(B)** Representative dose response curves for the sensitive cells from the partially sensitive populations. IC<sub>50</sub> values for AZD9291 growth inhibition are similar across all sensitive cells.

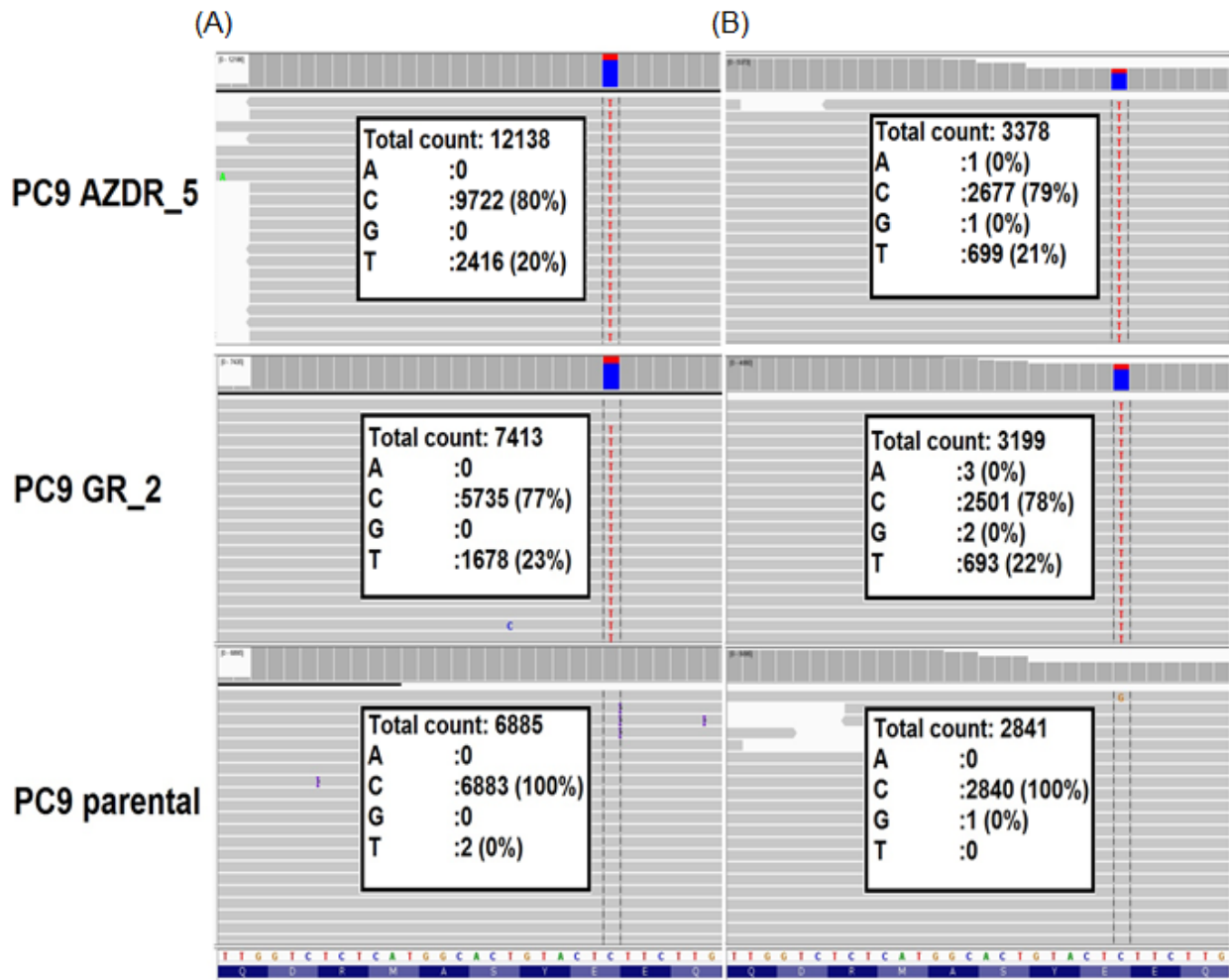
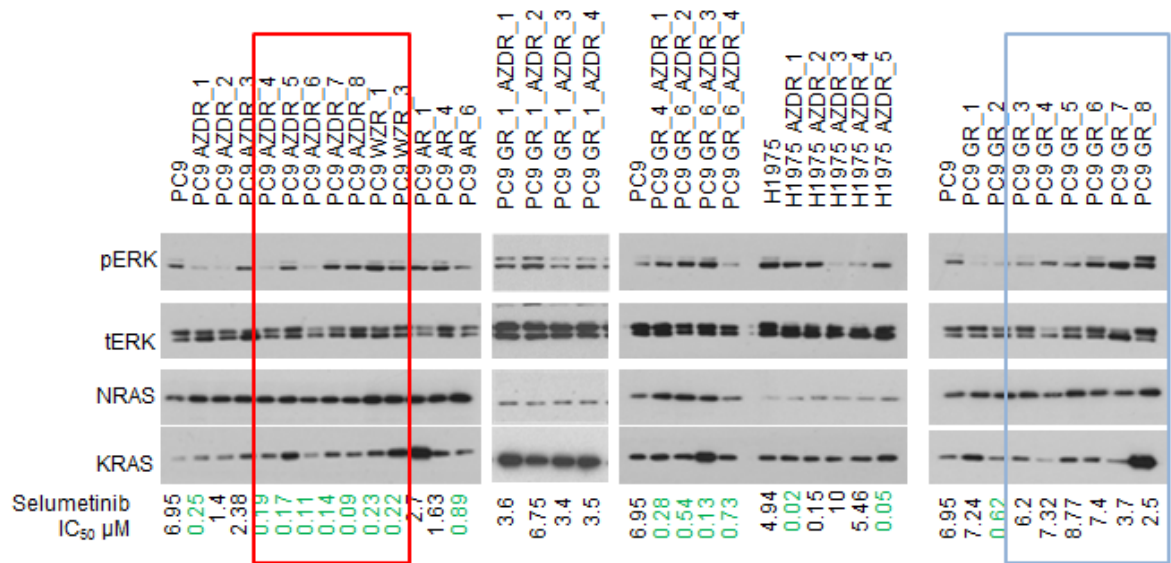


**Figure 39. Detection and Validation of a novel NRAS E63K mutation.**

Integrative Genomic Viewer (IGV) screen shots of the NRAS E63K mutation from orthogonal NGS platforms. (Table insert shows read depth and nucleotide counts for each sample.) **(A)** Life Technologies PGM platform: the E63K variant has an allele frequency of 20 and 23%, respectively for the two resistant samples. **(B)** Illumina platform: the E63K variant has an allele frequency of 21 and 22%, respectively for the two resistant samples. The parental sample, PC-9, shows no evidence of the NRAS E63K variant on either platform.



Green values represent resistant populations that are >5 fold more sensitive to selumetinib compared to the parental PC9 cells.  
 Red box highlights selumetinib sensitive resistant populations with variable levels of phosphorylated ERK.  
 Purple box highlights selumetinib refractory resistant populations with variable levels of phosphorylated ERK.

**Figure 40.** Lysates were prepared from parental PC9 and resistant populations analysed for levels of total and phosphorylated ERK, NRAS and KRAS by western blot.

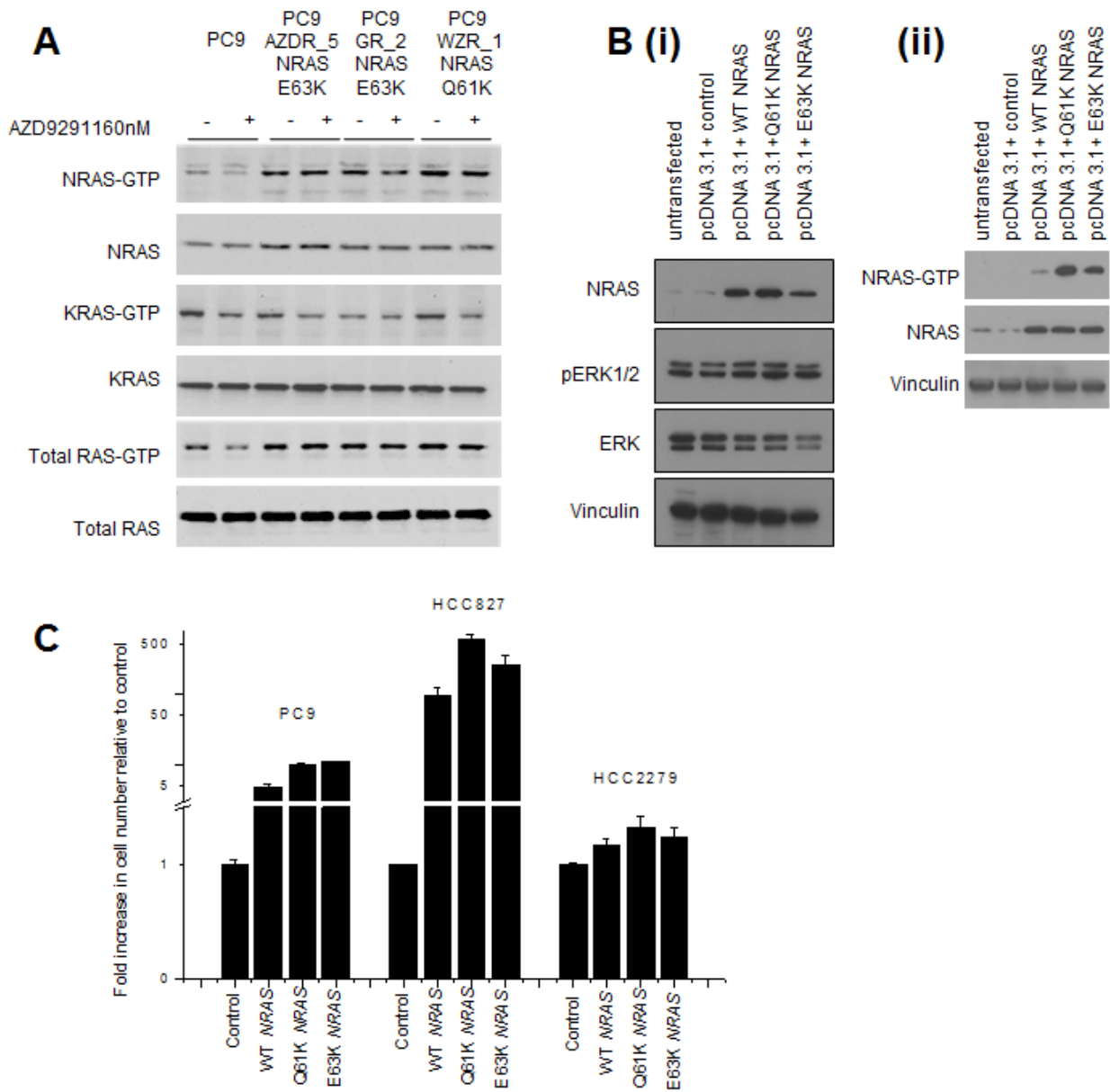


**Figure 41.** The novel NRAS E63K mutation is an activating mutation that when expressed enhances resistance to cell growth inhibition by gefitinib or AZD9291 in EGFRm cell lines.

**(A)** Resistant populations were cultured in media without EGFR inhibitor for 5 days prior to carrying out the assay. Lysates were prepared from parental and resistant cells serum starved overnight and treated for 6 hours +/- 160nM AZD9291. RAS activity was measured using RAS GTPase-specific pulldown assays. **(B) (i)** Lysates from PC9 cells transfected (electroporation) with pcDNA 3.1+ control and NRAS variant DNA constructs for 48 hours were immunoblotted for indicated proteins. **(ii)** Lysates were prepared from PC9 cells transfected (Fugene 6 reagent) with pcDNA 3.1+ control and NRAS variant DNA constructs for 48 hours. RAS activity was measured using RAS GTPase-specific pulldown assays.**(C)** EGFRm cells were transfected (Fugene 6 reagent) every 96 hours with indicated DNA constructs and cultured in media containing 160nM AZD9291 over a period of 12 days.

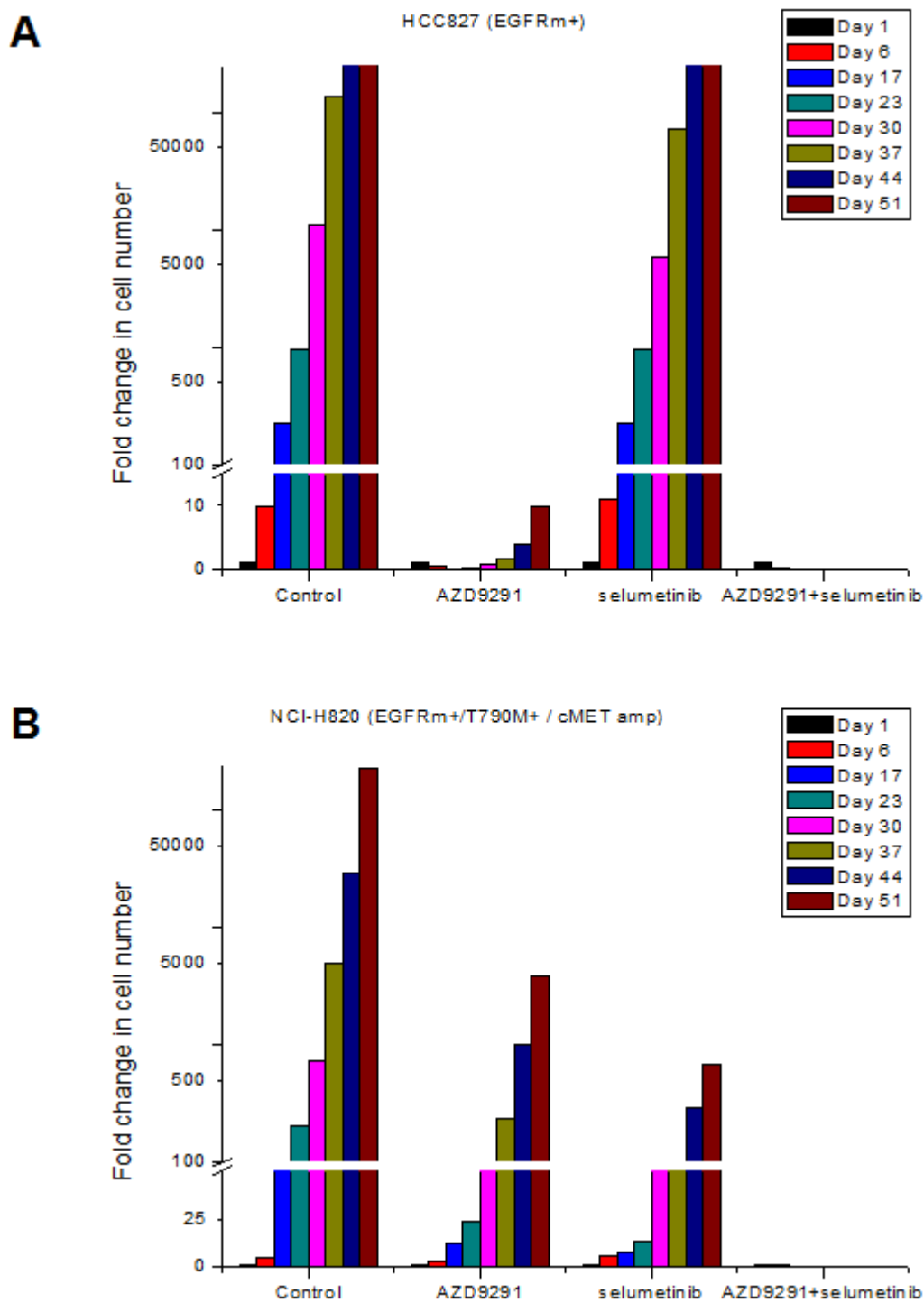


**Figure 42. In vitro combination of AZD9291 with selumetinib induces more profound phenotypic inhibition.**

(A) HCC827 and (B) NCI-H820 cells were chronically treated for 51 days with; DMSO, AZD9291, selumetinib or a combination of both AZD9291 with selumetinib. Fold increase in cell number was monitored over time.

**Table 23. Generation of resistant cell populations.**

Method used for generating resistant lines	EGFR inhibitor	Final conc. of EGFR inhibitor (nM)	Full name of resistant cell population	Abbreviated name of resistant cell population
Dose escalation	Gefitinib	1500	PC9_gefitinib resistant_1	PC9 GR_1
Dose escalation	Gefitinib	1500	PC9_gefitinib resistant_2	PC9 GR_2
Dose escalation	Gefitinib	1500	PC9_gefitinib resistant_3	PC9 GR_3
Dose escalation	Gefitinib	1500	PC9_gefitinib resistant_4	PC9 GR_4
Dose escalation	Gefitinib	1500	PC9_gefitinib resistant_5	PC9 GR_5
Dose escalation	Gefitinib	1500	PC9_gefitinib resistant_6	PC9 GR_6
Dose escalation	Gefitinib	1500	PC9_gefitinib resistant_7	PC9 GR_7
Dose escalation	Gefitinib	1500	PC9_gefitinib resistant_8	PC9 GR_8
Dose escalation	Afatinib	1500	PC9_afatinib resistant_1	PC9 AR_1
Dose escalation	Afatinib	1500	PC9_afatinib resistant_2	PC9 AR_2
Dose escalation	Afatinib	1500	PC9_afatinib resistant_3	PC9 AR_3
Dose escalation	Afatinib	1500	PC9_afatinib resistant_4	PC9 AR_4
Dose escalation	Afatinib	1500	PC9_afatinib resistant_5	PC9 AR_5
Dose escalation	Afatinib	1500	PC9_afatinib resistant_6	PC9 AR_6
Dose escalation	WZ4002	1500	PC9_WZ4002 resistant_1	PC9 WZR_1
Dose escalation	WZ4002	1500	PC9_WZ4002 resistant_2	PC9 WZR_2
Dose escalation	WZ4002	1500	PC9_WZ4002 resistant_3	PC9 WZR_3
Dose escalation	WZ4002	1500	PC9_WZ4002 resistant_4	PC9 WZR_4
Dose escalation	WZ4002	1500	PC9_WZ4002 resistant_5	PC9 WZR_5

Dose escalation	WZ4002	1500	PC9_WZ4002 resistant_6	PC9 WZR_6
Dose escalation	WZ4002	1500	PC9_WZ4002 resistant_7	PC9 WZR_7
Dose escalation	AZD9291	160	PC9_AZD9291 resistant_1	# PC9 AZDR_1
Dose escalation	AZD9291	160	PC9_AZD9291 resistant_2	# PC9 AZDR_2
Dose escalation	AZD9291	160	PC9_AZD9291 resistant_3	# PC9 AZDR_3
Dose escalation	AZD9291	160	PC9_AZD9291 resistant_4	PC9 AZDR_4
Single dose of compound	AZD9291	160	PC9_AZD9291 resistant_5	PC9 AZDR_5
Single dose of compound	AZD9291	160	PC9_AZD9291 resistant_6	PC9 AZDR_6
Single dose of compound	AZD9291	160	PC9_AZD9291 resistant_7	PC9 AZDR_7
Single dose of compound	AZD9291	160	PC9_AZD9291 resistant_8	PC9 AZDR_8
Dose escalation	AZD9291	1500	PC9_AZD9291 resistant_9	PC9 AZDR_9
Dose escalation	AZD9291	1500	PC9_AZD9291 resistant_10	PC9 AZDR_10
Dose escalation	AZD9291	1500	PC9_AZD9291 resistant_11	PC9 AZDR_11
Dose escalation	AZD9291	1500	PC9_AZD9291 resistant_12	PC9 AZDR_12
Dose escalation	WZ4002	1500	NCI-H1975_WZ4002 resistant	NCI-H1975 WZR
Dose escalation	Afatinib	1500	NCI-H1975_afatinib resistant	NCI-H1975 AR
Dose escalation	AZD9291	1500	NCI-H1975_AZD9291 resistant_1	NCI-H1975 AZDR_1
Dose escalation	AZD9291	1500	NCI-H1975_AZD9291 resistant_2	NCI-H1975 AZDR_2
Dose escalation	AZD9291	1500	NCI-H1975_AZD9291 resistant_3	NCI-H1975 AZDR_3
Dose escalation	AZD9291	1500	NCI-H1975_AZD9291 resistant_4	NCI-H1975 AZDR_4
Single dose of compound	AZD9291	160	NCI-H1975_AZD9291 resistant_5	# NCI-H1975 AZDR_5
Dose escalation	AZD9291	1500	PC9 gefitinib resistant_1_AZD9291 resistant_1	PC9_GR_1_AZDR_1
Dose escalation	AZD9291	1500	PC9 gefitinib resistant_1_AZD9291 resistant_2	PC9_GR_1_AZDR_2

Dose escalation	AZD9291	1500	PC9 gefitinib resistant_1_AZD9291 resistant_3	PC9_GR_1_AZDR_3
Dose escalation	AZD9291	1500	PC9 gefitinib resistant_1_AZD9291 resistant_4	PC9_GR_1_AZDR_4
Dose escalation	AZD9291	1500	PC9 gefitinib resistant_6_AZD9291 resistant_1	PC9_GR_6_AZDR_1
Dose escalation	AZD9291	1500	PC9 gefitinib resistant_6_AZD9291 resistant_2	PC9_GR_6_AZDR_2
Dose escalation	AZD9291	1500	PC9 gefitinib resistant_6_AZD9291 resistant_3	PC9_GR_6_AZDR_3
Dose escalation	AZD9291	1500	PC9 gefitinib resistant_6_AZD9291 resistant_4	PC9_GR_6_AZDR_4
Dose escalation	WZ4002	1500	PC9 vandetinib resistant_WZ4002 resistant	PC9VR_WZR
Dose escalation	Afatinib	1500	PC9 vandetinib resistant_afatinib resistant	PC9VR_AR

EGFR<sup>m+</sup> and EGFR<sup>m+/T790M</sup> cell lines were used to generate a panel of EGFR inhibitor resistant models. Cells were chronically treated with escalating concentrations of gefitinib, afatinib, WZ4002 or AZD9291 or a single concentration of AZD9291. Each cell line represents a pool of the resistant colonies that emerged following chronic treatment with EGFR inhibitor. Populations highlighted in yellow were those selected for further phenotypic and genetic analysis. # indicates populations selected for RPPA analysis.

**Table 24. Small molecule inhibitors.**

Compound	Inhibitor target	Reference
Selumetinib AZD6244 (ARRY-142886)	MEK1/2	Mol Cancer Ther. August 2007 6; 2209
AZD5363	AKT	Mol Cancer Ther. 2012 (4):873-87
AZD8055	mTORC1/mTORC2	Cancer Res. 2010; 70(1):288-98
AZD2014	mTORC1/mTORC2	Bioorg Med Chem Lett. 2013;23(5):1212-6
GDC-0941	Pan PI3K	J Med Chem. 2008; 51: 5522–5532
AZ_0012	AXL	AZ in-house compound
AZ_6592	MET	AZ in-house compound
AZ_1902	IGF-1R	AZ in-house compound
BMS-536924	IGF-1R	Journal of Medicinal Chemistry. 48 5639–5643
AZ_9424	HDAC	AZ in-house compound
AZD4547	FGFR	Cancer Res. 2012; 72(8); 2045–56
AZD1152 (HQPA)	Aurora kinase B	<a href="#">Clin Cancer Res.</a> 2007; 13(12):3682-8

**Table 25. IC<sub>50</sub> (µM) values from cell growth inhibition assays comparing compound sensitivity between parental and resistant cell populations.**

Cell population	GDC-0941 (Pan PI3K)	AZD5363 (AKT)	AZD8055 (mTOR)	AZD2014 (mTOR)	AZ_6592 (MET)	AZ_0012 (Axl)	selumetinib (MEK1/2)	AZ_1902 (IGF1R)	BMS-536924 (IGF1R)	AZD9291 (EGFR)	AZ_9424 (HDAC)	AZD4547 (FGFR)	AZD1152-HQPA (AURKB)
PC9	1.18 (±0.2)	6.16 (±2.8)	0.05 (±0.02)	0.37 (±0.08)	2.07 (±0.7)	1.4 (±0.5)	6.95 (±2.5)	2.16 (±0.6)	0.88 (±0.2)	0.008 (±0.002)	0.51 (±0.09)	5.47 (±0.15)	0.036 (±0.01)
PC9 GR 1	1.82 (±0.7)	6.79 (±3.1)	0.19 (±0.15)	ND	1.28 (±0.3)	0.94 (±0.4)	7.24 (±3.2)	1.33 (±0.6)	ND	1.12 (±0.5)	ND	3.97 (±1.06)	0.018 (±0.003)
PC9 GR 2	0.86 (±0.2)	6.6 (±2.6)	0.11 (±0.08)	ND	1.54 (±0.3)	2.01 (±0.5)	0.62 (±0.3)	1.23 (±0.3)	ND	2.8 (±0.4)	ND	8.25	ND
PC9 GR 3	0.99 (±0.2)	4.32 (±0.5)	0.05 (±0.02)	ND	1.2 (±0.2)	0.96 (±0.4)	6.2 (±3.6)	1.34 (±0.5)	ND	0.18 (±0.2)	ND	ND	ND
PC9 GR 4	1.07 (±0.2)	2.82 (±0.3)	0.04 (±0.01)	ND	3.03 (±0.7)	0.85 (±0.1)	7.32 (±2.3)	0.91 (±0.08)	ND	0.02 (±0.01)	ND	ND	ND
PC9 GR 5	0.73 (±0.1)	4.03 (±0.4)	0.04 (±0.01)	ND	2.29 (±0.6)	0.56 (±0.1)	8.77 (±1.5)	1.03 (±0.2)	ND	0.14 (±0.06)	ND	ND	ND
PC9 GR 6	1.34 (±0.3)	4.94 (±2.7)	0.08 (±0.03)	ND	1.81 (±0.9)	0.94 (±0.6)	7.44 (±2.6)	0.92 (±0.3)	ND	0.005 (±0.001)	ND	5.55 (±0.8)	0.015 (±0.007)
PC9 GR 7	1.43 (±0.8)	1.98 (±0.8)	0.03 (±0.01)	ND	1.83 (±0.07)	0.51 (±0.04)	3.7 (±0.99)	0.71 (±0.1)	ND	0.002 (±0.002)	ND	ND	ND
PC9 GR 8	1.42 (±0.3)	6.29 (±2.2)	0.27 (±0.15)	ND	2.02 (±0.3)	0.85 (±0.1)	2.48 (±1.4)	6.77 (±4.9)	ND	2.40 (±0.97)	ND	ND	ND
PC9 AR 1	1.61 (±0.2)	7.6 (±0.12)	0.23 (±0.05)	ND	1.73 (±0.75)	1.97 (±0.26)	2.7 (±0.23)	0.96 (±0.04)	ND	2.41 (±0.5)	ND	ND	ND
PC9 AR 4	0.57 (±0.2)	2.46 (±0.8)	0.029 (±0.01)	ND	1.84 (±0.3)	0.74 (±0.05)	1.63 (±1.1)	0.67 (±0.04)	ND	0.73 (±0.3)	ND	ND	ND
PC9 AR 6	0.77 (±0.3)	3.79 (±1.3)	0.044 (±0.03)	ND	4.98 (±1.7)	4.19 (±0.8)	0.89 (±0.6)	0.92 (±0.1)	ND	2.4 (±0.5)	ND	ND	ND
PC9 WZR 1	1.03 (±0.22)	5.05 (±2.1)	0.072 (±0.06)	ND	2.2 (±0.27)	1.67 (±0.19)	0.23 (±0.04)	0.87 (±0.09)	ND	1.99 (±0.03)	ND	ND	ND
PC9 WZR 3	0.58 (±0.04)	1.46 (±0.2)	0.022 (±0.006)	ND	1.47 (±0.7)	1.52 (±0.08)	0.22 (±0.1)	0.79 (±0.1)	ND	1.65 (±0.5)	ND	ND	ND
PC9 AZDR 1	0.87 (±0.4)	1.31 (±0.3)	0.072 (±0.04)	ND	1.76 (±0.5)	1.02 (±0.5)	0.25 (±0.06)	1.56 (±0.5)	ND	2.3 (±0.9)	ND	ND	ND
PC9 AZDR 2	1.17 (±0.4)	3.59 (±1.9)	0.033 (±0.007)	ND	1.66 (±0.7)	0.85 (±0.1)	1.4 (±0.9)	1.39 (±0.4)	ND	3.69 (±1.2)	ND	ND	ND
PC9 AZDR 3	0.75 (±0.1)	1.02 (±0.3)	0.038 (±0.02)	ND	1.32 (±0.4)	1.07 (±0.2)	2.38 (±0.9)	0.96 (±0.04)	ND	1.94 (±0.5)	ND	ND	ND
PC9 AZDR 4	0.57 (±0.05)	3.8 (±0.5)	0.031 (±0.004)	ND	3.45 (±0.2)	1.39 (±0.3)	0.19 (±0.1)	0.94 (±0.06)	ND	2.48 (±1.1)	ND	ND	ND
PC9 AZDR 5	ND	5.04 (±2.6)	ND	0.49 (±0.07)	1.8 (±0.1)	ND	0.17 (±0.05)	ND	0.67 (±0.02)	2.14 (±0.06)	0.54 (±0.01)	7.24 (±1.24)	0.034 (±0.01)
PC9 AZDR 6	ND	8.47 (±0.4)	ND	0.41 (±0.04)	1.42 (±0.5)	ND	0.11 (±0.03)	ND	0.64 (±0.002)	1.6 (±0.02)	0.49 (±0.02)	5.41 (±0.41)	0.051 (±0.002)
PC9 AZDR 7	ND	7.15 (±1.7)	ND	0.50 (±0.03)	2.32 (±0.1)	ND	0.14 (±0.03)	ND	0.66 (±0.01)	2.63 (±0.3)	0.65 (±0.01)	>10	0.031 (±0.001)
PC9 AZDR 8	ND	2.22	ND	0.23	1.02	ND	0.09	ND	0.24	1.23	0.26	4.16	0.04
PC9 GR 1 AZDR 1	ND	6.2 (±3.5)	ND	0.39 (±0.1)	1.5 (±0.1)	ND	3.6 (±0.7)	ND	0.7 (±0.1)	2.4 (±0.95)	0.5 (±0.06)	6.47 (±0.73)	0.012 (±0.001)
PC9 GR 1 AZDR 2	ND	3.3 (±1.1)	ND	0.49 (±0.06)	3.4 (±0.3)	ND	6.7 (±1.4)	ND	2.3 (±0.1)	2.7 (±1.2)	0.5 (±0.1)	>10	0.01 (±0.004)
PC9 GR 1 AZDR 3	ND	3.3 (±0.6)	ND	0.3 (±0.01)	2.1 (±0.13)	ND	3.4 (±0.5)	ND	1.6 (±0.3)	2.4 (±0.7)	0.4 (±0.1)	8.89 (±1.17)	0.013 (±0)
PC9 GR 1 AZDR 4	ND	5.8 (±0.1)	ND	0.56 (±0.16)	2.3	ND	3.6 (±2.6)	ND	2.2 (±1.2)	2.6 (±0.9)	0.5 (±0.1)	9.35	0.011
PC9 GR 6 AZDR 1	ND	1.10 (±0.05)	ND	0.27 (±0.1)	1.1 (±0.05)	ND	0.28 (±0.2)	ND	0.62 (±0.04)	1.35 (±0.05)	0.33 (±0.09)	3.53 (±0.06)	0.02 (±0.001)
PC9 GR 6 AZDR 2	ND	7.93 (±1.7)	ND	0.5 (±0.4)	1.5 (±0.2)	ND	0.54 (±0.3)	ND	0.82 (±0.1)	2.24 (±0.6)	0.55 (±0.1)	5.13 (±1.63)	0.02 (±0.002)
PC9 GR 6 AZDR 3	ND	1.57 (±0.4)	ND	0.43 (±0.04)	1.04 (±0.01)	ND	0.13 (±0.06)	ND	0.47 (±0.07)	1.48 (±0.3)	0.22 (±0.04)	4.38 (±0.57)	0.015 (±0.004)
PC9 GR 6 AZDR 4	ND	2.95 (±1.1)	ND	0.91 (±0.3)	0.88 (±0.07)	ND	0.73 (±0.5)	ND	0.52 (±0.08)	1.74 (±0.8)	0.34 (±0.05)	3.73 (±0.01)	0.02 (±0.004)
NCI-H1975	ND	1.34 (±0.4)	ND	0.21 (±0.04)	2.63 (±0.2)	ND	4.94 (±3)	ND	1.43 (±0.6)	0.016 (±0.01)	0.62 (±0.1)	8.91 (±0.9)	3.63 (±0.8)
NCI-H1975 AZDR 1	ND	0.36 (±0.02)	ND	0.12 (±0.06)	2.11 (±0.6)	ND	0.024 (±0.003)	ND	0.26 (±0.1)	2.52 (±0.4)	0.33 (±0.04)	4.05 (±0.45)	0.11 (±0.03)
NCI-H1975 AZDR 2	ND	0.49 (±0.2)	ND	0.14 (±0.02)	1.8 (±0.1)	ND	0.15 (±0.1)	ND	0.27 (±0.05)	2.21 (±0.2)	0.41 (±0.07)	2.56 (±0.26)	0.05 (±0.003)
NCI-H1975 AZDR 3	ND	0.84 (±0.1)	ND	0.22 (±0.004)	2.64 (±0.6)	ND	>10	ND	0.72 (±0.3)	3.04 (±0.4)	0.47 (±0.07)	4.06 (±0.14)	0.085 (±0.007)
NCI-H1975 AZDR 4	ND	0.59 (±0.2)	ND	0.17 (±0.05)	2.06 (±0.6)	ND	5.46 (±3.7)	ND	0.47 (±0.2)	2.67 (±0.7)	0.37 (±0.1)	5.04 (±0.49)	0.075 (±0.007)
NCI-H1975 AZDR 5	ND	0.76 (±0.7)	ND	0.17 (±0.08)	2.11 (±0.2)	ND	0.045 (±0.04)	ND	0.48 (±0.3)	2.58 (±0.6)	0.59 (±0.03)	5.15 (±1.11)	0.63 (±0.07)

represents cell lines which are at least 5 fold more sensitive to indicated inhibitor than in the relevant parental cell line.

represents cell lines which are at least 5 fold less sensitive to AZD9291 than in the relevant parental cell line.

Cells were treated with a dose response of indicated inhibitors alone for parental cells and in the presence of original EGFR inhibitor for resistant populations. Values highlighted in green in resistant populations represent >5 fold increased sensitivity to agent compared to the respective parental cell line. Values highlighted in pink in resistant populations represent >5 fold decreased sensitivity to AZD9291 compared to the respective parental line. Values represent an average of at least 2 independent experiments. Errors in brackets are standard deviation.

**Table 26. Genetic analysis of resistant cell populations.**

EGFR inhibitor and resistant concentration	Resistant population	EGFR T790M Status (Allele Freq)	Other alterations (Allele Freq or CNV)	Sequencing			aCGH	SnapShot	Sanger Sequencing	Western blot
				Lung/Illumina	PGM	WES/Illumina				
Parental	PC9	Not Detected	Not Detected	X	X	X	X			X
	NCI H1975	T790M (78%)	Not Detected	X		X				
gefitinib resistant (EGFRm+ setting)	PC9 GR_1	EGFR T790M (7%)	KRAS gain (5.43)	X	X	X	X			X
	PC9 GR_2	Not Detected	NRAS E63K (22%)	X	X		X			
	PC9 GR_3	EGFR T790M (11%)	Not Detected					X	X	
	PC9 GR_4	EGFR T790M (7%)	Not Detected					X	X	
	PC9 GR_5	EGFR T790M (7%)	Not Detected					X	X	
	PC9 GR_6	EGFR T790M (13%)	Not Detected	X	X	X	X			
	PC9 GR_7	EGFR T790M (9%)	Not Detected					X	X	
	PC9 GR_8	EGFR T790M (8%)	KRAS gain (7.06)	X	X		X			X
afatinib resistant (EGFRm+ setting)	PC9 AR_1	Not Detected	KRAS gain (24.6)				X			X
	PC9 AR_4	EGFR T790M (8%)	Not Detected				X	X	X	
	PC9 AR_6	EGFR T790M (8%)	NRAS gain (4.23)				X	X		
PC9 WZ4002 resistant (EGFRm+ setting)	PC9 WZR_1	Not Detected	NRAS Q61K					X	X	
	PC9 WZR_3	Not Detected	KRAS gain (2.64)				X			X
AZD9291 resistant (EGFRm+ setting)	PC9 AZDR_1	Not Detected	NRAS gain (2.5), MAPK1 (1.97), CRKL (1.84)	X	X		X			
	PC9 AZDR_2	Not Detected	NRAS G12V (2.4%)	X	X		X			
	PC9 AZDR_3	Not Detected	MAPK1(3.8), CRKL (3.46)	X	X		X			
	PC9 AZDR_4	Not Detected	Not Detected	X	X		X			
	PC9 AZDR_5	Not Detected	NRAS E63K (21%)	X	X		X			
	PC9 AZDR_6	Not Detected	NRAS E63K (24%)	X						
	PC9 AZDR_7	Not Detected	NRAS G12R	X						

			(20%)							
<b>AZD9291 resistant (EGFR+/T790M setting)</b>	PC9 GR_1_AZDR_1	T790M (4%)	KRAS gain (6.23)	X		X				X
	PC9 GR_1_AZDR_2	Not Detected	KRAS gain (5.66)	X		X				X
	PC9 GR_1_AZDR_3	T790M (7%)	KRAS gain (4.44)	X		X				X
	PC9 GR_1_AZDR_4	T790M (2%)	KRAS gain (5.46)	X		X				X
	PC9 GR_6_AZDR_1	EGFR T790M# (8%)	Not Detected	X		X				X
	PC9 GR_6_AZDR_2	EGFR T790M# (13%)	NRAS gain (2.4)	X		X				X
	PC9 GR_6_AZDR_3	EGFR T790M# (12%)	NRAS gain (3.68)	X		X				X
	PC9 GR_6_AZDR_4	EGFR T790M# (13%)	Not Detected	X		X				X
	NCI-H1975 AZDR_1	EGFR T790M* (75%)	Not Detected	X		X				
	NCI-H1975 AZDR_2	EGFR T790M* (86%)	Not Detected	X		X				
	NCI-H1975 AZDR_3	EGFR T790M* (99%)	Not Detected	X		X				
	NCI-H1975 AZDR_4	EGFR T790M* (92%)	NRAS Q61K (6%)	X		X				

DNA from 32 separate populations with acquired resistance to different EGFR inhibitors was analysed for gene mutation and/or gene copy number across a panel of cancer associated genes. Data represents genetic alterations detected in the resistant populations. Variants validated across at least 2 different assay platforms are indicated. Next generation sequencing, Sanger sequencing, comparative genomic hybridisation (CGH), SnaPshot mutation analysis and / or Western blot analysis were used as assay platforms to detect and validate genetic modifications. Bracketted values represent either gain as fold change relative to respective parental cells or percent allele frequency for mutations.

**Table 27. RPPA analysis of phosphorylated and total protein levels in PC9 and NCI-H1975 AZD9291 resistant populations compared to respective parental cells.**

Lysates from AZD9291 resistant and parental cells were prepared and analysed by RPPA. Phosphorylated and total protein levels in resistant cells were compared to levels in corresponding parental cells. See Excel file Supplementary Table S5 from [1].

## Supplementary information for Chapter V

No supplementary materials, methods or tables accompany this chapter.

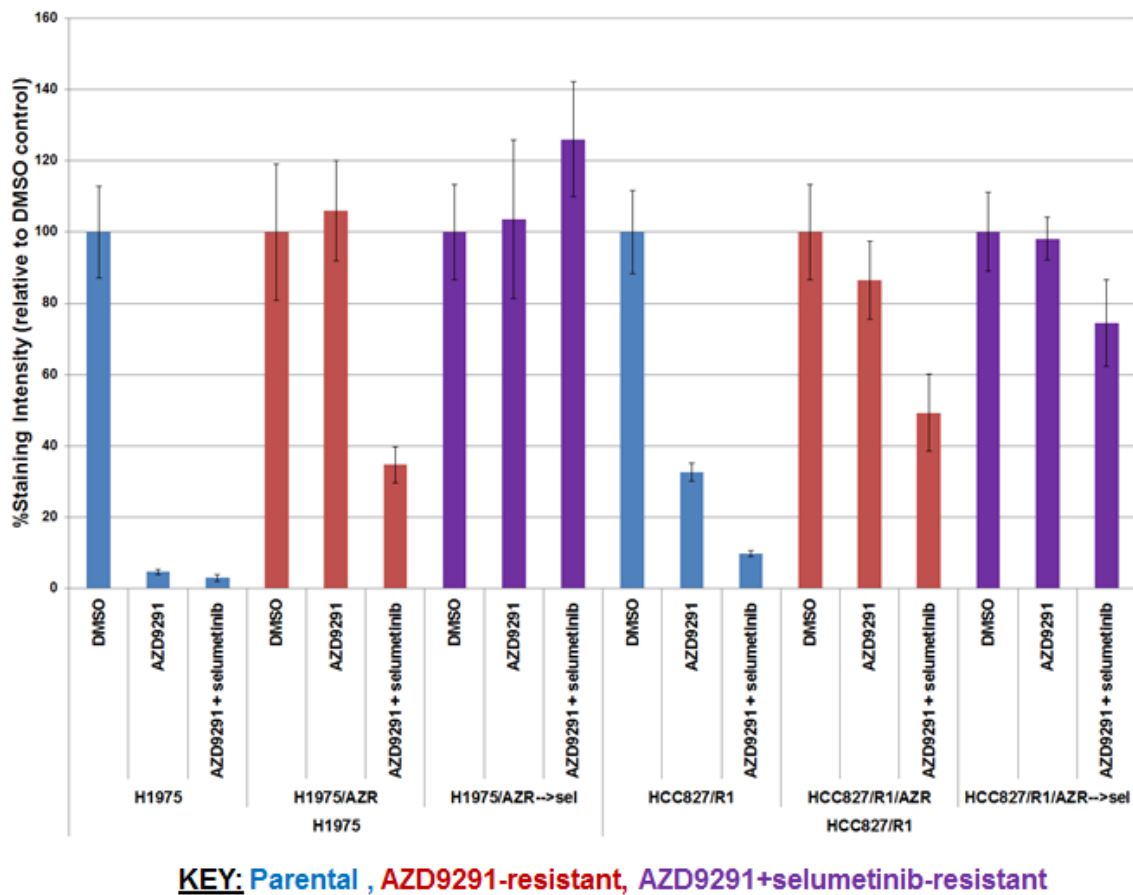
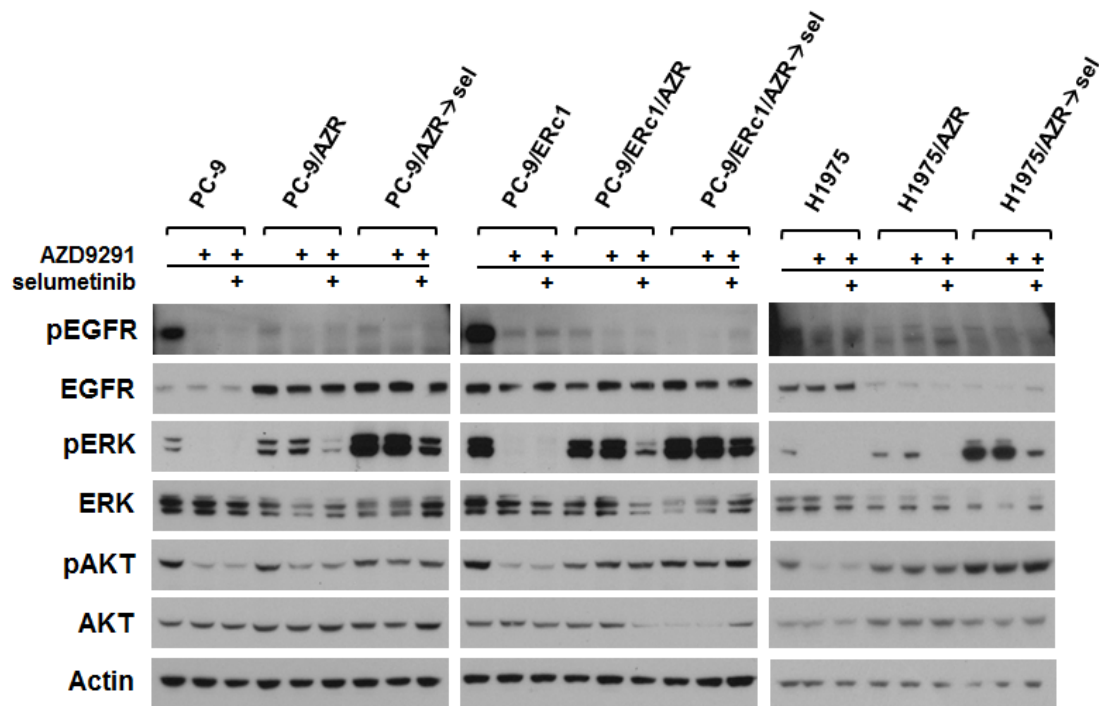


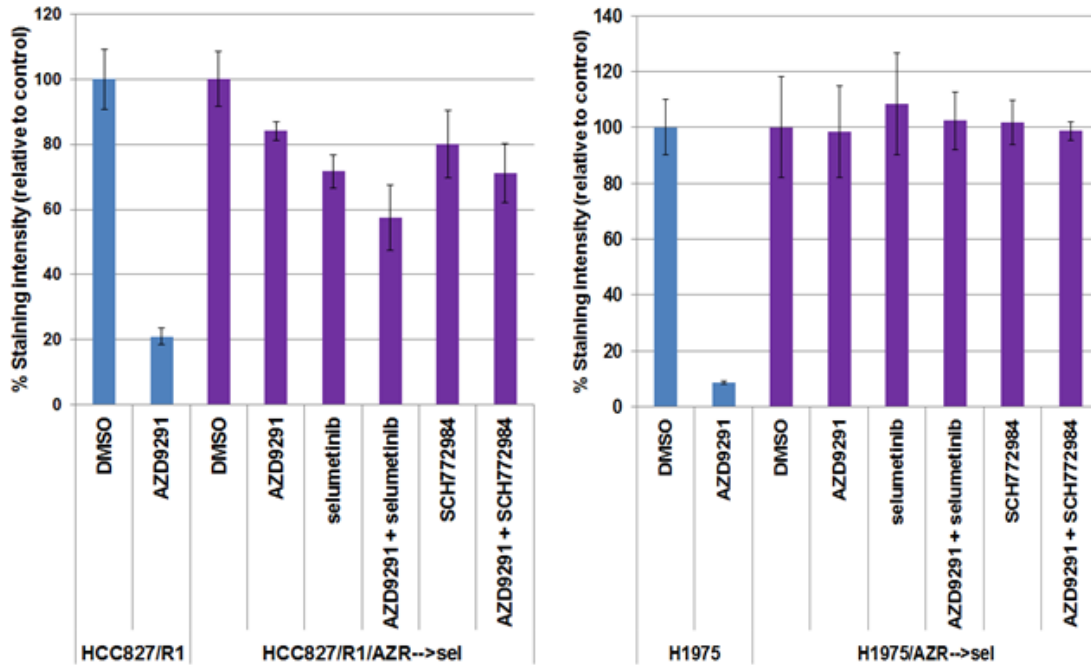
Figure 43. Characterization of additional cell line models of AZD9291 + selumetinib resistance.

Crystal violet assays demonstrate acquired resistance to AZD9291+selumetinib in the combination-resistant cells (H1975/AZR→sel and HCC827/R1/AZR→sel), as compared to their isogenic parental (H1975 and HCC827/R1) and AZD9291-resistant (H1975/AZR and HCC827/R1/AZR) counterparts. Cells were treated for 10 days with either AZD9291 [50nM], selumetinib [500nM], or the combination. Cells were fixed and stained with crystal violet. Staining intensity was measured to determine relative cell growth, and data are shown as a percentage of DMSO-treated cells. Error bars indicate one standard deviation.



**Figure 44. Increased phospho-ERK and/or phospho-AKT signaling in setting of AZD9291 + selumetinib resistance.**

Immunoblotting of parental (PC-9, PC-9/ERc1, and H1975), AZD9291-resistant (PC-9/AZR, PC-9/ERc1/AZR, and H1975/AZR), and AZD9291+selumetinib-resistant (PC-9/AZR→sel, PC-9/ERc1/AZR→sel, and H1975/AZR→sel) cells reveals increased baseline phospho-ERK and/or phospho-AKT in AZD9291+selumetinib-resistant cells. Phospho-ERK and phospho-AKT levels in AZD9291 + selumetinib-resistant cells are not affected by 6 hours of exposure to AZD9291 [50nM] plus selumetinib [500nM].



**KEY:** Parental , AZD9291+selumetinib-resistant

**Figure 45. Characterization of AZD9291 + selumetinib-resistant cell lines not sensitive to ERK inhibition.**

Crystal violet assays demonstrate the resistance of AZD9291+selumetinib-resistant cells (HCC827/R1/AZR→sel and H1975/AZR→sel) to inhibition by ERK inhibitor SCH772984. Cells were treated for 10 days with either AZD9291 [50nM], selumetinib [500nM], SCH772984 [500nM], or combinations thereof. Cells were fixed and stained with crystal violet. Staining intensity was measured to determine relative cell growth, and data are shown as a percentage of DMSO-treated cells. Error bars indicate one standard deviation.

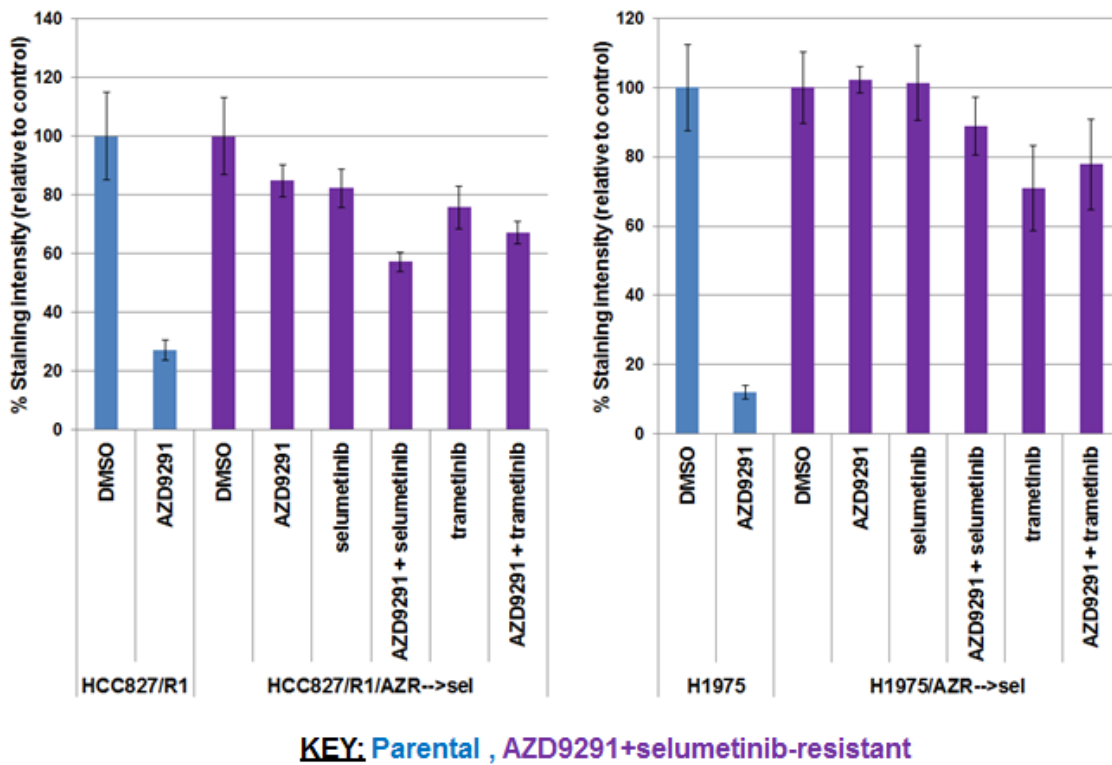


**Figure 46. Characterization of AZD9291 + selumetinib-resistant cell lines not sensitive to trametinib.**

Crystal violet assays demonstrate the resistance of AZD9291+selumetinib-resistant cells (HCC827/R1/AZR→sel and H1975/AZR→sel) to inhibition by MEK inhibitor, trametinib. Cells were treated for 10 days with either AZD9291 [50nM], selumetinib [500nM], trametinib [50nM], or combinations thereof. Cells were fixed and stained with crystal violet. Staining intensity was measured to determine relative cell growth, and data are shown as a percentage of DMSO-treated cells. Error bars indicate one standard deviation.

## **Supplementary information for Chapter VI**

No supplementary materials, methods, tables or figures accompany this chapter.

## REFERENCES

1. Eberlein, C.A., et al., Acquired resistance to mutant-selective EGFR inhibitor AZD9291 is associated with increased dependence on RAS signaling in preclinical models. *Cancer Res*, 2015.
2. Yu, H.A., et al., Analysis of tumor specimens at the time of acquired resistance to EGFR-TKI therapy in 155 patients with EGFR-mutant lung cancers. *Clin Cancer Res*, 2013. 19(8): p. 2240-7.
3. Ohashi, K., et al., Epidermal growth factor receptor tyrosine kinase inhibitor-resistant disease. *J Clin Oncol*, 2013. 31(8): p. 1070-80.
4. Sequist, L.V., et al., Genotypic and histological evolution of lung cancers acquiring resistance to EGFR inhibitors. *Sci Transl Med*, 2011. 3(75): p. 75ra26.
5. de Bruin, E.C., et al., Reduced NF1 Expression Confers Resistance to EGFR Inhibition in Lung Cancer. *Cancer Discov*, 2014. 4(5): p. 606-19.
6. Zhang, Z., et al., Activation of the AXL kinase causes resistance to EGFR-targeted therapy in lung cancer. *Nat Genet*, 2012. 44(8): p. 852-60.
7. Meador, C.B., et al., Beyond histology: translating tumor genotypes into clinically effective targeted therapies. *Clin Cancer Res*, 2014. 20(9): p. 2264-75.
8. Schiller, J.H., et al., Comparison of four chemotherapy regimens for advanced non-small-cell lung cancer. *N Engl J Med*, 2002. 346(2): p. 92-8.
9. Schiller, J.H., et al., Comparison of four chemotherapy regimens for advanced non-small-cell lung cancer. *N Engl J Med*, 2002. 346(2): p. 92-8.
10. Sandler, A., et al., Paclitaxel-carboplatin alone or with bevacizumab for non-small-cell lung cancer. *N Engl J Med*, 2006. 355(24): p. 2542-50.
11. Stehelin, D., et al., DNA related to the transforming gene(s) of avian sarcoma viruses is present in normal avian DNA. *Nature*, 1976. 260(5547): p. 170-3.
12. Weinstein, I.B. and A. Joe, Oncogene addiction. *Cancer Res*, 2008. 68(9): p. 3077-80; discussion 3080.
13. Pao, W. and K.E. Hutchinson, Chipping away at the lung cancer genome. *Nat Med*, 2012. 18(3): p. 349-51.
14. Cancer Genome Atlas Research, N., Comprehensive molecular profiling of lung adenocarcinoma. *Nature*, 2014. 511(7511): p. 543-50.
15. Vaishnavi, A., et al., Oncogenic and drug-sensitive NTRK1 rearrangements in lung cancer. *Nat Med*, 2013. 19(11): p. 1469-72.
16. Alexandrov, L.B., et al., Signatures of mutational processes in human cancer. *Nature*, 2013. 500(7463): p. 415-21.
17. Collins, F.S. and A.D. Barker, Mapping the cancer genome. Pinpointing the genes involved in cancer will help chart a new course across the complex landscape of human malignancies. *Sci Am*, 2007. 296(3): p. 50-7.
18. Pao, W., et al., EGF receptor gene mutations are common in lung cancers from "never smokers" and are associated with sensitivity of tumors to gefitinib and erlotinib. *Proc Natl Acad Sci U S A*, 2004. 101(36): p. 13306-11.
19. Paez, J.G., et al., EGFR mutations in lung cancer: correlation with clinical response to gefitinib therapy. *Science*, 2004. 304(5676): p. 1497-500.
20. Lynch, T.J., et al., Activating mutations in the epidermal growth factor receptor underlying responsiveness of non-small-cell lung cancer to gefitinib. *N Engl J Med*, 2004. 350(21): p. 2129-39.
21. Soda, M., et al., Identification of the transforming EML4-ALK fusion gene in non-small-cell lung cancer. *Nature*, 2007. 448(7153): p. 561-6.
22. Pillai, R.N. and S.S. Ramalingam, The biology and clinical features of non-small cell lung cancers with EML4-ALK translocation. *Curr Oncol Rep*, 2012. 14(2): p. 105-10.

23. Shaw, A.T., et al., Crizotinib versus chemotherapy in advanced ALK-positive lung cancer. *N Engl J Med*, 2013. 368(25): p. 2385-94.
24. Shaw, A.T. and J.A. Engelman, Ceritinib in ALK-rearranged non-small-cell lung cancer. *N Engl J Med*, 2014. 370(26): p. 2537-9.
25. Seto, T., et al., CH5424802 (RO5424802) for patients with ALK-rearranged advanced non-small-cell lung cancer (AF-001JP study): a single-arm, open-label, phase 1-2 study. *Lancet Oncol*, 2013. 14(7): p. 590-8.
26. Janne, P.A., et al., Selumetinib plus docetaxel for KRAS-mutant advanced non-small-cell lung cancer: a randomised, multicentre, placebo-controlled, phase 2 study. *Lancet Oncol*, 2013. 14(1): p. 38-47.
27. Blumenschein, G.R., Jr., et al., A randomized phase II study of the MEK1/MEK2 inhibitor trametinib (GSK1120212) compared with docetaxel in KRAS-mutant advanced non-small-cell lung cancer (NSCLC)dagger. *Ann Oncol*, 2015. 26(5): p. 894-901.
28. Lopez-Chavez, A., et al., Molecular profiling and targeted therapy for advanced thoracic malignancies: a biomarker-derived, multiarm, multihistology phase II basket trial. *J Clin Oncol*, 2015. 33(9): p. 1000-7.
29. Tolcher, A.W., et al., Antitumor activity in RAS-driven tumors by blocking AKT and MEK. *Clin Cancer Res*, 2015. 21(4): p. 739-48.
30. MacConaill, L.E., Existing and emerging technologies for tumor genomic profiling. *J Clin Oncol*, 2013. 31(15): p. 1815-24.
31. Metzker, M.L., Sequencing technologies - the next generation. *Nat Rev Genet*, 2010. 11(1): p. 31-46.
32. Meyerson, M., S. Gabriel, and G. Getz, Advances in understanding cancer genomes through second-generation sequencing. *Nat Rev Genet*, 2010. 11(10): p. 685-96.
33. Chmielecki, J. and M. Meyerson, DNA Sequencing of Cancer: What Have We Learned? *Annu Rev Med*, 2013.
34. Heitzer, E., P. Ulz, and J.B. Geigl, Circulating tumor DNA as a liquid biopsy for cancer. *Clin Chem*, 2015. 61(1): p. 112-23.
35. Sequist, L.V., et al., Activity of IPI-504, a novel heat-shock protein 90 inhibitor, in patients with molecularly defined non-small-cell lung cancer. *J Clin Oncol*, 2010. 28(33): p. 4953-60.
36. Socinski, M.A., et al., A multicenter phase II study of ganetespib monotherapy in patients with genotypically defined advanced non-small cell lung cancer. *Clinical Cancer Research*, 2013. 19(11): p. 3068-77.
37. Camidge, D.R., Bazhenova, L., Salgia, R., Langer, C.L., Gold, K.A., Rosell, R., Shaw, A.T., Weiss, G.J., Narasimhan, N.I., Dorer, D.J., Rivera V.M., Clackson, T.P., Conlan, M.G., Kerstein, D., Haluska, F.G., and Gettinger, S.N. , Safety and efficacy of brigatinib (AP26113) in advanced malignancies, including ALK+ non-small cell lung cancer (NSCLC). *J Clin Oncol* 33, 2015 (suppl; abstr 8062), 2015.
38. Sang, J., et al., Targeted inhibition of the molecular chaperone Hsp90 overcomes ALK inhibitor resistance in non-small cell lung cancer. *Cancer Discov*, 2013. 3(4): p. 430-43.
39. Sen, B., et al., Kinase-impaired BRAF mutations in lung cancer confer sensitivity to dasatinib. *Sci Transl Med*, 2012. 4(136): p. 136ra70.
40. Gautschi, O., et al., A patient with BRAF V600E lung adenocarcinoma responding to vemurafenib. *J Thorac Oncol*, 2012. 7(10): p. e23-4.
41. Rudin, C.M., K. Hong, and M. Streit, Molecular characterization of acquired resistance to the BRAF inhibitor dabrafenib in a patient with BRAF-mutant non-small-cell lung cancer. *J Thorac Oncol*, 2013. 8(5): p. e41-2.
42. Pitini, V., et al., Response to dasatinib in a patient with SQCC of the lung harboring a discoid-receptor-2 and synchronous chronic myelogenous leukemia. *Lung Cancer*, 2013. 82(1): p. 171-2.
43. Hammerman, P.S., et al., Mutations in the DDR2 kinase gene identify a novel therapeutic target in squamous cell lung cancer. *Cancer Discov*, 2011. 1(1): p. 78-89.
44. Mok, T.S., et al., Gefitinib or carboplatin-paclitaxel in pulmonary adenocarcinoma. *N Engl J Med*, 2009. 361(10): p. 947-57.
45. Mitsudomi, T., et al., Gefitinib versus cisplatin plus docetaxel in patients with non-small-cell lung cancer harbouring mutations of the epidermal growth factor receptor (WJTOG3405): an open label, randomised phase 3 trial. *Lancet Oncol*, 2010. 11(2): p. 121-8.

46. Maemondo, M., et al., Gefitinib or chemotherapy for non-small-cell lung cancer with mutated EGFR. *N Engl J Med*, 2010. 362(25): p. 2380-8.
47. Zhou, C., et al., Erlotinib versus chemotherapy as first-line treatment for patients with advanced EGFR mutation-positive non-small-cell lung cancer (OPTIMAL, CTONG-0802): a multicentre, open-label, randomised, phase 3 study. *Lancet Oncol*, 2011. 12(8): p. 735-42.
48. Rosell, R., et al., Erlotinib versus standard chemotherapy as first-line treatment for European patients with advanced EGFR mutation-positive non-small-cell lung cancer (EURTAC): a multicentre, open-label, randomised phase 3 trial. *Lancet Oncol*, 2012. 13(3): p. 239-46.
49. Sequist, L.V., et al., Phase III Study of Afatinib or Cisplatin Plus Pemetrexed in Patients With Metastatic Lung Adenocarcinoma With EGFR Mutations. *J Clin Oncol*, 2013. 31(27): p. 3327-3334.
50. Ramalingam, S.S., et al., Randomized phase II study of dacomitinib (PF-00299804), an irreversible pan-human epidermal growth factor receptor inhibitor, versus erlotinib in patients with advanced non-small-cell lung cancer. *J Clin Oncol*, 2012. 30(27): p. 3337-44.
51. He, M., et al., EGFR exon 19 insertions: a new family of sensitizing EGFR mutations in lung adenocarcinoma. *Clin Cancer Res*, 2012. 18(6): p. 1790-7.
52. Yasuda, H., et al., Structural, biochemical, and clinical characterization of epidermal growth factor receptor (EGFR) exon 20 insertion mutations in lung cancer. *Sci Transl Med*, 2013. 5(216): p. 216ra177.
53. Sequist, L.V., et al., Neratinib, an irreversible pan-ErbB receptor tyrosine kinase inhibitor: results of a phase II trial in patients with advanced non-small-cell lung cancer. *J Clin Oncol*, 2010. 28(18): p. 3076-83.
54. Sequist, L.V., et al., Rociletinib in EGFR-mutated non-small-cell lung cancer. *N Engl J Med*, 2015. 372(18): p. 1700-9.
55. Janne, P.A., et al., AZD9291 in EGFR inhibitor-resistant non-small-cell lung cancer. *N Engl J Med*, 2015. 372(18): p. 1689-99.
56. De Greve, J., et al., Clinical activity of afatinib (BIBW 2992) in patients with lung adenocarcinoma with mutations in the kinase domain of HER2/neu. *Lung Cancer*, 2012. 76(1): p. 123-7.
57. Cappuzzo, F., L. Bemis, and M. Varella-Garcia, HER2 mutation and response to trastuzumab therapy in non-small-cell lung cancer. *N Engl J Med*, 2006. 354(24): p. 2619-21.
58. Mazieres, J., et al., Lung cancer that harbors an HER2 mutation: epidemiologic characteristics and therapeutic perspectives. *J Clin Oncol*, 2013. 31(16): p. 1997-2003.
59. Malchers, F., et al., Cell-Autonomous and Non-Cell-Autonomous Mechanisms of Transformation by Amplified FGFR1 in Lung Cancer. *Cancer Discov*, 2014. 4(2): p. 246-57.
60. Marks, J.L., et al., Novel MEK1 mutation identified by mutational analysis of epidermal growth factor receptor signaling pathway genes in lung adenocarcinoma. *Cancer Res*, 2008. 68(14): p. 5524-8.
61. Ou, S.H., et al., Activity of crizotinib (PF02341066), a dual mesenchymal-epithelial transition (MET) and anaplastic lymphoma kinase (ALK) inhibitor, in a non-small cell lung cancer patient with de novo MET amplification. *J Thorac Oncol*, 2011. 6(5): p. 942-6.
62. Ohashi, K., et al., Characteristics of lung cancers harboring NRAS mutations. *Clin Cancer Res*, 2013. 19(9): p. 2584-91.
63. Bendell, J.C., et al., Phase I, dose-escalation study of BKM120, an oral pan-Class I PI3K inhibitor, in patients with advanced solid tumors. *J Clin Oncol*, 2012. 30(3): p. 282-90.
64. Drlon AE, S.C., Somwar R, Smith R, Ginsberg MS, Riely GJ, Rudin CM, Ladanyi M, Kris MG, Rizvi NA., Phase II study of cabozantinib for patients with advanced RET-rearranged lung cancers. *J Clin Oncol* 33, 2015 (suppl; abstr 8007), 2015.
65. Gautschi, O., et al., A patient with lung adenocarcinoma and RET fusion treated with vandetanib. *J Thorac Oncol*, 2013. 8(5): p. e43-4.
66. Bergethon, K., et al., ROS1 rearrangements define a unique molecular class of lung cancers. *J Clin Oncol*, 2012. 30(8): p. 863-70.
67. Shaw, A.T., et al., Crizotinib in ROS1-rearranged non-small-cell lung cancer. *N Engl J Med*, 2014. 371(21): p. 1963-71.
68. Su, Z., et al., A platform for rapid detection of multiple oncogenic mutations with relevance to targeted therapy in non-small-cell lung cancer. *J Mol Diagn*, 2011. 13(1): p. 74-84.
69. Dias-Santagata, D., et al., Rapid targeted mutational analysis of human tumours: a clinical platform to guide personalized cancer medicine. *EMBO Mol Med*, 2010. 2(5): p. 146-58.

70. Rekhtman, N., et al., Clarifying the spectrum of driver oncogene mutations in biomarker-verified squamous carcinoma of lung: lack of EGFR/KRAS and presence of PIK3CA/AKT1 mutations. *Clin Cancer Res*, 2012. 18(4): p. 1167-76.
71. Arcila, M., et al., Detection of KRAS and BRAF mutations in colorectal carcinoma roles for high-sensitivity locked nucleic acid-PCR sequencing and broad-spectrum mass spectrometry genotyping. *J Mol Diagn*, 2011. 13(1): p. 64-73.
72. Rikova, K., et al., Global survey of phosphotyrosine signaling identifies oncogenic kinases in lung cancer. *Cell*, 2007. 131(6): p. 1190-203.
73. Edwin, F., et al., A historical perspective of the EGF receptor and related systems. *Methods Mol Biol*, 2006. 327: p. 1-24.
74. Ullrich, A., et al., Human epidermal growth factor receptor cDNA sequence and aberrant expression of the amplified gene in A431 epidermoid carcinoma cells. *Nature*, 1984. 309(5967): p. 418-25.
75. Cohen, S., et al., A native 170,000 epidermal growth factor receptor-kinase complex from shed plasma membrane vesicles. *J Biol Chem*, 1982. 257(3): p. 1523-31.
76. Carpenter, G., et al., Characterization of the binding of 125-I-labeled epidermal growth factor to human fibroblasts. *J Biol Chem*, 1975. 250(11): p. 4297-304.
77. Cohen, S. and R.A. Fava, Internalization of functional epidermal growth factor:receptor/kinase complexes in A-431 cells. *J Biol Chem*, 1985. 260(22): p. 12351-8.
78. Roskoski, R., Jr., The ErbB/HER family of protein-tyrosine kinases and cancer. *Pharmacol Res*, 2014. 79: p. 34-74.
79. Mitsudomi, T. and Y. Yatabe, Epidermal growth factor receptor in relation to tumor development: EGFR gene and cancer. *FEBS J*, 2010. 277(2): p. 301-8.
80. Yarden, Y. and G. Pines, The ERBB network: at last, cancer therapy meets systems biology. *Nat Rev Cancer*, 2012. 12(8): p. 553-63.
81. Graus-Porta, D., et al., ErbB-2, the preferred heterodimerization partner of all ErbB receptors, is a mediator of lateral signaling. *EMBO J*, 1997. 16(7): p. 1647-55.
82. Parra, H.S., et al., Analysis of epidermal growth factor receptor expression as a predictive factor for response to gefitinib ('Iressa', ZD1839) in non-small-cell lung cancer. *Br J Cancer*, 2004. 91(2): p. 208-12.
83. Ladanyi, M. and W. Pao, Lung adenocarcinoma: guiding EGFR-targeted therapy and beyond. *Mod Pathol*, 2008. 21 Suppl 2: p. S16-22.
84. Pao, W. and J. Chmielecki, Rational, biologically based treatment of EGFR-mutant non-small-cell lung cancer. *Nat Rev Cancer*, 2010. 10(11): p. 760-74.
85. Fukuoka, M., et al., Multi-institutional randomized phase II trial of gefitinib for previously treated patients with advanced non-small-cell lung cancer (The IDEAL 1 Trial) [corrected]. *J Clin Oncol*, 2003. 21(12): p. 2237-46.
86. Miller, V.A., et al., Bronchioloalveolar pathologic subtype and smoking history predict sensitivity to gefitinib in advanced non-small-cell lung cancer. *J Clin Oncol*, 2004. 22(6): p. 1103-9.
87. Rossi, E.D., et al., Detection of common and less frequent EGFR mutations in cytological samples of lung cancer. *Acta Cytol*, 2014. 58(3): p. 275-80.
88. Honegger, A.M., et al., Point mutation at the ATP binding site of EGF receptor abolishes protein-tyrosine kinase activity and alters cellular routing. *Cell*, 1987. 51(2): p. 199-209.
89. Huse, M. and J. Kuriyan, The conformational plasticity of protein kinases. *Cell*, 2002. 109(3): p. 275-82.
90. Yang, J.C., et al., Clinical activity of afatinib in patients with advanced non-small-cell lung cancer harbouring uncommon EGFR mutations: a combined post-hoc analysis of LUX-Lung 2, LUX-Lung 3, and LUX-Lung 6. *Lancet Oncol*, 2015.
91. Cho, J., et al., Cetuximab response of lung cancer-derived EGF receptor mutants is associated with asymmetric dimerization. *Cancer Res*, 2013. 73(22): p. 6770-9.
92. Politi, K., et al., Lung adenocarcinomas induced in mice by mutant EGF receptors found in human lung cancers respond to a tyrosine kinase inhibitor or to down-regulation of the receptors. *Genes Dev*, 2006. 20(11): p. 1496-510.
93. Han, S.W., et al., Predictive and prognostic impact of epidermal growth factor receptor mutation in non-small-cell lung cancer patients treated with gefitinib. *J Clin Oncol*, 2005. 23(11): p. 2493-501.

94. Rosell, R., et al., Mutations in the tyrosine kinase domain of the EGFR gene associated with gefitinib response in non-small-cell lung cancer. *Lung Cancer*, 2005. 50(1): p. 25-33.
95. Taron, M., et al., Activating mutations in the tyrosine kinase domain of the epidermal growth factor receptor are associated with improved survival in gefitinib-treated chemorefractory lung adenocarcinomas. *Clin Cancer Res*, 2005. 11(16): p. 5878-85.
96. Arcila, M.E., et al., EGFR exon 20 insertion mutations in lung adenocarcinomas: prevalence, molecular heterogeneity, and clinicopathologic characteristics. *Mol Cancer Ther*, 2013. 12(2): p. 220-9.
97. Oxnard, G.R., et al., Natural history and molecular characteristics of lung cancers harboring EGFR exon 20 insertions. *J Thorac Oncol*, 2013. 8(2): p. 179-84.
98. Gschwind, A., O.M. Fischer, and A. Ullrich, The discovery of receptor tyrosine kinases: targets for cancer therapy. *Nat Rev Cancer*, 2004. 4(5): p. 361-70.
99. Wakeling, A.E., et al., ZD1839 (Iressa): an orally active inhibitor of epidermal growth factor signaling with potential for cancer therapy. *Cancer Res*, 2002. 62(20): p. 5749-54.
100. Hidalgo, M., et al., Phase I and pharmacologic study of OSI-774, an epidermal growth factor receptor tyrosine kinase inhibitor, in patients with advanced solid malignancies. *J Clin Oncol*, 2001. 19(13): p. 3267-79.
101. Vivanco, I., et al., Differential sensitivity of glioma- versus lung cancer-specific EGFR mutations to EGFR kinase inhibitors. *Cancer Discov*, 2012. 2(5): p. 458-71.
102. Park, J.H., et al., Erlotinib binds both inactive and active conformations of the EGFR tyrosine kinase domain. *Biochem J*, 2012. 448(3): p. 417-23.
103. Yu, H.A., G.J. Riely, and C.M. Lovly, Therapeutic strategies utilized in the setting of acquired resistance to EGFR tyrosine kinase inhibitors. *Clin Cancer Res*, 2014. 20(23): p. 5898-907.
104. Kris, M.G., et al., Efficacy of gefitinib, an inhibitor of the epidermal growth factor receptor tyrosine kinase, in symptomatic patients with non-small cell lung cancer: a randomized trial. *JAMA*, 2003. 290(16): p. 2149-58.
105. Shepherd, F.A., et al., Erlotinib in previously treated non-small-cell lung cancer. *N Engl J Med*, 2005. 353(2): p. 123-32.
106. Thatcher, N., et al., Gefitinib plus best supportive care in previously treated patients with refractory advanced non-small-cell lung cancer: results from a randomised, placebo-controlled, multicentre study (Iressa Survival Evaluation in Lung Cancer). *Lancet*, 2005. 366(9496): p. 1527-37.
107. Rosell, R., et al., Screening for epidermal growth factor receptor mutations in lung cancer. *N Engl J Med*, 2009. 361(10): p. 958-67.
108. Maemondo, M., et al., Gefitinib or chemotherapy for non-small-cell lung cancer with mutated EGFR. *New England Journal of Medicine*, 2010. 362(25): p. 2380-8.
109. Kim, E.S., et al., Gefitinib versus docetaxel in previously treated non-small-cell lung cancer (INTEREST): a randomised phase III trial. *Lancet*, 2008. 372(9652): p. 1809-18.
110. Mendelsohn, J. and J. Baselga, Epidermal growth factor receptor targeting in cancer. *Semin Oncol*, 2006. 33(4): p. 369-85.
111. Li, S., et al., Structural basis for inhibition of the epidermal growth factor receptor by cetuximab. *Cancer Cell*, 2005. 7(4): p. 301-11.
112. Bonner, J.A., et al., Radiotherapy plus cetuximab for squamous-cell carcinoma of the head and neck. *N Engl J Med*, 2006. 354(6): p. 567-78.
113. Baselga, J., et al., Phase II multicenter study of the antiepidermal growth factor receptor monoclonal antibody cetuximab in combination with platinum-based chemotherapy in patients with platinum-refractory metastatic and/or recurrent squamous cell carcinoma of the head and neck. *J Clin Oncol*, 2005. 23(24): p. 5568-77.
114. Herbst, R.S., et al., Phase II multicenter study of the epidermal growth factor receptor antibody cetuximab and cisplatin for recurrent and refractory squamous cell carcinoma of the head and neck. *J Clin Oncol*, 2005. 23(24): p. 5578-87.
115. Jonker, D.J., et al., Cetuximab for the treatment of colorectal cancer. *N Engl J Med*, 2007. 357(20): p. 2040-8.
116. Lynch, T.J., et al., Cetuximab and first-line taxane/carboplatin chemotherapy in advanced non-small-cell lung cancer: results of the randomized multicenter phase III trial BMS099. *J Clin Oncol*, 2010. 28(6): p. 911-7.
117. Pirker, R., et al., Cetuximab plus chemotherapy in patients with advanced non-small-cell lung cancer (FLEX): an open-label randomised phase III trial. *Lancet*, 2009. 373(9674): p. 1525-31.

118. Regales, L., et al., Dual targeting of EGFR can overcome a major drug resistance mutation in mouse models of EGFR mutant lung cancer. *J Clin Invest*, 2009. 119(10): p. 3000-10.
119. Mukohara, T., et al., Differential effects of gefitinib and cetuximab on non-small-cell lung cancers bearing epidermal growth factor receptor mutations. *J Natl Cancer Inst*, 2005. 97(16): p. 1185-94.
120. Janne, P.A., et al., Randomized phase II trial of erlotinib alone or with carboplatin and paclitaxel in patients who were never or light former smokers with advanced lung adenocarcinoma: CALGB 30406 trial. *J Clin Oncol*, 2012. 30(17): p. 2063-9.
121. Riely, G.J., et al., Clinical course of patients with non-small cell lung cancer and epidermal growth factor receptor exon 19 and exon 21 mutations treated with gefitinib or erlotinib. *Clin Cancer Res*, 2006. 12(3 Pt 1): p. 839-44.
122. Pao, W., et al., Acquired resistance of lung adenocarcinomas to gefitinib or erlotinib is associated with a second mutation in the EGFR kinase domain. *PLoS Med*, 2005. 2(3): p. e73.
123. Kobayashi, S., et al., EGFR mutation and resistance of non-small-cell lung cancer to gefitinib. *New England Journal of Medicine*, 2005. 352(8): p. 786-92.
124. Balak, M.N., et al., Novel D761Y and common secondary T790M mutations in epidermal growth factor receptor-mutant lung adenocarcinomas with acquired resistance to kinase inhibitors. *Clin Cancer Res*, 2006. 12(21): p. 6494-501.
125. Bean, J., et al., Acquired resistance to epidermal growth factor receptor kinase inhibitors associated with a novel T854A mutation in a patient with EGFR-mutant lung adenocarcinoma. *Clin Cancer Res*, 2008. 14(22): p. 7519-25.
126. Gorre, M.E., et al., Clinical resistance to STI-571 cancer therapy caused by BCR-ABL gene mutation or amplification. *Science*, 2001. 293(5531): p. 876-80.
127. Shah, N.P., et al., Multiple BCR-ABL kinase domain mutations confer polyclonal resistance to the tyrosine kinase inhibitor imatinib (STI571) in chronic phase and blast crisis chronic myeloid leukemia. *Cancer Cell*, 2002. 2(2): p. 117-25.
128. Godin-Heymann, N., et al., The T790M "gatekeeper" mutation in EGFR mediates resistance to low concentrations of an irreversible EGFR inhibitor. *Mol Cancer Ther*, 2008. 7(4): p. 874-9.
129. Sos, M.L., et al., Chemogenomic profiling provides insights into the limited activity of irreversible EGFR Inhibitors in tumor cells expressing the T790M EGFR resistance mutation. *Cancer Res*, 2010. 70(3): p. 868-74.
130. Yun, C.H., et al., The T790M mutation in EGFR kinase causes drug resistance by increasing the affinity for ATP. *Proc Natl Acad Sci U S A*, 2008. 105(6): p. 2070-5.
131. Bell, D.W., et al., Inherited susceptibility to lung cancer may be associated with the T790M drug resistance mutation in EGFR. *Nat Genet*, 2005. 37(12): p. 1315-6.
132. Yu, H.A., et al., Germline EGFR T790M mutation found in multiple members of a familial cohort. *J Thorac Oncol*, 2014. 9(4): p. 554-8.
133. Regales, L., et al., Development of new mouse lung tumor models expressing EGFR T790M mutants associated with clinical resistance to kinase inhibitors. *PLoS One*, 2007. 2(8): p. e810.
134. Bean, J., et al., MET amplification occurs with or without T790M mutations in EGFR mutant lung tumors with acquired resistance to gefitinib or erlotinib. *Proc Natl Acad Sci U S A*, 2007. 104(52): p. 20932-7.
135. Engelman, J.A., et al., MET amplification leads to gefitinib resistance in lung cancer by activating ERBB3 signaling. *Science*, 2007. 316(5827): p. 1039-43.
136. Takezawa, K., et al., HER2 amplification: a potential mechanism of acquired resistance to EGFR inhibition in EGFR-mutant lung cancers that lack the second-site EGFR T790M mutation. *Cancer Discov*, 2012. 2(10): p. 922-33.
137. Ohashi, K., et al., Lung cancers with acquired resistance to EGFR inhibitors occasionally harbor BRAF gene mutations but lack mutations in KRAS, NRAS, or MEK1. *Proc Natl Acad Sci U S A*, 2012. 109(31): p. E2127-33.
138. Ji, W., et al., Mechanisms of acquired resistance to EGFR-tyrosine kinase inhibitor in Korean patients with lung cancer. *BMC Cancer*, 2013. 13: p. 606.
139. Kwak, E.L., et al., Irreversible inhibitors of the EGF receptor may circumvent acquired resistance to gefitinib. *Proc Natl Acad Sci U S A*, 2005. 102(21): p. 7665-70.
140. Engelman, J.A., et al., PF00299804, an irreversible pan-ERBB inhibitor, is effective in lung cancer models with EGFR and ERBB2 mutations that are resistant to gefitinib. *Cancer Res*, 2007. 67(24): p. 11924-32.

141. Li, D., et al., BIBW2992, an irreversible EGFR/HER2 inhibitor highly effective in preclinical lung cancer models. *Oncogene*, 2008. 27(34): p. 4702-11.
142. Eskens, F.A., et al., A phase I dose escalation study of BIBW 2992, an irreversible dual inhibitor of epidermal growth factor receptor 1 (EGFR) and 2 (HER2) tyrosine kinase in a 2-week on, 2-week off schedule in patients with advanced solid tumours. *Br J Cancer*, 2008. 98(1): p. 80-5.
143. Miller, V.A., et al., Afatinib versus placebo for patients with advanced, metastatic non-small-cell lung cancer after failure of erlotinib, gefitinib, or both, and one or two lines of chemotherapy (LUX-Lung 1): a phase 2b/3 randomised trial. *Lancet Oncol*, 2012. 13(5): p. 528-38.
144. Janjigian, Y.Y., et al., Dual inhibition of EGFR with afatinib and cetuximab in kinase inhibitor-resistant EGFR-mutant lung cancer with and without T790M mutations. *Cancer Discov*, 2014. 4(9): p. 1036-45.
145. Pirazzoli, V., et al., Acquired Resistance of EGFR-Mutant Lung Adenocarcinomas to Afatinib plus Cetuximab Is Associated with Activation of mTORC1. *Cell Rep*, 2014. 7(4): p. 999-1008.
146. Zhou, W., et al., Novel mutant-selective EGFR kinase inhibitors against EGFR T790M. *Nature*, 2009. 462(7276): p. 1070-4.
147. Cross, D.A., et al., AZD9291, an irreversible EGFR TKI, overcomes T790M-mediated resistance to EGFR inhibitors in lung cancer. *Cancer Discov*, 2014.
148. Walter, A.O., et al., Discovery of a mutant-selective covalent inhibitor of EGFR that overcomes T790M-mediated resistance in NSCLC. *Cancer Discov*, 2013.
149. Walter, A.O., et al., Discovery of a mutant-selective covalent inhibitor of EGFR that overcomes T790M-mediated resistance in NSCLC. *Cancer Discov*, 2013. 3(12): p. 1404-15.
150. Ercan, D., et al., Reactivation of ERK signaling causes resistance to EGFR kinase inhibitors. *Cancer Discov*, 2012. 2(10): p. 934-47.
151. Cortot, A.B., et al., Resistance to irreversible EGF receptor tyrosine kinase inhibitors through a multistep mechanism involving the IGF1R pathway. *Cancer Res*, 2013. 73(2): p. 834-43.
152. Kwak, E.L., et al., Anaplastic lymphoma kinase inhibition in non-small-cell lung cancer. *N Engl J Med*, 2010. 363(18): p. 1693-703.
153. Sosman, J.A., et al., Survival in BRAF V600-mutant advanced melanoma treated with vemurafenib. *N Engl J Med*, 2012. 366(8): p. 707-14.
154. Demetri, G.D., et al., Efficacy and safety of imatinib mesylate in advanced gastrointestinal stromal tumors. *N Engl J Med*, 2002. 347(7): p. 472-80.
155. Chmielecki, J., et al., Optimization of dosing for EGFR-mutant non-small cell lung cancer with evolutionary cancer modeling. *Sci Transl Med*, 2011. 3(90): p. 90ra59.
156. Wacker, S.A., et al., Using transcriptome sequencing to identify mechanisms of drug action and resistance. *Nat Chem Biol*, 2012. 8(3): p. 235-7.
157. Boeva, V., et al., Control-free calling of copy number alterations in deep-sequencing data using GC-content normalization. *Bioinformatics*, 2011. 27(2): p. 268-9.
158. Boeva, V., et al., Control-FREEC: a tool for assessing copy number and allelic content using next-generation sequencing data. *Bioinformatics*, 2012. 28(3): p. 423-5.
159. Futreal, P.A., et al., A census of human cancer genes. *Nat Rev Cancer*, 2004. 4(3): p. 177-83.
160. Adzhubei, I.A., et al., A method and server for predicting damaging missense mutations. *Nat Methods*, 2010. 7(4): p. 248-9.
161. Krumm, N., et al., Copy number variation detection and genotyping from exome sequence data. *Genome Res*, 2012. 22(8): p. 1525-32.
162. Koboldt, D.C., et al., VarScan 2: somatic mutation and copy number alteration discovery in cancer by exome sequencing. *Genome Res*, 2012. 22(3): p. 568-76.
163. Sathirapongsasuti, J.F., et al., Exome sequencing-based copy-number variation and loss of heterozygosity detection: ExomeCNV. *Bioinformatics*, 2011. 27(19): p. 2648-54.
164. Ge, H., et al., FusionMap: detecting fusion genes from next-generation sequencing data at base-pair resolution. *Bioinformatics*, 2011. 27(14): p. 1922-8.
165. Onozato, R., et al., Activation of MET by gene amplification or by splice mutations deleting the juxtamembrane domain in primary resected lung cancers. *J Thorac Oncol*, 2009. 4(1): p. 5-11.
166. Goh, L., et al., Assessing matched normal and tumor pairs in next-generation sequencing studies. *PLoS One*, 2011. 6(3): p. e17810.
167. Govindan, R., et al., Genomic landscape of non-small cell lung cancer in smokers and never-smokers. *Cell*, 2012. 150(6): p. 1121-34.

168. Karolchik, D., et al., The UCSC Genome Browser Database. *Nucleic Acids Res*, 2003. 31(1): p. 51-4.
169. Hansen, R.S., et al., Sequencing newly replicated DNA reveals widespread plasticity in human replication timing. *Proc Natl Acad Sci U S A*, 2010. 107(1): p. 139-44.
170. Guelen, L., et al., Domain organization of human chromosomes revealed by mapping of nuclear lamina interactions. *Nature*, 2008. 453(7197): p. 948-51.
171. Furey, T.S. and D. Haussler, Integration of the cytogenetic map with the draft human genome sequence. *Hum Mol Genet*, 2003. 12(9): p. 1037-44.
172. Kong, A., et al., A high-resolution recombination map of the human genome. *Nat Genet*, 2002. 31(3): p. 241-7.
173. Jurka, J., Repbase update: a database and an electronic journal of repetitive elements. *Trends Genet*, 2000. 16(9): p. 418-20.
174. Irizarry, R.A., H. Wu, and A.P. Feinberg, A species-generalized probabilistic model-based definition of CpG islands. *Mamm Genome*, 2009. 20(9-10): p. 674-80.
175. Liu, L., S. De, and F. Michor, DNA replication timing and higher-order nuclear organization determine single-nucleotide substitution patterns in cancer genomes. *Nat Commun*, 2013. 4: p. 1502.
176. Weir, B.A., et al., Characterizing the cancer genome in lung adenocarcinoma. *Nature*, 2007. 450(7171): p. 893-8.
177. Kumar, P., S. Henikoff, and P.C. Ng, Predicting the effects of coding non-synonymous variants on protein function using the SIFT algorithm. *Nat Protoc*, 2009. 4(7): p. 1073-81.
178. Liu, J., et al., Genome and transcriptome sequencing of lung cancers reveal diverse mutational and splicing events. *Genome Res*, 2012. 22(12): p. 2315-27.
179. Campbell, P.J., et al., Identification of somatically acquired rearrangements in cancer using genome-wide massively parallel paired-end sequencing. *Nat Genet*, 2008. 40(6): p. 722-9.
180. Chiang, D.Y., et al., High-resolution mapping of copy-number alterations with massively parallel sequencing. *Nat Methods*, 2009. 6(1): p. 99-103.
181. Dahlman, K.B., et al., BRAF(L597) mutations in melanoma are associated with sensitivity to MEK inhibitors. *Cancer Discov*, 2012. 2(9): p. 791-7.
182. Li, H. and R. Durbin, Fast and accurate short read alignment with Burrows-Wheeler transform. *Bioinformatics*, 2009. 25(14): p. 1754-60.
183. DePristo, M.A., et al., A framework for variation discovery and genotyping using next-generation DNA sequencing data. *Nat Genet*, 2011. 43(5): p. 491-8.
184. Genomes Project, C., et al., A map of human genome variation from population-scale sequencing. *Nature*, 2010. 467(7319): p. 1061-73.
185. Reimers, M. and V.J. Carey, Bioconductor: an open source framework for bioinformatics and computational biology. *Methods Enzymol*, 2006. 411: p. 119-34.
186. Rozen, S. and H. Skaletsky, Primer3 on the WWW for general users and for biologist programmers. *Methods Mol Biol*, 2000. 132: p. 365-86.
187. Trapnell, C., L. Pachter, and S.L. Salzberg, TopHat: discovering splice junctions with RNA-Seq. *Bioinformatics*, 2009. 25(9): p. 1105-11.
188. Trapnell, C., et al., Transcript assembly and quantification by RNA-Seq reveals unannotated transcripts and isoform switching during cell differentiation. *Nat Biotechnol*, 2010. 28(5): p. 511-5.
189. Zakowski, M.F., et al., EGFR mutations in small-cell lung cancers in patients who have never smoked. *N Engl J Med*, 2006. 355(2): p. 213-5.
190. Janne, P.A., Ramalingam, S.S., Chih-Hsin Yang, J., Ahn, M-J., Kim, D-W., Kim, S-W., Planchard, D., Ohe, Y., Felip, E., Watkins, C., Cantarini, M., Ghiorghiu, S., Ranson, M., Clinical activity of the mutant-selective EGFR inhibitor AZD9291 in patients (pts) with EGFR inhibitor-resistant non-small cell lung cancer (NSCLC). *J Clin Oncol* 32:5s, 2014 (suppl; abstr 8009^).
191. Sequist, L.V., Soria, J-C., Gadgeel, S.M., Wakelee, H.A., Camidge, D.R., Varga, A., Solomon, B.J., Papadimitrakopoulou, V., Jaw-Tsai, S.S., Caunt, L., Kaur, P., Rolfe, L., Allen, A.R., Goldman, J.W., First-in-human evaluation of CO-1686, an irreversible, highly selective tyrosine kinase inhibitor of mutations in EGFR (activating and T790M). *J Clin Oncol* 32:5s, 2014 (suppl; abstr 8010^).
192. Kim, D.-W., Lee, D.H., Kang, J.H., Park, K., Han, J.-Y., Lee, J.-S., Jang, I.-J., Kim, H.-Y., Son, J., Kim, J.-H., Clinical activity and safety of HM61713, an EGFR-mutant selective inhibitor, in advanced non-small cell lung cancer (NSCLC) in patients (pts) with EGFR mutations who had received EGFR tyrosine kinase inhibitors (TKIs). *J Clin Oncol* 32:5s, 2014 (suppl; abstr 8011).

193. Cross, D.A., et al., AZD9291, an irreversible EGFR TKI, overcomes T790M-mediated resistance to EGFR inhibitors in lung cancer. *Cancer Discov*, 2014. 4(9): p. 1046-61.
194. Gong, Y., et al., Induction of BIM is essential for apoptosis triggered by EGFR kinase inhibitors in mutant EGFR-dependent lung adenocarcinomas. *PLoS Med*, 2007. 4(10): p. e294.
195. Ogino, A., et al., Emergence of epidermal growth factor receptor T790M mutation during chronic exposure to gefitinib in a non small cell lung cancer cell line. *Cancer Research*, 2007. 67(16): p. 7807-14.
196. Ramalingam, S., Ohe, Y., Nogami, N., Yang, J. C-H., Eberlein, C., Ashton, S., Mellor, M., Spitzler, P., Meador, C.B., Ichihara, E., Cross, D., Pao, W., Ballard, P., Hughes, G., Cantarini, M., Frewer, P., Ghiorghiu, S., Janne, P.A., Pre-clinical and Clinical Evaluation of AZD9291, a Mutation-specific Inhibitor, in treatment-naïve EGFR Mutated NSCLC. *ESMO*, 2014. Poster 454P.
197. Bauer, R.C., et al., Sequential inhibitor therapy in CML: in vitro simulation elucidates the pattern of resistance mutations after second- and third-line treatment. *Clinical Cancer Research*, 2013. 19(11): p. 2962-72.
198. Scher, H.I. and C.L. Sawyers, Biology of progressive, castration-resistant prostate cancer: directed therapies targeting the androgen-receptor signaling axis. *Journal of Clinical Oncology*, 2005. 23(32): p. 8253-61.
199. Arora, V.K., et al., Glucocorticoid receptor confers resistance to antiandrogens by bypassing androgen receptor blockade. *Cell*, 2013. 155(6): p. 1309-22.
200. Li, H. and R. Durbin, Fast and accurate long-read alignment with Burrows-Wheeler transform. *Bioinformatics*, 2010. 26(5): p. 589-95.
201. McKenna, A., et al., The Genome Analysis Toolkit: a MapReduce framework for analyzing next-generation DNA sequencing data. *Genome Res*, 2010. 20(9): p. 1297-303.
202. Van der Auwera, G.A., et al., From FastQ Data to High-Confidence Variant Calls: The Genome Analysis Toolkit Best Practices Pipeline, in *Current Protocols in Bioinformatics*. 2002, John Wiley & Sons, Inc.
203. Cibulskis, K., et al., Sensitive detection of somatic point mutations in impure and heterogeneous cancer samples. *Nat Biotechnol*, 2013. 31(3): p. 213-9.
204. Sherry, S.T., et al., dbSNP: the NCBI database of genetic variation. *Nucleic Acids Res*, 2001. 29(1): p. 308-11.
205. Wang, K., M. Li, and H. Hakonarson, ANNOVAR: functional annotation of genetic variants from high-throughput sequencing data. *Nucleic Acids Res*, 2010. 38(16): p. e164.
206. Gazdar, A.F., Activating and resistance mutations of EGFR in non-small-cell lung cancer: role in clinical response to EGFR tyrosine kinase inhibitors. *Oncogene*, 2009. 28 Suppl 1: p. S24-31.
207. Keating, G.M., Afatinib: a review of its use in the treatment of advanced non-small cell lung cancer. *Drugs*, 2014. 74(2): p. 207-21.
208. Kim, Y., et al., The EGFR T790M mutation in acquired resistance to an irreversible second-generation EGFR inhibitor. *Mol Cancer Ther*, 2012. 11(3): p. 784-91.
209. Nakagawa, T., et al., Combined therapy with mutant-selective EGFR inhibitor and Met kinase inhibitor for overcoming erlotinib resistance in EGFR-mutant lung cancer. *Mol Cancer Ther*, 2012. 11(10): p. 2149-57.
210. Kim, S.M., et al., Glycolysis inhibition sensitizes non-small cell lung cancer with T790M mutation to irreversible EGFR inhibitors via translational suppression of Mcl-1 by AMPK activation. *Mol Cancer Ther*, 2013. 12(10): p. 2145-56.
211. Shien, K., et al., Acquired resistance to EGFR inhibitors is associated with a manifestation of stem cell-like properties in cancer cells. *Cancer Res*, 2013. 73(10): p. 3051-61.
212. Vazquez-Martin, A., et al., IGF-1R/epithelial-to-mesenchymal transition (EMT) crosstalk suppresses the erlotinib-sensitizing effect of EGFR exon 19 deletion mutations. *Sci Rep*, 2013. 3: p. 2560.
213. Ware, K.E., et al., A mechanism of resistance to gefitinib mediated by cellular reprogramming and the acquisition of an FGF2-FGFR1 autocrine growth loop. *Oncogenesis*, 2013. 2: p. e39.
214. Yamauchi, M., et al., N-cadherin expression is a potential survival mechanism of gefitinib-resistant lung cancer cells. *Am J Cancer Res*, 2011. 1(7): p. 823-33.
215. Bedard, P.L., et al., Tumour heterogeneity in the clinic. *Nature*, 2013. 501(7467): p. 355-64.
216. Morabito, A., et al., Activity of gefitinib in a non-small-cell lung cancer patient with both activating and resistance EGFR mutations. *J Thorac Oncol*, 2013. 8(7): p. e59-60.

217. Tan, D.S., et al., Intertumor heterogeneity of non-small-cell lung carcinomas revealed by multiplexed mutation profiling and integrative genomics. *Int J Cancer*, 2014. 135(5): p. 1092-100.
218. Fukushima, S., et al., Mutually exclusive mutations of KIT and RAS are associated with KIT mRNA expression and chromosomal instability in primary intracranial pure germinomas. *Acta Neuropathol*, 2014. 127(6): p. 911-25.
219. van der Burgt, I., et al., Myopathy caused by HRAS germline mutations: implications for disturbed myogenic differentiation in the presence of constitutive HRas activation. *J Med Genet*, 2007. 44(7): p. 459-62.
220. Huang, M.H., et al., MEK inhibitors reverse resistance in epidermal growth factor receptor mutation lung cancer cells with acquired resistance to gefitinib. *Mol Oncol*, 2013. 7(1): p. 112-20.
221. Meriggi, F., et al., The Emerging Role of NRAS Mutations in Colorectal Cancer Patients Selected for Anti-EGFR Therapies. *Rev Recent Clin Trials*, 2014.
222. Misale, S., et al., Blockade of EGFR and MEK intercepts heterogeneous mechanisms of acquired resistance to anti-EGFR therapies in colorectal cancer. *Sci Transl Med*, 2014. 6(224): p. 224ra26.
223. Buonato, J.M. and M.J. Lazzara, ERK1/2 blockade prevents epithelial-mesenchymal transition in lung cancer cells and promotes their sensitivity to EGFR inhibition. *Cancer Res*, 2014. 74(1): p. 309-19.
224. Cheung, H.W., et al., Amplification of CRKL induces transformation and epidermal growth factor receptor inhibitor resistance in human non-small cell lung cancers. *Cancer Discov*, 2011. 1(7): p. 608-25.
225. Saki, M., M. Toulany, and H.P. Rodemann, Acquired resistance to cetuximab is associated with the overexpression of Ras family members and the loss of radiosensitization in head and neck cancer cells. *Radiother Oncol*, 2013. 108(3): p. 473-8.
226. Crystal, A.S., et al., Patient-derived models of acquired resistance can identify effective drug combinations for cancer. *Science*, 2014. 346(6216): p. 1480-6.
227. Niepel, M., et al., Profiles of Basal and stimulated receptor signaling networks predict drug response in breast cancer lines. *Sci Signal*, 2013. 6(294): p. ra84.
228. Thress, K.S., et al., Acquired EGFR C797S mutation mediates resistance to AZD9291 in non-small cell lung cancer harboring EGFR T790M. *Nat Med*, 2015.
229. Tricker, E.M., et al., Combined EGFR/MEK Inhibition Prevents the Emergence of Resistance in EGFR mutant Lung Cancer. *Cancer Discov*, 2015.
230. Meador, C.B., et al., Optimizing the Sequence of Anti-EGFR-Targeted Therapy in EGFR-Mutant Lung Cancer. *Mol Cancer Ther*, 2015. 14(2): p. 542-52.
231. Gilmartin, A.G., et al., GSK1120212 (JTP-74057) is an inhibitor of MEK activity and activation with favorable pharmacokinetic properties for sustained in vivo pathway inhibition. *Clin Cancer Res*, 2011. 17(5): p. 989-1000.
232. Nissan, M.H., et al., Loss of NF1 in cutaneous melanoma is associated with RAS activation and MEK dependence. *Cancer Res*, 2014. 74(8): p. 2340-50.
233. Gerlinger, M., et al., Intratumor heterogeneity and branched evolution revealed by multiregion sequencing. *N Engl J Med*, 2012. 366(10): p. 883-92.
234. Yap, T.A., et al., Intratumor heterogeneity: seeing the wood for the trees. *Sci Transl Med*, 2012. 4(127): p. 127ps10.
235. Piotrowska, Z., et al., Heterogeneity Underlies the Emergence of EGFR T790 Wild-Type Clones Following Treatment of T790M-Positive Cancers with a Third Generation EGFR Inhibitor. *Cancer Discov*, 2015.
236. Krebs, M.G., et al., Molecular analysis of circulating tumour cells-biology and biomarkers. *Nat Rev Clin Oncol*, 2014. 11(3): p. 129-44.
237. Ercan, D., et al., EGFR mutations and resistance to Irreversible pyrimidine based EGFR inhibitors. *Clin Cancer Res*, 2015.
238. Oxnard GR, R.S., Ahn MJ, Kim SW, Yu HA, Saka H, Horn L, Goto K, Ohe Y, Cantarini M, Frewer P, Lahn M, Yan, JCH., Preliminary results of TATTON, a multi-arm phase Ib trial of AZD9291 combined with MEDI4736, AZD6094 or selumetinib in EGFR-mutant lung cancer. *J Clin Oncol* 33, 2015 (suppl; abstr 2509), 2015.
239. Gajewski, T.F., H. Schreiber, and Y.X. Fu, Innate and adaptive immune cells in the tumor microenvironment. *Nat Immunol*, 2013. 14(10): p. 1014-22.
240. Postow, M.A., M.K. Callahan, and J.D. Wolchok, Immune Checkpoint Blockade in Cancer Therapy. *J Clin Oncol*, 2015. 33(17): p. 1974-1982.

241. Ward, R.A., et al., Structure- and reactivity-based development of covalent inhibitors of the activating and gatekeeper mutant forms of the epidermal growth factor receptor (EGFR). *J Med Chem*, 2013. 56(17): p. 7025-48.
242. Cingolani, P., et al., Using *Drosophila melanogaster* as a Model for Genotoxic Chemical Mutational Studies with a New Program, SnpSift. *Front Genet*, 2012. 3: p. 35.
243. Cingolani, P., et al., A program for annotating and predicting the effects of single nucleotide polymorphisms, SnpEff: SNPs in the genome of *Drosophila melanogaster* strain w1118; iso-2; iso-3. *Fly (Austin)*, 2012. 6(2): p. 80-92.
244. De Baets, G., et al., SNPeff 4.0: on-line prediction of molecular and structural effects of protein-coding variants. *Nucleic Acids Res*, 2012. 40(Database issue): p. D935-9.